THE UNIVERSITY OF WARWICK

Library Declaration and Deposit Agreement

1. STUDENT DETAILS

Please complete the following:

Full name: Frédéric PITIÉ

University ID number: 0859945

2. THESIS DEPOSIT

2.1 I understand that under my registration at the University, I am required to deposit my thesis with the University in BOTH hard copy and in digital format. The digital version should normally be saved as a single pdf file.

2.2 The hard copy will be housed in the University Library. The digital version will be deposited in the University's Institutional Repository (WRAP). Unless otherwise indicated (see 2.3 below) this will be made openly accessible on the Internet and will be supplied to the British Library to be made available online via its Electronic Theses Online Service (EThOS) service.
[At present, theses submitted for a Master's degree by Research (MA, MSc, LLM, MS or MMedSci) are not being deposited in WRAP and not being made available via EthOS. This may change in future.]

2.3 In exceptional circumstances, the Chair of the Board of Graduate Studies may grant permission for an embargo to be placed on public access to the hard copy thesis for a limited period. It is also possible to apply separately for an embargo on the digital version. (Further information is available in the *Guide to Examinations for Higher Degrees by Research*.)

2.4 *If you are depositing a thesis for a Master's degree by Research, please complete section (a) below. For all other research degrees, please complete both sections (a) and (b) below:*

(a) Hard Copy

I hereby deposit a hard copy of my thesis in the University Library to be made publicly available to readers (please delete as appropriate) EITHER immediately OR after an embargo period of ……..... months/years as agreed by the Chair of the Board of Graduate Studies.

I agree that my thesis may be photocopied. YES / ~~NO~~ (*Please delete as appropriate*)

(b) Digital Copy

I hereby deposit a digital copy of my thesis to be held in WRAP and made available via EThOS.

Please choose one of the following options:

EITHER My thesis can be made publicly available online. YES / ~~NO~~ (*Please delete as appropriate*)

OR My thesis can be made publicly available only after…..[date] (Please give date)
~~YES~~ / NO (*Please delete as appropriate*)

OR My full thesis cannot be made publicly available online but I am submitting a separately identified additional, abridged version that can be made available online.
~~YES~~ / NO (*Please delete as appropriate*)

OR My thesis cannot be made publicly available online. ~~YES~~ / NO (*Please delete as appropriate*)

3. GRANTING OF NON-EXCLUSIVE RIGHTS

Whether I deposit my Work personally or through an assistant or other agent, I agree to the following:

Rights granted to the University of Warwick and the British Library and the user of the thesis through this agreement are non-exclusive. I retain all rights in the thesis in its present version or future versions. I agree that the institutional repository administrators and the British Library or their agents may, without changing content, digitise and migrate the thesis to any medium or format for the purpose of future preservation and accessibility.

4. DECLARATIONS

(a) I DECLARE THAT:

- I am the author and owner of the copyright in the thesis and/or I have the authority of the authors and owners of the copyright in the thesis to make this agreement. Reproduction of any part of this thesis for teaching or in academic or other forms of publication is subject to the normal limitations on the use of copyrighted materials and to the proper and full acknowledgement of its source.

- The digital version of the thesis I am supplying is the same version as the final, hard-bound copy submitted in completion of my degree, once any minor corrections have been completed.

- I have exercised reasonable care to ensure that the thesis is original, and does not to the best of my knowledge break any UK law or other Intellectual Property Right, or contain any confidential material.

- I understand that, through the medium of the Internet, files will be available to automated agents, and may be searched and copied by, for example, text mining and plagiarism detection software.

(b) IF I HAVE AGREED (in Section 2 above) TO MAKE MY THESIS PUBLICLY AVAILABLE DIGITALLY, I ALSO DECLARE THAT:

- I grant the University of Warwick and the British Library a licence to make available on the Internet the thesis in digitised format through the Institutional Repository and through the British Library via the EThOS service.

- If my thesis does include any substantial subsidiary material owned by third-party copyright holders, I have sought and obtained permission to include it in any version of my thesis available in digital format and that this permission encompasses the rights that I have granted to the University of Warwick and to the British Library.

5. LEGAL INFRINGEMENTS

I understand that neither the University of Warwick nor the British Library have any obligation to take legal action on behalf of myself, or other rights holders, in the event of infringement of intellectual property rights, breach of contract or of any other right, in the thesis.

Please sign this agreement and return it to the Graduate School Office when you submit your thesis.

Student's signature: F.PITIE …… Date: 10/06/2013

UNIVERSITY OF WARWICK

High Temperature Thermal Energy Storage

Encapsulated Phase Change Material Particles: Determination of Thermal and Mechanical Properties

Frédéric PITIÉ

November 2012

A thesis submitted in fulfilment of the requirements for the degree of Doctor of Philosophy in Engineering

University of Warwick, School of Engineering,

Coventry, CV4 7AL

ACKNOWLEDGMENT

I could not have achieved this thesis without the guidance, help and motivation of many people, all part of this acknowledgement:

My PhD promoters, Prof. Dr. Changying Zhao, Prof. Dr. Zacharie Tamainot-Telto and Prof. Dr. Jan Baeyens, for supervising and guiding me.

Dr. Gustavo Cáceres, and the University Adolfo Ibañez team, for their warm welcome and assistance during part of the theoretical simulations, carried out within the Cáceres' team in Santiago de Chile. Special thanks to Dalila Fernandes and Cristóbal Parrado, for the profound discussions and collaboration.

The internal and external members of my thesis committee, for their assessment constructive criticism.

Dr. Astrid 鄭宜玫, for providing me with moral support in times of difficulty.

My parents and family, for their support from the very beginning of my project. I am dedicating this Thesis to my father and my grandfather who inspired me in my professional life.

Enfin et surtout, merci à toi, Émilie, pour ton soutien contre vents et marées.

DECLARATION

Except where clearly indicated, the work reported in this thesis is an account of my own independent research at the University of Warwick carried out between May 2009 and October 2012.

Essential parts of Chapters 2, 3 and 5 were adapted and published before the present thesis was completed. Published papers are attached in the appendices.

The research reported in this thesis has not been submitted, either wholly or in part, for a degree at another institution.

Frédéric Pitié Warwick, November 2012

NOMENCLATURE

Abbreviations

BFB, CFB	Bubbling and Circulating fluidized bed, respectively
CAES	Compressed Air Energy Systems
CAF	Core Annulus Flow
DRF	Dilute riser flow
DRU	Dense riser up-flow
DSC	Differential Scanning Calorimeter
EIA	Energy Information Administration
ES	Energy Storage
FES	Flywheel Energy Storage
HTTES	High Temperature Thermal Energy Storage
IEA	International Energy Agency
OECD	Organisation for Economic Co-operation and Development
PCM	Phase Change Material
PHS	Pumped Hydro-Storage
TES	Thermal Energy Storage
TFBB	Turbulent Fluidized Bed at the Bottom
TPA	Ton Per Annum

Symbols

a, b	Dimensionless parameters of equation (5.7)
A_{ex}	Surface area of the heat exchanger, m²
C	Solid to gas heat capacity, C_p/C_g
C_p, C_g	Specific heat capacity of solid and gas respectively, J kg^{-1} K^{-1}
c_{pi}	Specific heat, J kg^{-1} K^{-1}
D	Riser equivalent diameter, m
d_p	Average particle diameter, m
E	Energy, J
f	Fraction
f_d	Time fraction of contact by the dense phase
G	Solids circulation flux, kg m^{-2} s^{-1}
G_{sh}	Particles horizontal exchange flux, kg m^{-2} s^{-1}
h	Enthalpy, kJ kg^{-1}
h_c	Contact transfer resistance, W m^{-2} K^{-1}
h_d	Heat transfer coefficient during dense phase contact, W m^{-2} K^{-1}
h_{ij}^{rad}	Radiation heat transfer coefficient, W m^{-2} K^{-1}
h_g	Heat transfer coefficient of gas, W m^{-2} K^{-1}
h_{gc}	Gas convective transfer coefficient, W m^{-2} K^{-1}
h_l	Heat transfer coefficient of lean gas phase contact, W m^{-2} K^{-1}
h_m	Heat transfer coefficient of the suspension, W m^{-2} K^{-1}
h_r	Heat transfer coefficient by radiation, W m^{-2} K^{-1}
h_{sr}	Heat transfer coefficient by radiation from the suspension to the wall, W m^{-2} K^{-1}
h_{tot}	Total effective heat transfer coefficient, W m^{-2} K^{-1}
$h(\overline{\theta})$	Surface renewal heat transfer coefficient, W m^{-2} K^{-1}
ID, OD	Inner and outer diameter respectively, m
K	Bulk modulus, *Pa*
k_g	Thermal conductivity of gas, W m^{-1} K^{-1}
M	Loading ratio, kg/kg

Nu	Nusselt number
P	Pressure, Pa
Pr	Prandtl number
R,r	Radius, m
Re	Reynolds number
s_i	Entropy, J kg^{-1} K^{-1}
T	Temperature, K
T_b, T_w	Bulk and wall temperature, respectively, K
t_g, t_p	Residence time of gas and particles in the riser, respectively, s
u	Displacement
U	Superficial air velocity through the riser, m s^{-1}
U_{TR}	Transport velocity of particles, m s^{-1}
V	Volume, m^3
$\bar{v}_p$	Average velocity of particle, m s^{-1}
α	Coefficient of linear expansion, K^{-1}
β_i	Isothermal compressibility
δ_g	Gas gap thickness, m
ΔT	Temperature difference, K
ε	Strain
E_y	Young's modulus, Pa
ε	Voidage of the riser
ε_B	Voidage of the TFBB
ε_{sus}	Cross sectional average suspension voidage
φ	Slip factor
λ, μ	Lamé's constant, Pa
λ_i	Thermal conductivity, W m^{-1} K^{-1}
ν	Poisson ratio
ρ_i	Density of phase, kg m^{-3}
ρ_g, ρ_p	Density of gas and solids respectively, kg m^{-3}

ρ_{sus}	Suspension density, kg m^{-3}
θ, ϕ	Angle, *rad*
$\bar{\theta}$	Average contact time of the particle packets at the wall, s
σ	Stress, *Pa*
ζ	$\zeta = \sqrt{1.82\log(\mathrm{Re}) - 1.64}$

TABLE OF CONTENTS

LIST OF FIGURES

LIST OF TABLES

1 INTRODUCTION AND OBJECTIVES

The purpose of this chapter is to identify the potential value of new phase-change materials that we study throughout this document. The first section introduces briefly the global energy background. Particular attention is given to problems of depletion of fossil fuels and global warming. The second section describes the potential applications for energy recovery and storage in the industrial and power generation sector. The third section shows the needs for thermal energy storage seems to be best placed to meet short and medium term performance requirements and costs imposed by targeted applications. Then, the next section shows the use of powder circulation to significant improvement in the process of capture and storage systems, heat exchangers and hence investment costs. Finally, the objectives and structure of the PhD are given.

1.1 Introduction

Phase Change Materials have been used for centuries, e.g. as large blocks of ice stored in winter to provide cooling in summer, or more recently, as encapsulated beads of wax incorporated into the loom of winter gloves' fabric to improve the conservation of body heat. Nowadays, new PCM applications are constantly developed and examined, however of more complex constitution and mostly for industrial energy applications.

Since the Industrial Revolution, energy supply has progressively become a vital issue. The Kyoto Protocol crystallized the concerns of the public regarding the emission of greenhouse gases and the need to reduce the use of fossil fuels (Asif and Muneer, 2007). The global economic crisis since 2008 added additional challenges (IEA and OECD, 2011). This global concern about energy and CO_2 emissions, lead worldwide governments to enact new policies and financial incentives in support of renewable energies, enhancing their implementation and development despite the economic regression, whilst simultaneously creating valuable new business opportunities for companies involved in this energy sector. One of the hot topics in the energy strategy is the capture and storage of thermal energy and waste heat recovery. Both advanced energy utilisation schemes call for the development and new usage of existing and/or new materials. These new materials, and their potential use, are the subject of the present PhD thesis. The layout of the present chapter is illustrated in Figure 1. Each of the parallel topics is subsequently dealt with.

Figure 1: Layout of chapter 1.

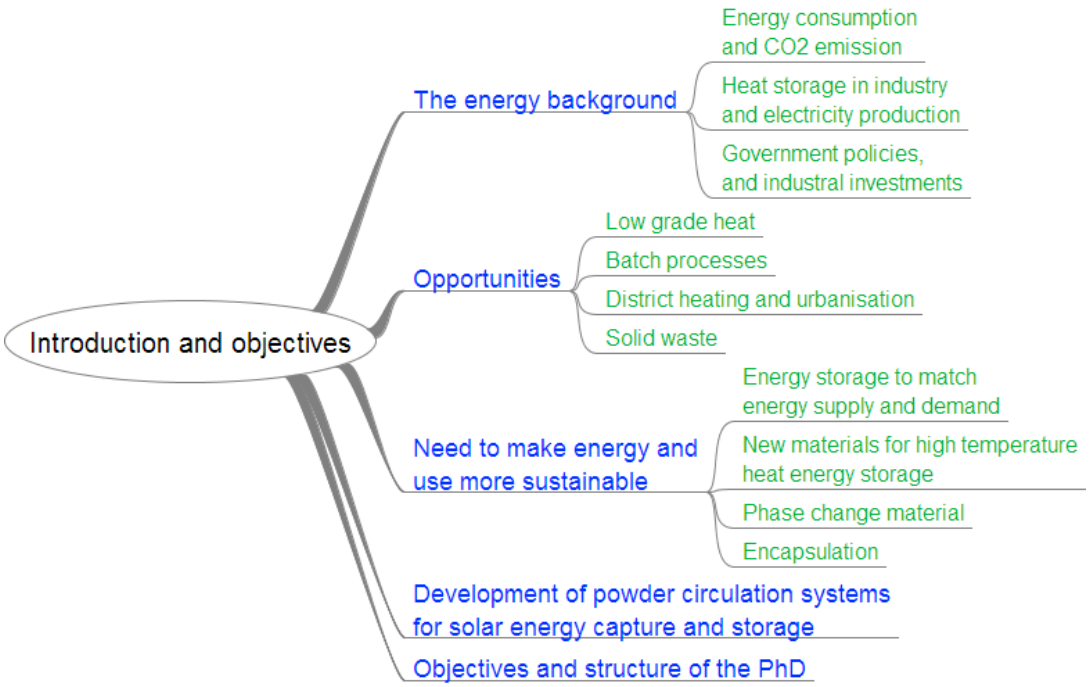

1.2 The energy background

1.2.1 Energy consumption and CO_2 emissions

Based upon current statistics and predictions of energy consumption, the U.S. Energy Information Administration in 2011 predicated an increase of the total world energy use from 148 10^9 MWh in 2008 to 181 10^9 MWh in 2020, and to 225 10^9 MWh in 2035 (EIA, 2011). Since liquid fuels remain an important source of energy, albeit with depleting reserves, their prices are expected to remain and/or exceed 130$/barrel. The *EIA* also predicated an increase of coal and gas as major sources from 60% currently to 64% in 2030.

Because of the use of fossil fuels, current global CO_2 emissions are at 30.6 10^9 TPA of CO_2 (against 28.2 10^9 TPA in 2005). Without effective measures, it is however expected that world energy-related emissions of CO_2 will further increase to 33.5 10^9 TPA in 2015 and 43.2 10^9 TPA in 2035. The rising price of fossil fuel, and its influence on the environment, fosters the need for energy preservation. Finally, reducing the dependency on fossil fuel will also reduce the impact of the fossil fuel price on the economic performance, as previously observed when

the ‘1973 oil crisis’ has been held responsible for subsequent economic recession and a period of excessive inflation (Barsky and Kilian, 2004).

1.2.2 Heat storage in industry and electricity production

Since the Kyoto Protocol, the Organisation for Economic Co-operation and Development (OECD) and International Energy Agency (IEA) have been urging to reduce both the emission of CO_2 while producing energy, and the waste while consuming it (Lopez, 2007).

There is still a considerable scope for improving energy efficiency. As of the early 2000s, the industrial energy use represented 25% of the total energy use in the UK (Department of Trade and Industry (UK), 2012). The industrial sectors of the chemical, food and beverage, steel and iron, and pulp and paper productions represented more than 50% of the industrial energy usage. Furthermore, the energy cost represented up to 10% of the total production cost in the food sector, 5% in the chemical sector, and between 30% and 45% in the steel industry (Marechal and Muller, 2008). Higher energy costs are reflected in the prices of the produced goods and efficient energy savings will ensure that these important industries remain competitive, whilst maintaining the activity level of associated sectors (construction, printing, etc…). Thermal energy losses occur in each operating unit (e.g. compressors, evaporators, boilers, etc.), and these losses increase with the increasing number of operating units of the process industry, thus providing incentives to improve process efficiency by reducing the number of operation units. In general, both the industry and energy production sectors should improve their energy balance through three key concepts being (i) the suppression of any loss of heat or electricity by applying heat recovery technologies and stacked use of energy; (ii) substitution of current low efficiency energy-producing processes; and (iii) substitution of low efficiency raw material by durable alternatives.

As a major consumer of energy in general, and a key producer of waste heat, the industrial sector is the special target to improve its processes. Co-generation, thermal waste heat recovery and stacked energies seem to be key topics in a strategy to improve energy efficiency. In a short

or medium term, waste heat recovery and *high temperature thermal energy storage* (HTTES) are crucial concepts to implement such solutions, and even power plants can use HTTES to improve the energy balance of their operations, since HTTES increases the flexibility and availability of heat and electricity in traditional or sustainable power plants.

1.2.3 Government policies, and industrial investments

Governments worldwide are enacting policies and drafting regulations to reduce CO_2 emissions to fight climate change, thus further forcing industries to invest in more sustainable technologies. In the UK, a target of 80% reduction in emissions by 2050 has been set by the Climate Change Act 2008 and more recently, an 'interim target' of a 34% cut by 2020 was imposed and made legally binding in the April 2009 Budget.

A recent survey by Ernst & Young reported that many companies have already increased their ecologically friendly investments (The Economist, 2011), with (i) 44% confirming that their company's spending on sustainability had increased since the 2008 financial crisis; (ii) another 44% confirmed a "status quo" (a surprising feat considering that public spending on sustainability has also taken a hit); and even mining companies (operating in places with difficult access to the national grid), such as BHP and investing in energy efficiency and clean energy as a result of the failing price of renewable energy and the rising price of crude oil.

As a result of these investments and economics factors, small positive changes in energy efficiency can result in considerable money saving. Large companies (with more than 500 employees) are hence keen to adopt ambitious emissions-reduction schemes. A survey of over 500 large companies by the Carbon Disclosure Project claimed that 59% of emission-reducing investments made so far have a three years payback period (Carbon Disclosure Project, 2011). The high cost of renewable energy and the rising prices of crude oil provide extra impetus for companies to invest in energy efficiency and clean energy technologies and practices. Innovative solutions must reduce emissions and maximise economic growth. Industries usually

resort to investments with the shortest possible payback such as heat recovery and reduction of losses.

In the UK, the Small and Medium-sized enterprises (SMEs) deserve a special attention since they account for 45% of the industrial energy use, while their processes and plants are often less optimised due to the lack of financial means. According to a recent study by the Carbon Trust (2010), they also represent the greatest energy saving potential with an average potential saving of 20% compared with a possible 8% for larger companies only.

The imposed reduction in CO_2 emissions will require a combination of detailed strategies and tactics (Chu *et al.*, 2013), including (i) a mix of energy generation technologies; (ii) a reduction in energy usage through the use of incentives, technologies, taxes and quotas; (iii) maximising CO_2 absorption, such as carbon sequestration by both natural means and by technical developments; and (iv) the development of highly-efficient energy capture, recovery and storage methods.

The implementation of strategies and tactics will however introduce uncertainties or risks on economic growth (Stern, 2007), therefore acceptance of these measures will only be achieved if the impact on economic growth is minimised by taking the uncertainties into account and by constantly updating information on the latest energy efficient technologies and practices.

1.3 Major opportunities

1.3.1 Low grade heat

Waste heat sources can be of high grade and low grade according to the viability of recovery within the processes. There use "of low grade heat" is not widespread since it is a technical and economic challenge to obtain useful exergy and energy from low grade heat. The temperature range of low grade heat sources is typically between ambient temperature

and 250°C (Institution of Electrical Engineers, 1994; Department of the Environment, and Energy Efficiency Office, 1996).

The market potential for surplus/waste heat from industrial processes in the UK is between 10 TWh (1 TerraWh = 10^{12}Wh) to 40 TWh (BERR, 2008; Carbon Trust, 2010; McKenna, 2009). These figures demonstrate a significant potential resource which has remained unexploited to (BERR, 2008; Carbon Trust, 2010; McKenna, 2009). Figure 2 shows that the potential for waste heat recovery in the UK process industries is significant, and the complete recovery of this heat would exceed the output of many of the renewable energy sources currently used in the UK.

Figure 2: Comparison of the Waste Heat Recovery potential and the use of various renewable resources in UK (adapted from (Department of Energy & Climate Change, 2012; Law *et al.*, 2012).

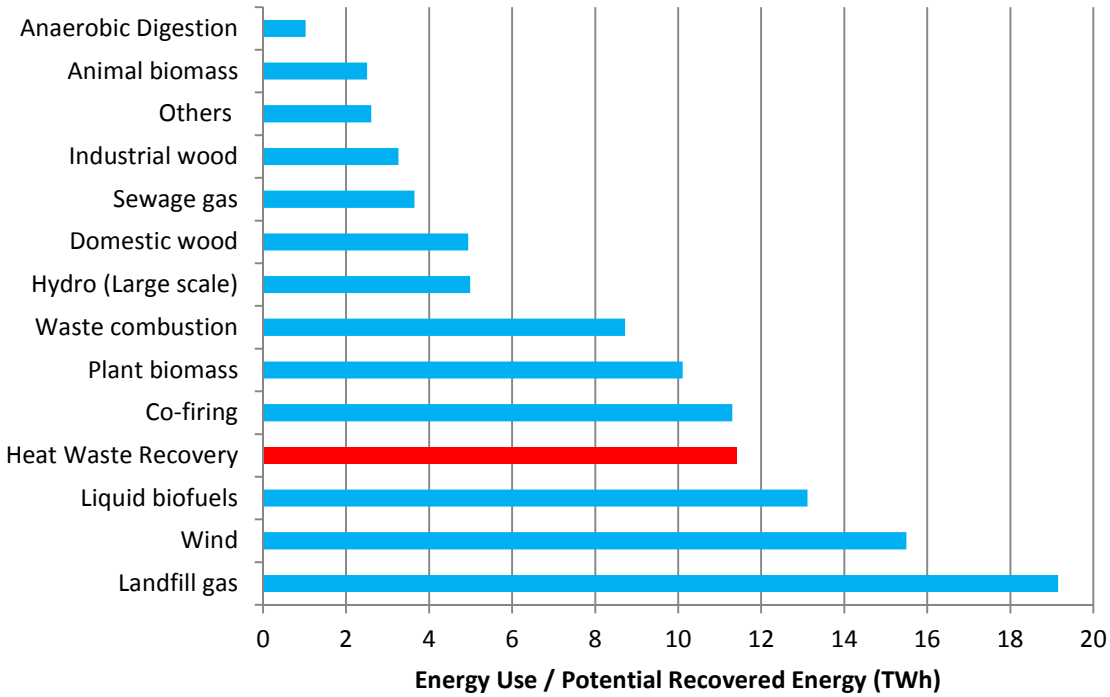

A large amount of low grade heat is available in the process industry as e.g. water from cooling towers with gas temperatures between 35°C and 55°C, and stack exhausts with a broader temperature range, between 30°C and 250°C.

The barriers associated with low grade heat utilisation (Ammar *et al.*, 2012; Law *et al.*, 2012) include:

- The need to match the sources with potential end-users around the process plant;
- The production of electricity but limited to temperatures in excess of 70°C for the most advanced Rankine cycle derivatives. The low thermal efficiencies of waste heat conversion technologies are presented in Figure 2;
- The difficulty in harnessing the potential of the waste water streams available at lower temperatures (between 35 and 55°C), whilst achieving economical benefits;
- The insufficient knowledge about the economic distance from the heat source to the heat sink, especially for district heating systems. There are also stringent geographic limitations since steam with a temperature of 120-250°C can be transported only to a distance of approximately 3 to 5 km due to the high pressure drop in the steam circuit, with progressive condensation as a result. This condensation is even increased due to the gradual extraction and condensation of the steam by the users along the pipeline, reducing the free cross sectional pipe area for steam flow and increasing the pressure drop even further. Water at a temperature of 90-175°C performs better, at about 30km (Bujak, 2008).
- The heat losses, the total cost for pipeline installation, and pumping cost (Hlebnikov and Siirde, 2008).

Table 1 Comparison of performance characteristics of waste heat technologies (Markides and Smith, 2011).

Sources	Technology	η_{th}	η_{ex}	Heat source	Relative cost
(Saleh *et al*., 2007; Shengjun *et al*., 2011)	ORC	8-20%	25-45%	100-300°C	Intermediate
(Borsukiewicz-Gozdur and Nowak, 2010; Chen *et al*., 2011; Shengjun *et al*., 2011)	Supercritical ORC	10-25%	30-50%	100-300°C	High
(Arslan, 2010; Engelhard, 2006; Nag and Gupta, 1998; Ogriseck, 2009; Valdimarsson, 2006)	Kalina Cycles	10-20%	40-50%	100-200°C	Intermediate
(Markides and Smith, 2011; Smith, 2006, 2004; Solanki et al., 2012)	TFO	1-5%	5-20%	30-150°C	Low

*ORC: Organic Rankine Cycles
**TFO: Thermofluidic oscillators
η_{th}: thermal efficiency
η_{ex} :exergy efficiency

1.3.2 Batch vs. Continuous processes

It is well-known in the process industry that continuous processes are usually more efficient towards the use of energy and resources than batch processes. Process expert Nigel Fletcher from Foster Wheeler claimed that continuous processing is the future goal of the process industry (Fletche, 2010).

A few industrial sectors, such as the pharmaceutical, specialty chemicals and brewing ones, are still applying batch processes instead of the continuous approach.

Batch processes involve the needs:

- to handle and process intermediate batches, transport intermediates to and from the warehouse, dispense them to the next stage and repeat these operations for every intermediate, thus consuming a large amount of operating and processing time;
- to have energy-intensive heating and cooling for each batch process, whereas cooling and heating are only needed during start up and shut down for the continuous process;
- long processing times are associated with a high energy consumption to maintain desirable temperatures, such as in the breweries;

- to provide larger buildings to accommodate a larger overall size of the reactors for batch than for continuous processes, potentially adding a cost for space heating.

In the pharmaceutical industry, batch reaction times can be several hours longer than in the equivalent continuous processing (Fletche, 2010). A pilot plant, built by Foster Wheeler for pharmaceutical production, was able to produce the final bulk product in less than two days using the continuous processing, compared to 18 months when applying the original batch processing (Fletche, 2010). However, a lot of work still has to be done for wider industrial applications, be it in the pharmaceutical or specialty chemicals industries.

1.3.3 District heating and urbanisation

Before discussing problems faced by district heating, it is important to clear the misconceptions regarding urbanisation, as urbanisation and district heating are mutually dependable.

Cities have often been blamed for causing environmental problems due to the high concentration of people, enterprises, motor vehicles and waste. Cities are said to be responsible for 75% of the global energy consumption and have been blamed for generating 80% of the world's greenhouse gas emissions (United Nations *et al.*, 2007) hence contributing disproportionately to the global climate change (Grimm et al., 2008; Grimmond, 2007; Sánchez-Rodríguez et al., 2011). Calculations of the ecological footprints of cities have also tended to stress the area of land a city requires to supply its needs (Girardet, 1998). The Clinton Foundation (2012) suggested that cities contribute to 75% of greenhouse gas emissions while comprising 2 per cent of land mass only.

These ecological consequences are however not so much driven by urbanisation as such, but by the rapid increase in consumption levels and in the number of people with

high-consumption lifestyles. When comparing rural and urban populations with similar incomes, urban inhabitants generally have lower consumption and less waste generation (Satterthwaite, 2011).

Economies of scale, proximity and agglomeration facilitate the provision of economic district energy systems that minimise environmental impacts (Satterthwaite, 1999). Detailed analyses of urban greenhouse gas emissions for individual cities per capita indicated that urban residents tend to generate a substantially smaller volume of greenhouse gas emissions than residents elsewhere in the same country (Dodman, 2009). The per capita emissions from London are the lowest in the UK, being 6.18 tonnes per capita in 2006 while the national average was 11.19 tonnes per capita (Dodman, 2009). A regional analysis of UK greenhouse gas emissions shows that the regions with the highest per capita greenhouse gas emissions are the relatively rural Northeast, Yorkshire and the Humber, whereas London has the lowest figure, followed by the highly urbanised West Midland (Dodman, 2009).

The concentration of people and industries in large cities provides the opportunity for technological innovations, such as combined heat and power and waste-to-energy generation plants that can generate electricity and efficient district heating (or cooling) especially if the urban site is not situated too far from the waste heat source that would otherwise render district heating (or cooling) thermodynamically and/or economically unfeasible (Ammar et al., 2012; Bujak, 2008).

Zhou *et al.* (2012) stated that there is a lack of suitable design tools to demonstrate and compare the energy and economic benefits of distributed energy systems with that of a centralized system. An energy systems engineering framework must be designed towards the optimal design of distributed energy systems. To minimise the overall cost, and whenever applicable, the framework should include electricity, heating, cooling and hot water loads;

together with a utility tariff structure, and technical/financial information about various technologies.

The characteristics of distributed/district energy systems foster energy efficiency (Zhou *et al.*, 2012), since (i) distributed energy systems can avoid the difficult planning and construction processes associated with large plants and long distance transmission; (ii) if the power grid fails, distributed energy systems can continuously supply energy to customers, thereby enhancing energy security; (iii) the various scattered waste sources and renewable energy (solar, wind and geothermal), can be integrated into the distributed energy systems to provide energy collectively.

The potential benefits of distributed energy systems may however not be fully exerted, because of the highly fluctuating energy demands and some renewable resources may cause problems to the efficient and safe operation of distributed energy systems (Akorede et al., 2010; Bayod-Rújula, 2009; Pepermans et al., 2005).

1.3.4 Solid waste to Energy applications

The European Landfill directive (1999/31/EC) prohibits the disposal of untreated solid waste into landfills. It outlines that the disposal of untreated waste is no future option, and that other options are to be developed to utilise the potential of waste-derived fuels for heat and electricity production. This led some countries, like the UK, to impose a stringent waste legislation, like the Landfill Taxation and the Landfill Allowance Trading Scheme. Solid recovered fuel (SRF) is a solid waste that complies with the CEN standard, i.e. CEN343:2005 ANAS (European Committee for Standardization, 2005). The lower heating value of SRF is approximately 20 MJ/kg (dry basis) (Hilber *et al.*, 2007).

As of 2008, plans for potential incinerator locations in the UK were in place for at least 30 sites (Letsrecycle, 2008). Some of the electricity generated from waste is deemed to be from a Renewable Energy Source (RES) and is thus eligible for tax credits if privately operated.

Incineration processes featuring energy recovery, have been recognised to bring benefits from both economic and environmental perspectives (Van Caneghem et al., 2012; Van de Velden et al., 2007). Sheffield has been using waste heat from its waste incinerator to provide district heating to more than 130 buildings since 1988 (Sheffield City Council, 2012).

In the United States of America, incineration was granted qualification for renewable energy production tax credits in 2004 (United States Environmental Protection Agency, 2012).

In most of the EU countries, waste-to-energy plants are considered as renewable energy producers, hence being granted "green power" benefits.

1.4 The need to make energy use and generation more sustainable

1.4.1 Energy storage to match energy supply and demand

We need energy - electrical or thermal - but in most cases where and when it is not available. Energy storage technologies are a strategic and necessary component for the efficient utilization of renewable energy sources and energy conservation. There is an important potential for substituting fossil fuel combustion by using heat that would otherwise be wasted. These energy sources can be used more efficiently through the addition of short and long term energy storage. Such storage facilities enable an extensive and more efficient use of the fluctuating energy sources by matching the energy supply with demand.

Low cost, fossil fuel-based electricity has always served as a formidable cost competitor for electrical power generation and traditional power plants store their energy resource on site in the form of a stock of e.g. coal, oil, nuclear fuel or even water behind a dam. The Alternating Current (A.C.) electricity grid requires that supply and demand is always matched on a second by second basis, and electricity network and transmission system operators have arrangements in place to ensure that this requirement is always met. The traditional electricity market is therefore largely based on fuels sold and traded as commodities, and used to generate electricity to instantaneously match supply with demand. A future electricity system predominantly or

solely supplied by renewable energy sources will therefore find it difficult to meet the fundamental stability requirement of AC networks to constantly match supply and demand (Naish *et al.*, 2008).

1.4.2 New materials for high temperature heat energy storage

HTTES is the storing of thermal energy at high temperature which can be drawn upon at a later time to perform some operations (Gil *et al.*, 2010). Progress made in the development of HTTES materials is described in Section 1.4.3. below, and further detailed in Chapter 2.

Despite the stake pointed out by HTTES, very few industrial sectors apply energy storage. As further discussed in Chapter2, the electricity storage is used more often than heat storage, thus stressing the pressing need to develop adequate methods for conserving heat. In the development of such applications, there are three priorities being (i) the development and use of low-cost materials with a long life and thermo chemical stability; (ii) the design of efficient thermal exchanger and storage architectures; (iii) the development of strategies which can be easily adapted to industrial settings.

There are three main types of storage media as a function of the underlying phenomena being the sensible and/or latent heat storage, and the application of reversible chemical reactions: they store heat in materials which change of temperature, change of phase or change through chemical reaction, respectively. For high temperature purposes, sensible heat has already been extensively studied and experimented at a large scale (Medrano *et al.*, 2010). Regarding chemical heat storage, despite its attractive application for long term energy storage, it is still at an early stage of laboratory research (Pilkington Solar International GmbH, 2000). Latent heat allows more compact, efficient and therefore economical systems to operate.

1.4.3 Phase change material

Phase change materials (PCM) mainly use the liquid-solid transition to store latent heat. Largely studied for thermal storage use (Sharma *et al.*, 2009), PCM are made from very different types of material as shown in the Figure 3.

Figure 3: Classification of energy storage materials (Zalba *et al.*, 2003).

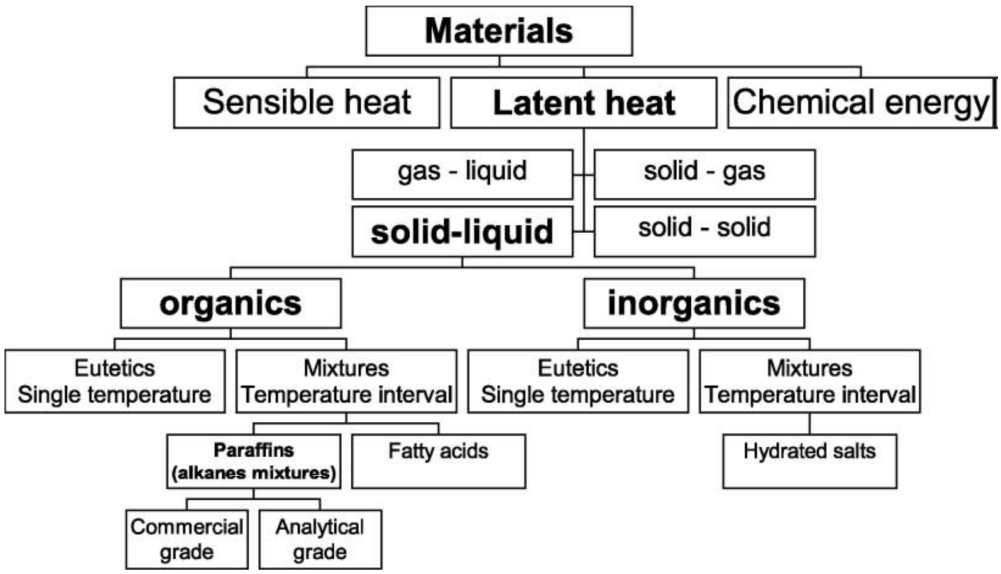

For high temperature purposes, salts had been chosen as the cheapest and most efficient PCMs to store heat energy. But due to their low thermal conductivity, they have slow charging and discharging rates. In order to enhance their thermal properties, different techniques have been studied (Jegadheeswaran and Pohekar, 2009): metal foams or supports, porous media in graphite, or fin heat exchangers. Results from Acem *et al*. (2010) and Pincemin *et al*. (2008) proved that a micro-encapsulation in a graphite matrix is a possible and efficient solution.

1.4.4 Encapsulation

The composite graphite-salt system has to deal with a problem of mixture stability during the first charging-discharging cycle (Lopez, 2007). The graphite releases the molten salt from its matrix because of its volume expansion. The packed bed of capsules of PCM does not face this problem (Regin *et al.*, 2008). Although the micro-encapsulation of PCM had been previously used to produce slurries (Agyenim *et al.*, 2010), or for building applications (Castellón *et al.*,

2007), it has not yet been used for high temperature purposes. Such a free surface micro-encapsulation will allow extending thermal exchanges to a maximum surface. Although encapsulation does not significantly alter the heat capacity of the phase change material, it allows the PCM to undergo its phase change in a confined environment, thus adding the latent heat of phase change (mostly melting-solidification) to the heat storage capacity of the PCM. The volumetric heat storage capacity is hence considerably increased.

1.5 The development of powder circulation systems for solar energy capture and storage

More energy from the sunlight strikes the earth in 1 hour, than all of the energy consumed by humans in an entire year (Lopez, 2007). In fact, solar energy dwarfs all other renewable and fossil-based energy resources combined. Solar energy is of unsteady nature, both within the day (day-night, clouds) and within the year (winter-summer). The storage of solar energy is critical if a significant portion of the total energy needs to be provided by solar energy, and to provide a durable and widespread primary energy source, solar energy must be captured, stored and used in a cost-effective fashion.

Peaks of solar energy are recorded in some “hot” spots of the Globe as seen on Figure 4, e.g. the Mojave Desert (USA), the Sahara and Kalahari Desert (Africa), the Middle East, Western South America and Central Australia, although other regions also offer a sufficient potential, as indicated in the world solar energy map below: most of the countries, except those above latitude 40°N, are subject to annual average irradiations in excess of 1.3 MWh/m². A major part of China also meets this criterion.

Figure 4: World solar insulation rate (Ahlenius, 2008).

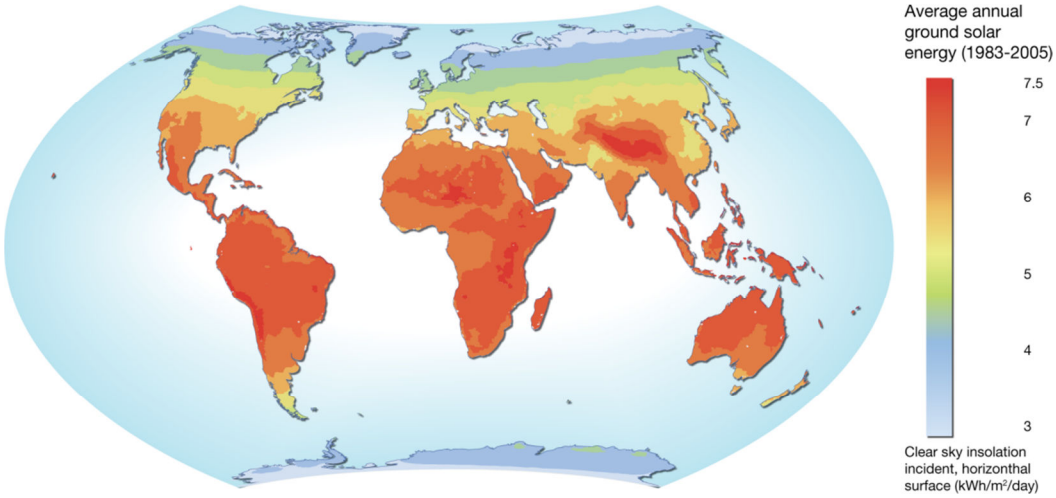

(Source: NASA. 2008. NASA Surface meteorology and Solar Energy (SSE) Release 6.0 Data Set, Clear Sky Insolation Incident On A Horizontal Surface. http://eosweb.larc.nasa.gov/sse/ (Accessed April 24, 2008))

A recent assessment by the USA DOE confirmed the solar potential of several facilities in the USA:

Location	Facility	Capacity (MW)
Virginia	Bath County	2722
New Jersey	Mt. Hope	2000
California	Castaic Dam	1566
Michigan	Ludington	1872
California	Pyramid Lake	1495

In Europe, significant developments have taken place in France and Spain. Especially the solar towers of Southern Spain (Torresol, Catalunya) are of major importance in the further development (50 MW installed, 35MW supplementary planned for 2012) (Barlev *et al.*, 2011; Torresol Energy Investments, 2012). These solar energy capture systems now make use of molten salts as heat transfer medium, with problems including mainly expensive construction materials, high pressure drops in the circulation loops and associated high pumping costs, possible failure of the system in case of a breakdown, large storage capacities required for the moderate energy density only. Molten salt systems, e.g. have a maximum operating temperature of ~550 °C due to the decomposition into nitrites; they moreover have a high viscosity at lower temperature thus increasing the pressure losses and increasing the pumping costs. A minimum temperature of 260 °C is necessary to avoid solidification, and for safety reasons a heat-tracing

is required for the whole circuit in case of insufficient heat captured, night-time, shut-down periods. Synthetic oils risk decomposition and coking if heated more than 350 °C. Their low recovery efficiency in the boiler is (350 - 90)/350 = 74 % only, and they also need "tracing" which is 5% of the crude production. Supercritical CO_2 is still in development and results of the first application in Australia are not yet convincing.

A 4 year EU Framework VII research program, called CSP :"concentrated solar power" will involve the solar towers of Torresol and the pilot scale solar concentration plant of the French CNRS (Centre National des Recherches Scientifiques) in Font Romeu. The objective is to improve the energy capture and storage efficiency and effectiveness of these available EU solar capture projects, through using alternative capture and storage media.

To replace the molten salt or oil circulation, it is proposed to use a powder circulation system since powders have virtually no temperature limitation (T up to 900 °C is possible). Their specific heat is comparable to oils and salts. They also present a high storage capacity per unit weight due to the higher operating ΔT, and finally provide a highly efficient boiler operation [~ (900 - 90)/900 = 90 %].

In a 2012 paper, entitled "Thermal energy storage: How previous findings determine current research priorities", the state-of-the-art in high temperature energy storage was assessed, and the needs for future development to assure a breakthrough were established (Fernandes *et al.*, 2012). These needs include the development of high capacity storage systems, preferably using sensible and latent heat storage media. Phase changes in solids (melting-solidification) involve a major heat of transformation, about 2 or 3 times the sensible heat capacity at the given temperature range.

These powder circulation systems could be of 2 kinds, i.e. (i) Silicium Carbide or similar powders, with high specific heat, that facilitate sensible heat storage; or (ii) the use of Phase Change Materials, whereby an inorganic salt is coated by an inert shell, so that both sensible and

latent heat can be used for heat storage. Within the range of 500 to 750°C, a possible core-material could be Sb_2O_3 (melting ~ 560°C), coated e.g. by SiC or Ni.

Although the literature on the solar energy capture and storage in powder systems is still scarce, a few references already highlight the potential (Burgaleta et al., 2011; Price et al., 2002). New concepts of thermal energy storage systems are being developed for concentrated solar plants: integrated receiver/storage systems using a fluidized bed storage concept, as illustrated in the Figure 5 below. In the concepts shown, particles of SiC or SiO_2 flow through a heat exchanger where they collect the heat from a concentrated solar beam. The particles are then conveyed to the hot storage tank. The powder is either fluidized in the exchanger, or is of the moving bed type with a minimum amount of air passed through it. Due to the very high heat transfer coefficient between a heat exchanger wall and a fluidized or aerated moving powder bed, powders are quickly heated and reach very high temperatures in the receiver, thus helping to improve the efficiency and storage rates of the plant (Rovira *et al*., 2011; Torresol Energy Investments, 2012).

At present, this specific solution needs to be further developed, and is the secondary objective of the PhD research, since several problems with powder circulation systems need to be resolved (Gil *et al.*, 2010).

Figure 5: Schemes of function of a fluidized bed integrated storage system (Medrano *et al.*, 2010) and the riser solar energy capture and storage (Pitié *et al.*, 2012).

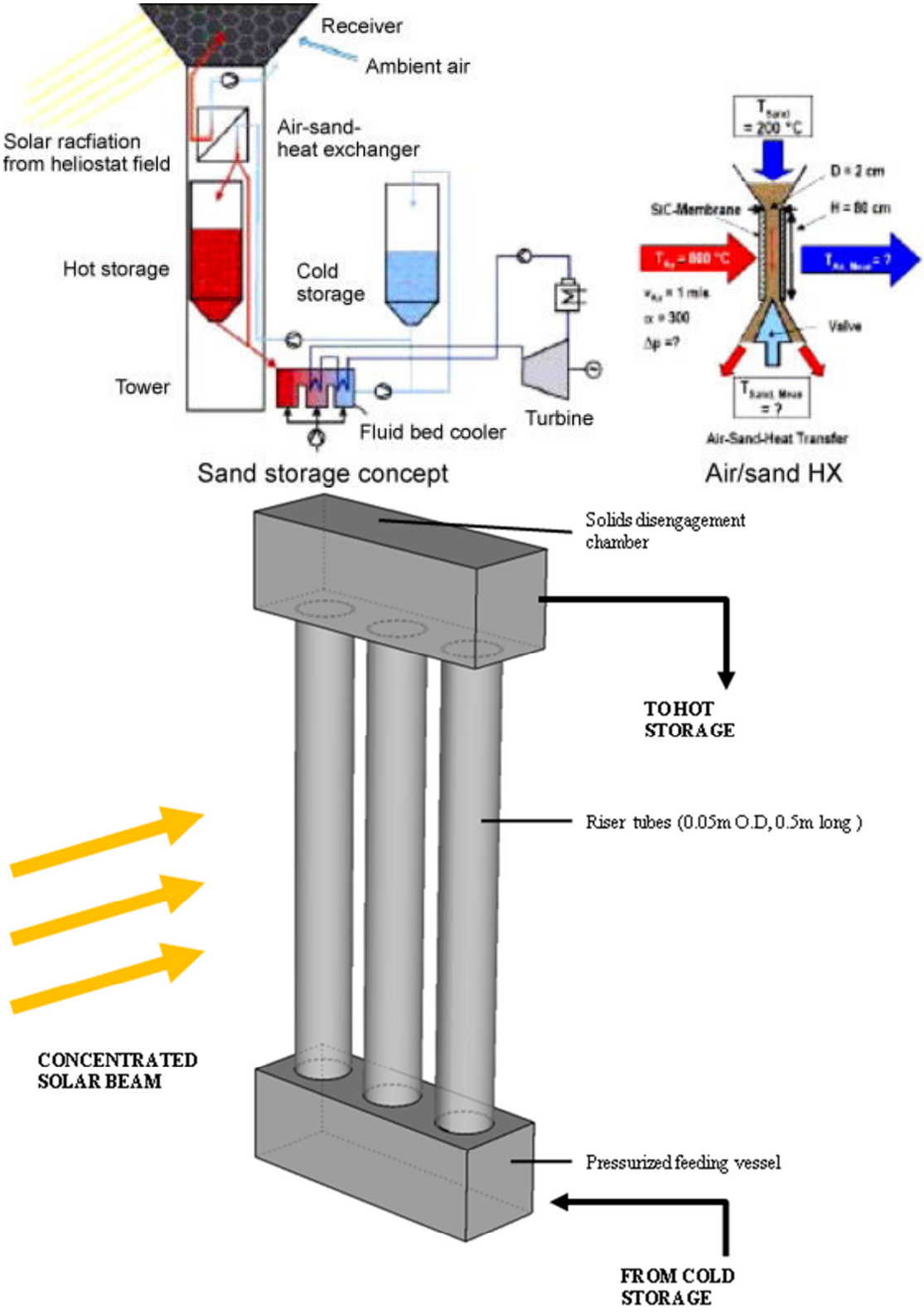

1.6 Objectives and structure of the thesis project.

The previous general background briefly reviewed the worldwide energy consumption and the need to develop advanced and highly-efficient energy caption/storage systems. The PhD hence has two major objectives: (i) establish the fundamental criteria to be met by PCM systems; (ii) assess the heat transfer characteristics of a powder circulation heat capture and storage.

Chapters 2 and 3 deal with the first objective, whereas chapter 4 and 5 will provide solutions and results with respects to the second objective.

Chapter 2 will review the logical sequence from the general idea of saving energy and the specific needs in HTTES to the selection of one particular material. The technologies available allow combining PCM salts with ceramic particles coating.

In order to predict thermo-mechanical behaviour of such material, the two presented models will be used to develop the first step of this thesis project.

Chapter 3 will expose the adaptation of previous models to the selected material. In a first step, demonstration of the original model is performed again in order to highlight the steps that should be adapted to the new material. Then, general work in continuous mechanic is used to develop the modelling of a ceramic encapsulated molten salt PCM. A first analytical modelling is done using MATLAB. Then COMSOL is used for a finite element method analysis.

Chapter 4 will illustrate the different techniques for thermal energy storage and/or transfer. The ways in which these could benefit from encapsulated PCM for high temperature purpose are considered. Three media are examined: solid, liquid, and gas. Improvements brought by new materials are then analysed.

Chapter 5 will provide initial insights in the mechanism of circulating fluidised beds, and their use as energy storage systems. The research was performed at the Katholieke Universiteit

Leuven, where pilot-scale experimental rigs are available. It is intended to test the selected solution at the CNRS solar collector of Font-Romeu (France), in 2014 for a 1 MW scale concentration plant.

Chapter 6 will finally provide a summary of the essential findings of the research, whilst highlighting areas of additionally required research.

2 INTRODUCTION TO THERMAL ENERGY STORAGE: "HOW PREVIOUS FINDINGS DETERMINE CURRENT PRIORITIES" AND OBJECTIVES OF THE PHD-RESEARCH

Thermal energy storage is an expanding field within the subject of renewable energy technologies. This introduction assesses the different possibilities available for energy storage, and then compares of various materials for High Temperature Thermal Energy Storage (HTTES):

- *Several attributes and needs of each solution are listed.*
- *One particular priority issue is using the latent heat as one of the most efficient ways to store thermal energy.*
- *The particle made of a phase-change material (PCM) encapsulated in a silicon carbide (SiC) shell is optimising the thermal properties of the material for latent heat energy storage.*
- *The results of previous studies show that mechanical and thermal properties of spherical shells and PCMs were studied in a separate and non-combined way.*

The introduction highlights the potential for an advanced study of thermo-mechanical properties of SiC shells coated PCM, and this advanced study is the major subject of the present research.

2.1 Introduction

The efficient use of energy is of growing importance. Developing highly effective energy saving solutions is paramount in the current energy demand context. The objective of this chapter is to review the available information on the high temperature thermal energy storage (HTTES), in order to define the priority research objectives to complete the fundamentals needed for their widespread application. The review part specifically focuses upon (i) the underlying storage mechanisms and its potential, (ii) the essential materials and properties that delineate temperature ranges of application, and (iii) the illustration of particular solutions to high temperature thermal energy storage. After a brief description of thermal energy storage (TES), the advantages of storing both sensible and latent heat are discussed. As a specific case, we demonstrate the effectiveness of storage involving latent heat and how it leads to the selection of a phase change material (PCM) for specific applications, whilst highlighting its appropriate characteristics, its current weaknesses, and the multiple solutions to improve the thermal properties of PCM. The selected solution involves a SiC shell coated PCM. Both SiC and PCMs two materials have been previously studied, mostly towards their applicability and advantages. From assessing these previous studies which were part of extensive research programs, it is clear that there is an urgent need to develop a thermo-mechanical modelling of such a composite. The layout of the present part is illustrated in Figure 6. Each of the parallel topics is subsequently dealt with. Essential parts of this chapter were adapted and published before the present thesis was completed. Published paper is attached in the appendices.

Figure 6: Layout of chapter 2

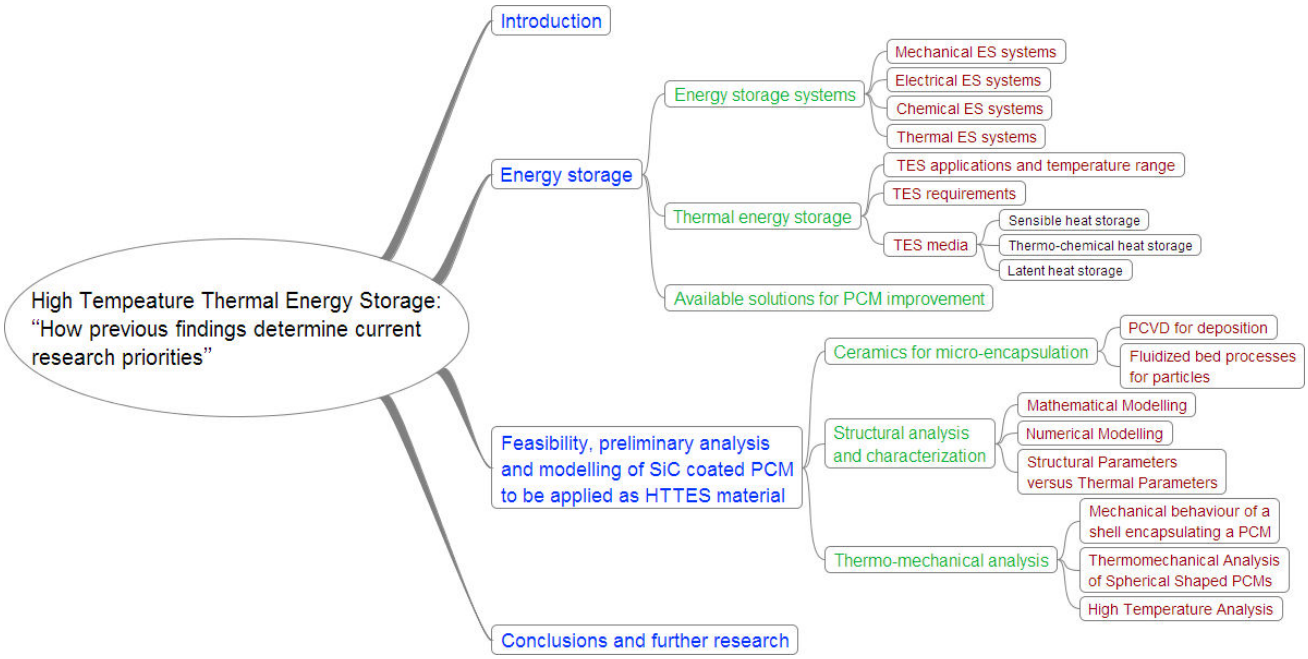

2.2 Energy storage

Energy Storage (ES) is the storage of some kind of energy that can be drawn upon at a later time and usefully re-applied in a given operation. It has the potential of increasing the effective use of energy equipment and is normally applied to balance the possible mismatch between the supply of, and demand for energy (Gil *et al*., 2010). The imperativeness of ES results from the need of having the energy production decoupled from its supply and distribution, and to support the intermittent nature of producing alternative energy (Chen *et al*., 2009). An energy storage process is based on three fundamental steps: charging (loading), storing and discharging (releasing) (Gil *et al*., 2010). As a result, ES applications facilitate energy management, help bridging power supply/needs and power quality, and increase the system reliability (Chen *et al*., 2009). Energy forms include mainly mechanical, chemical, electrical or thermal energy, and all of them can be stored using an appropriate method, system or technology as described below.

2.2.1 *Energy storage systems*

Every system or technology of ES had been developed in order to answer specific needs (Chen *et al*., 2009). They are classified by the form of energy stored, as shown in Figure 7

Figure 7: Classification of energy storage systems (Gil *et al*., 2010)

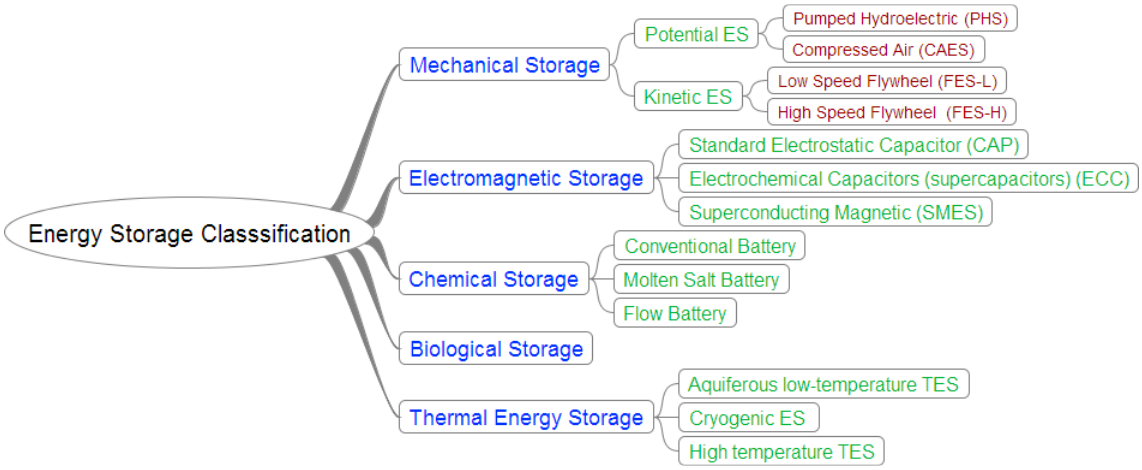

2.2.1.1 *Mechanical ES systems*

Mechanical ES systems are either of potential or kinetic nature.

Figure 8: Flywheel system (Chen *et al*., 2009)

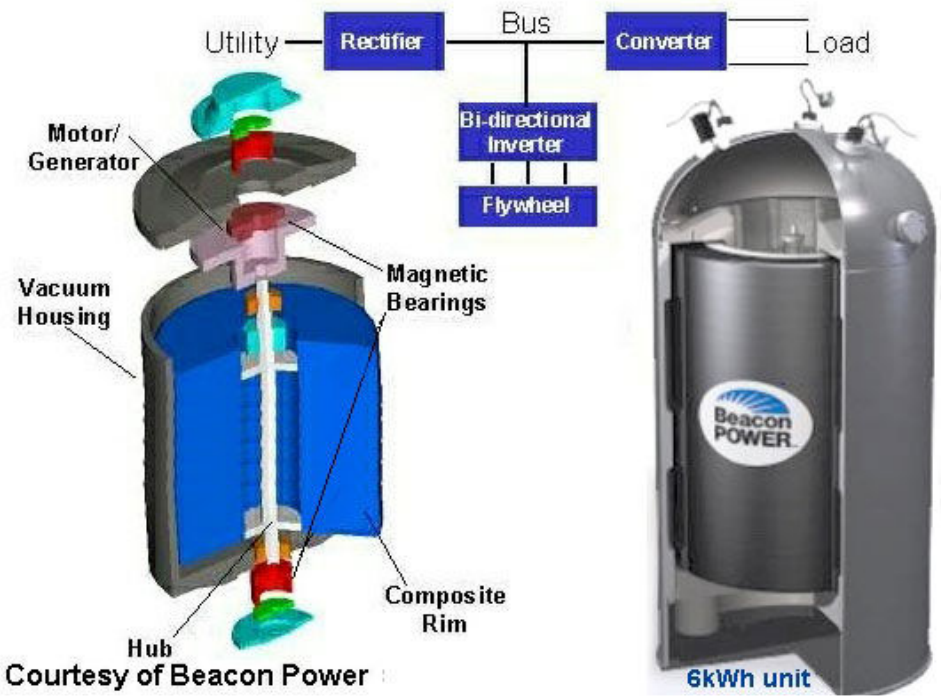

Kinetic energy storage systems are usually flywheels with low or high rotational speeds (FES) (Chen *et al.*, 2009). In such a system, energy is stored by increasing the angular momentum of a rotating disc with an electric motor (Figure 8). Electricity is released on demand with a generator. Low speed flywheels have their discs rotating up to 10 000 rpm, while high speed ones see their rotation speed go up to 100000 rpm. The main loses come from the frictions of the bearings supporting the disc. The short period of releasing the energy, from 5 up to 50 seconds, limits the application of FES for quality energy supply (Bradbury, 2010).

Potential energy storage systems include pumped hydroelectric (PHS) and compressed air energy systems (CAES) at small and large scale (Chen *et al.*, 2009).

Figure 9: Pumped Hydro-Storage (PHS) (Chen *et al.*, 2009)

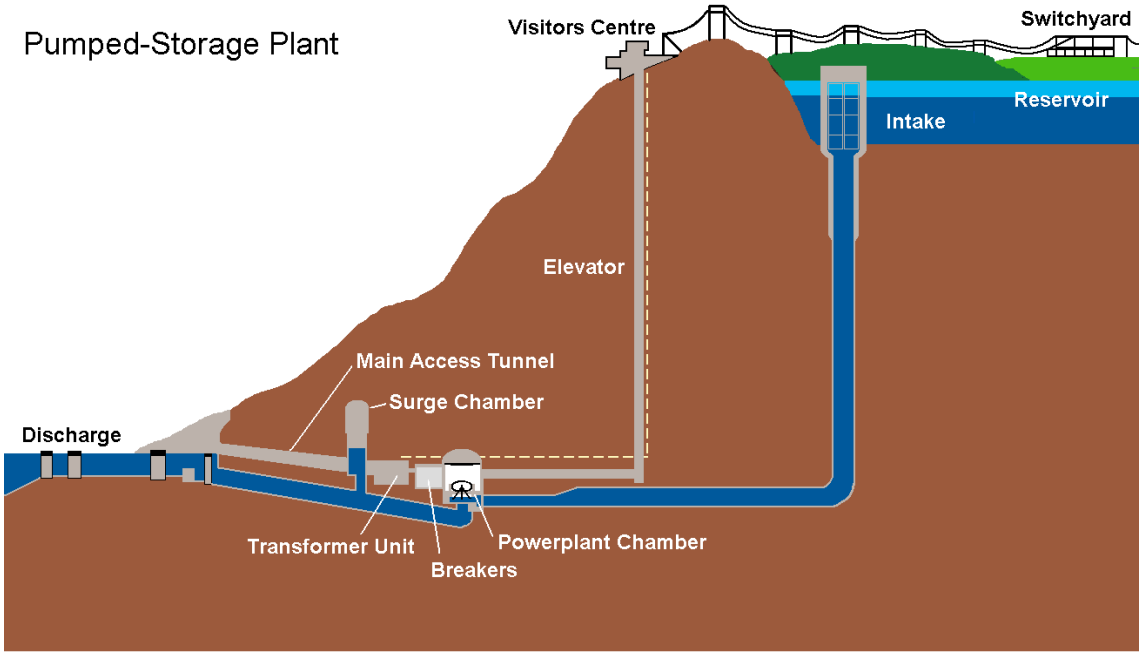

As seen on Figure 9, PHS is composed of two reservoirs with a height difference. Energy is stored by pumping water in the upper reservoir, and released while the water drives a turbine while going down through the pipe linking the reservoirs (Chen *et al.*, 2009). Some variations present underground reservoirs or use seawater (Bradbury, 2010). The efficiency of the system is first limited by the efficiency of the turbines and the pump, then by the loss of the stored

water by evaporation or its friction in the pipes. With low maintenance costs, this type of energy storage is mainly used for commodity storage.

Figure 10: Compressed Air Energy Storage (CAES) (Chen *et al.*, 2009)

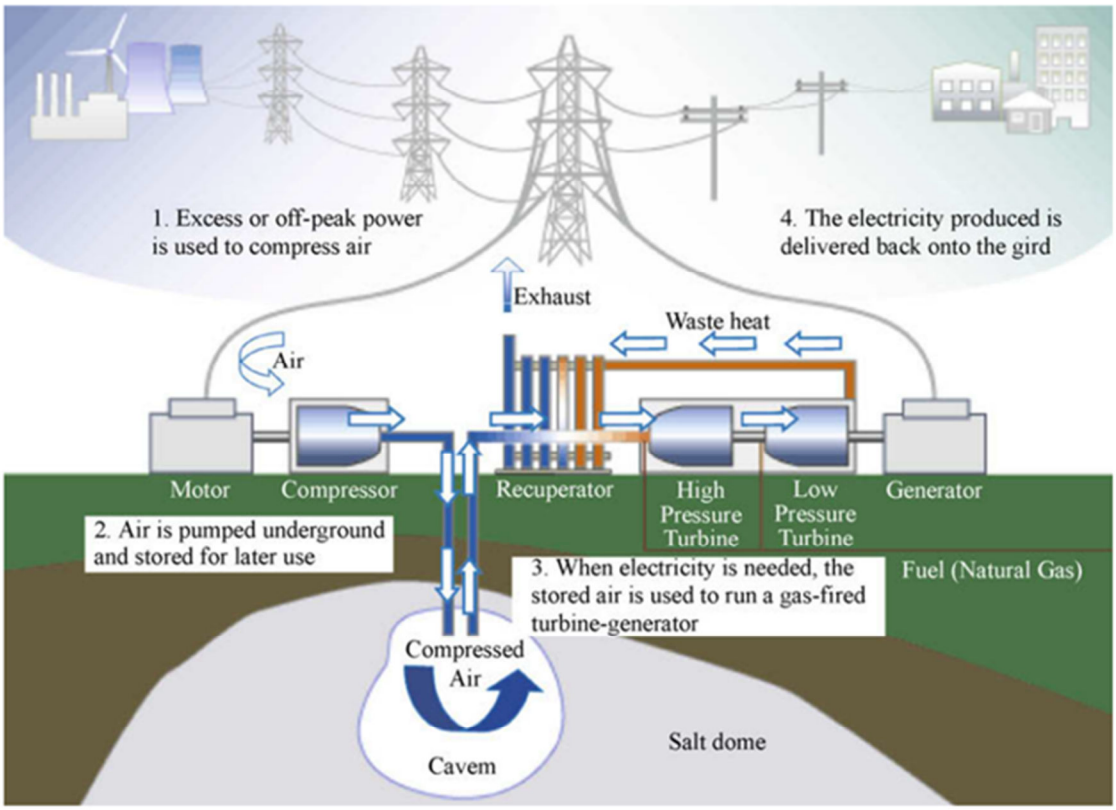

As seen on Figure 10, compressed air energy storage systems use an underground cavern to store air to a high pressure (4-8 MPa) (Chen *et al.*, 2009). It is pumped at off-peak time and released when needed. Air is then combusted with fuel in a high pressure turbine. Such a system is designed to sustain frequent charging/discharging cycles. Despite a low capital cost, CAES have a high efficiency and a long storage period (Chen *et al.*, 2009).

Potential energy storage are the only commercially available technologies capable of very large scale energy storage deliverability (<100MW per unit) (Chen *et al.*, 2009).

2.2.1.2 Electrical ES systems

The electrical ES is the only technology that charges, stores and returns electric energy: it uses standard electrostatic capacitors (CAP), electrochemical capacitors (super-capacitors) (ECC), and superconducting magnetic energy storage (SMES).

Figure 11: Capacitor/super capacitor (Chen *et al*., 2009).

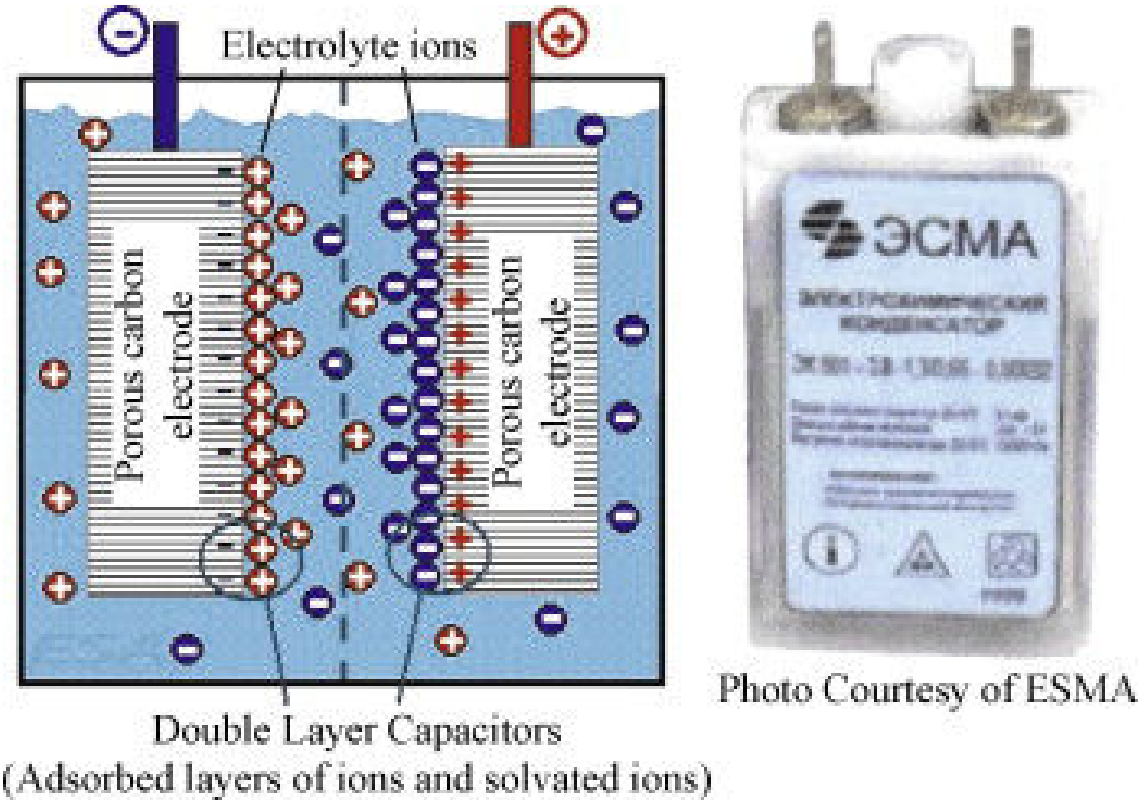

When charged by a direct-current source, capacitors store electricity by physically separating positive and negative charges—unlike batteries which do so chemically (Chen *et al*., 2009). They are made of two metal plates separated by a non-conducting layer called dielectric. Capacitors charge faster than batteries but still present a low energy density. Hence, large capacitors are too expensive. Super-capacitors get better energy storage capacities by replacing solid dielectric with an electrolyte solution (Chen *et al*., 2009). Because of self-discharge loss, capacitors, like flywheels, present high energy dissipations and short durations. Hereafter, capacitors are also used in power quality applications.

Figure 12: Energy Storage Method Using Superconducting Phenomenon (Nomura *et al*., 2010)

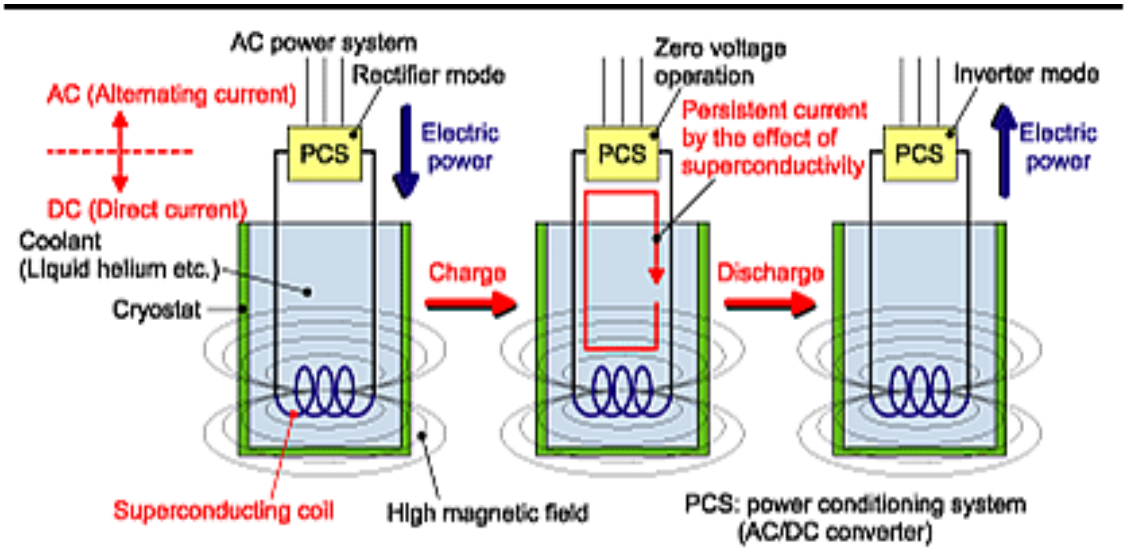

Figure 12 shows the working mechanism of a SMES. Electric energy is directly store into electric current. Once the current is charged, it circulates indefinitely in an inductor made of superconducting material. With no moving parts, such a system presents an efficiency rate up to 98%, and a very low maintenance cost. The high level of cycle life and the very quick response time make it suitable for applications in power quality problems and voltage stability for large industrial customers (Bradbury, 2010; Chen et al., 2009).

2.2.1.3 Chemical ES systems

Chemical ES groups three main types of batteries; i.e. the conventional, molten salt, and flow batteries (Chen *et al*., 2009) (Figure 13).

Figure 13: Schematic of flow battery (Chen *et al.*, 2009)

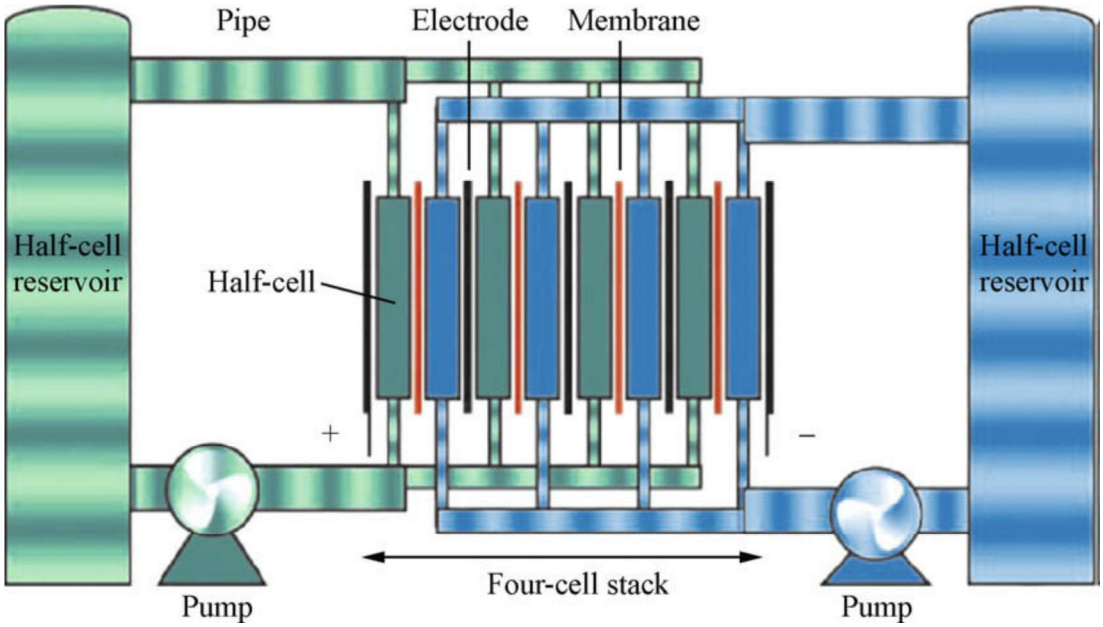

Conventional batteries are made of one or more electrochemical cells. Each cell contains a solid, paste, or liquid electrolyte together with a positive electrode (anode) and a negative electrode (cathode). Reversible electrochemical reactions occur at the two electrodes. While discharging, the reaction generates a flow of electrons through an external circuit. Charging is allowed by applying an external voltage across the two electrodes. Variations would use different products or shapes for the electrodes. Several technologies have been developed to increase the storage capacities known as "advanced rechargeable batteries": flow batteries (Figure 13), high temperature systems, lithium systems (Bradbury, 2010). The main advantage of batteries is that you can increase the size of the system by combining them in series or parallel (Bradbury, 2010; Chen et al., 2009). The major problems of batteries are their high cost, their low energy and charge densities, and the environmental impact of the components (Chen *et al.*, 2009).

2.2.1.4 Thermal ES systems

The Thermal Energy Storage (TES) systems cover a large range of temperatures and applications (Chen *et al*., 2009) and are further detailed in this chapter because of their expected high technological strength and market potential.

Several reviews have previously described ES technologies and systems (Chen *et al*., 2009; Bradbury, 2010). Data are collated in Table 2 by Bradbury (Bradbury, 2010): the wide range of their characteristics, costs and efficiencies illustrates that development and application are at different stages. Levelized costs include investment, maintenance and operating costs. The intrinsic investment and maintenance costs differ widely amongst the technologies, explaining the significant variation of the energy costs included in the Tables below.

Table 2 Main characteristics of mechanical energy storage systems (Bradbury, 2010):

	Mechanical Storage			
	PHS	CAES	FES-LS	FES-HS
Parameter				
Roundtrip Efficiency [%]	70-85	57-85	70-95	70-95
Self-discharge [%Energy/day]	~ 0	~ 0	100	1.3-100
Cycle Lifetime [cycles]	N/A	N/A	20k-100k	20k-100k
Expected Lifetime [Years]	30-60	20-40	15-20	15-20
Specific Energy [Wh/kg]	0.5-1.5	30-60	10-30	10-30
Specific Power [W/kg]	0	0	400-1.5k	400-1.5k
Energy Density [kWh/m^3]	0.5-1.5	3-6	20-80	20-80
Power Density [kW/m^3]	0	0.5-2	1k-2k	1k-2k
Costs				
Power Cost [$/kW]	600-2k	400-800	250-360	250-400
Energy Cost [$/kWh]	0-23	2-140	230-60k	580-150k
Balance of Plant Costs (BOP)[$/kW]	270-580	270-580	110-600	110-600
Power Conversion System Costs (PCS)[$/kW]	0-4.8	46-190	0-120	0-1200
Operation and Maintenance (OM) Fixed Cost[$/kW-y]	3-4.4	1.6-29	6-22	6-22

Table 2 (continued): Main characteristics of electrical energy storage systems (Bradbury, 2010):

	Electrical Storage		
	CAP	ECC	SMES
Parameter			
Roundtrip Efficiency [%]	60-70	90-98	90-98
Self-discharge [%Energy/day]	40	20-40	10-15
Cycle Lifetime [cycles]	50k	10k-100k	100k
Expected Lifetime [Years]	5	20	20-30
Specific Energy [Wh/kg]	0.05-5	2.5-15	0.5-5
Specific Power [W/kg]	100k	500-5k	500-2k
Energy Density [kWh/m^3]	2-10	0	0.2-2.5
Power Density [kW/m^3]	100k	100k	1k-4k
Costs			
Power Cost [$/kW]	200-400	100-360	200-350
Energy Cost [$/kWh]	500-1k	300-94k	1k-83k
BOP Cost [$/kW]	180-580	180-580	140-650
PCS Cost [$/kW]	50-12k	50-12k	60-12k
O&M Fixed Cost [$/kW-y]	6-16	6-16	9.2-30

Table 2 (continued): Main characteristics of chemical energy storage systems (Bradbury, 2010):

	Chemical Storage				
	Conventional Battery			Molten Salt Bat.	
	Lead Acid	NiCad	Li-ion	NaS	ZEBRA
Parameters.					
Roundtrip Efficiency [%]	70-82	60-70	85-98	70-90	85-90
Self-discharge [%Energy/day]	0.033-0.3	0.067-0.6	0.1-0.3	0.05-20	15
Cycle Lifetime [cycles]	100-2k	800-3.5k	1k-10k	2.5k-2.5k	2.5k
Expected Lifetime [Years]	3-20	5-20	5-15	5-15	10-14
Specific Energy [Wh/kg]	30-50	50-75	75-200	150-240	100-120
Specific Power [W/kg]	75-300	150-300	150-315	150-230	150-200
Energy Density [kWh/m^3]	50-80	60-150	200-500	150-250	150-180
Power Density [kW/m^3]	10-400	0	0	0	220-300
Costs					
Power Cost [$/kW]	175-600	150-1500	175-4000	150-3000	150-300
Energy Cost [$/kWh]	150-400	600-1500	500-2500	250-500	100-200
BOP Cost [$/kWh]	120-600	120-600	120-600	120-600	120-600
PCS Cost [$/kW]	58-180	50-180	0	0-120	0-120
O&M Fixed Cost [$/kW-y]	1.8-52	6-32	12-30	23-61	23-61

Table 2 (continued): Main characteristics of chemical energy storage systems (Bradbury, 2010):

	Chemical Storage		
	Flow Battery		
	ZnBr	Polysulfide-bromide	Vanadium Redox
Parameters.			
Roundtrip Efficiency [%]	60-75	57-75	60-85
Self-discharge [%Energy/day]	0.24	~ 0	0.2
Cycle Lifetime [cycles]	2k	2k	12k-14k
Expected Lifetime [Years]	5-10	10-15	5-15
Specific Energy [Wh/kg]	30-50	10-50	10-30
Specific Power [W/kg]	0	0	0
Energy Density [kWh/m^3]	30-60	16-60	16-33
Power Density [kW/m^3]	0	0	0
Costs			
Power Cost [$/kW]	175-2500	330-2500	175-1500
Energy Cost [$/kWh]	150-1000	120-1000	150-1000
BOP Cost [$/kWh]	120-600	120-600	120-610
PCS Cost [$/kW]	0-120	60-120	36-120
O&M Fixed Cost [$/kW-y]	15-47	18-96	24-65

The comparison shows that each technology has a specific field of applications and answers a specific need. Thermal Energy Storage is presented here as a solution for numerous applications.

2.2.2 Thermal energy storage

With Thermal Energy Storage (TES), heat is transferred to storage media during the charging period, and released at a later stage during the discharging step, to be usefully applied e.g. in generating high pressure steam for power block (Rankin cycle) in solar plants, or as heat carrier in high temperature industrial processes, such as metallurgical transformations (Pincemin et al., 2008b). In terms of storage media, a variety of choices exists depending on the storage media system selected, the temperature range and the specific application.

2.2.2.1 TES applications and temperature range

Thermal energy storage includes a number of different technologies, each one with its own specific performance, application and cost. TES systems based on sensible heat storage offer a storage capacity ranging from 10 kWh/t to 50 kWh/t and storage efficiencies between 50% and 90%, dependent on the specific heat of the storage medium and thermal insulation. Phase

change materials (PCM) can offer higher storage capacity and storage efficiencies between 75% to 90%. In most cases, storage is based on a solid/liquid phase change with energy densities in the order of 100 kWh/m^3 (e.g. ice). Thermo-chemical storage (TCS) systems can reach storage capacities of up to 250 kWh/t, with operation temperature in excess of 300°C and efficiencies between 75% and nearly 100% (IEA and OECD, 2011).

Low temperature thermal energy storage (LTTES) operates in a temperature range below 200°C and has been extensively investigated and developed. Cold Thermal Energy Storage applications can be found mostly in building cooling (Castellón *et al.*, 2007), while LTTES applications are in building heating, solar cooking, solar water boilers and air-heating systems, and in solar greenhouses (Regin *et al.*, 2008; Sharma *et al.*, 2009). For instance, Figure 14 shows the commercially tested system of "Solar Collectors and Seasonal Energy Store".

Figure 14: Schematic of a Solar Collectors and Seasonal Energy Store System (Colclough *et al.*, 2011)

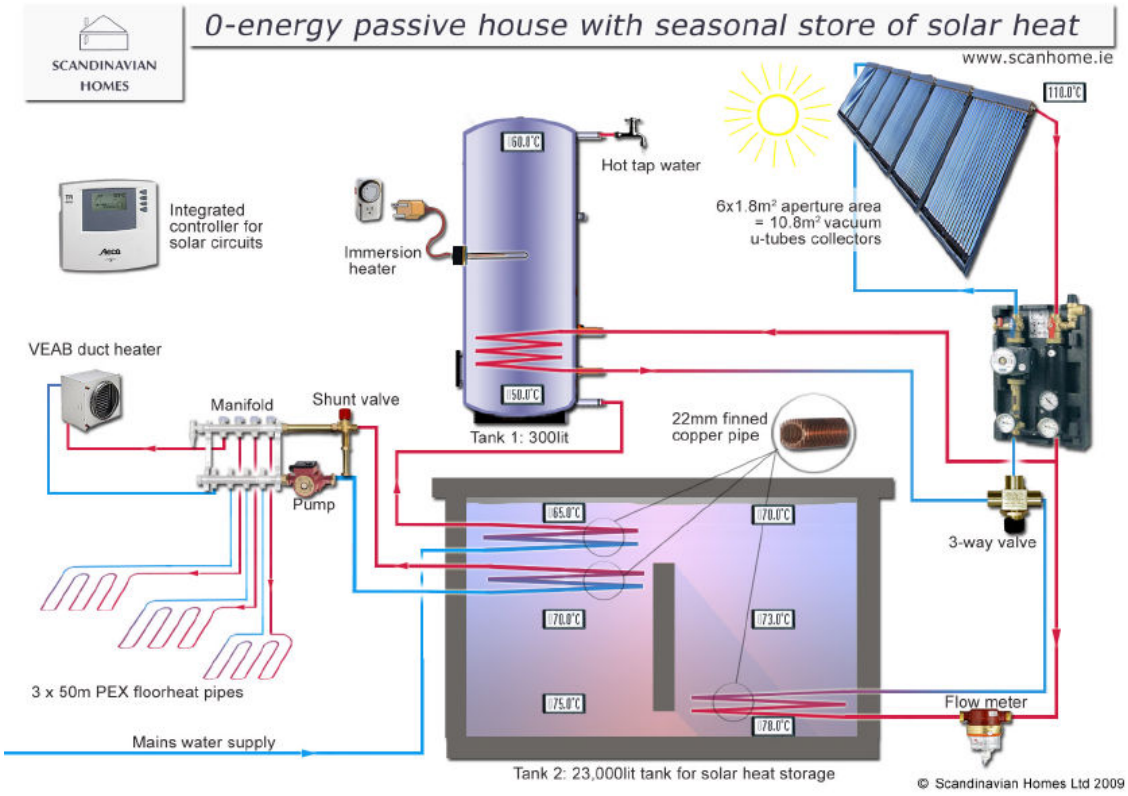

High temperature thermal energy storage (HTTES) plays a vital role in renewable energy technologies and waste heat recovery. There is a wide range of industrial applications where

waste heat can be recovered, as in the manufacturing of construction materials (e.g. clay brick or cement kilns) mining and in the metallurgical industry in general (Maruoka et al., 2002; Tamme et al., 2008). Today, most HTTES usages are however focused upon applications of solar thermal energy (Laing et al., 2011; Medrano et al., 2010). Figure 15 is an overview of a large scale testing system for HTTES in concentrated solar plants. This system is currently being extensively studied for high temperature energy storage in a direct steam generation concentrated solar plant (Laing et al., 2011; Medrano et al., 2010), it combines two different use for molten salts material i.e. sensible and latent heat.

Figure 15: Overview of a three-part thermal energy storage system for DSG combining sensible and latent heat storage (Laing *et al.*, 2011)

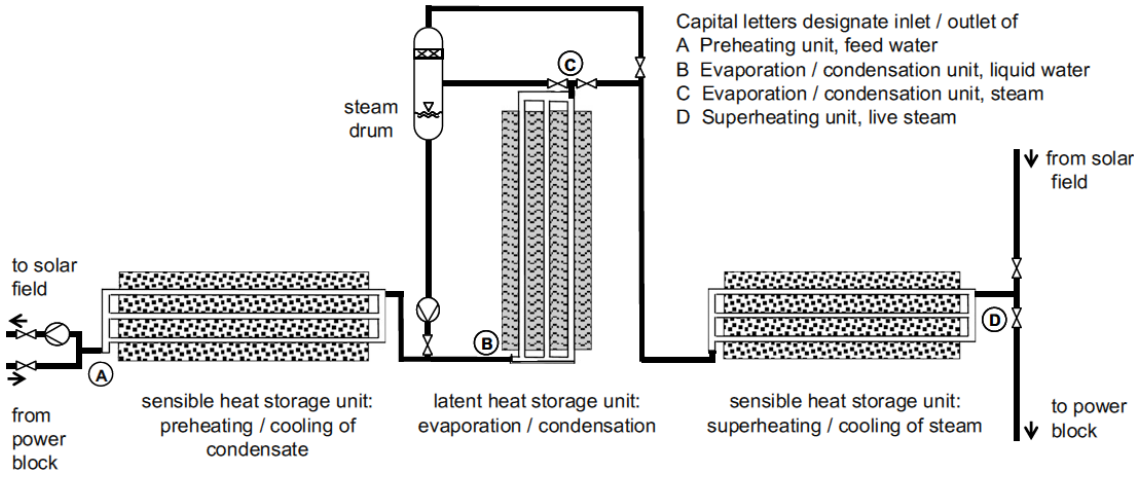

TES applications are the subject of constant innovative research and the designs as shown in the numerous reviews (Gil *et al.*, 2010; Chen *et al.*, 2009; Bradbury, 2010; Sharma *et al.*, 2009; Medrano *et al.*, 2010; Agyenim *et al.*, 2010; Ibrahim *et al.*, 2008; Jegadheeswaran *et al.*, 2010; Jegadheeswaran and Pohekar, 2009; Kenisarin, 2010; Sharma and Sagara, 2005; Zalba *et al.*, 2003). The current chapter presents a guideline for a specific TES solution.

2.2.2.2 TES requirements

In order to make HTTES a more plausible and attractive alternative for improving the efficiency of industrial processes and solar engineering, some requirements must be fulfilled.

HTTESs firstly need to stably operate in a high range of temperatures, which in the present context is specified from 200°C to an as high a temperature limit as possible. Secondly, the material used as storage media must be inexpensive, available in big quantities and compatible with a cost-effective system design (Gil *et al*., 2010). Several additional facts need to be considered when deciding on the storage media for a HTTES, and the most important requirements are presented by Alba *et al*. (Zalba *et al*., 2003):

(i) Energy capacity: high energy density in the storage material;

(ii) Efficiency: good transfer between the heat transfer fluid (HTF) and the storage medium;

(iii) Mechanical and chemical stability of the storage material during the multiple charging/discharging cycles;

(iv) Safety: compatibility between HTF, heat exchanger and/or storage medium;

(v) Lifespan: complete reversibility in multiple charging/discharging cycles;

(vi) Low heat losses;

(vii) Ease of control;

(viii) Adequate maximum load;

(ix) Appropriate nominal temperature and;

(x) Specific enthalpy drops in load.

Meeting all these requirements needs innovative engineering approaches shaped by the development and research into the fields of storage media. The latter is due to the difficulty of selecting an adequate and stable storage material that matches both (i) and (ii) requirements described above. The combination of high efficiency and high energy density requirements can lead to the development of a storage media that makes viable the design of cost-efficient HTTES, and it is a challenge that demands novel ideas and pioneering efforts.

2.2.2.3 TES media

An assertive material selection involves choosing an adequate form of thermal storage, which can be found in three types, being the thermal storage as sensible heat, the thermal

storage as latent heat when phase transformations are accounted for, and the thermo-chemical storage as a result of combining endothermic and exothermic reactions occurring with the media. The energy released or absorbed by a material as its temperature is reduced or increased is called sensible heat, and the specific heat (c_p) is the relevant characteristic. The energy required to convert a solid into a liquid, or a liquid into a gas (material phase change) is called latent heat with e.g. heats of fusion and condensation recognised for their high value. The capacity of energy storage is significantly higher when latent heat storage complements the sensible heat storage. The third and less developed category of heat storage, the thermo-chemical heat storage, uses the reversible endothermic/exothermic reactions of some reactions as detailed below.

2.2.2.3.1 Sensible heat storage

Sensible heat storage materials undergo no phase change within the temperature range required for the storage application (Fernandez *et al*., 2010). Table 3 summarizes the main characteristics of the most common solid and liquid sensible HTTS materials (Fernandez et al., 2010; Nallusamy et al., 2007).

Within the indicated solids, concrete and cast ceramics have been extensively studied due to their low costs, good thermal conductivities and moderate specific heats (Domański and Fellah, 1998; Tamme, 2006). In terms of liquids, molten salts are widely used in power tower systems, being liquid at ambient pressure, providing an efficient and low cost medium, having their operating temperatures compatible with current high-pressure and high-temperature turbines (temperature range over 120°C to 600°C), whilst being non-flammable and non-toxic (Tamme, 2006; Yang et al., 2010). These molten salts are already used in the chemical and metallurgical industries as heat-transport fluid. This experience provides knowledge for molten salt used in other fields than solar plants (Kearney *et al*., 2003). From Table 3, it is clear that the main candidates for liquid sensible heat storage are either a solar salt, i.e. a binary salt consisting of 60% of $NaNO_3$ and 40% of KNO_3, that melts at 221°C and is kept liquid at 288°C in an

insulated storage tank; or HitecXL, a ternary salt consisting of 48% Ca $(NO_3)_2$, 7% $NaNO_3$, and 45% of KNO_3 operating beyond its melting point of 130°C (Kearney *et al*., 2004).

Table 3 Main Characteristics of sensible heat storage solid and liquid materials

Storage Medium	Temperature		Average Density (kg/m^3)	Average Heat Conductivity (W/m K)	Average Heat Capacity (kJ/kg K)	Volume Specific Heat Capacity (kWh_t/m^3)	Costs per kg (US$/ kg)	Costs per kWh_t (US$/ kWh_t)
	Cold (°C)	Hot (°C)						
Solid Storage Medium								
Sand-rock-mineral oil	200	300	1700	1	1.3	60	0.15	4.2
Reinforced Concrete	200	400	2200	1.5	0.85	100	0.05	1
NaCl (solid)	200	500	2160	7	0.85	150	0.15	1.5
Cast iron	200	400	7200	37	0.56	160	1	32
Silica fire bricks	200	700	1820	1.5	1	150	1	7
Magnesia fire bricks	200	1200	3000	1	1.15	600	2	6
Liquid Storage Medium								
HITEC Solar Salt	120	133	1990	0.60	-	-	-	-
Mineral oil	200	300	770	0.12	2.6	55	0.3	4.2
Synthetic oil	250	350	900	0.11	2.3	57	3	42
Silicon oil	300	400	900	0.1	2.1	52	5	80
Nitrite salts	250	450	1825	0.57	1.5	152	1	12
Nitrate salts	265	565	1870	0.52	1.6	250	0.5	3.7
Carbonate salts	450	850	2100	2	1.8	430	2.4	11
Liquid	270	530	850	71	1.3	80	2	21

Sensible heat materials have been widely studied and are currently applied in solar thermal plant applications, despite important disadvantages that can affect the storage system design and stability. Kearney *et al*. (2002) investigated molten salts and demonstrated such disadvantages. Most molten salts have a high freezing point (around 100°C), and the high outlet temperature results in heat losses and in requiring more expensive piping and materials (Brosseau et al., 2005; Kearney et al., 2002). The high freezing point may be a problem for solar power plants because of the required heat trace during non-functioning periods. Furthermore, the sensible

fraction of thermal energy is seldom fully recovered due to the required temperature difference as heat transfer driving force. Another important disadvantage consists in the low energy storage density of sensible heat materials, which are required in large volumes or quantities in order to deliver the amount of energy storage necessary for HTTES applications. The above mentioned problems can imply significant increments in the costs of sensible heat storage systems.

2.2.2.3.2 Thermo-chemical heat storage

The main advantage of the thermo-chemical heat storage systems consists in the potentially high energy density of the occurring reversible chemical reactions, which can be even higher than what is usually encountered for the other thermal storage processes (Gil et al., 2010; Oelert et al., 1982). Materials that have been mostly investigated for chemical storage are the SnO_x/Sn and ammonia system. In the former case, the metal oxide/metal reactions are possible and technically feasible; occurring at a temperature of 980 K, and SnO_2 (solid) is reduced with CH_4 while it floats on top of liquid Sn. For the latter case, ammonia is dissociated producing hydrogen and nitrogen. The exothermic reaction heat from ammonia synthesis is suitable for electric power generation in conventional Rankin Cycles. Despite its high energy density, thermo-chemical heat storage is considered to be an expensive alternative and is, at the present, at early stages of development (Oelert *et al*., 1982).

2.2.2.3.3 Latent heat storage

Latent heat storage is based on the heat absorption or heat release that occurs when a storage material undergoes a phase change. Latent storage systems based on phase change materials (PCMs) with solid-liquid transition are considered to be very efficient in comparison to liquid-vapour and solid-solid transitions (Regin *et al*., 2008). Liquid-gas transition requires a large volume recipient for the PCM and the solid-solid transition presents a low value of latent heat. Therefore these last two alternatives are not considered appropriated choices. (Do Couto Aktay et al., 2008). A large number of materials are known to melt with a high heat of fusion within different ranges of temperature. No material yet studied has all the optimal characteristics required for a PCM, and the selection of a PCM for a given application requires careful

consideration of the properties of the various substances and/or mixtures (Kenisarin, 2010). The main characteristics required for PCMs are indicated in Table 4 (Regin *et al*., 2008).

Table 4 Main desirable characteristics of PCMs

Thermal properties	Phase change temperature suitable within the desired operating range. High latent heat per unit mass. High specific heat. High thermal conductivity for both solid and liquid phases.
Physical properties	High energy density. Low density variation during phase change. No super cooling during freezing.
Chemical properties	Chemical stability. No chemical decomposition. Compatibility with container materials construction (e.g. vessels and piping). Non-toxic, non-inflammable and non-explosive.
Economic Factors	Available in large quantities. Inexpensive

As an example, commercial or potential substances used as PCM are shown in Table 5, Table 6, and Table 7 (Nallusamy *et al*., 2007)**.**

Table 5 Organic compounds for potential use as PCM.

Organic Compounds	Melting Point (°C)	Heat of Fusion (kJ/kg)
Ammediol	112	285
Neopentyl glycol	125	45.3
Neopentylglycol diacrylate	126	44.3
Isomalt	147	275
Adipic acid	152	247
Dimethylol propionic acid	153	275
Tromethamine	172	27.6
Trimethylolethan	198	44.6
Pentaerythritol	260	36.9

Table 6 Inorganic substances for potential use as PCM and commercial compounds

Inorganic Compounds	Melting Point (°C)	Heat of Fusion (kJ/kg)	Density (kg/m^3)	Specific Heat (kJ/kg.K)	Thermal Conductivity (W/m.K)
$Mg(NO_3).2H_2O$	130	275	n.a	n.a.	n.a
Hitec XL: 48%$Ca(NO_3)_2$-45%KNO_3-7%$NaNO_3$	140	n.a.	1992	1.44	0.519
Hitec: KNO_3-$NaNO_2$-$NaNO_3$	142	84	1990	1.34.	0.6
68%KNO_3-32%$LiNO_3$	144	75	n.a	n.a.	n.a
Isomalt	147	252	n.a	n.a.	n.a
$LiNO_3$-$NaNO_3$	195	n.a.	n.a.	n.a.	n.a.
KNO_3/$NaNO_3$ eutetic	223	105	n.a.	n.a.	0.8
$NaNO_3$	307/308	74	2260/2257	n.a.	0.5
KNO_3/KCl	320	116	2100	1.21	0.5
KNO_3	333/336	266/116	2110	n.a.	0.5
KOH	380	149.7	2044	n.a.	0.5
$MgCL_2$/KCl/NaCl	380	400	1800	0.96	n.a.
$NaCO_3$-$BaCO_3$/MgO	500-850	n.a.	2600	n.a.	5
$AlSi_{12}$	576	560	2700	1.038	160
$AlSi_{20}$	585	460	n.a.	n.a.	n.a
$MgCl_2$	714	542	2140	n.a.	n.a
80.5%LiF-19.5%CaF_2 eutetic	767	790	2100/2670	1.97/1.84	1.7/5.9
NaCL	800/802	492/466.7	2160	n.a.	5
LiF	850	1800 MJ/m^3	n.a.	n.a.	n.a.
Na_2CO_3	854	275.7	2533	n.a.	2
KF	857	452	2370	n.a.	n.a.
K_2CO_3	897	235.8	2290	n.a.	2

Table 7 Inorganic substances for potential commercial compounds

Commercial compounds	Melting Point (°C)	Heat of Fusion (kJ/kg)	Density (kg/m^3)	Specific Heat (kJ/kg K)	Thermal Conductivity (W/m.K)
Paraffin RT110	112	213	n.a.	n.a.	n.a.
Inorganic E117	117	169	1450	2.61	0.7
Organic A164	164	306	1500	n.a.	n.a.

Current experimented uses of PCMs for thermal storage involve low to moderate temperatures (10-100°C) and include solar water-heating systems, solar air-heating systems, solar cookers, solar greenhouses (for curing and drying processes), building acclimatization as in a PCM Trombe wall (Figure 16), PCM wallboards (Castellón *et al*., 2007), under-floor heating systems and ceiling boards (Regin *et al*., 2008; Sharma *et al*., 2009).

Figure 16: Test cubicles with inclusion of PCM in concrete (a) and results (b) (Castellón *et al*., 2007)

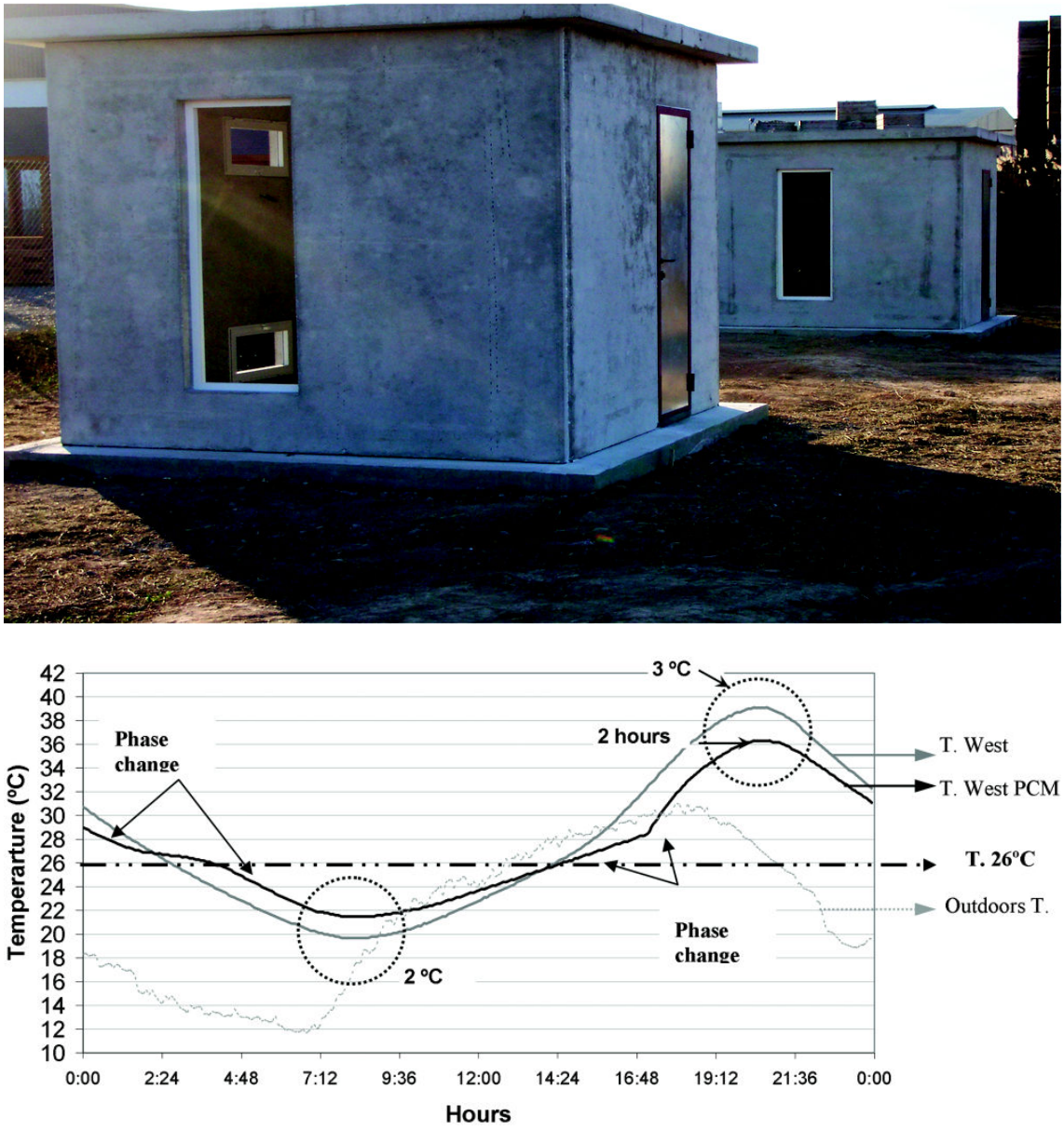

Though PCMs usage in HTTES has been experimented for solar plant applications, it has not yet been commercially used in a solar plant (Gil *et al*., 2010; Laing *et al*., 2011).

The development of high temperature thermal storage using PCMs is of increasing interest since they are moderately expensive, have high energy density, can in the future be available in large quantities (Zalba *et al*., 2003), and are able to store and release thermal energy at a constant temperature most of the times (Regin *et al.*, 2008; Sharma *et al.*, 2009). However, most of PCMs have a low thermal conductivity, leading to low charging and discharging rates and sometimes non suitable field of temperature in the material. Therefore, using PCMs for energy storage in high temperature range applications requires considering new aspects of material selection and development. In addition to adapting PCM's melting points to a high temperature range, their characteristics need to be improved in order to increase the *efficiency of the charging and discharging* processes.

Based on this information, several studies or papers consider the development of novel phase change materials for high temperature purpose a very important subject of study, and several researchers are engaged in an extensive programme of research to provide an adequate theoretical background and a description of the fundamentals. The successful completion of this research will help create fundamental and advanced knowledge on the subject, as well as support the development of cost-effective high temperature thermal storage systems oriented for the improvement of renewable energy technologies and energy-efficient industrial processes. The facts and findings of previous research form the guidelines to the research priorities, and are dealt with below.

2.2.3 Available options for PCM development

To improve the efficiency of the charging and discharging processes of PCMs, the most relevant parameter to be studied is their thermal conductivity. In order to increase the thermal conductivity of PCMs, several heat transfer enhancement techniques have been studied (Jegadheeswaran and Pohekar, 2009), such as:

(i) the use of metal carrier structures made of steel or stainless steel;

(ii) a dispersion of high conductivity material i.e. copper, silver or aluminium particles, within the PCM;

(iii) the impregnation of high conductivity porous materials, either as a metal foam (copper, steel or aluminium), or as porous material like graphite;

(iv) the use of high conductivity, low density materials such as carbon fibres and paraffin composites; and

(v) the micro-encapsulation of PCMs using graphite (Lopez, 2007), polymers, nickel film coating of PCM copper spheres (Maruoka and Akiyama, 2003).

The general review of these techniques illustrated in Figure 17 was undertaken by Agyenim *et al*. (2010), and the encapsulation of PCM in shells was determined as being one of the most promising and suitable approaches at the present stage of the project investigation. As described below and explained in detail in the following sections, coating shells improve heat transfer rates in PCMs significantly, thus being an attractive approach for developing and improving latent heat storage media.

The reasons behind this selection are the result of the detailed assessment, which summaries as follows:

(i) Incorporating metal structures into the PCM has been addressed as one of the thermal conductivity enhancement techniques by some researchers, who investigated metal structures made of steel or stainless steel in different geometries, such as cylindrical and spherical geometries, and in different arrangements (Ettouney et al., 2006; Khodadadi and Hosseinizadeh, 2007; Velraj et al., 1999; Zeng et al., 2007). In order to achieve a significant reduction of melting/solidification time, an important system volume is necessary. With the increase of the volume, however, comes with the rise of the cost. Due to the constrains demonstrated by the review, this heat transfer enhancement technique does not fulfil our research interests.

Figure 17: Heat transfer enhancement methods employed in phase change material research (Agyenim *et al.*, 2010)

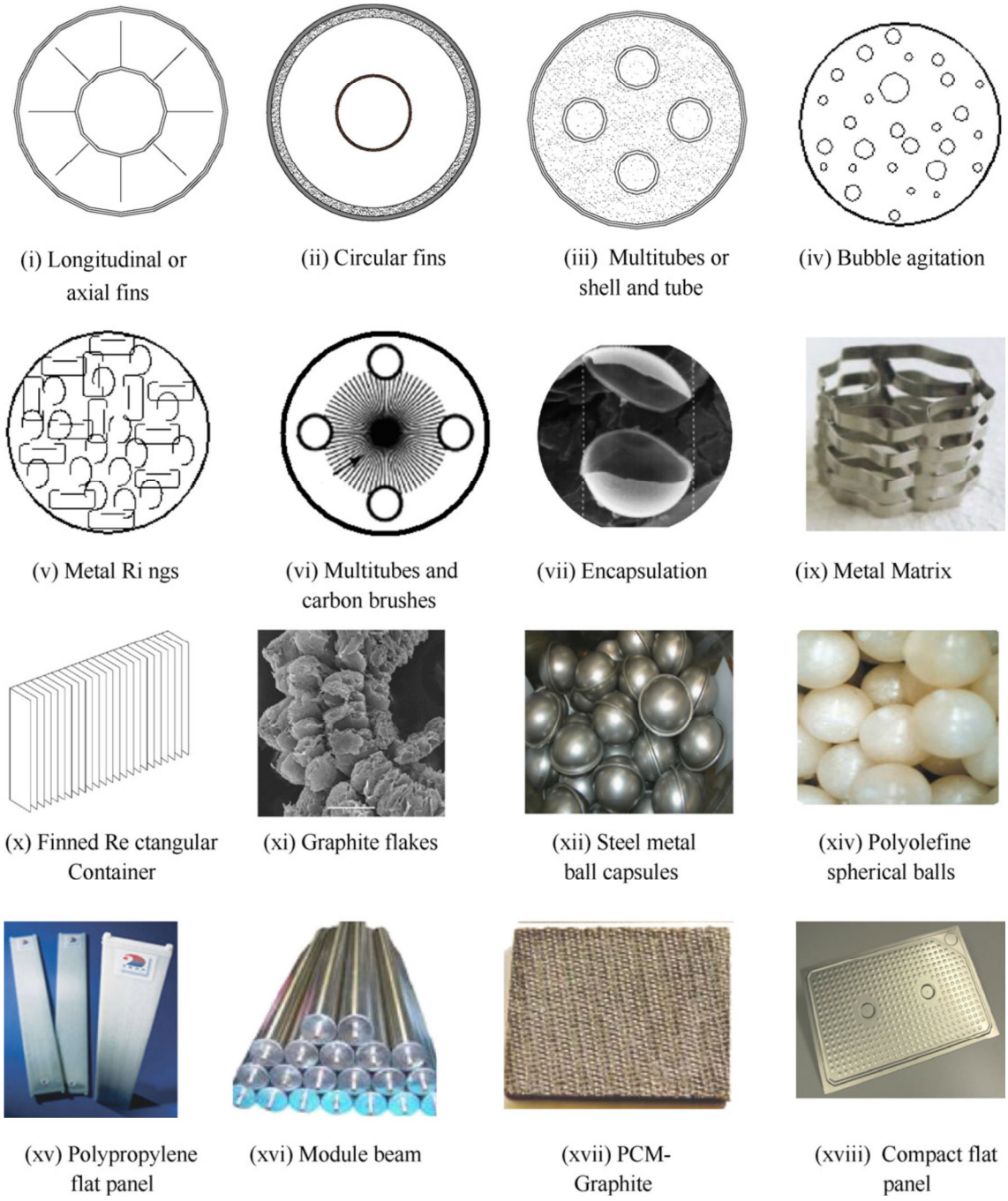

(ii) Dispersion of high conductivity particles into the PCM is a relatively simple technique to enhance the thermal conductivity of PCM. Studies involving dispersion of metal particles like copper, silver and aluminium have been undertaken (Elgafy and Lafdi, 2005; Khodadadi and Hosseinizadeh, 2007; Mettawee and Assassa, 2007). They

showed that, at any given condition, there is a range of optimum particle fractions and it is suggested to choose lower values in the band to ensure a high mass of PCM to increase the amount of energy stored. Hence, an appropriate combination of particle thermal conductivity and particle mass fraction is quite important when the conductive particles are to be dispersed in the PCM to enhance the performance of the unit. These results conclude that there is a limitation in terms of PCM/particle combination that could be applied, and further research is necessary.

(iii) High conductivity particles should also be compatible with all PCMs. Due to the relatively high density; the metal particles/metal structures may settle at the bottom of the TES container and add considerable weight to the system. According to Fukai *et al*. (2000), not all metal particles are compatible with all PCMs. For example, paraffin and aluminium are compatible, while copper and nickel are not compatible. Similarly, aluminium and copper are not compatible with some salt hydrates. Hence, there has been a search for low-density high conductivity additives which should be compatible with all PCMs. Since the densities of carbon fibres are lower than those of metals and the thermal conductivities are almost equal to that of aluminium and copper, carbon fibres can be better alternatives to enhance the thermal performance of LTTES systems. This heat transfer enhancement technique has been widely studied, as previously mentioned (Elgafy and Lafdi, 2005; Fukai et al., 2003, 2002; Hamada et al., 2005, 2003). The review has revealed that both the phase change and/or the charging and discharging rate (melting/solidification) can be increased considerably by adding high conductivity substances. In general, however, these additives may lead to the loss of storage capacity of pure PCM. The loss in storage capacity limits the mass/ volume fraction of additives. It should therefore be mentioned that this technique has a limited potential for developing LTTES systems for industrial applications, where a high storage capacity of PCMs is needed to accomplish the industrial requirement of non-intermittent high temperature steam production.

(iv) In view of the above mentioned constraints, impregnation of high conductivity porous materials in PCMs constitutes an attractive alternative for improving the heat transfer processes in PCMs. The use of a porous matrix has gained increasing attention because of its light weight and high specific surface area for heat transfer (Wu and Zhao, 2001). Porous structures can be even matrices made of aluminium, copper, etc., or naturally available porous materials such as graphite. Since the porous material is impregnated in the PCM, the problem of particle segregation at the bottom of the TES container is reduced.

(v) The thermal performance of micro-encapsulated PCMs is expected to exceed conventional PCMs since small PCM particles provide larger heat transfer area per unit volume and will provide a higher heat transfer rate. Micro-encapsulated PCMs moreover add advantages like less reaction of PCM with container material, and the ability to withstand volume change during phase change (Hawlader *et al*., 2003). This heat transfer enhancement technique has been widely studied for different combinations of PCMs and coating shells (Chen et al., 2008; Choi et al., 2001; Hawlader et al., 2003; Lopez, 2007; Maruoka and Akiyama, 2003; Pitié et al., 2011; Sarı et al., 2010; Zou et al., 2004). These studies mainly focused on the preparation and characterization of micro-encapsulated PCMs, without extensive comparison of the performance of micro-encapsulated PCM with that of pure PCM, and more comparative work is needed in order to assess the performance enhancement due to micro-encapsulation of commonly used PCMs. Such approach requires a great deal of experimental work, only at its incipient stage at present.

The main challenge of this approach would be to develop a compatible and efficient encapsulation of the PCM by a high conductivity material, suitable for high temperature purposes. The composite graphite-salt has to deal with a problem of mixture's stability of on the first charging-discharging cycle (Lopez, 2007). The graphite lets the molten salt escape from its matrix because of its volume expansion. The packed bed of capsules of PCM does not face this

problem (Regin *et al*., 2008). Although the micro-encapsulation of PCM had been already used to produce slurries (Agyenim *et al*., 2010), or for building applications (Castellón *et al*., 2007), it has not been used yet for high temperature purposes. Such a free surface micro-encapsulation will allow for extending thermal exchanges to a maximum surface. More specifically, the research should provide a proper modelling of SiC shell coating selected salts as PCM. Therefore, *structural mechanic* of the SiC shell and *thermo-mechanical behaviour* of the PCM need to be studied in conjunction with a *charging/discharging efficiency analysis*.

2.3 Feasibility, preliminary analysis and modelling of SiC coated PCM to be applied as HTTES material

In this work, ceramic encapsulated PCMs have been selected as potential HTTES solution. This part of the literature is considering the previous studies conducted on the different aspects of this solution.

2.3.1 Ceramics for micro-encapsulation

Ceramics have good properties such as mechanical resistance and relative chemical neutrality in high temperatures (Ubrig, 2007). Hence, we consider micro-encapsulation of salt PCM by coating them within ceramic spherical shells. SiC is already used in nuclear energy processes as a coating material: it protects fissionable fuel material from the chemical corrosive and mechanical erosive environment (Alkan *et al*., 2001). The better mechanical strength, extreme chemical resistance, and high thermal conductivity of SiC compared to graphite (Zhu *et al*., 1999) could offer major advantages when coating PCM pellets with SiC.

2.3.1.1 PCVD for deposition

The high temperature of ceramics manufacturing process (more than 800°C) could make those materials unsuitable for coating salts which have a melting temperature between 200°C and 500°C. But thanks to the Plasma Enhanced Chemical Vapour Deposit (PCVD), the temperature of deposit can be reduced as low as 80°C for SiO-SiN composed ceramics (Ubrig,

2007). PCVD is a process that uses a plasma torch to deposit thin films of chemical components from gas state to a solid state (Dagdag, 2005). This technology is already used to protect electronic components (Chung *et al*., 2005) or nuclear fuel from high temperature aggressive environments (Kim *et al*., 2000). PCVD ceramics coating is the chosen solution to produce an efficient material for high temperatures use. However, this process should be able to be applied on micro-sized particles.

2.3.1.2 Fluidized bed processes for particles

Fluidized beds are used as a technical process which has the ability to promote high levels of contact between gases and solids (Geldart, 1973). It is possible to coat particles thanks to a PCVD process combined to a fluidized bed (Cadoret *et al*., 2009; Czok *et al*., 2005; Czok and Werther, 2005; Harth *et al*., 1997). But despite their small size, melting coated PCM particles will face a volume expansion that can provoke the shell cracking and the destruction of the material (Maruoka and Akiyama, 2003).

2.3.2 Structural analysis and characterization

Several studies in solid mechanic of isolated hollow spheres have already been undertaken. Efforts have been made to determine the proper modelling for elastic and plastic deformation of shells. However, there are no studies attempting to develop a model specifically to a SiC spherical shell coating a PCM for HTTES. The present review presents a few interesting approaches to the mechanical characterization of spherical shells and porous materials in general, which provide starting points for further investigations related to SiC spherical shells coating a PCM.

2.3.2.1 Mathematical Modelling

Mechanical modelling of spherical shells under inner pressure has been done for different sets of parameters: plastic or elastic deformations, homogenous or heterogeneous materials (Cailletaud, n.d.; Delogu, 2007; Eslami et al., 2005, 1997; Gao, 2003; Gao et al., 2009; Hrudey

and Haddow, 1973; Jabbari et al., 2003; Poultangari et al., 2008). Complexity of the model increases with the number of parameters. The stress strain analysis of a an homogenous material is the simplest case if the deformation stays elastic, plastic deformation of an heterogeneous increasing the difficulty to get an analytical solution (Eslami et al., 2005; Jabbari et al., 2003; Poultangari et al., 2008).

2.3.2.2 Numerical Modelling

Numerical models of spherical shells under inner pressure can be found. For instance, Delogu developed one in order to predict the behaviour of nanometres sized particles (Delogu, 2007). The change in scale had to be studied with different tools than usual mechanical continuum. Numerical analysis can be used as well when the mechanical behaviour of the shell is under influence of both mechanical and thermal constrains.

2.3.2.3 Structural Parameters versus Thermal Parameters

The study of the relation of structural parameters with thermal conductivity, thermal diffusivity and latent heat in a porous material impregnated with PCM was done for a graphite matrix integrated with paraffin wax (Zhong *et al*., 2010). The research determined:

(i) an almost linear relation between thermal conductivity and the bulk density of the graphite matrix, as well as between the latent heat of the composite and the mass ratio of the paraffin wax in the matrix;

(ii) a small pore-size and thicker walls in the matrix resulted in a higher thermal diffusivity;

(iii) a large pore-size and thinner walls in the matrix resulted in a larger latent heat.

A similar analysis relating structural and thermal parameters will be carried out in our research, which will instead consider a SiC shell coating a selected salt submitted to a high temperature.

2.3.3 Thermo-mechanical analysis

The thermo-mechanical behaviour analysis is important to predict the effect of various cycles of charging and discharging of thermal energy when the PCM is subjected to high and low temperatures. It also provides information about how this condition influences the stress parameters. The purely mechanical behaviour of isolated hollow sphere in absence of temperature variation has been widely studied to determine the tensile properties of these materials. We consider the understanding of the mechanical behaviour of spherical shell a first step to later combine with thermal analysis; therefore the review of particularly relevant literature on this subject has been undertaken. Additionally, the thermo-mechanical review for both isolated hollow spherical shell material and coating PCM has also previously been presented.

2.3.3.1 Mechanical behaviour of a shell encapsulating a PCM

The mechanical stress analysis of a shell under inner pressure due to the volume expansion of a coated material has already been studied, and the work of e.g. Maruoka *et al*. assesses the thermal-stress while the coating material is strained by the volumetric expansion of the melting PCM (Maruoka and Akiyama, 2003). In the research of Maruoka *et al*, the PCM is a pellet of lead or copper encapsulated by a nickel coating shell. The experiments and modelling evaluate the required conditions to avoid the cracking of the shell under the inner pressure, without considering the heat storage efficiency of the PCM. The coating material has an elasto-plastic behaviour while the SiC shell of the present study has a pure elastic behaviour.

Upadhyaya *et al*. developed a stress analysis of an egg-shell strained by the volumetric expansion of its content, whereby the thermo-elastic behaviour of the coating is modelled by applying a thin shell theory (Upadhyaya *et al*., 1985). Upadhyaya *et al*. showed that it is possible to use Hooke's laws to make a simple model of the full-filled shell stress-strain behaviour. The difference of the current paper with that of Upadhyaya *et al*. is that the eggshell

does not coat a PCM. This study is used as a first step to model the SiC shell fully filled with a melting PCM.

2.3.3.2 Thermomechanical Analysis of Spherical Shaped PCMs

The thermo-mechanical analysis of porous graphite impregnated with PCMs was also performed in order to develop of a mathematical model of porous materials plastic behaviour (Lopez *et al*., 2010). This research is focused on help understanding salt melting within the graphite matrices and for proposing reliable ways for composite materials improvement. The mathematical modelling was able to determine the relation between the pore-elastic-plastic deformation versus temperature and pressure time history, as well as liquid-crystals equilibrium conditions. An important observation was that, under melting, the salt volume expansion will be constrained by the graphite matrix and pressure in pores will thus increase. Main consequences of this pressurization are a progressive increase of the salt melting temperature and a progressive reduction of its latent heat. For melting progress, materials have to be heated up to a melting point which is continuously increasing. Hence, a significant part of the energy supplied to the material will be used to heat it up (sensible heat instead of latent heat). Control of graphite densification during materials elaboration would be an easy way for increasing porosity (voids) within the graphite matrix skeleton and hence to reduce its rigidity and to increase the pore wall thickness. However, this will also lead to a reduction of the effective thermal conductivity. Even though the porous material of this previous study slightly differs from a spherical shell, the results could be considered as a preliminary approach of the interaction between the PCM and the SiC shell.

2.3.3.3 High Temperature Analysis

There are a reduced number of investigations that focus on heat transfer through a porous material embedded in PCMs at high temperature. The core interest of the investigations resides in proving the feasibility of porous material for increasing heat transfer rates through PCMs subjected to high temperature.

A large scale experimentation of graphite and salt composite applied to a thermal solar plant showed a very important result (Pincemin et al., 2008b); salt leakage was observed during the first cycles of charging/ discharging of the PCM and, therefore, all contact surfaces between PCM and graphite foam were lost. An analysis showed that, under thermal cycling, salt leakage can be mainly attributed to impurities and remaining mechanical stresses. The result points to potential problems that shall be considered in the present and further investigations of metal foams behaviour at high temperatures.

A mathematical model especially relevant for our research was developed for a graphite and salt composite (Lopez *et al*., 2010). The methods used for this research were based on energy conservation equations, pressure-dependent liquid–crystal equilibriums, linear elasticity laws and Poiseuille-like flow. The model provided a broad poro-elasto-plastic analysis and was able to determine required actions for achieving more desirable properties of the composite, which are the reduction of the pore-wall rigidity, the increase of the pore walls thickness, increasing pores connectivity or, in general, creating void space.

From this literature review, it is clear that thermo-mechanical and structural parameters play an important role in the heat transfer behaviour of SiC shell-PCMs composites. However, the few existing approaches lack mathematical modelling to predict how the interaction of those particular parameters will affect the stability and energy flux through the composite subjected to high temperatures.

The present research addresses these issues and tries to present a novel approach to the thermo-mechanical behaviour predictions by developing a model that incorporates all of the crucial aspects mentioned above and which influence the efficiency of charging and discharging processes of PCMs.

2.4 Objectives of the research

The aim of this review was to examine the current state of art in order to delineate the required further development of a high temperature model of SiC shell coated PCM. The parameters involved in the process of loading and releasing of thermal energy have to be investigated and adjustments to improve the material's heat flux behaviour have to be determined.

This work is leading to focus on the study of one major thermal storage parameter: the rate of loading and releasing of energy in PCMs coated by ceramic shell, and the logical extension of this general work results in the study of (i) the metal foam structure characterization, (ii) the analysis of the composites' thermo-mechanical behaviour, and (iii) the combination of these two particular topics to accurately analyse and predict heat transfer processes through a SiC shell coating PCMs.

Current research related to heat transfer enhancement by encapsulating PCMs at high temperatures relies only on experimental studies that were developed without the aid of mathematical and numerical modelling (Maruoka and Akiyama, 2003).

In order to achieve our objectives, research must analyse the thermo-mechanical stress in a ceramic shell in order to quantify the influence of stress boundary effects on the integrity of the material. Additionally, it has to determine the latent heat storage response to a SiC shell mechanical characterization subjected to high temperature heating conditions during normal operation of loading and releasing of thermal energy in salts. The research has to be carried out by linking each methodology duly selected and adapted for the above-mentioned analysis, to then improve the knowledge and insight of heat transfer processes in SiC shell coating PCMs.

SiC ceramics have in general a good thermal conductivity, but it is not enough to consider SiC as good materials because graphite has also excellent conductivity. Then we can also consider the good mechanicals properties as stiffness of SiC to support high volume expansion

without cracking which is one problem of graphite matrix. Manufacturing SiC as coating shell is correct way to improve their thermo-mechanical properties.

3 THERMO-MECHANICAL ANALYSIS OF CERAMIC ENCAPSULATED PHASE-CHANGE-MATERIAL (PCM) PARTICLES.

As discussed in Chapter 2, thermal energy storage (TES) is of growing importance, and involving both the storage of sensible and latent heat, offering major benefits towards the overall efficiency of the process. Latent heat storage is indeed particularly attractive, since it can store the energy as the latent heat of fusion at a constant temperature, thus providing a high energy storage density. The low temperature encapsulated phase change materials (PCM) for building applications have been extensively investigated mostly in rigid cells. This form of latent heat storage is already used in buildings, based mostly on paraffins. A different solution uses microcapsules that significantly increase the surfaces, or for industrial applications, macro-encapsulation whereby steel or graphite fins with good thermal conductivity are arranged in-parallel in the storage material thus ensuring efficient heat transfer.

A final solution relies on covering appropriate latent heat materials with an inert rigid or elastic shell. The compound particle, commonly referred to as PCM-particle, has the broadest application since it can be used in fixed, moving or fluidized bed heat capturing systems. These PCM-particles are not yet available commercially. It is however important to determine the behaviour of these compound particles in a heat storage systems, both thermally and mechanically. Determined characteristics and limitations will then help direct the manufacturing of PCM particles.

The present chapter therefore studies the encapsulation of salts PCM material within elastic shells. The mechanical feasibility of such a spherical shell coating of a melting material is first investigated. The influence of encapsulation on the melting process of PCMs is thereafter studied for this particular geometrical case, including the complex interactions with the melting temperature of PCMs. The stored energy and pressure variation due to the volume change during the melting process are examined. It is shown that the encapsulated PCMs particles can

melt without cracking the coating shell only under specific conditions. These conditions are of paramount importance in the successful development and production of PCMs.

3.1 Introduction

The layout of the present chapter is illustrated in Figure 18. Each of the parallel and successive topics is subsequently dealt with. Essential parts of this chapter were adapted and published before the present thesis was completed. Published paper is attached in the appendices.

Figure 18: Layout of the chapter 3

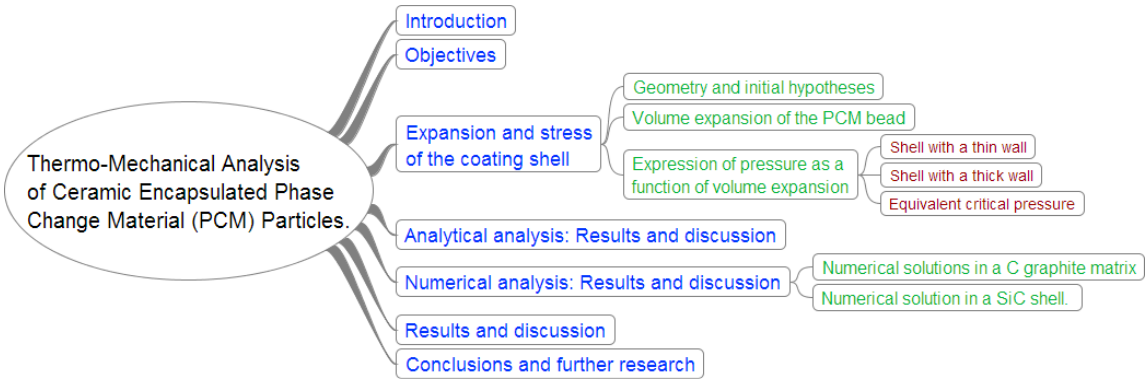

As seen in the first chapter of the present thesis, high temperature thermal energy storage (HTTES) plays a vital role in renewable energy and waste heat recovery. Although there is a wide range of industrial applications, most HTTES usages are found in solar thermal technologies (Gil et al., 2010; Tamme et al., 2008), aerospace applications (Chow, 1996), the steelmaking industry (Maruoka *et al.*, 2002). One of HTTES solutions proposed is using latent heat of phase change materials (PCM); different salts are used as PCMs, since they are cheap, available in large quantities, and have good thermal storage properties (Regin *et al.*, 2008). Despite these advantages, salts have low thermal conductivities, leading to slow heat charging and discharging rates with low heat energy storage efficiency (Agyenim *et al.*, 2010).

In order to increase the thermal conductivity, several heat transfer enhancement techniques have been studied (Agyenim et al., 2010; Bauer et al., 2006), such as mixing graphite and nitrate salts under isotropic pressure (Morisson et al., 2008; Pincemin et al., 2008a, 2008b). The graphite has naturally good thermal properties, and its mixture with nitrate salts compensates the low thermal conductivity of PCM (Afanasov et al., 2009; do Couto Aktay et al., 2008). This

composite material has been widely studied by Lopez *et al*. (2008, 2010), and referred to as graphite encapsulated PCM salt. This studied composite is considered as a solid sphere of PCM nitrate salts encapsulated in a thick shell of graphite (Figure 19). Since the graphite shell is part of a plain material, it is modelled as an elastic material with a mobile internal wall and a non-moving symbolic external wall, leading to variations of melting temperature, enthalpy and energy function of this modelled sphere.

Figure 19: Salt bead coated in a Graphite matrix (Lopez *et al.*, 2010).

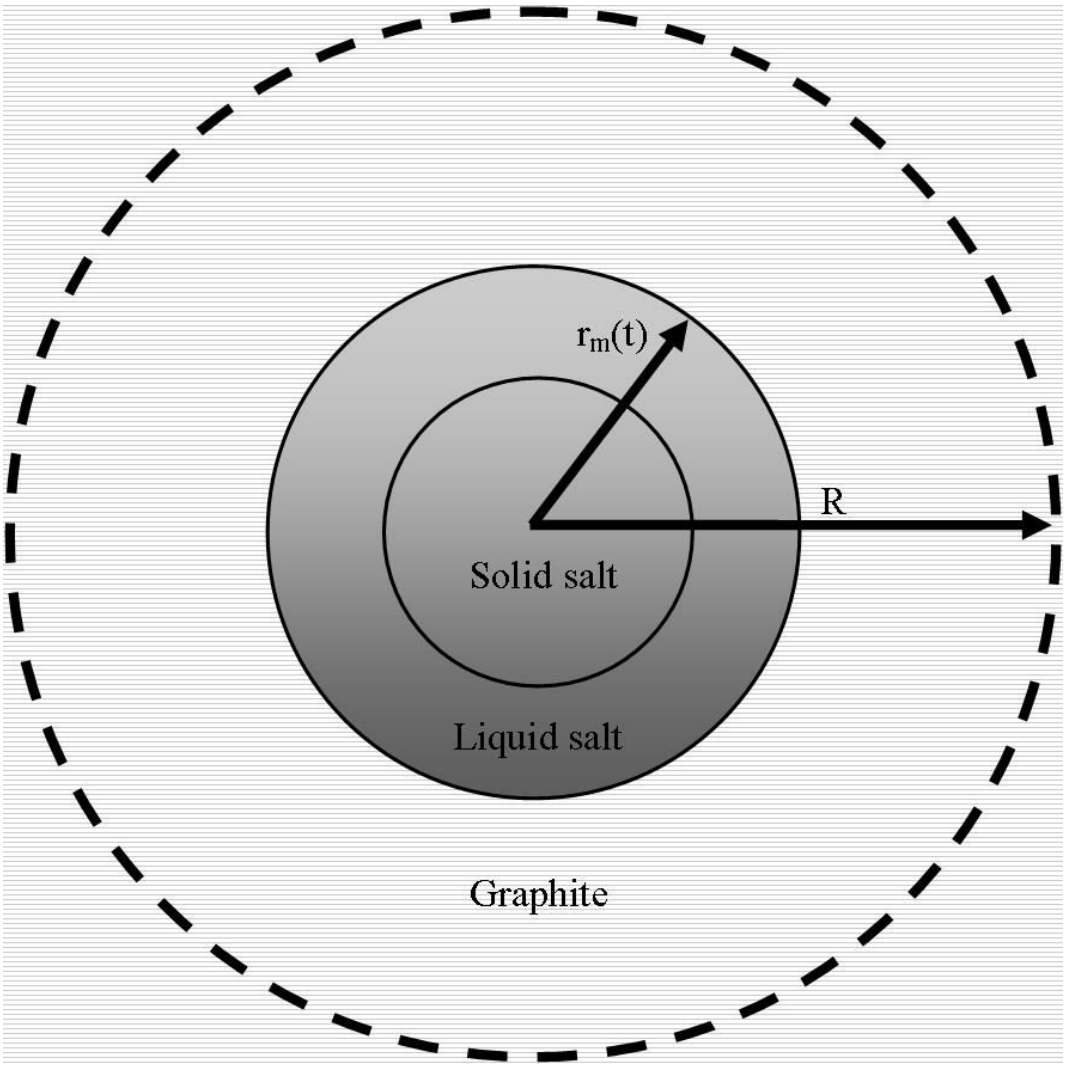

The current research further develops the model of the closed solid sphere proposed by Lopez *et al.* (2010), and their results have been used to verify the code used in the current chapter. The starting hypotheses are thereafter extended to a shell of Silicon Carbide (SiC) with a free mobile external wall, as illustrated in Figure 20.

Figure 20: Salt particle coated in a ceramic shell.

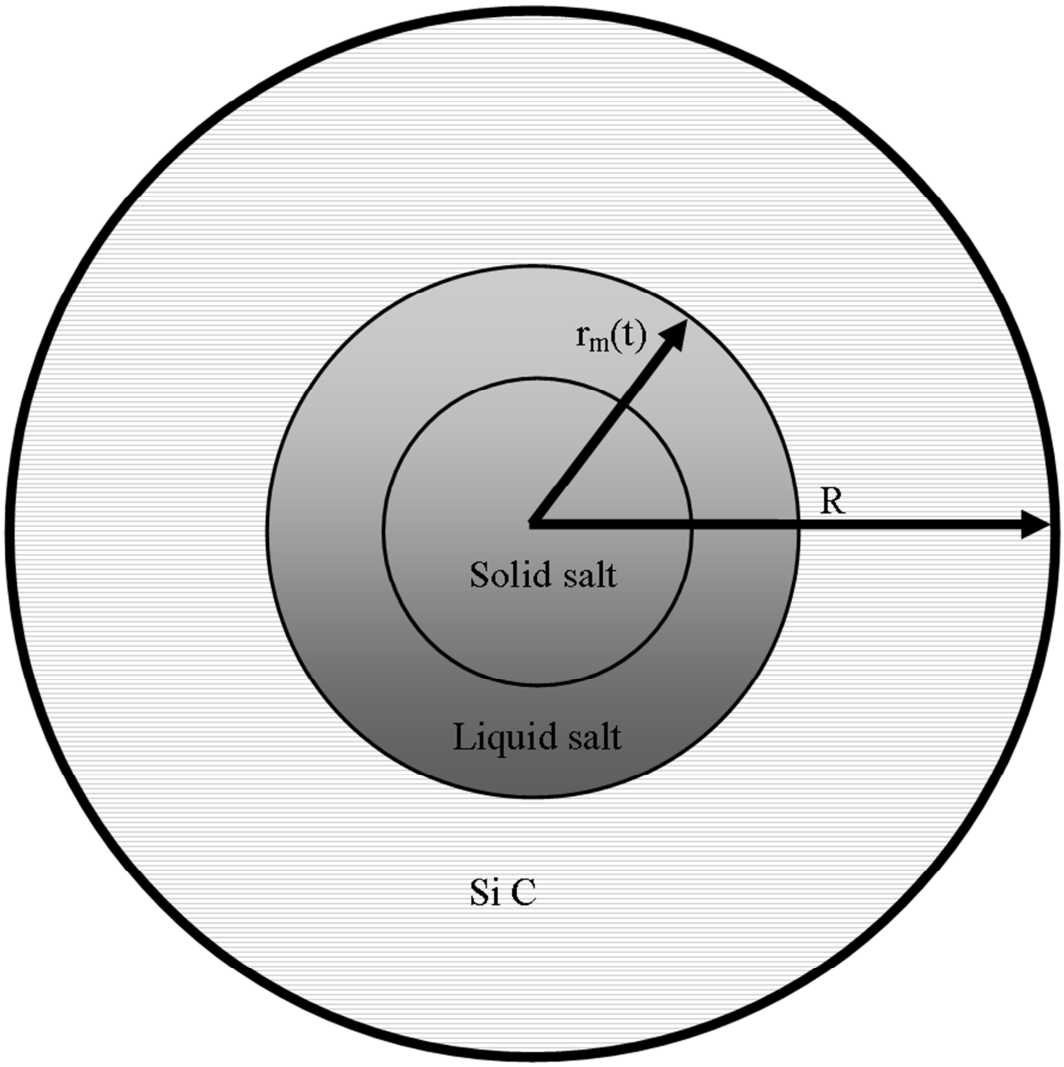

Encapsulating a salt bead (diameter ≈ 1mm) into a SiC shell as a HTTES material is proven to be more efficient for heat transfer by increasing the surface area of heat exchange (Bezian *et al.*, 2007; Bounaceur *et al.*, 2007). Because the SiC shell is a free surface, no strain and displacement are imposed on the external wall as initial conditions (Figure 20).

SiC is already used in nuclear energy processes as a coating material: it protects fissionable fuel material from the chemical corrosive and mechanical erosive environment (Alkan *et al.*, 2001). The better mechanical strength, extreme chemical resistance, and high thermal conductivity of SiC compared to graphite (Zhu *et al*., 1999) could offer major advantages when coating PCM pellets with SiC.

The mechanical stress analysis of a shell under inner pressure due to the volume expansion of a coated material has already been studied, and the work of e.g. Maruoka and Akiyama (2003) assesses the thermal-stress while the coating material is strained by the volumetric expansion of the melting PCM. In the research of Maruoka *et al.* (2002), the PCM is a pellet of lead or copper encapsulated by a nickel coating shell. The experiments and modelling evaluate the required conditions to avoid the cracking of the shell under the inner pressure, without considering the heat storage efficiency of the PCM. The coating material has an elastoplastic behaviour while the SiC shell of the present study has a pure elastic behaviour.

Upadhyaya *et al.* (1985) developed a stress analysis of an egg-shell strained by the volumetric expansion of its content, whereby the thermo-elastic behaviour of the coating is modelled by applying a thin shell theory. Upadhyaya *et al.* showed that it is possible to use Hooke's laws to make a simple model of the full-filled shell stress-strain behaviour. The difference of the current chapter with that of Upadhyaya *et al.* is that the eggshell does not coat a PCM. This study is used as a first step to model the SiC shell fully filled with a melting PCM.

The thermo-mechanical behaviour of encapsulated PCMs has not yet been fully studied for HTTES purposes. Encapsulation of free PCM particles may be a solution to increase the low thermal conductivity and protect the salt, with a coating film of silicon carbide (SiC) being a possible example (Alkan *et al.*, 2001). The high thermal resistance of such a material would protect the PCM of aggressive external conditions, although the coating is subjected to volumetric expansion. The aim of this work is to investigate the thermo-mechanical conditions for an elastic material shell as coating of PCM without cracking. This attempt studies the thermo-dependent mechanical model of a PCM sphere with a SiC coating in a free surface shell rather than with fixed walls.

3.2 Objectives

The main objective is to provide a thermo-mechanical model to describe the behaviour of a free spherical PCM coated by SiC.

Previous work of Lopez *et al.* presents a model of confined melting in composite materials made of graphite and a PCM (Figure 19) (Lopez *et al.*, 2010). The present work extends it to PCM coated by SiC (Figure 20). This modelling defines respectively (i) stress and expansion of the coating shell, and (ii) inner pressure, melting temperature, enthalpy, isentropy, and total energy of the coated particle. The final target is to design and proportion a SiC encapsulation of PCM by using the modelled strengths.

3.3 Expansion and stress of the coating shell

The geometry of the problem and the analysis of the stress-strain behaviour of the shell are developed for three different cases. The first spherical shell with a fixed external wall as presented in the work of Lopez *et al.* is used as a reference to validate our code (Lopez *et al.*, 2010). Then a thermo-mechanical stress analysis with the thin shell theory is used to express the inner pressure function of volumetric expansion (Upadhyaya *et al.*, 1985). The Lame's equations, extended to a thick spherical shell (Eslami *et al.*, 2005), are then used to develop a more accurate model. Finally, the maximum pressure supported by a thick shell is calculated with the Von Mises' yield criterion or octahedral shear stress criterion (Pellissier Tanon, 1988). This criterion is valid for ductile material and is not appropriate for brittle material such as SiC. However, as developed in section 3.3.3, the choice of this criterion was made in order to reduce the maximum stress limit for the modelling of the material mechanical behaviour.

3.3.1 Geometry and initial hypotheses

The geometry of a coated particle is shown in Figure 19. The study develops the model of a salt spherical particle coated in a graphite shell with a non-moving external wall $\left(\frac{R(t)}{dt} = 0\right)$ to validate the code using the results of Lopez *et al.* (2010). The current work thereafter uses a silicon carbide (SiC) free surface shell instead of the graphite fixed wall.

The present chapter uses the hypotheses of Lopez *et al.* (Figure 19) to validate the code thanks to the study of the non-moving external wall of the graphite coating shell (Lopez *et al.*,

2010). The main hypotheses applied in the model of Lopez concerning the liquid phase of the salt are:

a) The density ρ_l, specific heat c_{pl} and thermal conductivity λ_l are constant, independent of pressure and temperature.
b) The liquid pressure within the shell is uniform
c) As a result of the salt viscosity in its liquid state ($\sim 6 \times 10^{-3} kg.m^{-1}.s^{-1}$) and shell size ($\sim mm$), convective heat transfer will be negligible;
d) The viscous energy dissipation is also neglected.

For the salt in the solid state it is assumed that:

e) It can be considered as homogeneous, with constant values of density ρ_s, specific heat c_{ps} and thermal conductivity λ_s,
f) It is non-deformable.

The shell wall (graphite or silicon carbide) is considered to be:

g) homogeneous, isotropic and exhibiting a linear elastic behaviour;
h) at known and uniform temperature.

At the interfaces, the following conditions are proposed:

i) an equality of phases temperature and heat flux continuity at the melting front;
j) an equality of temperature and pressure at the graphite/salt interface.

Spherical symmetry coming from hypotheses b) and h) allows reducing the original three-dimensional problem of transfer to a one-dimensional one (Lopez *et al.*, 2010).

In the present work, the new hypothesis of a SiC shell with an external free surface does not modify any other hypotheses.

3.3.2 Volume expansion of the PCM bead

In the different following cases, the volume expansion of the PCM at a time t is:

$$\Delta V = V_l + V_s - V_{s0} = V_{s0}\left(\frac{\rho_s - \rho_l}{\rho_l}\right) f^* \tag{3.1}$$

with $V_s = V_{s0}(1 - f^*)$ where $f^*$is, at a time t, the fraction of the initial volume of salt V_{s0} which has been molten (molten salt fraction in the following), and ρ_i $(i = [s, l])$ represents the phase density (Lopez *et al.*, 2010).

3.3.3 Expression of pressure as a function of volume expansion

In a shell with a non-moving external wall, the initial radius$R$ is supposed to be fixed; the internal wall, i.e. initial radius r_{m0}, is under a uniform increasing pressure due to the volume expansion of the melting salt (ΔV). From the hypotheses that the wall is homogeneous, isotropic and showing a linear elastic behaviour and that the liquid pressure within the shell is uniform, the inner pressure is:

$$P = P_0 - K\frac{V_m - V_{m0}}{V_{m0}} = V_{s0}\left(\frac{\rho_s - \rho_l}{\rho_l}\right) f^* \tag{3.2}$$

where P_0 represents the initial shell pressure (atmospheric), K is the bulk modulus of the shell wall, V_{m0} is the initial volume of the wall (before its deformation) and V_m is the wall volume at shell pressure P (Lopez *et al.*, 2010).

$$\Delta V = -(V_m - V_{m0}) \tag{3.3}$$

Introducing this expression in equation (3.1) yields:

$$P(t) = P_0 + K\left(\frac{\rho_s - \rho_l}{\rho_l}\right)\left(\frac{V_{s0}}{V_{m0}}\right) f^*(t) \tag{3.4}$$

This equation allows calculating the pressure in the closed graphite non-moving wall shell as a function of the fraction of molten salt in the model (Lopez *et al.*, 2010). The current work

uses this formula as a basis to validate the used code. Once the code is validated for a non-moving external wall, the next step is to extend it to a moving wall.

3.3.3.1 Shell with a thin wall

The second case is a free surface thin shell. The external wall is no longer fixed, R can increase. The thin shell theory is used to validate the change in the code between moving and non-moving wall. The thin shell theory is a classical approximation in mechanical studies when the shell thickness is a maximum 10% of the inner radius (Upadhyaya *et al.*, 1985).

According to the thin shell model (Upadhyaya *et al.*, 1985), the relation between pressure and volume variation is:

$$\Delta V = 3\, V_{s0} \left(\alpha \Delta T + P \left(\frac{1-\nu}{2\, \mathrm{E}_y} \right) \left(\frac{r_{m0}}{R - r_{m0}} \right) \right) \tag{3.5}$$

with the value of ΔV from equation (3.1) it becomes:

$$P(t) = \frac{2}{3} \left(\frac{E_y}{1-\nu} \right) \left(\frac{R - r_{m0}}{r_{m0}} \right) \left(\frac{\rho_s - \rho_l}{\rho_l} f^*(t) - 3\, \alpha\, \Delta \mathrm{T} \right) \tag{3.6}$$

where E_y, ν, α, and ΔT are, respectively, the Young's modulus, the Poisson's ratio, the coefficient of linear expansion, and the change of temperature of the shell material, R and $\mathrm{r_{m0}}$ are, respectively, the external and the internal radius of the shell. This equivalence is true under the condition of thin shells, i.e. $r_{m0} \gg R - r_{m0}$.

This equation allows calculating the pressure in the closed SiC free surface shell as a function of the fraction of molten salt in the model. The current work uses this formula to validate its code for a free surface SiC shell. Once the code is validated for a thin shell, the next step is to extend it to a thick shell to increase the accuracy of the model.

3.3.3.2 Shell with a thick wall

In the case of a thick shell, the Lamé's equations are solved without ignoring the radial component of the stress. The approximation of the mechanical model of the current work is more accurate.

In a spherical coordinates system r, θ, ϕ, the studied volume has a spherical symmetry, and it includes a homogenous and isotropic material; the boundary conditions have also a spherical symmetry. In this case, the displacement, strain, and stress fields are:

$$\begin{cases} u = u_r = f(r) \\ u_\theta = u_\phi = 0 \end{cases} \tag{3.7}$$

$$\begin{cases} \varepsilon_{rr} = g_1(r) \\ \varepsilon_{\theta\theta} = \varepsilon_{\phi\phi} = g_2(r) \\ \varepsilon_{r\theta} = \varepsilon_{r\phi} = \varepsilon_{\phi\theta} = 0 \end{cases} \tag{3.8}$$

$$\sigma_{rr} = h_1(r), \sigma_{\theta\theta} = \sigma_{\phi\phi} = h_2(r), and \sigma_{r\theta} = \sigma_{r\phi} = \sigma_{\phi\theta} = 0 \tag{3.9}$$

The strain-displacement relations are:

$$\begin{cases} \varepsilon_{rr} = u' \\ \varepsilon_{\theta\theta} = \dfrac{u}{r} \end{cases} \tag{3.10}$$

where $(')$ denotes differentiation with respect to r (Eslami et al., 2005). The stress-strain relations are:

$$\begin{cases} \sigma_{rr} = \lambda(\varepsilon_{rr} + 2\varepsilon_{\theta\theta}) + 2\mu\varepsilon_{rr} - (3\lambda + 2\mu)\alpha\Delta T \\ \sigma_{\theta\theta} = \lambda(\varepsilon_{rr} + 2\varepsilon_{\theta\theta}) + 2\mu\varepsilon_{\theta\theta} - (3\lambda + 2\mu)\alpha\Delta T \end{cases} \tag{3.11}$$

where λ and μ are Lamé constants related to the modulus of elasticity E_y and Poisson's ratio ν as

$$\lambda = \frac{\mathrm{E}_y \nu}{(1+\nu)(1-2\nu)} \qquad \mu = \frac{\mathrm{E}_y}{2(1-\nu)} \tag{3.12}$$

(Eslami *et al.*, 2005). The equilibrium equation in the radial direction, disregarding the body force and the inertia term is

$$\sigma_{rr}{}' + \frac{2}{r}(\sigma_{rr} - \sigma_{\theta\theta}) = 0 \tag{3.13}$$

The boundary conditions are:

$$\sigma_{rr}(r = r_{m0}) = -P, \text{ and} \sigma_{rr}\ (r = R) = 0 \tag{3.14}$$

Solving the equations (3.7) to (3.12), and with the boundary conditions (3.14), yields the elastic description of the system as:

$$u\ (r) = r\ \Delta T\alpha + \frac{r_{m0}^3}{R^3 - r_{m0}^3}\left(\frac{R^3}{4\,r^2\mu} + \frac{r}{3\,\lambda\ +\ 2\,\mu}\right)P \tag{3.15}$$

$$\varepsilon_{rr}\ (r) = \Delta T\alpha\ + \frac{r_{m0}^3}{R^3 - r_{m0}^3}\left(-\frac{R^3}{2\,r^3\mu} + \frac{1}{3\,\lambda\ +\ 2\,\mu}\right)P \tag{3.16}$$

$$\varepsilon_{\theta\theta}\ (r) = \Delta T\alpha\ + \frac{r_{m0}^3}{R^3 - r_{m0}^3}\left(\frac{R^3}{4\,r^3\mu} + \frac{1}{3\,\lambda\ +\ 2\,\mu}\right)P \tag{3.17}$$

$$\sigma_{rr}(r) = -\ \frac{r_{m0}^3}{R^3 - r_{m0}^3}\left(\frac{R^3}{r^3} - 1\right)P \tag{3.18}$$

$$\sigma_{\theta\theta}(r) = \frac{r_{m0}^3}{R^3 - r_{m0}^3}\left(\frac{R^3}{2r^3} + 1\right)P \tag{3.19}$$

For $r = r_{m0}$, the volume displacement is written:

$$\Delta V = \frac{4}{3}\pi\left(\left(r_{m0} + u(r_{m0})\right)^3 - r_{m0}^3\right) \tag{3.20}$$

re-arranged using equation (3.1):

$$u(r = r_{m0}) = r_{m0}\left(\sqrt[3]{\frac{\rho_s - \rho_l}{\rho_l}f^*(t) + 1} - 1\right) \tag{3.21}$$

which combined with equation (3.15) gives:

$$P(t) = \frac{2(R^3 - r_{m0}^3)\mathrm{E}_y\left(\sqrt[3]{\frac{\rho_S - \rho_l}{\rho_l} f^*(t) + 1} - (1 + \alpha\,\Delta\mathrm{T})\right)}{r_{m0}^3(1+\nu) + R^3(2-4\nu)} \quad (3.22)$$

This equation allows calculating the pressure in the closed SiC free surface shell as a function of the fraction of molten salt in the model. Once the code is validated for a thick shell, the next step is to estimate the critical pressure that will make the shell crack.

3.3.3.3 Equivalent critical pressure

Under a maximum stress, the shell will crack and loose the encapsulated PCM (Maruoka and Akiyama, 2003). According to the Von Mises criterion, the yield condition of pressure, named equivalent pressure P_e, in the shell is:

$$P_e = \frac{2}{3}\left(1 - \frac{r_{m0}^3}{R^3}\right)\sigma_y \quad (3.23)$$

where σ_y is the yield strength of the coating material (Gao, 2003). The Von Mises' criterion describes the stress equivalent to the elastic limit of the material. Choice is made of this criterion in order to have a factor of safety for the maximum stress the shell can take. The Von Mises' criterion is always a smaller value than maximum principle stress, but it is aligned in the direction that has to support the maximum shear load (Pellissier Tanon, 1988). According to the fact that ceramics are non-plastic materials at room temperature, the tensile strength is taken as yield strength.

It is however important to mention that the criterion of Von Mises has only been validated for metals. Since the calculations are developed for a PCM encapsulated with a ceramic coating, supposed to be homogeneous, the application of the Von Mises criterion seemed plausible. Moreover the 3-dimensional nature of the calculation seemed most appropriate for the spherical geometry under consideration. Certainly the basis of Von Mises can be questioned towards the supposedly homogeneous ceramic encapsulation, but it is the only scientific approach available, and results of the calculations confirm what is normally expected for a coated particle. If

encapsulated PCM particles were available at the time of this study, the fracture limit could have been determined and compared with the Von Mises criterion. Unfortunately, E-PCMs are still in full development, and it was recently announced that a first production of E-PCMs was examined by Terranova (USA), only at a research stage, but with good prospects of further development.

Knowing this criterion, the hypothesis is that the maximum tensile strength is reached at the maximum volumetric expansion i.e. when all the PCM is molten ($f^*(t) = 1$). For fixed PCM material properties and volume, and fixed coating material properties, the external radius R, chosen as a variable, can be optimised to reduce the shell stress to the minimum value possible. Then, solving the equation $P(R)=P_e(R)$, for any values of t, gives:

$$R_{min0} = \sqrt[3]{\frac{4\nu - 2}{3\frac{E}{\sigma_y}\left(1 + \Delta T\,\alpha - \sqrt[3]{\frac{\rho_{s0}}{\rho_{l0}}}\right) + (1 + \nu)}}\, r_{m0} \tag{3.24}$$

R_{min0} is the minimum value of the external radius of the shell under the maximum acceptable pressure P_e that prevents the shell from cracking. The condition for the existence of the shell is then $\frac{R_{min0}}{r_{m0}} > 1$ which, according to (5.24), can be simplified as:

$$\sqrt[3]{\frac{\rho_{s0}}{\rho_{l0}}} < 1 + \Delta T\,\alpha + (1 - 5\nu)\frac{\sigma_y}{3E_y} \tag{3.25}$$

This final criterion expresses the fact that the spherical shell will not crack under the condition that the change of densities of the melting PCM, written $\sqrt[3]{\frac{\rho_{s0}}{\rho_{l0}}}$, is less than the combination of the thermo-mechanical properties of the shell material.

In the current work, the mechanical stress analysis of the spherical shell proceeds according to three steps:

(i) The study from the work of Lopez *et al.* (2010) gives the relation between volume expansion and inner pressure of a graphite shell with a non-moving external wall. The current work takes this expression as a basis to start the discussion about a free surface particle.

(ii) The relation between volume expansion and inner pressure of a SiC shell with a moving external wall is calculated using the theory of thin shells. This relation is used to estimate the mechanical behaviour of the shell.

(iii) A more accurate description is given by the thick shell model. The maximum pressure that the shell can support before cracking is estimated using the von Mises criterion. This estimation is used to calculate the minimum external radius possible. The condition of existence of this external radius is used to set a thermo-mechanical criterion for SiC coating of PCM.

The new description of pressure as a function of the fraction of molten salt in a SiC shell is used to compare the thermal behaviour of PCM in two case: one with a graphite non-moving external wall shell, and one other with a SiC thick shell.

3.4 Full description of PCM in a closed shell at thermodynamical equilibrium

Equations governing salt melting of a solid sphere (Figure 19) are established in the research of Lopez *et al.* (2010): the external shell radius is noted R and is assumed to be constant during melting. This hypothesis is due to the geometry chosen of a graphite matrix. In the current chapter with a selected free surface SiC shell, R is not constant. Both cases are reproduced in the following demonstration. The position of the shell/salt interface and the melting front at time t are referred as $r_m(t)$ and $r_f(t)$ respectively (Lopez *et al.*, 2010).

The different variables of a first order solid↔liquid transformation were demonstrated (Lopez *et al.*, 2010), and the approach deals with simple univariant equilibrium because no

component changes occur during the transformation. In that case, both phases exist along a single curve in the temperature-pressure domain (*T,P*) (Lopez *et al.*, 2010).

The system of PCM encapsulated in a closed shell is fully described by the following equations (Lopez *et al.*, 2010):

The conservation of energy is written:

$$\frac{\partial\left[\left(\rho c_p\right)_{eq} T(r,T)\right]}{\partial t} = \frac{1}{r^2}\frac{\partial}{\partial r}\left(\lambda_{eq} r^2 \frac{\partial T(r,t)}{\partial r}\right) - \rho_s \Delta h_m \frac{df_s(r,t)}{dt} \tag{3.26}$$

where $\left(0 < r < r_m(t)\right)$, $\left(\rho c_p\right)_{eq}$ and λ_{eq} are, respectively, the equivalent heat capacity and the equivalent thermal conductivity. They are given by:

$$\begin{cases} \left(\rho c_p\right)_{eq} = \rho_l c_{pl}(1 - f_s) + \rho_s c_{ps} f_s \\ \lambda_{eq} = \lambda_l(1 - f_s) + \lambda_s f_s \end{cases} \tag{3.27}$$

Boundary conditions of the problem are:

$$\forall t, \begin{cases} T(r,t) = T_m(t) r = r_m(t) \\ -\lambda_{eq} \left.\dfrac{\partial T(r,t)}{\partial r}\right|_{r=0} = 0, r = 0 \end{cases} \tag{3.28}$$

where $T_m(t)$ is the temperature of the shell wall (assumed to be known and uniform).

With the solid fraction $f_s(r,t)$:

$$f_s(r,t) = 0.5\left[\tanh\left(\frac{T_m(P) - T(r,t)}{\Delta T}\right) + 1\right] \tag{3.29}$$

where ΔT defines the interval where the curve is smoothed. The global variables are:

$$f^*(t) = 1 - \frac{3}{r_{m0}^3} \int_0^{r_m(t)} r^2 f_s(r,t)\, \mathrm{d}r \tag{3.30}$$

$$P(t) = P_0 + K\left(\frac{\rho_s - \rho_l}{\rho_l}\right)\left(\frac{V_{s0}}{V_{m0}}\right) f^*(t) \tag{3.31.a}$$

$$P(t) = \frac{2(R^3 - r_{m0}^3)\mathrm{E}}{r_{m0}^3(1+\nu) + R^3(2-4\nu)}\left(\sqrt[3]{\frac{\rho_s - \rho_l}{\rho_l} f^*(t) + 1} - (1 + \alpha\,\Delta\mathrm{T})\right) \tag{3.31.b}$$

The two different expressions of the pressure stem from the different cases studied earlier. The first one describes the pressure in a non-moving external wall shell, and the second expression gives the pressure in a free surface shell.

The displacement of the internal wall is:

$$\Delta r_m(t) = r_{s0}\left[\sqrt[3]{1 + \frac{\rho_l - \rho_s}{\rho_s} f^*(t) - 1}\right] P \tag{3.32}$$

$\Delta r_m(t) = r_m(t) - r_{m0}$ represents the displacement of the interface graphite/salt with respect to its initial position $r_{m0} = r_{s0} = r_m\ (t = 0)$.

The melting temperature function of the pressure equation given by Lopez (2007) is

$$T_m(P) = T_0 + \frac{-b + \sqrt{b^2 - 4ac}}{2a}$$

$$\text{With} \begin{cases} a = -\frac{1}{2}\left(\frac{c_{pl0} - c_{ps0}}{T_0}\right) \\ b = -(s_{l0} - s_{s0}) + \left(\frac{\alpha_{l0}}{\rho_{l0}} - \frac{\alpha_{so}}{\rho_{so}}\right)(P - P_0) \\ c = \left(\frac{1}{\rho_{l0}} - \frac{1}{\rho_{so}}\right)(P - P_0) - \frac{1}{2}\left(\frac{\beta_{l0}}{\rho_{l0}} - \frac{\beta_{so}}{\rho_{so}}\right)(P - P_0)^2 \end{cases} \tag{3.33}$$

values of parameters s_{l0}, s_{s0}, ρ_{l0}, ρ_{s0}, c_{pl0}, c_{ps0}, α_{l0}, α_{s0}, β_{l0}, and β_{so} are usually available in standard thermodynamic data bases.

The relationship between both enthalpy and entropy function of the pressure at thermodynamic equilibrium is:

$$\Delta h_m(T_m, P) = -\Delta s_m(T_m, P)T \tag{3.34}$$

with:

$$\Delta s_m = (s_{l0} - s_{s0}) + \left(\frac{c_{pl0} - c_{ps0}}{T_0}\right)(T_m - T_0) - \left(\frac{\alpha_{l0}}{\rho_{l0}} - \frac{\alpha_{so}}{\rho_{so}}\right)(P - P_0) \tag{3.35}$$

The equation of density, admitting that values of state of reference are T_0 and P_0, is:

$$\frac{1}{\rho_i} = \frac{1}{\rho_{i0}}[1 + \alpha_i(T - T_0) - \beta_i(P - P_0)] \tag{3.36}$$

Figure 21 shows the relative evolution of the density of molten salt as a function of the fraction of molten salt: $\frac{(\rho_i - \rho_{i0})}{\rho_{i0}}$.

Figure 21: Relative density function of fraction of molten salt

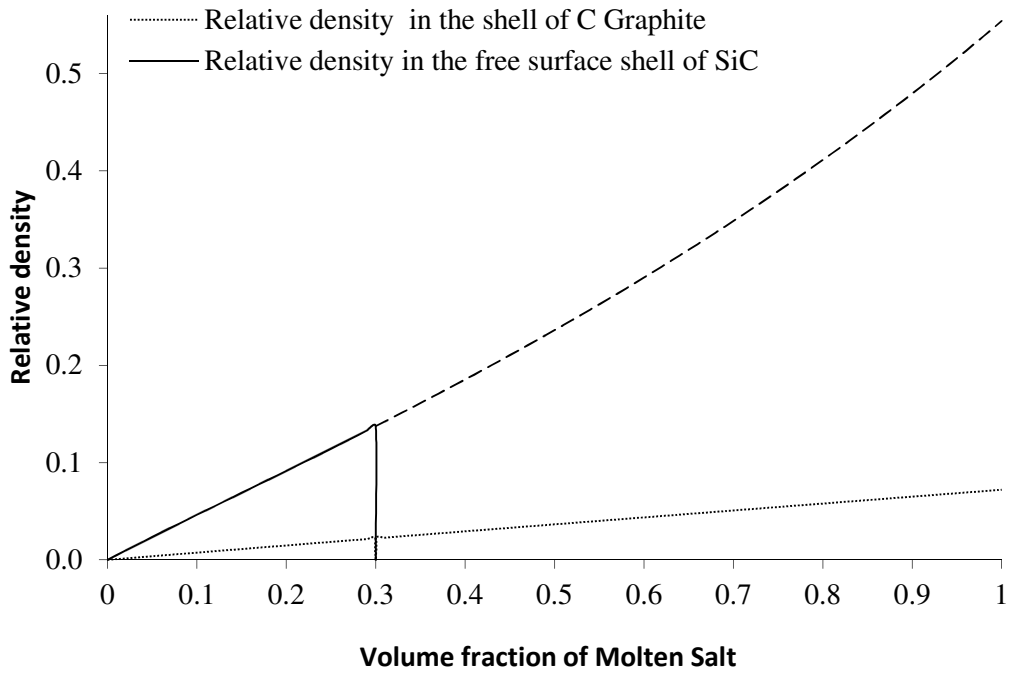

As shown later (Figure 22), and due to the higher mechanical strength of SiC, the inner pressure is 6.3 times higher than in a graphite shell. The density of the liquid phase ρ_l is then increased and is no longer considered as a constant as shown in Figure 21. This graph shows that the variation of density can be ignored at low pressures but not at high pressures.

The full energy stored during the fusion in the shell is given by Lopez *et al.* (2010):

$$E(f^*) = \int_0^{f^*} V_{s0} \frac{\rho_s - \rho_l}{\rho_l} P \, df + \int_0^{f^*} \rho_s V_{s0} \, \Delta h_f \, df + \int_{T(f=0)}^{T(f^*)} V_{s0} \left(\rho_l Cp_l f + \rho_s Cp_s (1-f)\right) dT \tag{3.37}$$

The first term represents the energy used for shell deformation, the second term represents the energy required for melting a volume fraction $f^*$of salt, and the third term is the sensible heat accumulation. This expression intends to describe the ratio of each type of energy in the global system of the PCM closed shell.

The mechanical, thermal and thermo-dynamical behaviour of the PCM coated in a graphite wall or a SiC shell is fully given by the equations listed before. The two behaviours are now analysed and compared.

3.5 Analytical analysis: Results and discussion

In a first attempt to validate the understanding of the Lopez model (Lopez *et al.*, 2010), the thermo-dynamical properties at $P_0 = 10^5 Pa$ of the (KNO_3)/($NaNO_3$) salt are listed in Table 8.

The following calculations will focus on two sets of geometrical and mechanical values of the shell:

- $K_m = 8 \times 10^9 Pa$ representing the graphite matrix properties.
- $E_{SiC} = 476 \times 10^9 Pa, \nu_{SiC} = 0.19$, and $\alpha_{SiC} = 3.810^{-6}\mathrm{K}^{-1}$ representing the SiC shell properties.
- $R = 1.2mm$ and $r_m = 1mm$

Table 8 Properties of (KNO_3)/($NaNO_3$) salt (Lopez *et al.*, 2010, Janz, 1967)

	Properties	Symbol	Value	Unit
Salt in liquid state	Density	ρ_{l0}	2096	$\mathrm{kg.\,m^{-3}}$
	Specific heat	Cp_l	1500	$\mathrm{J.\,kg^{-1}.\,K^{-1}}$
	Compressibility	β_l	1.86E-10	$\mathrm{Pa^{-1}}$
	Thermal expansion	α_l	3.7E-4	$\mathrm{K^{-1}}$
	Thermal conductivity	λ_l	0.8	$\mathrm{W.\,m^{-1}.\,K^{-1}}$
Salt in solid state	Density	ρ_{s0}	2192	$\mathrm{kg.\,m^{-3}}$
	Specific heat	Cp_s	1430	$\mathrm{J.\,kg^{-1}.\,K^{-1}}$
	Compressibility	β_s	0	$\mathrm{Pa^{-1}}$
	Thermal expansion	α_s	0	$\mathrm{K^{-1}}$
	Thermal conductivity	λ_s	1	$\mathrm{W.\,m^{-1}.\,K^{-1}}$
S↔L	Melting temperature at P0	T_{f0}	223	°C
	Melting enthalpy at (Tf0,P0)	Δh_{f0}	105	$\mathrm{kJ.\,kg^{-1}}$

An analytical computation using MATLAB provides a first estimation of the results. The calculation of the inner pressures is illustrated in Figure 22. The inner pressure of the graphite non-moving wall is traced according to eq. 3.31 with the data from the original work of Lopez *et al.* (2010) and Janz (1967), and the original work of Lopez *et al.* (2010) is used as a reference to validate the code. The pressures' equivalent respectively to the tensile strength and the von Mises criterion strength of SiC, i.e. P_e from Eq. (3.23), are traced as to compare the evolution of the inner pressure in the SiC shell to the limits of the material.

Figure 22: Inner pressure of the shell as a function of fraction of molten salt.

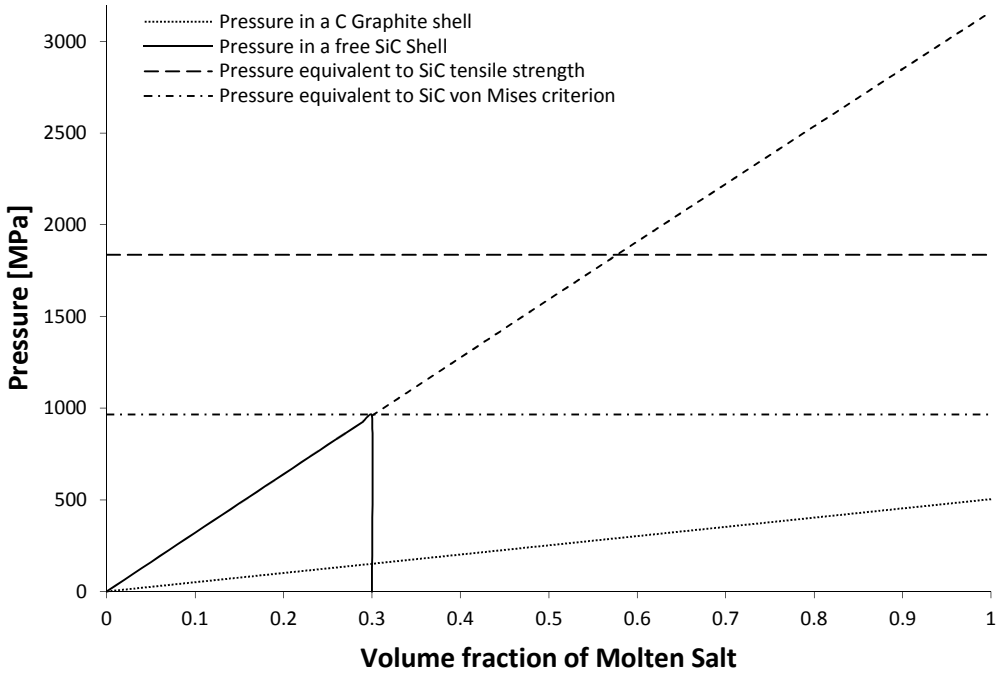

In both cases on Figure 22, the pressures are higher than common ones in use with molten salts. The value of pressure in the graphite is the same as the value presented in the original results. The SiC shell pressure is 6.3 times higher than the pressure in graphite while the ratio of the bulk modulus exceeds 32. The shell shape reduces the inner pressure compared to the non-moving external wall. Once a third of the salt is molten, the shell is strained up to its maximum octahedral shear stress criterion equivalent or von Mises criterion. Later in the chapter, the proportion of molten salt that sets the inner pressure equivalent to von Mises criterion stress is referred to as the cracking limit. The SiC shell presents a maximum pressure when the cracking limit indicates an impossibility to encapsulate a PCM with a SiC coating, and it becomes impossible to consider the PCM trapped in a closed shell anymore.

The following figures are still considering up to 100% of molten salt to compare the SiC case to the graphite one.

While considering the melting temperature from Eq. 3.33 in Figure 23, the theoretical model in the graphite cell is not in conformity with the original model (Lopez *et al.*, 2010). The

maximum melting temperature found here is 567K, lower than in the original result of 574K in Lopez *et al.* (2010). This phenomenon results from the difference between the original values of the compressibility and thermal expansion of liquid salt from Lopez *et al.* (2010) and the values used in the present work. Despite the difference, the increase of melting temperature of the PCM bead coated in a graphite wall is visible. The coated PCM does no longer melt at constant temperature. For achieving a complete melting in the graphite cell, the salt should be heated up to 567 K, while the maximum temperature before the SiC shell cracks is 651 K.

Figure 23: Melting temperature of the PCM as a function of fraction of molten salt.

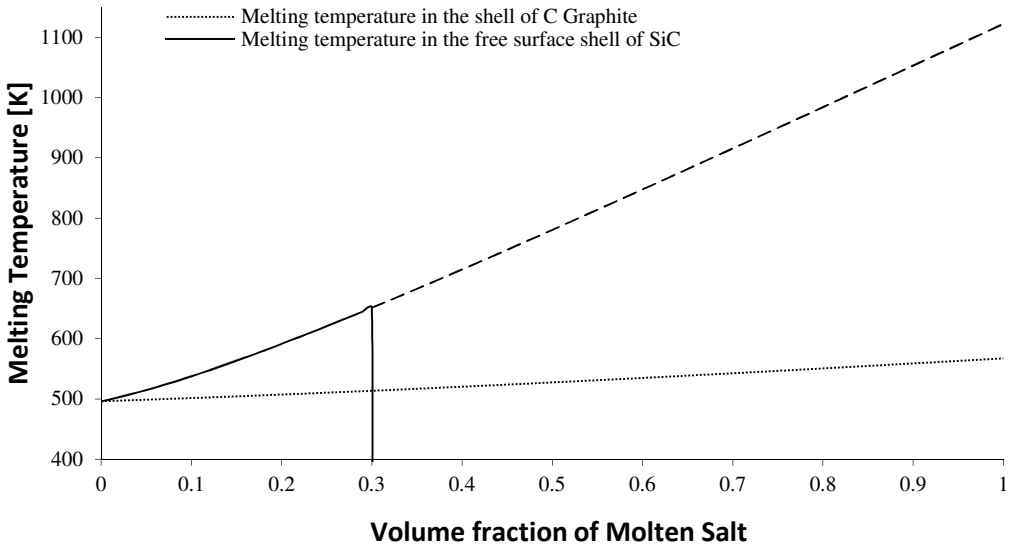

The problem of the higher temperatures needed for a free SiC shell appears. Considering the fact that only a third of the PCM can melt before the shell cracks, the maximum temperature reached by the salt is still below the maximum acceptable temperature for the material.

In Figure 24, the data of latent heat in a graphite shell, from Eq. 3.34, do not match the original model by Lopez *et al.*, (2010) because of the different values for the thermal expansion and the liquid compressibility of the salt. Despite that, this graph shows the same impact of too high a pressure on the latent heat as in the Lopez work (Lopez *et al.*, 2010). As the melting temperature and inner pressure rise, the latent heat decreases. For the SiC shell, until a third of the shell melts, the latent heat decreases by almost 50%. The effect of a loss of latent heat

storage energy is observed, and the high pressures impact it significantly. Once 60% of the salt is molten, the pressure is higher than what PCM is allowing, and it is not capable of melting anymore, which explains the nil latent heat.

Figure 24: Latent heat of the PCM bead as a function of fraction of molten salt.

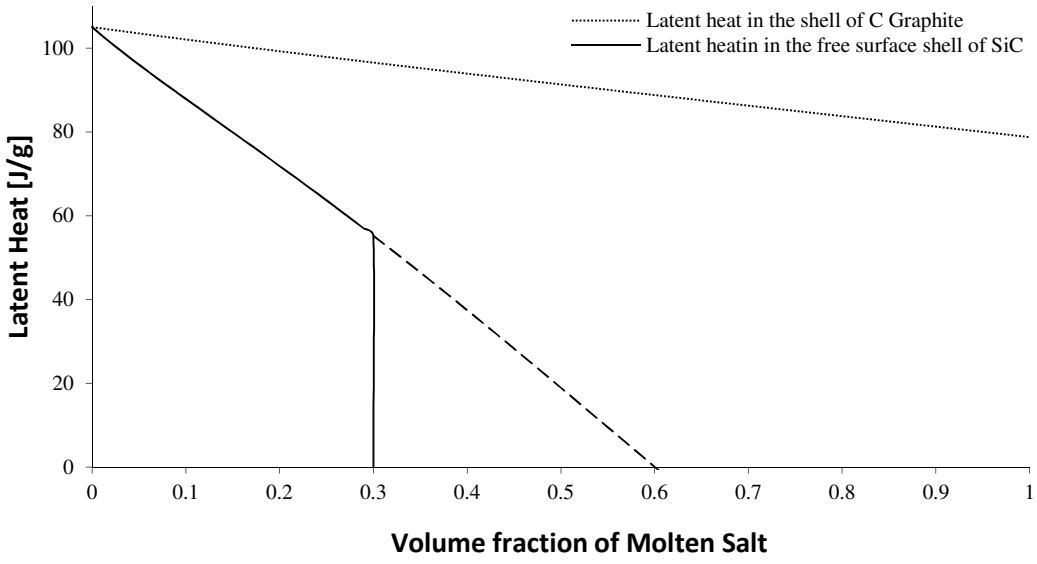

Figure 25 and Figure 26, respectively, illustrate the energy stored within the graphite and SiC shells according to Eq. 3.37.

Figure 25: Energy of the PCM bead coated in a graphite shell as a function of fraction of molten salt.

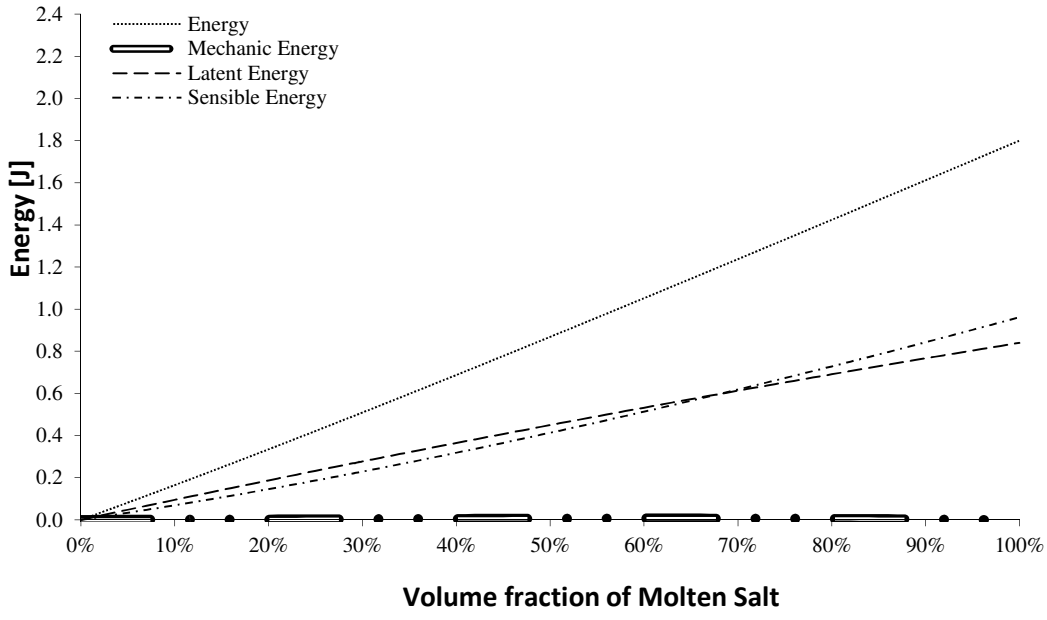

Figure 26: Energy of the PCM bead coated in a SiC shell as a function of fraction of molten salt.

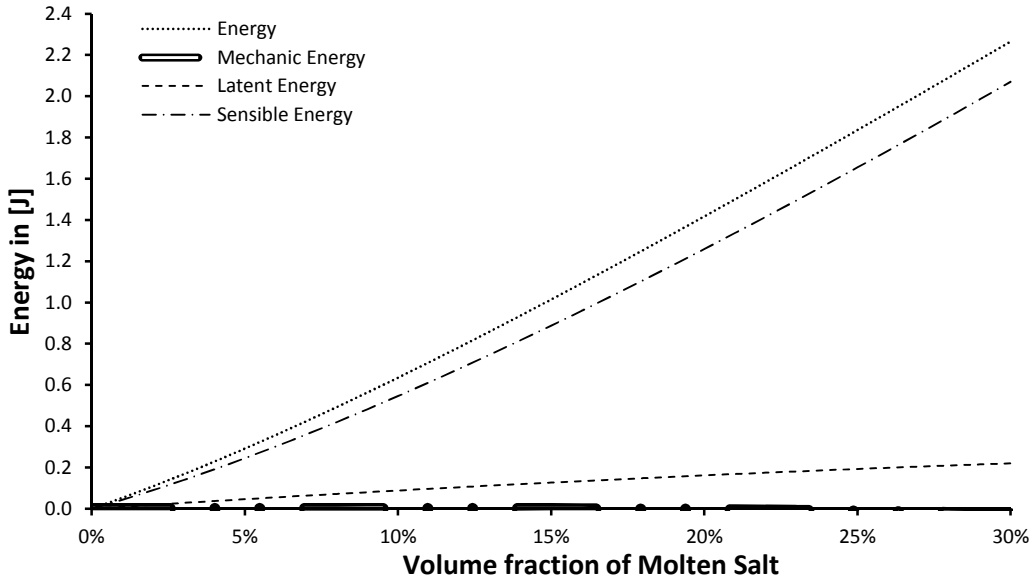

In both types of shell, the mechanical energy is negligible compared to the total energy. Sensible energy and latent energy represent an average identical share of the total of the energy needed to melt a PCM bead coated in a graphite shell. According to Lopez *et al.* (2010), the energy required to melt the bead of PCM coated graphite is higher than an equivalent volume of PCM at constant temperature. In the SiC shell coating, the high pressure renders the capacities of latent heat energy storage of the less efficient, and the sensible energy PCM is more important than the latent one.

The pressure that the SiC shell imposes on the PCM is 6.3 higher than the pressure in a graphite shell. This higher pressure involves an increasing melting temperature, a decreasing latent heat, and a reduction of the energy stored by the PCM bead.

3.6 Numerical analysis: Results and discussion

A second analysis was performed to understand the dynamic thermo-mechanical behaviour of a PCM encapsulated in a SIC shell using COMSOL. COMSOL is an engineering and finite element analysis software. It was used in order to approximate a solution to the equation 3.26 of conservation of energy.

Properties at $P_0 = 10^5 Pa$ of the (KNO_3)/($NaNO_3$) salt used in the numerical analysis are the same than information used with MATLAB and listed in Table 8.

3.6.1 Numerical solutions in a graphite matrix

In order to validate our code, the first solution estimated has the same parameters than previous works of Lopez *et al.* (2010). Evolutions of pressure and temperature function of the proportion of molten salt are the same as those predicted with MATLAB (Figure 22 and Figure 23).

Figure 27 and Figure 28 respectively show the evolution of latent heat and energy functions in terms of the proportion of molten salt. Values calculated using COMSOL are similar to original Lopez values, even if they tend to be different from the MATLAB results. These differences come from the fact that the numerical analysis was performed using the density as a constant and not as a variable. When the model was translated from MATLAB to COMSOL, the density being a variable function of the temperature, it was creating a recursive loop that COMSOL was not able to solve. Therefore, it has been chosen to set the density as a constant parameter in the modelling with COMSOL.

Figure 27: Evolution of the Latent heat function of the proportion of molten salt in a graphite matrix.

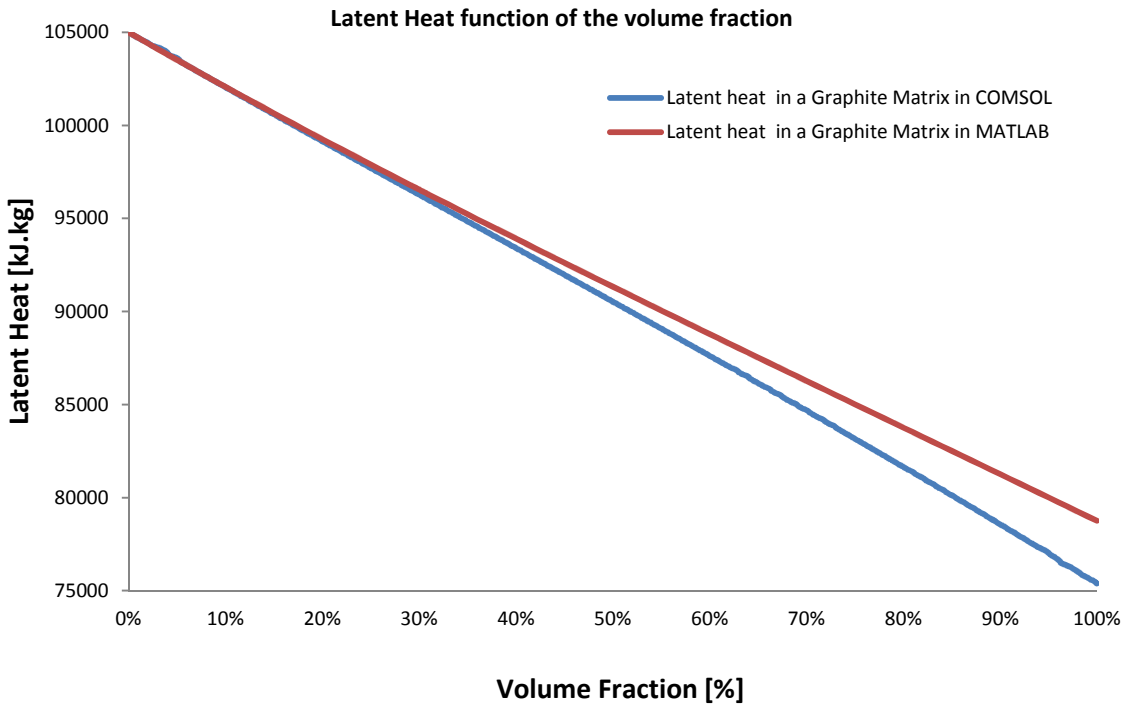

Figure 28: Evolution of energies function of the proportion of molten salt in a graphite matrix.

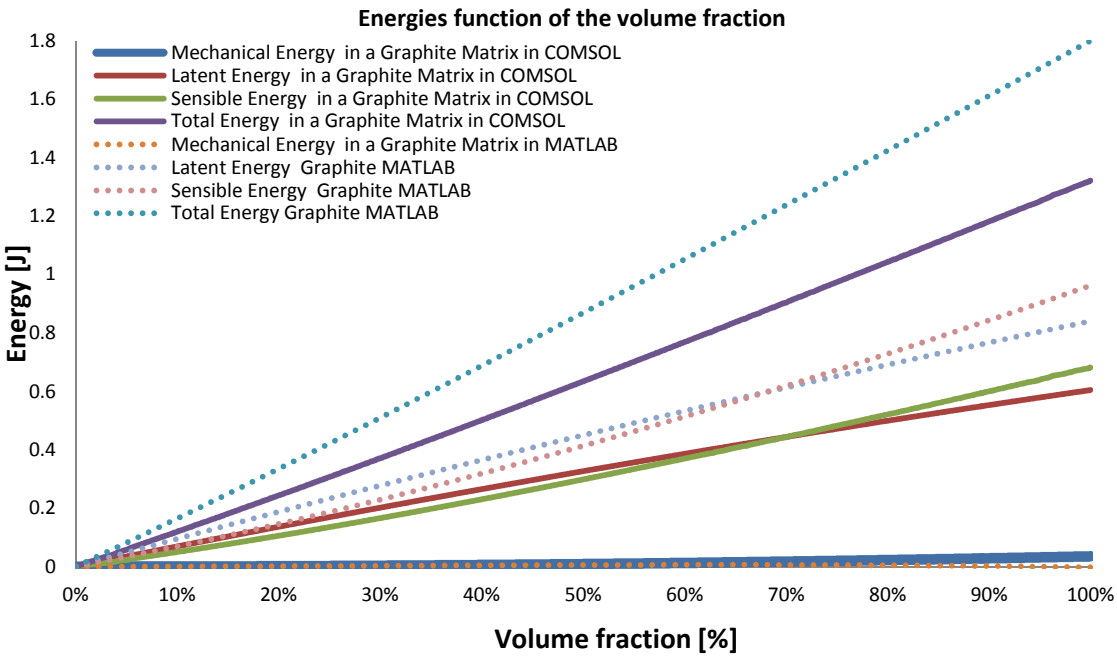

The model described in Section 5 is used for the dynamical simulation of salt melting within a graphite matrix. At time t = 0, the shell is assumed to beat uniform temperature T_{ini} and

pressure P_0. Then the initial heating temperature T_{ini} of the system is set at 150°C,$\forall r, T(r, t = 0) = T_m(t = 0) = T_{ini} < T_f(P_0)$ and $P(t = 0) = P_0$, P_0 being the atmospheric pressure. The temperature of the shell is maintained constant for the first 200 seconds. The constant external temperature is to check the stability of the system before heating. From 200 till 1800 seconds, the temperature is then increased up to 300°C, where after it is constant for the last 200 seconds as illustrated in Figure 29.

Figure 29: Evolution of Temperatures and Pressure as a function of time in a graphite matrix.

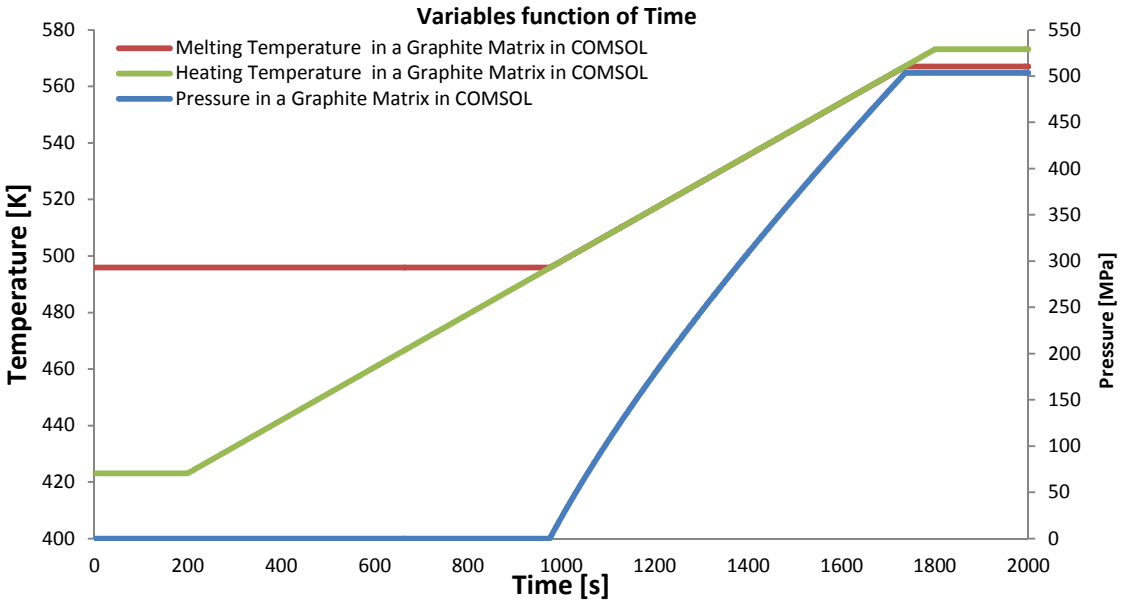

Figure 29 illustrates the evolution of heating temperature, melting temperature and pressure as a function of time, and Figure 30 depicts the evolution of the fraction of molten salt as a function of time. From 0 to 974 seconds, the heating temperature increases up to 222°C while the melting temperature is constant at 222°C.

At 975 seconds, the salt bead starts to melt, then f*, fraction of molten salt, increases. At the same time, pressure increases because of the variation of the volume of salt within the spherical graphite shell. Hence, the melting temperature increases too. At 1738 seconds, f* value reaches 1 (Figure 30), and the whole salt bead is molten. The melting temperature stops increasing at 294°C while the heating temperature, imposed, further increases to 300°C. The pressure of the

graphite matrix stops increasing at 503MPa, and stays constant. Such results conform to the original results by Lopez *et al.* The differences between our and the original results come from the initial value of the isothermal compressibility of the liquid salt. Indeed, the original work was considering a non-compressible liquid salt with a value of $1.86E^{-20}Pa^{-1}$ while the present work considers a value of $1.86E^{-10}Pa^{-1}$ according to literature data (Janz, 1967).

Figure 30: Evolution of fraction of melting salt as a function of time in a C graphite matrix.

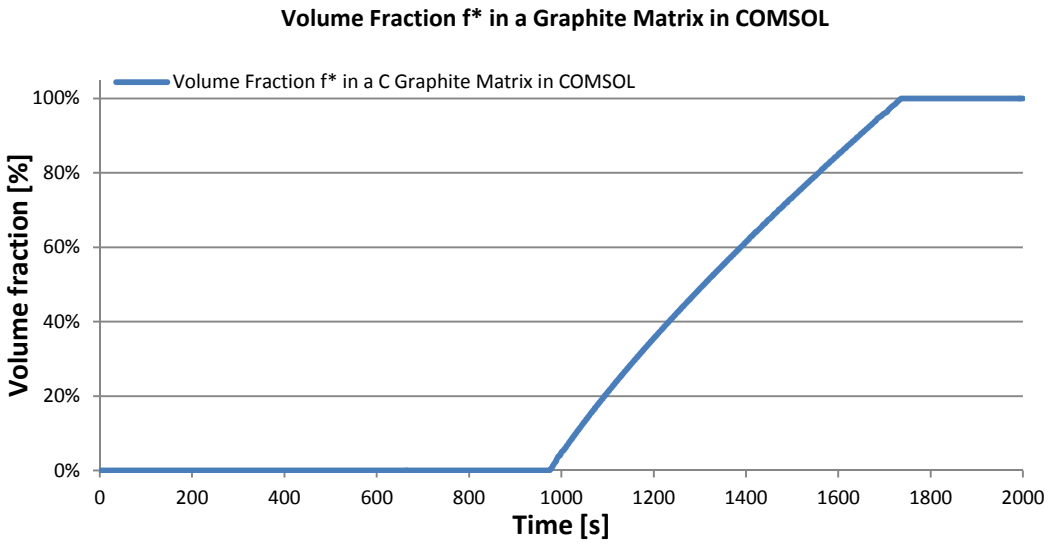

Energies of the salt bead in a graphite shell evolve in the same way than in the previous work (Figure 31). Mechanical energy is negligible compares to latent and sensible energies which remain of the same order of magnitude.

Figure 31:Evolution of energies as a function of time in a graphite matrix.

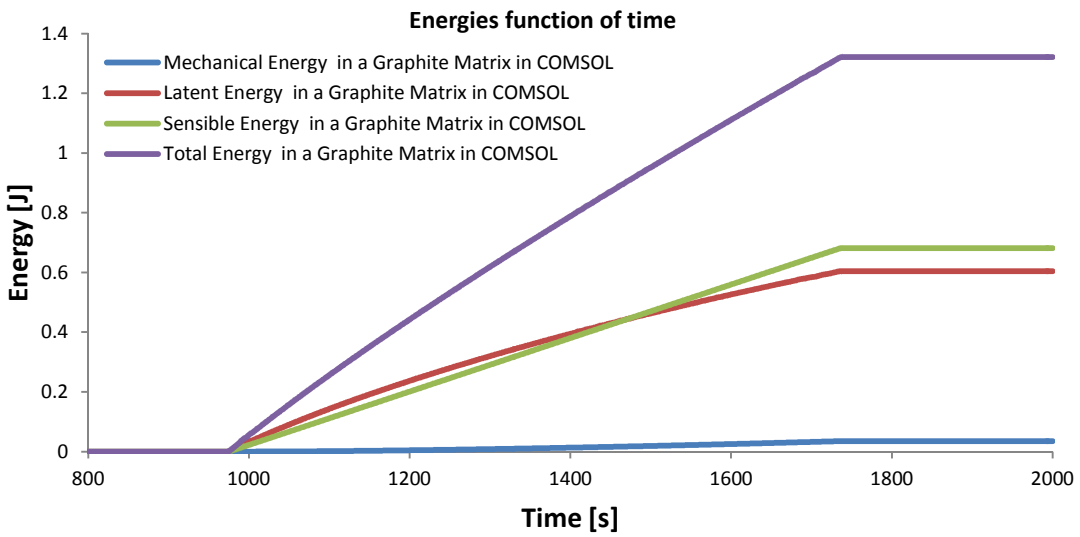

The results given by the dynamic simulation of the melting salt bead encapsulated in a graphite shell validate the code generated. The next step in the numerical analysis is to use the expression of the pressure in the SiC shell.

3.6.2 Numerical solution in a SiC shell.

In this part of the numerical analysis, the non-moving wall of the graphite matrix is replaced by the SiC shell. Parameters of the modelling in COMSOL have the same values than those used in the previous case apart from the pressure taken from equation (3.22).

As in the case with a graphite matrix, the temperature of the shell is maintained constant at 800°C for the first 200 seconds. The constant external temperature is to check the stability of the system before heating. From 200 till 7000 seconds, the temperature increases to 800°C, where after it is constant for the last 500 seconds. Figure 32 shows the evolution of the pressure, the heating temperature and the melting temperature as functions of time.

Figure 32: Evolution of Temperatures and Pressure function of time in a SiC shell.

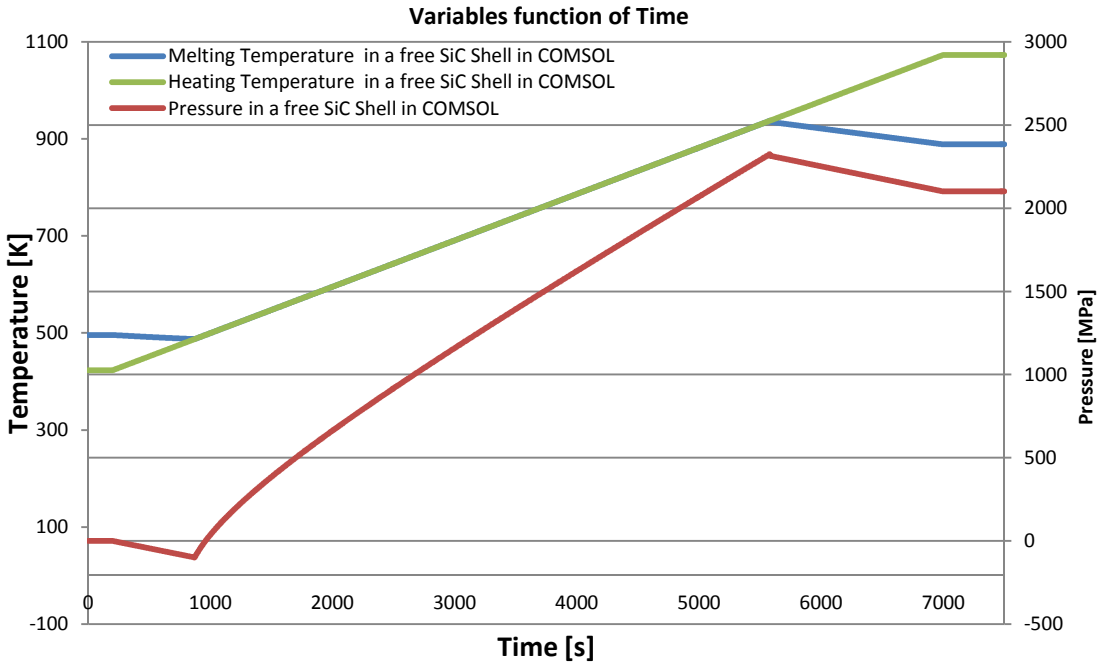

When the heating temperature starts increasing, the pressure in the SiC shell decreases to negative values. This behaviour does not match a physical phenomenon, but the result of is the thermal stress component of the pressure $(1 + \alpha\,\Delta T)$ which set the negative values. While the SiC shell temperature increases, the thermal expansion of the coating material is not compensated in the model by the thermal expansion of the salt bead. Hence, it creates a vacuum effect in the modelling. The main consequence of this vacuum effect is a decrease of the melting temperature before the salt starts melting. As seen in Figure 33, the melting of the salt starts at 200 seconds and finishes at 5583 seconds. At the same time, both the pressure and, hence, the melting temperature increase. Once the whole salt bead is given as molten, the heating temperature keeps increasing. The pressure and melting temperature decrease due to the thermal expansion of the SiC shell.

Figure 33: Evolution of fraction of melting salt as a function of time in a SiC shell.

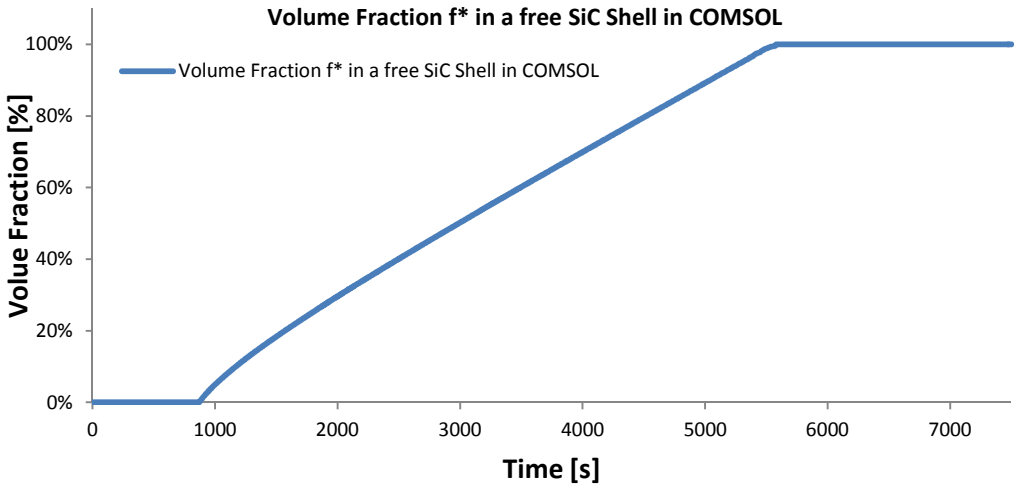

The reductions in the pressure and melting temperature show the limit of the modelling to describe the reality of the phenomenon, but highlight their actual existence.

Figure 34 shows the comparison between the results using MATLAB and those using COMSOL.

Figure 34: Evolution of Temperatures and Pressure as a function of the proportion of molten salt in a SiC shell.

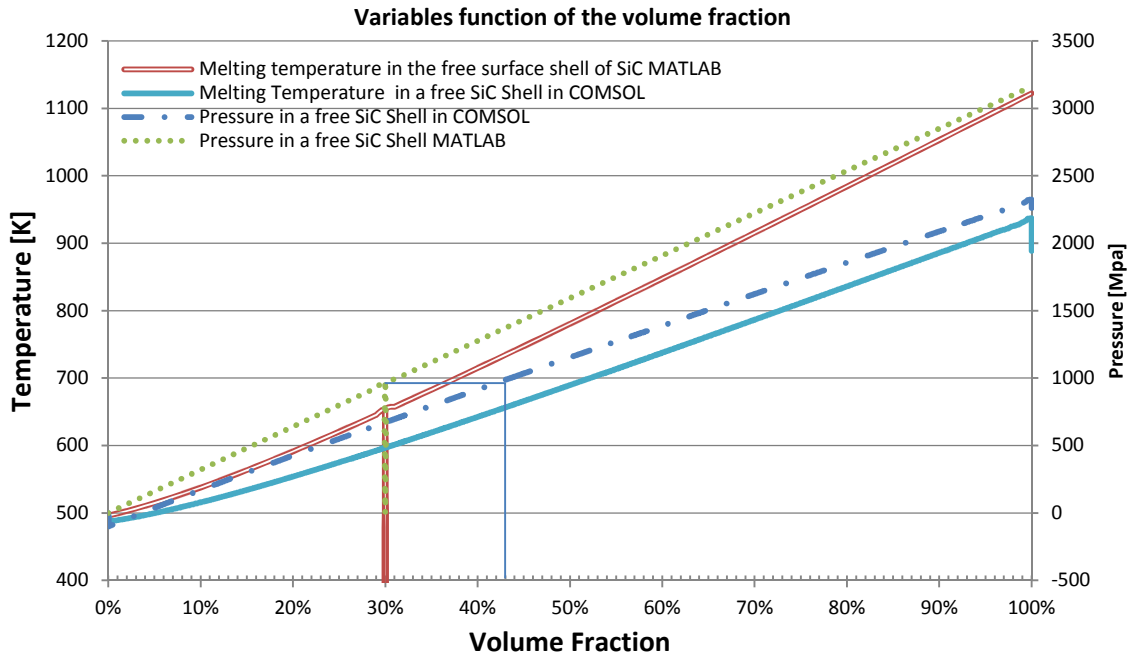

In MATLAB, the thermal gradient was not included in the calculation of the pressure and the melting temperature. Hence, the graph of pressure and melting temperature present a difference of slope. The limit of the critical maximum pressure is no longer reached at 30% of molten salt, as was the case in the MATLAB simulation. In COMSOL, the maximum pressure is reached at 42% of molten salt as shown in Figure 34. This proportion of molten salt is reached on 2585 seconds. According to the criteria calculated with equation 23, the shell reaches its maximum yield stress and cracks. The graphs then provide hypothetical values of the thermo-dynamical behaviour of the melting salt. The latent heat and energies values are also affected by the reduction of pressure. As seen in Figure 35, the latent heat still presents a negative slope with values going reaching zero, meaning that melting of the salt is no longer possible.

Figure 35: Evolution of Latent Heat function of the proportion of molten salt in a SiC shell.

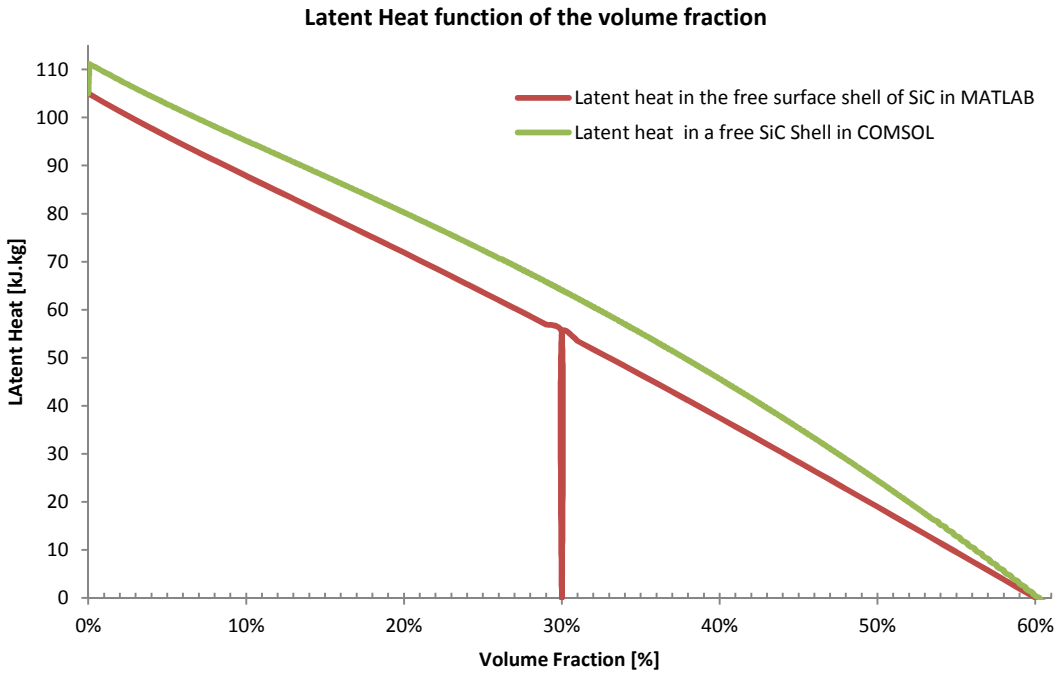

In Figure 36, the energies also present a reduction in values. The mechanical energy can still be neglected. The latent heat energy values remain close to the values estimated with MATLAB, while the sensible energy values are almost divided by 2. When the energies in a

graphite matrix are compared to the energies stored by a salt bead in a SiC shell, the proportion of latent heat energy is reduced from 50% to 13%.

Figure 36: Evolution of energies as functions of the proportion of molten salt in a SiC shell.

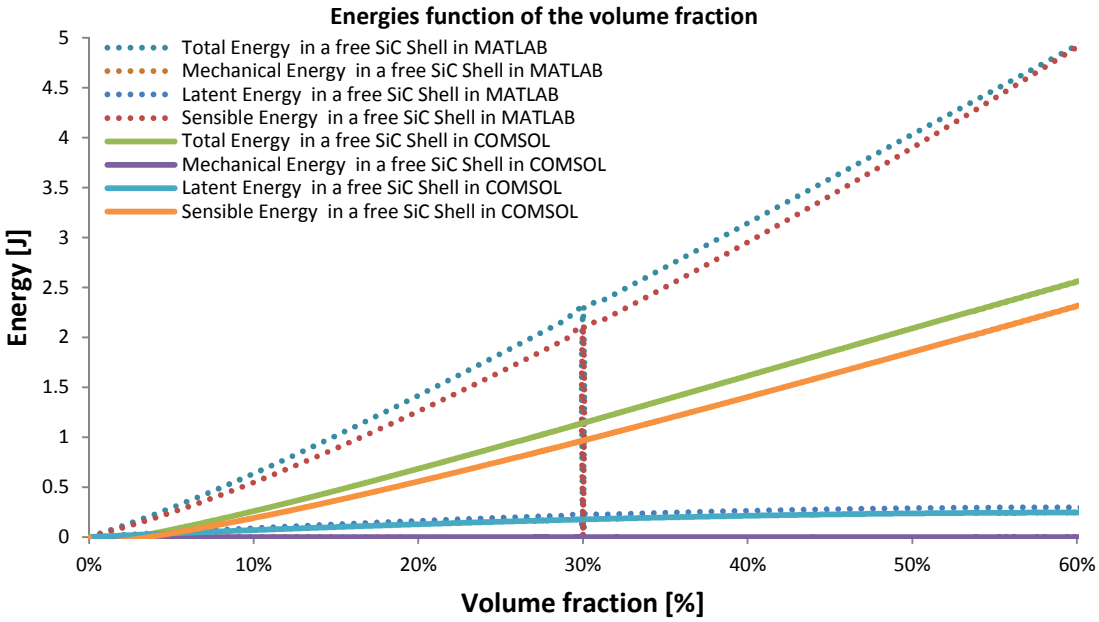

This gap is also visible in the Figure 37 that shows the evolution of the energies as functions of time. The evolutions of the energies are traced from 0 to 7500 seconds despite the fact that the SiC is meant to crack at 2585 seconds. The charts in Figure 37 highlight the positive and negative parts of both mathematical and numerical analysis.

The influence of the high pressure appears with the high values of the sensible heat energy. While the negatives values of energies before the salt starts melting show the limits of the model. The decreasing of the latent heat energy tends to prove that the salt cannot melt under too high pressure. The proportion of the three different types of energy which are sum to compose the total, confirms that under high pressure the latent heat energy storage is less efficient.

Figure 37: Evolution of energies as a function of time in a SiC shell.

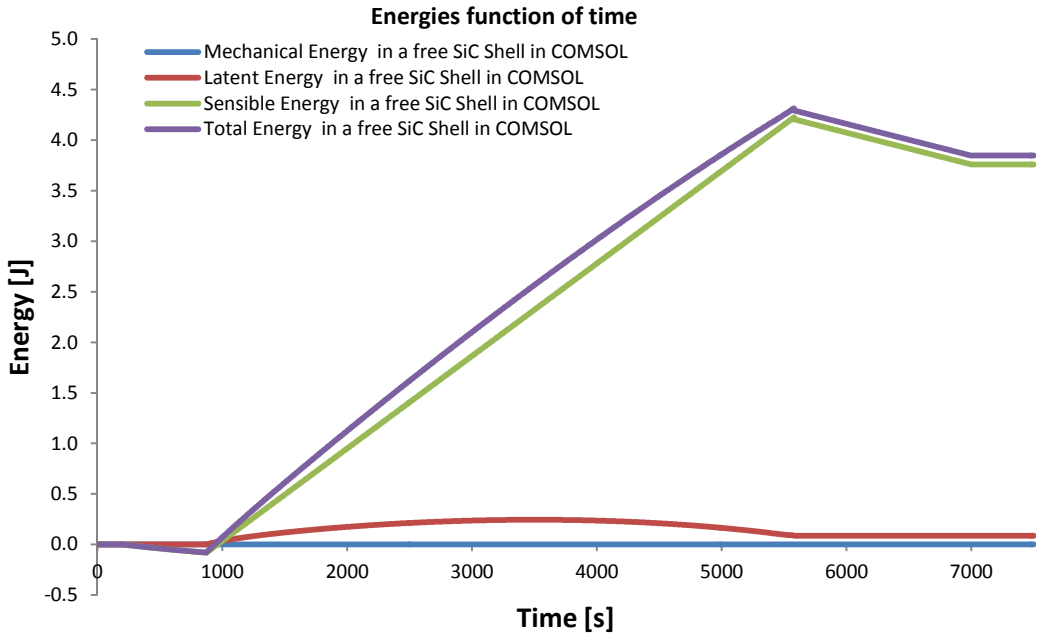

The numerical analysis provides information on the dynamical behaviour in addition the mathematical analysis. It tends to confirm the previous results found and it also highlights the limits of the model. The thermal expansion of the SiC shell is then proved to have an impact on the melting of the coated salt bead. But the negative values do not reflect the reality of this influence. The thermal expansion of the different materials that compose the SiC encapsulated salt bead should therefore be modelled in order to take its influence into consideration.

3.7 Conclusions

The mechanical model of a PCM coated in a spherical shell was calculated in three cases. A non-moving external wall graphite shell refers to the work of Lopez *et al.*(2010) which is taken as a reference to this work. A thin SiC free surface shell is used to estimate the inner pressure of the shell under volumetric expansion of PCM. The thick shell model of a shell coating melting PCM is finally used together with the von Mises criterion to define the conditions when the shell cracks under the inner pressure. The computed inner pressure is higher than the limit of the SiC material, which tends to show that this kind of encapsulation is not possible with this particular PCM.

In a second part of the chapter, the thermal dependent mechanical behaviour of a high temperature melting PCM is studied. The original work is fully adapted to the new hypotheses. Despite the fact that the predicted energy does not match with the original model, the model seems to be viable, since this mismatch is the result of the fact that the data used in the chapter have been estimated from the thermal properties of separate elements of the PCM. The expression of the energy of the system is proven to be adapted to a free surface coated particle. The study in high pressure conditions shows that the density of the PCM cannot be considered as a constant with the new hypotheses. The total energy needed to melt the whole bead of PCM increases with the inner pressure due to the coating material. The proportion of latent heat energy decreases with the high pressure.

In a third part of the chapter, the numerical analysis approaches the thermal dependent mechanical behaviour of a high temperature melting PCM in time. The code of the numerical analysis is validated by reproducing the result of previous works. However, the strength and limitations of the actual model are highlighted. The high increase in pressure is confirmed to reduce the efficiency of the latent heat energy storage for a SiC encapsulated salt bead. The thermal expansion of the shell is shown to have an influence when the salt starts to melt. But negative values of the pressure show the limitations of the model to analyse the thermal expansion of both salt and SiC shell.

Encapsulation on a macro-scale (for sizes in excess of about 10 mm) is already achieved, and will be presented by Zhang et al. during the ICEPE2013 and SDEWES2013 conferences, respectively in Frankfurt (June 2013) and Dubrovnik (September 2013). Publications are not yet available. Encapsulation of smaller particles (< 1 mm) is in development by the same research team, with plasma vapour deposition and tumbling electrolytic coating having been tested. Results so far do not yet permit an application on laboratory or larger scale, due to the micro-leaks present in the deposit coating layer (Ni, Cr, SiC).

The research indicates that the interest of coating a PCM with a SiC shell is strongly determined by the PCM properties, namely the PCM should have a high latent heat but a low volumetric expansion, thus leading to a smaller increase of pressure during the melting process.

4 POTENTIAL APPLICATIONS FOR THERMAL ENERGY STORAGE USING CERAMIC ENCAPSULATED PCM.

Whereas the previous chapters (i) delineated the overall concept of energy storage and thermal energy storage; and (ii) developed the fundamental principles that govern the properties of PCMs, the present chapter will illustrate different techniques for thermal energy storage and/or transfer. The ways in which these could benefit from encapsulated PCM for high temperature purpose are considered. Three media are examined: solid, liquid, and gas. Improvements brought by new material involving PCM are then analysed.

4.1 Introduction

The layout of the present chapter is illustrated in Figure 38. Each of the parallel topics is subsequently dealt with.

Figure 38: Layout of chapter 4.

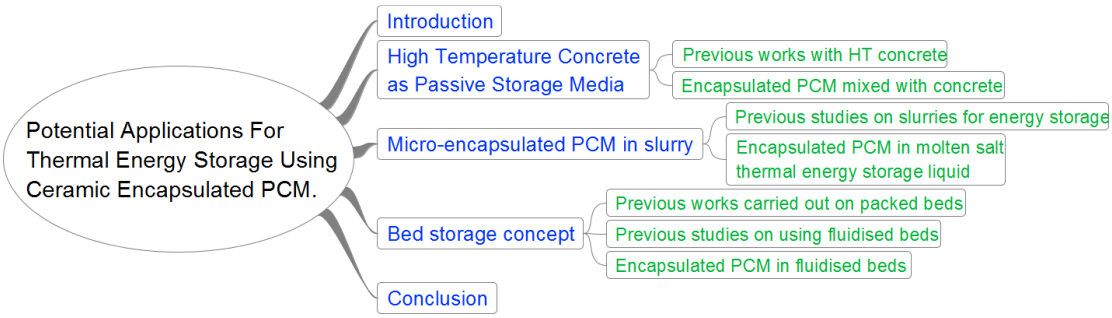

To further illustrate the practical use of the results reported in previous chapters, design approaches for thermal energy storage installations are further elaborated. The first chapter demonstrated that ceramic encapsulated molten salt PCM had distinct advantages in high temperature thermal heat storage (HTTES). The mathematical modelling of the second chapter highlighted the conditions required to encapsulate a PCM salt in a ceramic shell. The high melting temperature PCM latent heat improves the energy density compared to a purely sensible heat storage material. The ceramic shell coated the PCM moreover prevents the PCM from melting and leaking, whilst also increasing the thermal conductivity and the heat exchange surface of the PCM.

The present chapter defines applications where ceramic encapsulated PCMs offer a sufficient improvement in latent heat energy storage, and to enumerate the component requirements for the use of molten salt as encapsulated PCM, i.e., with SiC shells. This will be demonstrated by describing potential applications of HTTES or High Temperature Heat Transfer in three typical case studies:

- The encapsulated PCM is mixed within a high temperature (HT) concrete for passive heat energy storage.
- The encapsulated PCM is mixed to a liquid heat transfer fluid (HTF).
- The encapsulated PCM is used in a solid-gas conveying system as heat carrier.

In these case studies, the coated PCM interacts with a different phase being: solid, liquid, gas.

4.2 High Temperature Concrete as Passive Storage Media.

At the Plataforma Solar de Almeria (PSA) in Southern Spain, tests were run by Ciemat and the German Aerospace Centre (DLR). They proved that both castable ceramics and high temperature concrete are suitable as solid media sensible heat storage systems (Medrano *et al*., 2010). Figure 39 shows the concrete storage modules tested between 1991 and 1994. The system used the standard HTF in the solar field, which transferred its heat through a system comprising an array of pipes embedded in the solid storage media. When the heat energy collected from the sun exceeds the quantity needed for electricity production, the heat is stored by the solid storage media by increasing its temperature. Then, when the energy collected from the sun is insufficient, the thermal energy recycled to the HTF.

Figure 39: View of a high temperature concrete storage system (Medrano *et al*., 2010).

DLR examined the performance, durability and cost of using these solid thermal energy storage (TES) media in parabolic trough power plants (Figure 40). Thanks to this study and, it appears that the high temperature concrete is cost effective, the enhanced material strength and easier handling as show in Table 9.

Table 9 Thermal properties of HT concrete, ceramic and molten salts (Py *et al*., 2011).

Materials	HT concrete	HT Ceramics	molten salts
density [kg/m^3]	2750	3500	900 - 2600
C_p [J/ (kg.K)]	916	866	1500
$\rho \times C_p$ [kJ/ (m^3.K)]	2519	3031	1350 - 3900
λ [W/ (m.K)]	1.0	1.35	~ 0.15 – 2.0
coeff. of thermal expansion [10^{-6}/K]	9.3	11.8	---
price [euros/tonne]	80	4500 - 9000	500 -750

Figure 40. Illustration of the storage test plant in PSA (Medrano *et al*., 2010).

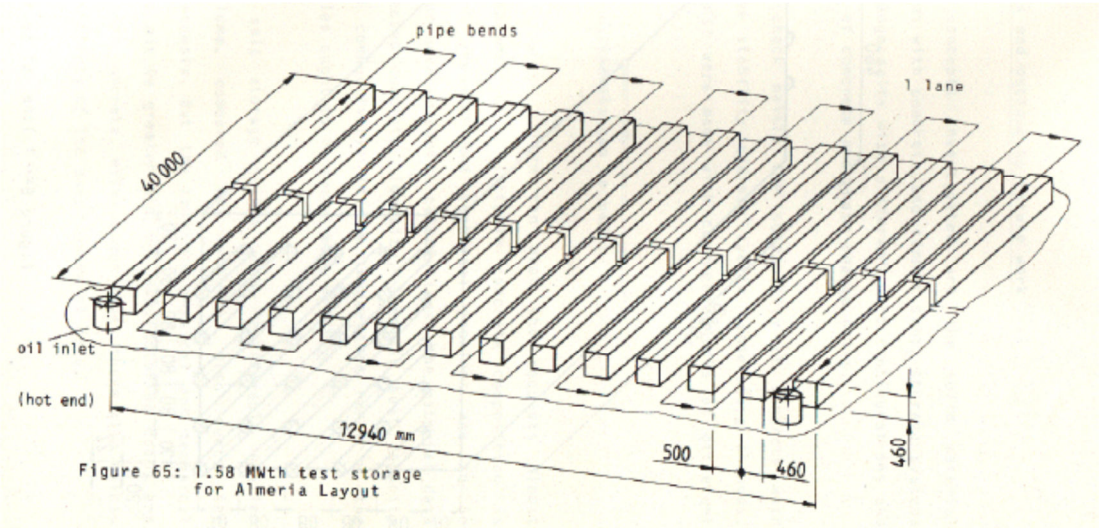

Further tests were carried out in 2004 at the Plataforma Solar de Almeria. The thermal energy was provided by a parabolic trough loop with a maximum thermal power of 480 kW. The storage temperatures reached were within a range of 340-390°C (Medrano *et al*., 2010).

In order to raise this technology to pre-commercial status for use in solar power plants, a 2009 follow-up project was designed by Laing *et al*. (2011) (Figure 15). A three component thermal storage system, combining sensible and latent heat storage was tested for application in DSG power plants (Laing *et al*., 2011).Investigations and experiments supported the hypothesis that high-temperature concrete could serve as sensible heat storage up to 500°C.

Within the limitations of the solid concrete structure, the incorporation of phase-change materials will undoubtedly be beneficial since capable of absorbing a high quantity of energy (sensible and latent heat), while keeping the temperature of the matrix close to the melting point of the phase change.

This use of encapsulated PCM mixed with concrete was demonstrated for applications at ambient temperatures (Cabeza et al., 2011; Castellón et al., 2007; Sharma et al., 2009). Those recent studies focused on the possibility of using micro-encapsulated PCM in concrete without losing any of the concrete initial characteristics, achieving high energy savings in cooling

power. For instance, the test cubicles illustrated in Figure 16 have three panels made of concrete including 5% of PCM achieving a permanent difference of 2°C between a PCM loaded concrete and an un-loaded concrete, demonstrating that HT concrete could benefit from the incorporation of SiC encapsulated PCM molten salt.

Further to the tentative results of chapter 3, we believe that the improvement of HT concrete properties and characteristics are related to specific properties of adding SiC encapsulated PCM molten salt, i.e.

- SiC is fully compatible with concrete towards particle size range and mechanical properties (John et al., 2011a, 2011b).
- Thermal property of the loaded concrete mixture will not be affected by the inclusion of SiC thanks to its high thermal conductivity.
- Encapsulated PCM would add a latent heat storage component to the sensible heat storage of the original concrete system thereby reducing the volume of material needed for a required heat capture and storage. Price and manufacturing process would benefit from the improvement of the material.
- The original system integration of concrete modules would guarantee good adaptation of the material to scaling up since involving change in the process of producing the concrete when admixing these particles: current research has given a first evidence of their advantage (Bai and Xu, 2011; John et al., 2011a; Laing, 2007).
- The final thermal storage capacity of the new material can be easily proof-tested.

Although, no further studies have yet explored the application of the HT concrete with a proportion of encapsulated PCM, it is evident that the combination of both materials would take advantage of their properties to conserve thermal energy, and thus may lead to a new mixed material worthy of further development. It is however possible that the costs of research and development would mean higher costs at the outset, and that economies of scale would

obviously lead to a reduction in the price in the long term, needed to implement practical and efficient applications (Medrano *et al*., 2010).

4.3 Micro-encapsulated PCM in slurry.

4.3.1 Previous studies on slurries for energy storage.

A micro-encapsulated PCM slurry is a suspension where the PCM is dispersed at 15-20wt% of the weight without significantly altering the physical properties of the liquid (density, viscosity) (Chen *et al*., 2008; Delgado *et al*., 2012). In the studies at low temperatures, PCM is microencapsulated using a polymeric capsule and dispersed in water (Chen et al., 2008; Delgado et al., 2012; Yamagishi et al., 1999). The experimental analysis using a slurry with a 10wt% concentration of paraffin was conducted by Delgado *et al.* to investigate the effectiveness of its properties as a thermal storage material and as a heat transfer fluid (Delgado *et al*., 2012). The results obtained demonstrated an increase of approximately 25% in the convective heat transfer coefficient when compared to water. The increase in the efficiency in heat transfer of the liquid is the result of improving the overall heat capacity of the material through applying the latent heat properties of the PCM (Chen *et al*., 2008).

Similarities of shape between the polymeric capsule and the ceramic encapsulated PCMs tend to indicate that the latter could be used to improve the heat transfer coefficient for high temperature slurry applications, as described below.

Nano-particle Enhanced Ionic Liquids (NEILs) are a class of low-melting organic compounds with discrete charges that cause a significant decrease in their vapour pressure. At atmospheric pressure, this property prevents volatilization of an ionic liquid (IL), which would recommend its use as a thermal fluid and for energy storage materials (Bridges et al., 2011; Wu et al., 2001). The feasibility of using ionic liquids as liquid thermal storage media and heat transfer fluids in a solar thermal power plant has been the subject of additional investigations (Wu *et al*., 2001). According to Bridges *et al.*, nano-particle enhanced ILs have been shown to increase the heat capacity of the IL without adverse secondary effects on the ILs' thermal

stability (Bridges *et al*., 2011). The IL physical properties were shown to be only affected in cases of high nano-particle loading. Those similarities between high and low temperature slurries' properties tend to indicate that a high temperature equivalent of an encapsulated PCM slurry is possible.

Further to the results of chapter 3, we believe that the improvement of HT slurries' properties and characteristics are related to specific properties of adding SiC encapsulated PCM molten salt. Heat transfer fluid and heat storage liquid have been proven to be more efficient as a result of the incorporation of particles in the liquid. For instance, Concentrated Solar Plants could benefit from such a technology as described below.

4.3.2 Encapsulated PCM in molten salt thermal energy storage liquid.

New concentrated solar plants have been under development for some time (Luptowski, 2011). These new designs involve a heat storage unit as part of the production process. Figure 41 shows how heat transfer fluid is used as sensible heat storage material. Using a unique molten salt for both of these applications reduces the cost and improves the global performance of the system (Gil et al., 2010; Luptowski, 2011; Price et al., 2002).

Figure 41: Schematics of a parabolic through power plant, with two-tank storage system (Luptowski, 2011).

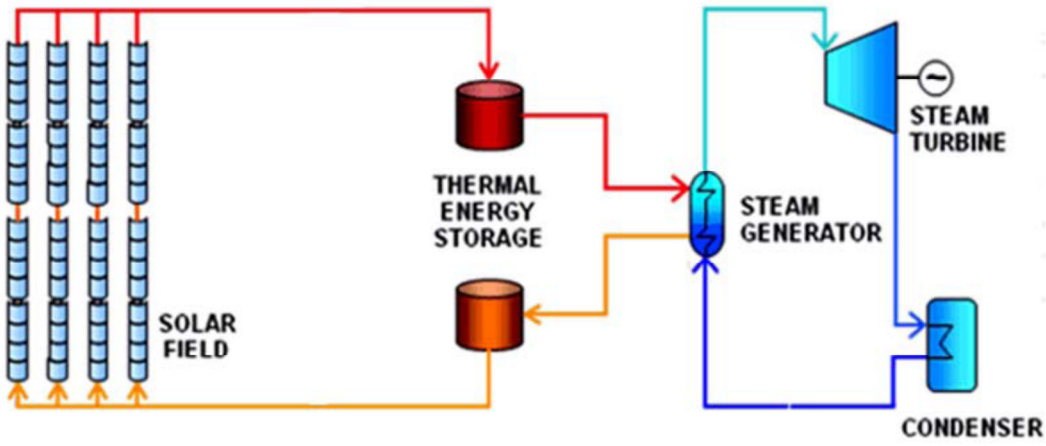

Such a system could benefit from a heat transfer fluid which incorporates encapsulated particles of PCM. The heat transfer capacities would be improved by the high conductivity of the SiC and the high energy density of the PCM. In comparison with a conventional thermal fluid, e.g. Santotherm 350, the specific heat will be increasingly by a fraction of ≈3 whilst the energy density will increase by about 5.

The main issues for developing salt-PCM modifications would be the loss of fluidity of the high temperature slurry. Further studies have to prove if the addition of particles increases the thermal properties of the HTF without affecting the viscosity and associated pumping power needed. Existing CSP would then see their global efficiency improved by the higher energy density of the HTF.

4.4 Bed storage concept.

High heat transfer coefficients can be achieved between an encapsulated PCM and a gas flow thanks to the high exchange surface. There are two different concepts: in packed beds, the PCM is not moving and is used only for heat energy storage; in moving beds, the encapsulated PCM is used for the transport and storage of the heat energy.

Powder beds are of 4 types: fixed, moving, bubbling and circulating fluidized beds. When a gas is passed through a bed of powders, the bed will remain fixed at very low gas flow rates. Since there is no particle movement, the heat transfer coefficient is mostly determined by the convection heat transfer of the gas flow only (order of magnitude < 20 to 50 W/m²K). When the drag force of the gas flow exceeds the bed weight per unit cross sectional area, the bed will fluidize and bubbles will occur. The bubbling activity will increase at increased gas flow rates. Due to the turbulent movement of the particles, induced by the bubble flow, the heat trtansfer coefficient will significantly increase, with measured values of 100 W/m²K for coarse particles, to 700 W/m²K for fine (~100 µm) particles. In circulating fluidized beds, obtained at a gas flow rate that carries all particles out of the bed, hence requiring a recycle to keep the bed inventory,

the heat transfer coefficient is again high due to the intensive particle mixing. Values between 150 to 500 W/m²K are achieved, as further demonstrated in Chapter 5.

4.4.1 Previous works in carried out on packed beds.

The following example of encapsulated PCMs packed bed is quoted several times in this thesis as a pioneer for heat waste recovery at very high temperature (Maruoka and Akiyama, 2003, 2002; Maruoka et al., 2002).

The steam reforming of methane is an essential endothermic reaction in the chemical and metallurgy industries, involving the direct reduction in the production of hydrogen and carbon monoxide. The hydrogen and carbon monoxide generated are thus made available to synthesize methanol. Figure 42 illustrates the system developed by Maruoka and Akiyama to recycle waste heat energy. A packed bed of Nickel coated beads of copper accumulates the excess heat from the LD converter in the steel production (Linz Donawitz process). The latent heat energy stored is further used to produce hydrogen and carbon monoxide.

Figure 42: Schematic diagram of the proposed process consisting of the LD converter and the PCM heat storage reactor (Maruoka and Akiyama, 2002).

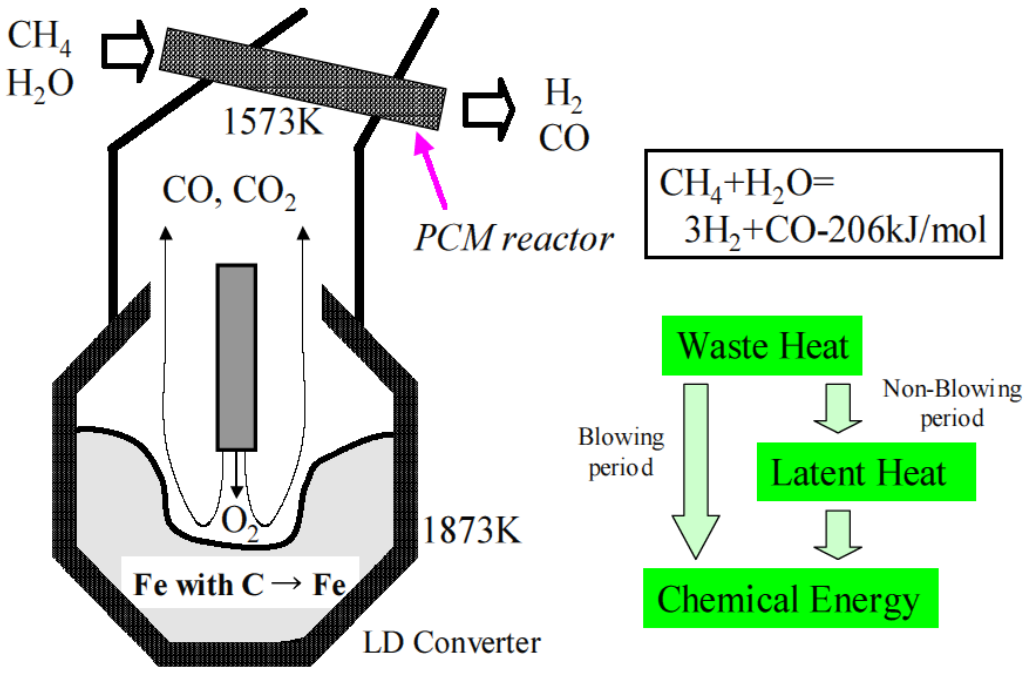

The high temperature encapsulated PCMs are demonstrating their full potential with that particular application.

4.4.2 Previous studies on using fluidized beds.

The circulating fluidized bed (CFB) is increasingly used in chemical reactors and in physical gas-solid processes (e.g. drying). New concepts of thermal energy storage systems are being developed for concentrated solar energy capture/storage systems or industrial waste heat recovery. They use a fluidized bed as transfer and storage medium to replace thermal fluids or molten salts (Chen *et al*., 2005).

In the first case, an air-to-sand exchanger is installed in the receiver tower in order to minimize the losses. The sand is fluidized in the exchanger and air is passed through it. The exchange of heat between the air and the moving sand is excellent thanks to the fluidization of the sand. The air circulating reaches very high temperatures in the receiver, and carries the heat to the storage and the production unit. Such a system helps to improve the efficiency and storage rates of the plant (Figure 5 a). The typical set-up of Figure 5 b, applicable in solar towers and in waste heat recovery, applies a dense particle bed conveyed within a tube bundle to capture the heat at bed temperatures between 500 and 750 °C, thereafter using the stored heat in a bubbling fluidized bed steam boiler (European Union, 2011). A CFB shares many of its advantages with traditional bubbling fluidized beds (BFB), including temperature uniformity and excellent heat transfer. The continuous carry-over of particles implies solids' collection and return equipment. In solar energy capture systems, solar heat will be captured at the outside tube wall, and subsequently transferred to the circulating solids.

At present, this specific solution is still in its development stages and several problems are still, as yet, to be resolved (Medrano *et al*., 2010).

4.4.3 Encapsulated PCM in fluidised beds.

A new system for the storage of low temperature thermal solar energy, which consists of a bubbling fluidized bed filled with granular phase change materials, has been undergoing tests in Madrid since 2010. In this system, the main advantages of both technologies are combined: the high heat transfer coefficients of bubbling fluidized beds and the high thermal energy storage capacity in the reduced volume of phase change materials. The project is focused on storage at specifically low temperatures.

Such a technology combined with SiC encapsulated molten salt PCM would be capable of combining the benefits of both technologies. The thermal conductivity of the particles, which are the result of their ceramic coating, would optimise the heat exchange. As in HT concrete, the latent heat would increase the amount of energy stored. The life cycle of the system and aging of the particles would require a careful study. If the shells of the PCM were to break or leak, the result would be leakage of the molten salt from the shell and consequent damage to the fluidised bed, by corrosion, defluidization and possible sintering of the bed material if low melting eutectics can be formed.

4.5 Conclusion

Existing systems incorporating high temperature thermal energy storage technologies are subject to further research and analysis to discover how further improvements can be applied to them. The physical properties of SiC shell coated PCM could provide appreciable benefit in these kinds of systems.

An effect of the addition of these particles would be that high temperature concrete could acquire greater thermal conductivity, and hence the thermal storage capacity would be increased. In spite of this, the manufacturing processes employed in producing HT concrete would barely need to undergo any change.

Slurries are also undergoing further study to analyse their potential to extend their applications to high temperature heat transfer fluids and thermal energy storage materials. The replacement of nano-particles by encpasulated PCM would increase the energy density of the materialbecause heat transfer capacities would be improved by the high conductivity of the SiC and the high energy density of the PCM.

Finally, there is an increasing interest in the use of encapuslated particles in fluidized. Encapsulated PCM would bring higher energy density and stabilised working temperatures.

Further research and analysis of all those potential new applications of encapsulated particles will be required in order to precise the field of applications available. Results of a first study on CFB is display in the next chapter.

5 HEAT TRANSFER TO THE RISER-WALL OF A CIRCULATING FLUIDISED BED (CFB)

An alternative to using molten salts in high temperature energy capture and storage systems, relies upon the use of circulating powder suspensions. These systems have also found their introduction in solar energy capture and storage, as described in Chapter 4.

Since the amount of heat captured by the container wall (ΔH, MJ/s), needs to be evacuated by the flowing suspension, two parameters are of major importance: (i) the suspension circulation rate (G_s, kg/s), its apparent specific heat (C_p, kJ/kg.K), and the temperature increase of the suspension in the energy receiver ($T_{out} - T_{in}$, °K) must enable the continuous evacuation of the heat supplied; and (ii) the heat transfer coefficient between wall and suspension flow (h, W/m²K), together with the temperature difference between wall and bulk flowing suspension (T_{wall}- T_{bed}, K) will determine the area of the heat exchanging surface required (A_{ex}, m²). This results in $\Delta H = G_s\, C_p\, (T_{out}-T_{in}) = h\, (T_{wall}-T_{bed})\, A_{ex}$

The heat transfer coefficient from the heat transfer surface to the gas-solid suspension is a strong function of the solids circulation rate, and needs to be determined as design parameter and as function of the operating conditions of the gas-solid suspension.

The present Chapter investigates the heat transfer coefficient for different operating gas velocity and solids circulation flux, whilst covering the different hydrodynamic solid flow regimes of dilute, core-annulus or dense mode. Measured values of the wall-to-bed heat transfer coefficients are compared with empirical predictions of both Molodstof and Muzyka (1985)*, and Golriz and Grace* (2002)*. The application of a packet renewal mechanism at the wall is also investigated, and introducing the predicted solid contact time at the wall provides a very fair estimate of the heat transfer coefficient.*

5.1 Introduction

The layout of the present chapter is illustrated in Figure 43. Each of the parallel topics is subsequently dealt with. Essential parts of this chapter were adapted and published before the present thesis was completed. Published paper is attached in the appendices.

Figure 43: Layout of Chapter5.

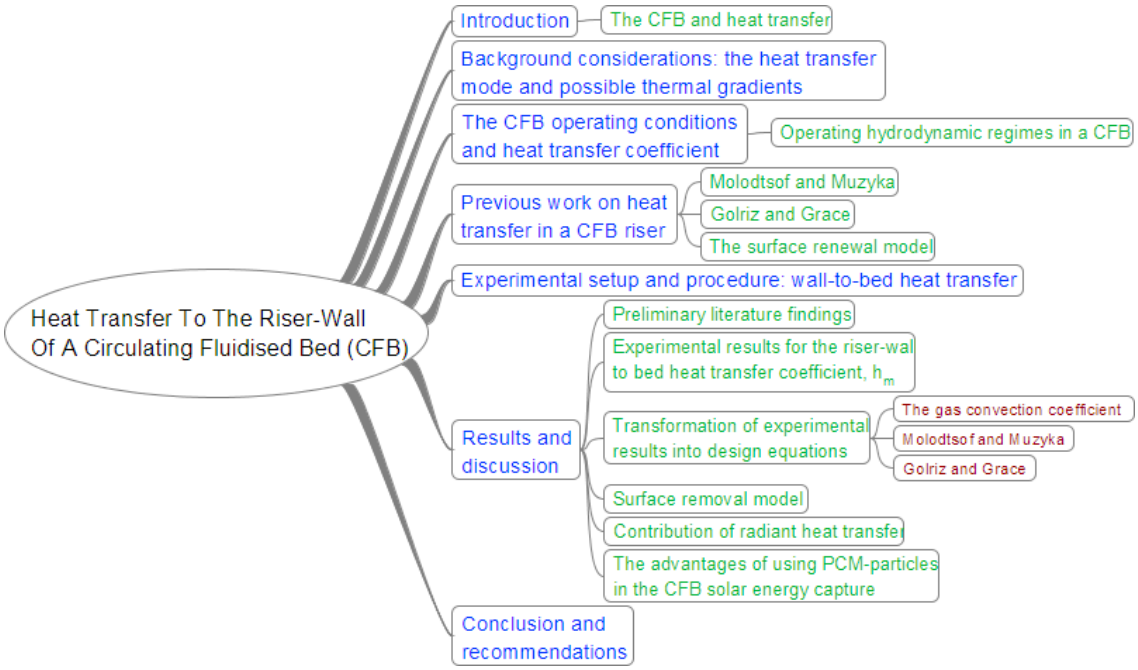

5.1.1 The CFB and heat transfer

The circulating fluidized bed (CFB) regime is of increasing importance for gas-solid reactions (e.g. combustion, calcination, SO_2 removal from combustion gases), for gas-catalytic reactions (e.g. maleic anhydride from butane, acrylonitrile, aniline), and for physical gas-solid processes such as drying or VOC adsorption. A recent development is the use of a circulating fluidized bed in solar energy capture and storage systems, to replace thermal fluids or molten salts as transfer and storage medium (European Union, 2011). Reviews of the different gas-solid and gas-catalytic applications are given in e.g. Mahmoudi *et al.* (2012), Chan *et al.* (2010). Fernandes *et al.* (2012) introduce the use in solar energy systems.

Layouts of different applications are illustrated in Figure 44.

Figure 44: Illustration of different CFB layouts, with heat transfer.

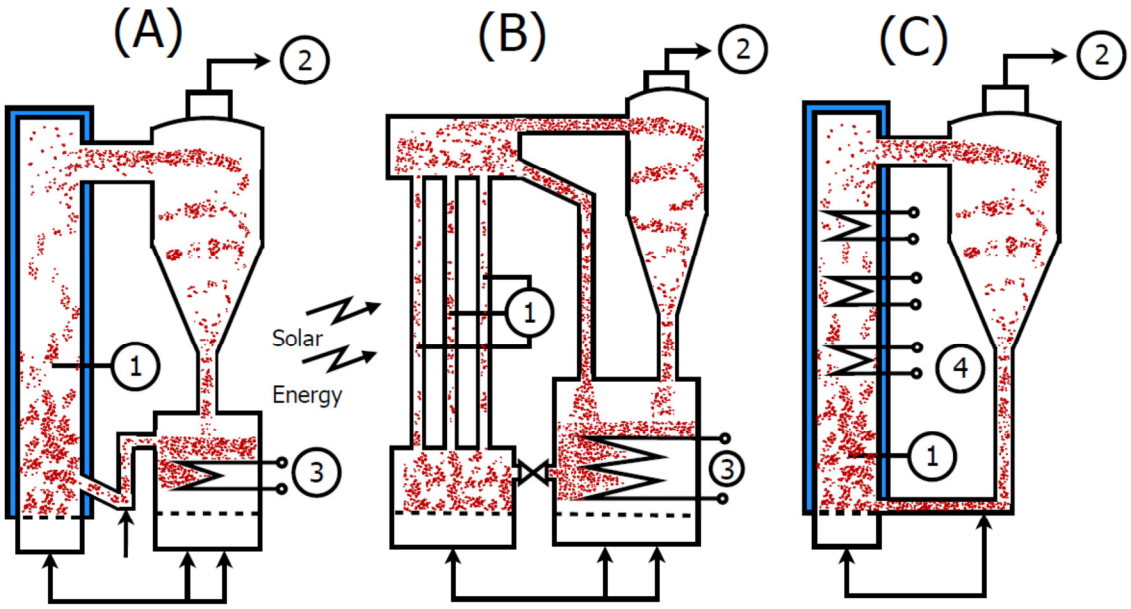

1) Riser, with wall-mounted heat exchanger in (A) and (C)
2) exhaust to further treatment or de-dusting
3) heat exchange surface in secondary bubbling fluidised bed
4) in-riser heat exchanger

(A) Application for gas-solid reaction, e.g. combustion
(B) Application in solar energy capture and storage
(C) Application for gas-catalytic reaction, with in-bed heat transfer

A CFB shares many of its advantages with traditional bubbling beds, including temperature uniformity and excellent heat transfer, while allowing higher gas throughput and having a greater ability to handle agglomerating particles. The circulation of particles requires solids' collection and return equipment: the overall CFB setup hence consists of a riser, a cyclone, a downcomer and a return valve (often executed as non-mechanical valve), as illustrated in Figure 44.

Most reactions carried out in the CFB are endothermic or exothermic and hence require an exchange of heat between the gas-solid suspension and heat transfer surfaces, located either at the wall of the riser, inside the riser, externally in a low-velocity fluidized bed in the return loop of the solids, or as a traditional downstream heat exchanger on the exhaust gas (superheater or economizer tube-bundle). Mostly membrane water-wall surfaces are used in combustion or other exothermic applications. For other systems, it might be impossible to provide sufficient heat transfer surface at the wall of the riser (unless extremely tall). It is then necessary to embed

surfaces in the riser itself, as is mostly the case for highly exothermic gas-catalytic reactions. In solar energy capture systems, solar heat will be directed onto the outside riser wall, and subsequently transferred to the circulating solids.

Despite the high gas and solid velocities, particle erosion and attrition in a CFB are limited, as demonstrated previously by Van de Velden and Baeyens (2007). In general, powder losses are well below 50 kg/day, and need to be supplemented weekly. With 50 tons of sand present in a CFB system, weekly losses are below 0.5 %.

Geldart classified the various powders according to the particle size and absolute density. Very coarse powders (> 400 µm at 2600 kg/m³, classified as D-powders) are difficult to fluidize, and more adapted to spouted bed operation. Very fine powders (< 30 µm at 2600 kg/m³) are classified as C-powders, because of their inherent cohesive nature: they agglomerate mostly due to Vanderwaals forces, and cannot be fluidized.

In between the C and D powders, Geldart made a distinction between A (= aeratable) and B (Bubbling) powders. Both powders can easily be fluidized, and flow readily. A powders are however aeratable, meaning that they are characterized by a significant bed expansion prior to bubbling. Their minimum bubbling gas velocity exceeds the minimum fluidization velocity by a factor of about 2. B-powders are in the bubbling fluidization mode, as soon as the gas velocity exceeds the minimum fluidization velocity.

The gas flow velocity to convey particles is also a function of the particle size and density.

Although both A and B-powders can be used in CFB-applications, industrial preference goes to A-type powders because of the lower gas flow rate needed, and the ease of particle circulation due to their aeratability.

Given the wear caused by particles moving rapidly upwards and downwards, CFB reactors seldom employ internal surfaces. Hence, the design problem of greatest interest is how to predict the heat transfer coefficient at the wall of a CFB. The design of the heat transfer surface

requires the knowledge of the heat transfer coefficient between the flowing gas-solid suspension and the surface itself. The present Chapter investigates first experimental results obtained towards the heat transfer coefficient as measured in a riser for Geldart A-type particles with average particle size, d_{sv}, of approximately 75 μm, representative of most industrial CFB applications. The objectives of the research objective are: (i) to determine the wall-to-bed heat transfer coefficient for different operating conditions of gas flow and solids' circulation flux, thus covering the different operating modes of the riser flow (dilute, core-annulus, dense) and (ii) to compare experimental results with existing model approaches. The different operating modes have been classified by Mahmoudi *et al.* (2012) in terms of the dominant flow parameters, being the superficial gas velocity U (corrected for the velocity of onset circulating mode, U_{TR}) and the solids circulation flux G. The resulting diagram is represented in Figure 45. Since solids flow modes will determine the heat transfer coefficient, a summary discussion of these flow modes will be given in Section 5.3.

Figure 45: Hydrodynamic operating modes of a CFB riser, expressed as G versus U-UTR depending on the different hydrodynamic flow modes (Mahmoudi *et al.*, 2012)

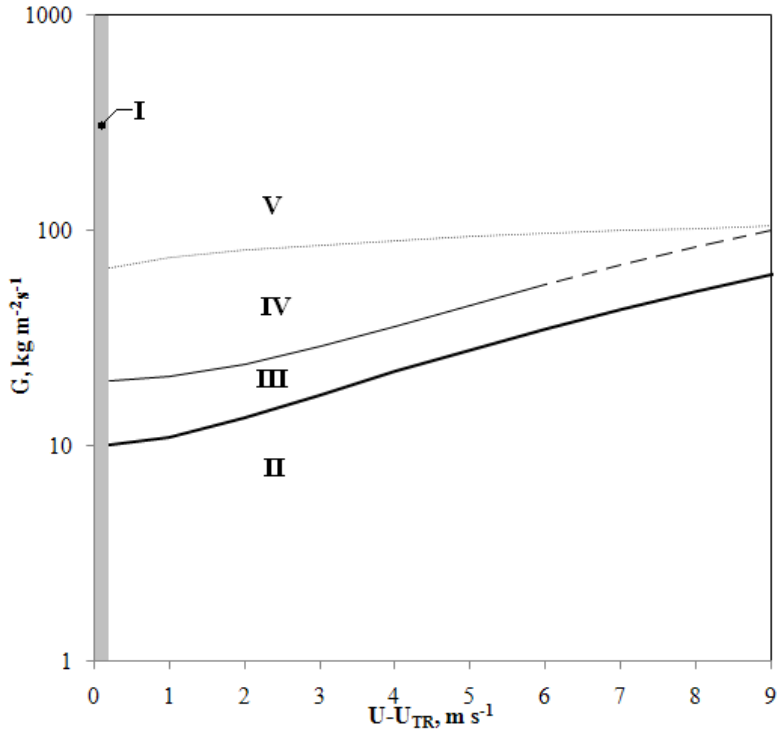

Zone I: Transition zone and/or inaccuracy in U_{TR} prediction
Zone II: dilute riser flow (DRF)
Zone III: core-annulus flow (CAF) only
Zone IV: CAF with turbulent fluidized bed at the bottom (TFBB)
Zone V: dense riser up-flow (DRU)
——— transition DRF - CAF: $G = 10 + (U - U_{TR})^{1.8}$
——— transition CAF - CAF with TFBB: $G = 20 + (U - U_{TR})^{2}$
·····transition CAF with TFBB - DRU: $G = 60 + 15 (U - U_{TR})^{0.5}$
– – – Range of operating conditions where CAF mode is no longer reported and only DRF and DRU prevail.

5.2 Background considerations: the heat transfer mode and possible thermal gradients

Since particles should rapidly achieve a uniform temperature during heat capture, the present section assesses the main objective of the study: “how can thermal gradients in and around the particle be avoided?” Application of the basic principles of both heat transfer to the particle and of heat conduction within the particle, allows to determine the required working conditions. The temperature uniformity throughout the particles can be determined by the heat

conduction law of Fourier, here applied in non-stationary regime and for the simple case of a spherical particle:

$$\frac{\partial T}{\partial t} = \frac{k_p}{\rho_p c_p}\left(\frac{\partial^2 T}{\partial r^2} + \frac{2}{r}\frac{\partial T}{\partial r}\right) \quad (5.1)$$

With

- k_p: heat conductivity of the particle at temperature T (W $m^{-1}K^{-1}$)
- c_p: specific heat capacity of particle at temperature T (J $kg^{-1}K^{-1}$)
- ρ_p: density of the particle (kg m^{-3})

when heated at a rate β (K s^{-1}):

$\partial T/\partial t = \beta$ for r = 0 to R (= $d_p/2$) and $\partial T/\partial r = 0$ for r = 0 (in the core)

The solution is given by Carslaw and Jaeger (1986) as:

$$\Delta T_{max} = (T_R - T_c) = \beta\, d_p^2/(24\,\alpha) \quad (5.2)$$

Applied for various values of β and with e.g. the characteristic properties of an inorganic particle at 773 K, i.e. k_p = 0.60 W $m^{-1}K^{-1}$, c_p = 1 150 J $kg^{-1}K^{-1}$ and ρ_p = 2800 kg m^{-3}, results are a set of curves in function of the diameter as shown in Figure 46.

Figure 46: Maximum temperature difference (ΔT_{max}) between the surface and core of the particle in function of the particle diameter at different heating rates (β).

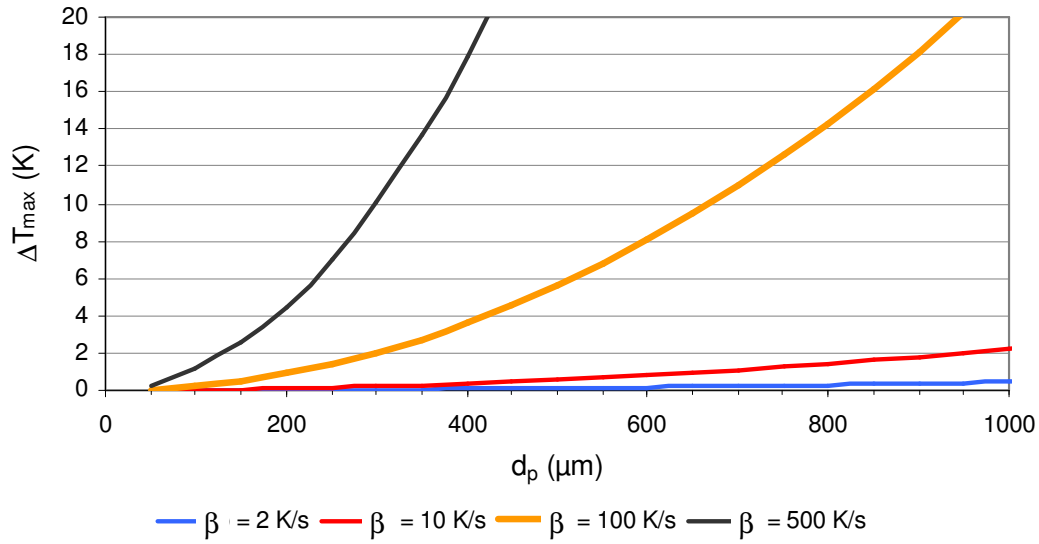

These calculations show that the temperature differences between the particle surface and core are very limited, certainly when considering that the surrounding temperature is 773K.

The heating rate will vary with the heating technique applied, between minimally 1.5 K s^{-1} in a TGA (thermogravimetic analysis), to a >> 100 K s^{-1} in a BFB or CFB (Baeyens and Geldart, 1980). In order to minimize ΔT_{max} (< 10 K) even at high heating rates, it is appropriate to use small inorganic particles (sand, SiC,…) below 400 µm. No significant thermal gradient will occur in these small particles, even when working at slow heating rates: the core and the surface of the particle will behave thermally in a similar way.

Solar energy capture and subsequent heat release require a fast heat transfer from the exchanger wall to/from the particles. This heat transfer is conditioned by the degree of gas and solid turbulence achieved in the collector. The heat transfer coefficient depends on the gas-solid contacting mode. It ranges from 10 W $m^{-2}K^{-1}$ for a static bed, to 50 - 100 W $m^{-2}K^{-1}$ in a fixed bed with forced gas circulation (as in TGA), and several hundreds of W $m^{-2}K^{-1}$ for BFB and CFB (Baeyens and Geldart, 1980). This explains why the fluidized beds are specifically

considered as top technologies for solar energy systems. The heat transfer coefficient in a CFB was previously measured by various investigators, with values of 300 to 600 $Wm^{-2}K^{-1}$.

Since not only external convection but also internal conduction is important, the overall picture is expressed by the Biot-number, as the ratio of the internal resistance to heat penetration and the external convection resistance to heat transfer.

$$Bi = (d_p/k_p) / (1/h) \quad (5.3)$$

For the 100 µm particle at 773 K, with a thermal conductivity k_p of 0.6 $Wm^{-1}K^{-1}$, the values are as follows:

- h = 300 W $m^{-2}K^{-1}$ Bi = 100.10-6 . 300 / 0.60 = 0.05
- h = 500 W $m^{-2}K^{-1}$ Bi = 100.10-6 . 500 / 0.60 = 0.08
- h = 700 W $m^{-2}K^{-1}$ Bi = 100.10-6 . 700 / 0.60 = 0.12

The Biot-number is < 1 in all cases, implying that the external resistance associated with convective heat transfer largely dominant for smaller particles. This remains valid for particle sizes below ~700 µm. Bi is only > 1 for coarser particles. This result confirms Figure 46 where limited increasing ΔT_{max} values are noticed with increasing β values (achieved at high convection heat transfer rates), for smaller particles, but significant differences occur for coarser particles. Operating a CFB collector at d_p < ~400 µm is hence certainly indicated to avoid thermal gradients within the particle. Fortunately, CFB operations are restricted to particle sizes of similar magnitude (Mahmoudi *et al.*, 2012).

5.3 The CFB operating conditions and heat transfer coefficient

The heat transfer to the wall of a CFB riser can be assumed to involve additive components due to conduction, convection and radiation. Many researchers have approached the phenomenon with a two-phase structure, somewhat similar to that described for bubbling fluidised beds (BFB) (Baeyens and Geldart, 1980). The two phases are however different from

those in bubbling beds, since no bubbles are present, but with the flow at the wall in the core-annulus (CAF) operating mode dominated by streamers or clusters travelling mostly downward, but interspersed with periods where there is upwards flow of the powder suspension. In dilute or dense riser flow, the solids flow is dominantly upwards. Complementing experiments in a bubbling bed, CFB experiments by Wu *et al.* (1989) with small flush-mounted heat transfer surfaces have shown rapidly varying local instantaneous heat transfer coefficients, with the fluctuations corresponding to the arrival of streamers at the heat transfer surface. Hence, the processes governing heat transfer are indeed similar in BFB and CFB, with packets of particles contacting the wall, and exchanging heat according to the known film penetration model (Kunii and Levenspiel, 1991). Several factors are however make the flow configuration more complex:

- The voidage distribution in bubbling beds is essentially binary, varying between a discrete dense phase voidage and nearly pure voids inside bubbles. The voidage distribution in a riser tends to be continuous and widely dispersed.
- The powder flow in the CFB riser can reverse directions, moving both upwards and downwards, especially in the CAF operating mode.

Boiler makers and other manufacturers of large CFB units estimate the heat transfer coefficient on confidential experience from previous units, with adjustments to account for such factors as changes in mean particle diameter, suspension density and membrane surface geometry. Published empirical correlations, widely used in bubbling fluidized beds, are not common for circulating fluidized beds. Instead, two semi-empirical models have been proposed in the literature based on the periodic renewal of particle clusters at the heat transfer surface. As indicated in equation (5.4), one treats the heat transfer as being additively composed of conduction/convection and radiation (Chen *et al.*, 2005).

$$h_{tot} = f_d h_d + (1 - f_d) h_l + h_r \tag{5.4}$$

where h_{tot}, h_d, h_l and h_r are the total effective heat transfer coefficient, the heat transfer coefficient during dense (particle) phase contact, the heat transfer coefficient during lean gas phase contact and the heat transfer coefficient for radiation, respectively. f_d is the time fraction of contact by the dense phase (Chen *et al.*, 2005).

The experimental data available for predicting the heat transfer in CFBs are mostly from larger CFBs, with cross-sectional areas varying from 2.4 to 88 m², as summarized by Golriz and Grace (2002). While the limited number of data is disadvantage, there is one significant advantage of larger scale equipment, being the fact that large risers are tall enough to guarantee that both the flow and the heat transfer are fully developed (Golriz and Grace, 2002). In small scale CFBs, relevant measurements should only be made in the fully developed riser flow, i.e. at a distance from the recycle entry and the exit geometry (Chan *et al.*, 2009; Mahmoudi *et al.*, 2011).

5.3.1 Operating hydrodynamic regimes in a CFB

The riser operating modes are vital to design a CFB for a required process of either gas-solid or gas-catalytic nature. Different operating modes provide different solid residence times and mixing behaviour, which define both the efficiency/yield of the reactions and the heat transfer. Literature gives evidence of distinct operating modes as a result of observed differences both in slip factors, and in the range of particle velocities and their associated residence time distribution (Mahmoudi *et al.*, 2012), resulting in the definition of 4 distinctive solids hold-up regimes in the riser, as illustrated in Figure 45, with the different operating modes (dilute, dense, core-annulus, combined) being a function of U and G in the riser.

The various flow regimes have distinct characteristics towards solids flow, and hence towards heat transfer. For these different regimes, the particle velocity has been expressed by equation (5.5), introducing the slip factor, φ, resulting in:

$$\bar{v}_p = \frac{U}{\varepsilon\varphi} \tag{5.5}$$

The slip factor is the ratio between the real particle velocity, and the theoretical particle velocity calculated on the basis of the interstitial gas velocity (U/ε) and the terminal particle velocity. If particles behave individually, the theoretical calculation holds, and the slip factor is close to 1. In **Dilute Riser Flow (DRF)**, the solids are predominantly moving upwards with negligible downward flow. In DRF-regime, the slip factor, φ, has a reported value between 1 and 1.2 (Chan et al., 2010; Hartge et al., 1988). In **Core-annulus Flow (CAF)**, the solids motion is an upward core flow and unsteady downward (cluster or streamer) flow in the annulus. Particles cluster together (in fact behaving as a particle cluster with higher terminal velocity than the individual particle), and the real particle velocity if lower than the calculated value. The ratio, i.e. the slip factor, then achieves values close to 2. The solids velocity can be predicted by equation (5.5), with φ values close to 2 (Chan et al., 2010; Matsen, 1976; Ouyang and Potter, 1993). The regime of the **Core-annulus Flow (CAF) with Turbulent Fluidised Bottom Bed (TFBB)** is characterized by an axial voidage profile of typical S-nature, due to the appearance of a Turbulent Fluidised Bottom Bed (TFBB). The residence time for CAF with TFBB is significantly longer than CAF itself and DRF due to the existence of the fully mixed TFBB. Chan *et al.* (2009) demonstrated that the residence time for solids in TFBB alone can range from 10 to 20s. The voidage of the TFBB ranges from 0.7 to 0.9 and can be predicted by the empirical equation (5.6) (King, 1989):

$$\varepsilon_B = \frac{U+1}{U+2} \tag{5.6}$$

The characteristics of the CAF region above the TFBB are similar to the above sole CAF flow, as described before. The **Dense Riser Upflow (DRU)** regime has almost similar characteristics to DRF, the main difference being that the φ values are fractionally higher, ranging between 1.2 and 1.6 with an average of 1.3 (Chan et al., 2010).

These various hydrodynamics regimes show an evolution of bed voidage with height in the riser, characteristic for the various operating modes. Average voidages range from approximately 0.98 in dilute flow (DRF); 0.7-0.9 in a bottom fluidised bed (TFBB), 0.95-0.98 in core-annulus mode (CAF), to ~ 0.9 in dense riser up-flow DRU respectively (Brems et al., 2011; Smolders and Baeyens, 2001a, 2001b).

Each regime more or less shows a similar behaviour in the **Acceleration Zone** with the exception of CAF with TFBB mode, where two acceleration zones exist to include the **Initia**l **Acceleration Zone** at the base of the TFBB, and a secondary acceleration zone at the transition between TFBB and CAF. The tentative delineation of the regimes is shown in Figure 45 (Mahmoudi *et al.*, 2012).

Commercial risers of e.g. combusters and calciners, are reported in CAF operation in the range of $U\text{-}U_{TR}$ = 0.5 to 5 m/s and G-values of 10 to about 80 kg/m^{2}s. CFB operations in DRU-mode are reported in mostly gas-catalytic operations for $U\text{-}U_{TR}$ values in excess of about 8 m/s and G-values between 150-1200 kg/m^{2}s. These reported combined (U,G) ranges are in good agreement with the proposed operation diagram of Figure 45

5.4 Previous work on heat transfer in a CFB riser

5.4.1 Molodtsof and Muzyka

Work undertaken on vertically flowing suspensions has been reviewed in great detail by Muzyka (1985) and Grace (1990). As long as convective heat transfer between the suspension and the surface is considered, with the exclusion of radiant heat transfer, the major concern is to predict the variation of the heat transfer coefficient with solids loading and gas velocity in various riser geometries. Various empirical correlations and models (mostly for bed-to-wall heat transfer) have been proposed (Basu and Nag, 1987; Wu *et al.*, 1989), but Grace (1990) summarized the situation as follows: “no existing correlations give consistent agreement with the available data”.

The theoretical approach proposed by Molodstof *et al.* (1984) and by Molodtsof and Muzyka (1989) is based upon the rigorously derived general probabilistic equations for multiphase flow (Molodstof, 1985). According to their treatment, the wall-to-suspension heat transfer coefficient can be expressed as a function of the loading ratio, M, and of the heat capacity ratio, C:

$$\frac{h_m}{h_g} = \frac{(1 + MC)^2}{1 + aMC + b(MC)^2} \tag{5.7}$$

The equation relates the heat transfer coefficient of the suspension, h_m, to that of the gas alone, h_g, flowing in the same pipe at the same gas flow rate. The loading ratio, M, expressed as kg solids/kg gas, together with the solids-to-gas heat capacity ratio, $C = C_p / C_g$, are the dominant parameters. The dimensionless parameters a and b in equation (5.7) are compound factors involving dimensionless radial concentration, velocity, and temperature profiles. They are generally unknowns, as the profiles are unknown, and depend upon design parameters (pipe diameter, particle size distribution and physical properties), and upon the superficial gas velocity. With a and b fitted from experimental results for the specific gas-solid system under scrutiny, the trend of reported heat transfer results, obtained at a constant wall heat flux, was shown to be in good agreement with predictions of equation (5.5) (Muzyka, 1985). It was therefore considered interesting to assess the CFB-validity of equation (5.7), as well as the effect of the flow structure on the heat transfer.

5.4.2 Golriz and Grace

Golriz and Grace (2002) devised a model for large units (> 1 m ID) based on the assumptions of fully developed conditions and radially uniform clusters at the wall, hence valid for CAF operation. At any instant, some portions of the surface are bare, while other portions of the surface are covered by clusters, each separated from the wall by a thin gas gap of thickness δ_g. Different heat transfer mechanisms are assumed for the bare and covered portions. For the

bare sections, transfer is by gas convection (denoted by subscript 'gc') and by radiation from the suspension to the wall (subscript 'sr'). The rest of the wall is covered by clusters/streamers providing a parallel transfer path. The transfer rate is then assumed to be controlled by a particle horizontal exchange flux, G_{sh}. The combined expression of the heat transfer coefficient is given as a total heat transfer coefficient, h_{tot}, as follows:

$$h_{tot} = \left(h_{gc} + h_{sr}\right)\left(1 - f\right) + \frac{f}{\frac{1}{G_{sh}C_p + h_{be}^{rad}} + \frac{1}{\left(k_g / \delta_g\right) + h_{ew}^{rad}}} \tag{5.8}$$

For operation at temperatures below 600 °C, the radiation contribution is negligible (Baeyens and Geldart, 1980).

The parameters of the equation are correlated by different equations.

The fractional coverage f accounts for the scale of the unit as follows:

$$f = 1 - \exp\left[-25000\left(1 - \frac{2}{\exp(0.5D) + \exp(-0.5D)}\right)\left(1 - \varepsilon_{sus}\right)\right] \tag{5.9}$$

where D is the riser equivalent diameter (4x cross sectional area/perimeter) in metres. For large units, f approaches unity, meaning that the entire wall becomes covered by clusters. An alternative relationship giving somewhat lower values of f as D increases has been suggested by Dutta and Basu (2003). The gas convective transfer coefficient, h_{gc}, was obtained from the well-known Dittus-Boelter correlation (Welty, 1974).

The gas gap thickness is estimated from:

$$\delta_g = 0.0282\ d_p \left(1 - \varepsilon_{sus}\right)^{-0.59} \tag{5.10}$$

where d_p is the average particle diameter and ε_{sus} is the cross sectional average suspension voidage (Lints and Glicksman, 1993).

An expression for the lateral solids flux was obtained by fitting all heat transfer data for units of hydraulic diameter $\geq$ 1 m where the suspension densities, $\rho_{sus} = \rho_p (1 - \varepsilon_{sus}) + \rho_g \varepsilon_{sus}$, were greater than or equal to 5 kg/m^3, leading to:

$$G_{sh} = 0.1093 + 0.0225 \ln(\rho_{sus}) \quad (5.11)$$

This approach provides a quantitative means of estimating heat transfer coefficients for the design of large-scale CFB units. However, it is not considering such factors as the interaction between radiation and convection, the heat transfer resistance in the tube wall and on the steam side, the upward/downward motion of the powder at the wall, and the highly three-dimensional nature of the membrane wall surface. A more advanced model that accounts for these factors is proposed by Xie *et al.* (2003b) and by Xie *et al.* (2003a).

The fundamental radiation approach of Gorliz and Grace can however be simplified. The effect of operating at higher temperature, i.e. generally> 600 °C, is twofold and includes the effect of both the increasing thermal properties of mainly the gas phase, and the direct contribution of radiation heat transfer. The effect of the thermal properties of the fluidizing gas is reflected to a major extent in the temperature dependence of the increasing gas thermal conductivity as T increases, and increasing the heat transfer coefficient proportionally with $\sqrt{k_g}$ (Baeyens and Geldart, 1980; Kunii and Levenspiel, 1991). The additive effect of radiation itself is expressed in equation (5.4), with an increasing contribution to heat transfer as T increases, however function of the size and nature of the fluidized solids (Baskakov, 1985). Adapted results of Baskakov are illustrated in Figure 47 for particle sizes as commonly used in CFB applications (Baskakov, 1985). This figure provides a rule of thumb estimate.

Figure 47: Fractional component of total heat transfer coefficient attributable to radiation, wall temperature 850°C, and for three mean particle sizes (adapted from (Baskakov, 1985))

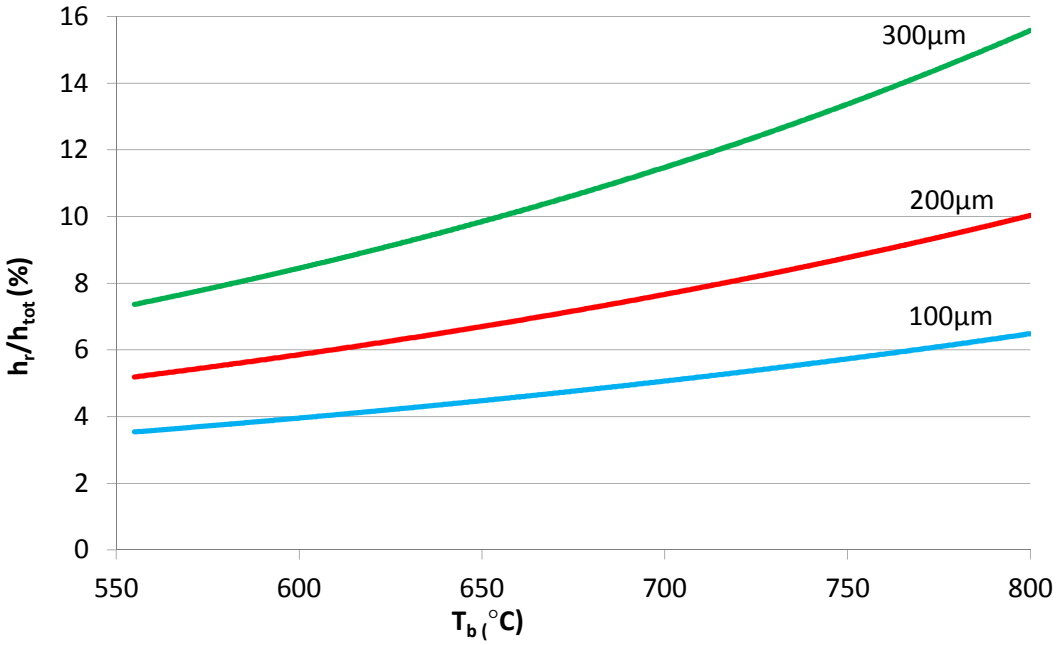

The radiation component can also be estimated by using the Stefan-Boltzman equation:

$$h_r = 5.673 \times 10^{-8} \varepsilon_r (T_w^4 - T_b^4) / (T_w - T_b) \quad (5.12)$$

with wall (T_w) and bed (T_b) temperatures in absolute values, and ε_r as reduced emissivity to account for the different emissive properties of the surface (ε_s) and bed (ε_b), according to:

$$\varepsilon_r = 1 / [(1/ \varepsilon_s + 1/ \varepsilon_b) - 1] \quad (5.13)$$

ε_b assumes values of 0.59 for Al_2O_3 and ZrO_2, 0.8 for clay, 0.85 for sand and 0.95 for fused MgO.

Because of the effect of the hot surface on the immediately adjacent particles, the bed temperature there will be higher than the bulk temperature, and allowance should be made for this when using the bulk temperature in equation (5.18). Baskakov suggests to use an apparent emissivity (ε_{app}) instead of ε_r (Baskakov, 1985).

Figure 48: Apparent emissivity (adapted from (Baskakov, 1985))

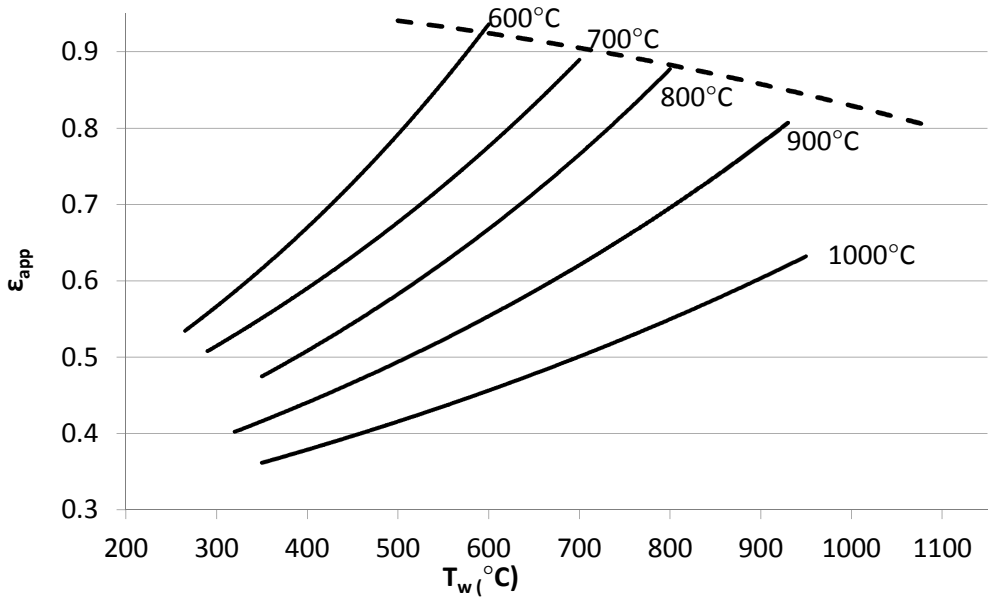

The values of ε_{app} will be a function of the operating temperatures, as illustrated in Figure 48 (Baskakov, 1985). A reasonable value for alumina would be between 0.6 and 0.7, and somewhat lower for sand. ε_r may be as low as 0.1 when using a shiny metal surface.

5.4.3 The surface renewal model

Since the heat transfer is determined by the transient heat transfer of the transfer wall to packets of particles in contact, a surface renewal model can possibly be applied, as developed by Baeyens and Geldart (1980) for bubbling fluidized bed applications.

$$h(\bar{\theta}) = \frac{h_c}{1 + \frac{6h_c}{\rho_p C_p d_p}\bar{\theta}} \tag{5.14}$$

where $h(\bar{\theta})$ is the average heat transfer coefficient from the suspension to the wall, h_c is a contact transfer resistance, and $\bar{\theta}$ is the average contact time of the particle packets at the wall. The experimental results will also be used to check the applicability of such a packet renewal mechanism.

5.5 Experimental setup and procedure: wall-to-bed heat transfer

The riser and CFB are depicted in Figure 49. The riser consists of a 50 mm ID pipe approximately 2.5 m high. Solids circulation was achieved via a 100 mm ID downcomer and 50 mm ID L-valve. Air is supplied through a distributor plate and leaves the system through a cyclone after the riser exit. Pressure taps are located along the height of the riser and connected to a data acquisition system. Flow rates and pressure drops were monitored. A concentric wall heater of 10 cm length was installed at 1.2m above the re-entry joint of the L-valve, hence within the fully-developed riser flow made. Heat supply was by hot water or thermal fluid (Santotherm 350). The downcomer was water-cooled through a 0.2 m long concentric cooler. The wall surface temperature was measured using a resistance thermocouple welded onto the wall. Additional Thermocoax thermocouples (0.1 mm OD) were installed at various locations in the riser and downcomer, as well as in the feeding and overflow lines of the fluid, as indicated in Figure 49. The heat input was set at such a value, that the bed temperature ranged from 30 to 40°C.

Figure 49: Layout of the experimental set-up

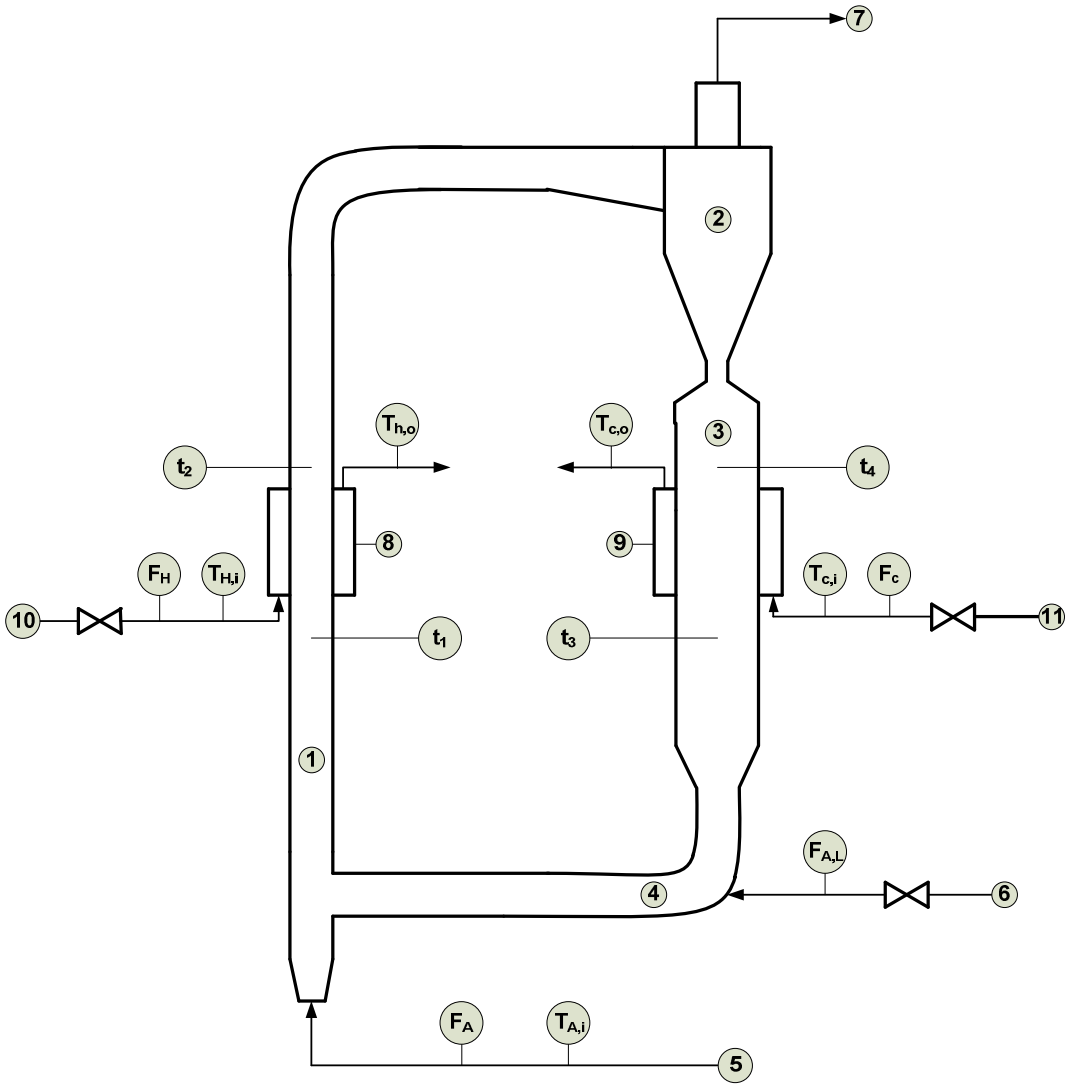

(1) riser 50 mm I.D., (2) HE Stairmand cyclone, (3) downcomer 100 mm I.D., (4) L-valve 50 mm I.D., (5) air from speed-controlled blower, (6) compressed air, (7) vent to bag house filter, (8) co-axial heating section, (9) co-axial cooling section, (10) supply of thermal fluid, (11) supply of cooling water; F_H, F_C, F_A, $F_{A,L}$: respectively flow meters of thermal fluid, cooling water, riser air, L-valve air; T: temperature probes for respective fluids; t: temperature probes inside riser and downcomer.

The experiments consisted of starting the gas flow to the riser, followed by the flow of the fluidizing gas to the solids feeder. The flow rates of gas and solids were then set to the desired values, the heat input into the system was fixed, and the system was allowed to stabilize over a period of about one hour, during which flow rate, temperatures, and pressures were monitored and recorded.

The axial pressure profile was recorded during each experiment in order to make sure that the suspension entering the heated section was in fully developed flow conditions.

From the known exposed surface area, A_{ex}, and measured temperature difference, ΔT, the heat transfer coefficient was calculated for the given heat input as:

$$h_m = \frac{Q}{A_{ex}\Delta T} \tag{5.15}$$

The measurements were performed for the gas flow alone and for the gas-solid suspension at various solid/gas ratios. The heat transfer coefficient to the gas-solid suspension, h_m, was also expressed as h_m/h_g ratio. The bed material used was rounded sand of the following characteristics: d_p = 75 µm, ρ_p = 2260 kg/m^3, and C_p = 1.05 kJ/kg.K.

Various combined (U,G) values were tested in order to scan the different riser hydrodynamic regimes: these conditions are illustrated in Figure 50, using the Mahmoudi *et al* regime diagram as a basis (Mahmoudi *et al.*, 2012). Clearly, all operating modes were assessed by the experiments.

Figure 50: Experimental (U,G) conditions in comparison with the riser flow modes.

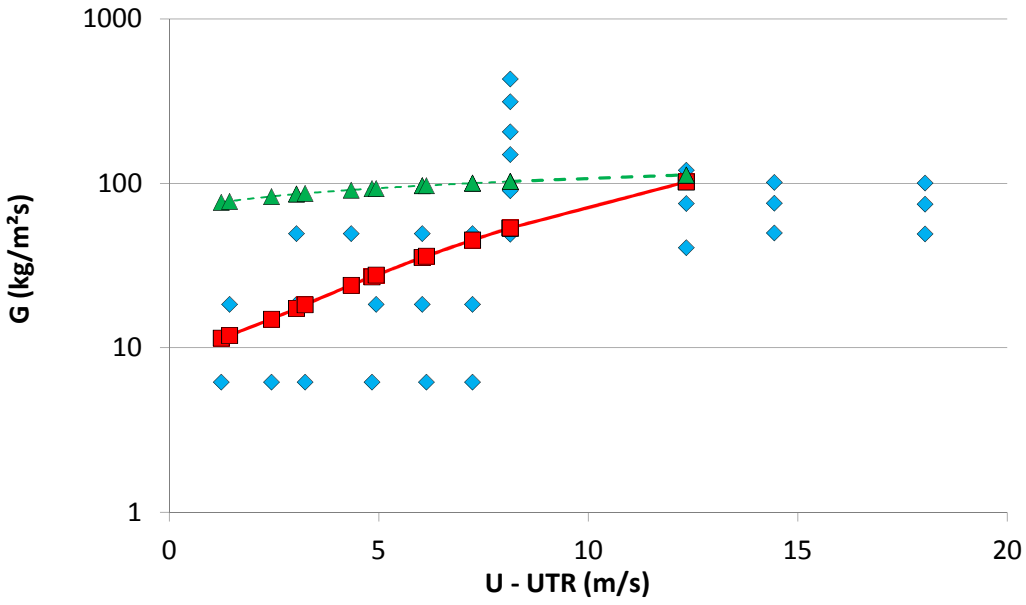

5.6 *Results and discussion*

5.6.1 *Preliminary literature findings*

In a previous research, Everaert *et al.* (2006) studied the heat transfer coefficient to an in-bed heat transfer surface in a 0.1 m I.D. riser, expressed as h_m and related to the sole gas flow convection heat transfer coefficient h_g (Everaert *et al.*, 2006).Experiments were carried out in the DRF and CAF operating modes. It was demonstrated that (i) the heat transfer coefficient in the core is significantly higher than at the wall; (ii) the core region extends to approximately 85% of the riser radius (0.05 m), hence with an annulus thickness of approximately 7.5 mm; and (iii) Increasing the gas flow rate at a given solid circulation rate significantly reduces the suspension heat transfer coefficient.

The Everaert *et al.* paper moreover quantitatively determines the radial dependence of the heat transfer coefficient, as illustrated in Figure 51 (Everaert *et al.*, 2006).

Figure 51: Effect of the radial position of the heater in the riser on the heat transfer coefficient h_m (expressed as ratio) at U_g = 7.8 m/s.

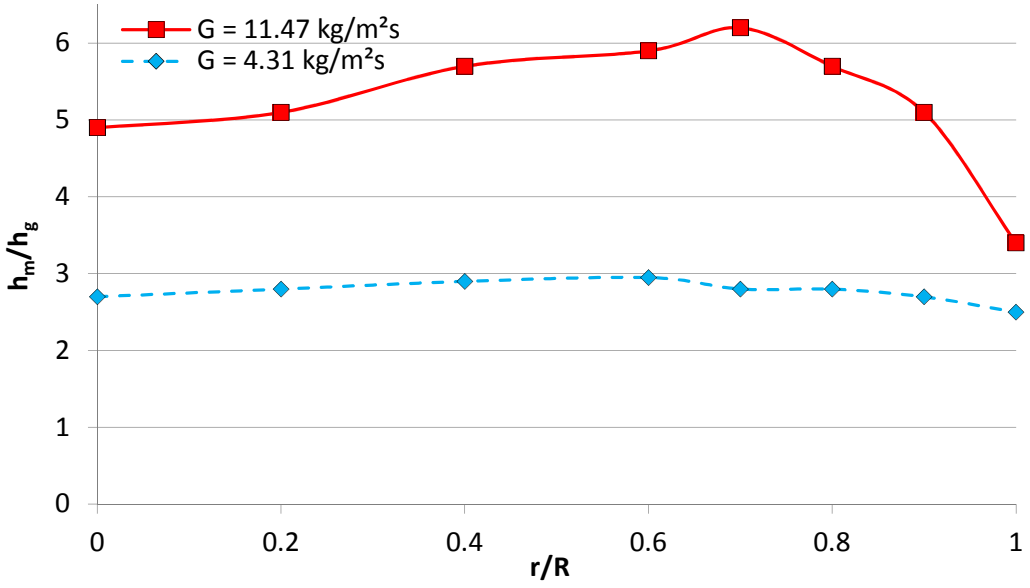

It can be seen that the wall-to-bed heat transfer coefficient is about 20 to 40% lower that the in-bed surface heat transfer coefficient. Even in dilute flow, i.e. at the low *G* values of Figure

51, the solids contribute significantly to the overall heat transfer coefficient, since the ratio h_m/h_g exceeds ~ 2.

5.6.2 *Experimental results for the riser-wall to bed heat transfer coefficient, h_m*

Experimental results are illustrated in Figure 52: h_m is a strong function of the (U,G) combination, especially at lower G values, thus also of the hydrodynamic operating mode of the riser. Experimental results will further be developed in terms of the approaches of Section 5.4.

Figure 52: Experimental results, expressed as hm for different (U,G) combinations

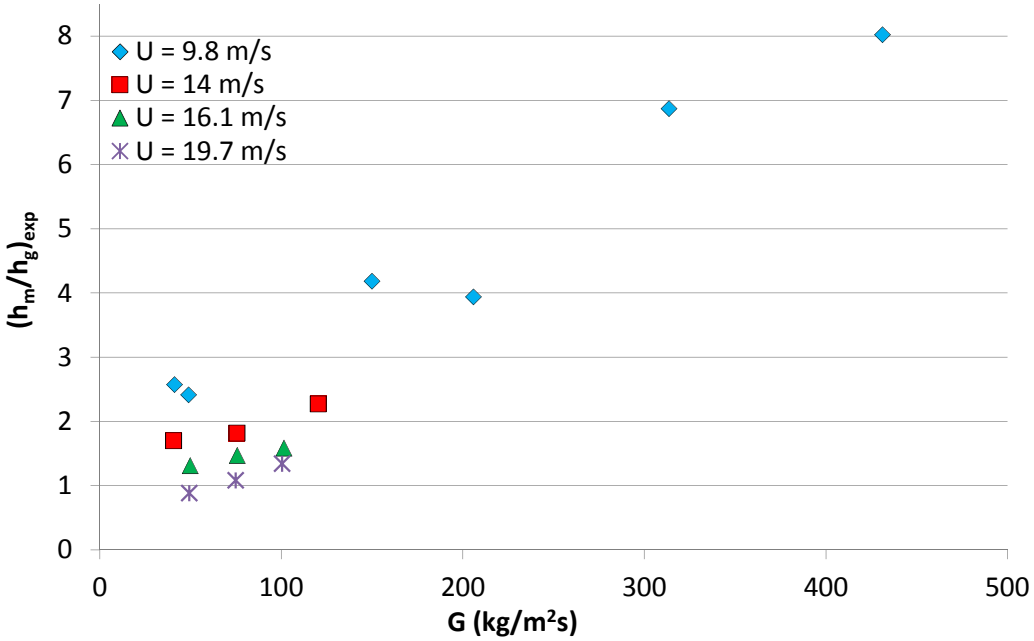

At $G = 0$, h_m should assume the h_g heat transfer coefficient, only a function of U.

5.6.3 *Transformation of experimental results into design equations*

5.6.3.1 *The gas convection coefficient.*

Essential in the use of the semi-experimental equations, is the prediction of the heat transfer coefficient when solids are absent, i.e. the heat transfer coefficient between the heat transfer surface and a pure gas flow in the riser, h_g. The equation used to predict h_g in the present

treatment was presented by Gnielinski to cover gas flow in the transitional and turbulent flow regime (Gnielinski, 2007):

$$Nu = \frac{h_g D}{k_g} = \frac{\left(\frac{\zeta}{8}\right)(\mathrm{Re} - 1000)\,\mathrm{Pr}}{1 + 12.7\sqrt{\frac{\zeta}{8}}\left(\mathrm{Pr}^{2/3} - 1\right)}\left(1 + \left(\frac{D}{L}\right)^{2/3}\right) \tag{5.16}$$

with $\zeta = \sqrt{1.82 \log(\mathrm{Re}) - 1.64}$ and other symbols defined in the Nomenclature.

5.6.3.2 Molodtsof and Muzyka

All results were expressed as h_m/h_g values.

In order to compare the experimental results with the trend of variations predicted by equation (5.7), a new dimensionless variable, *Y*, was defined as follows:

$$Y = \frac{1}{MC}\left(\frac{(1+MC)^2}{h_m/h_g} - 1\right) \tag{5.17}$$

As a result, the Molodtsof and Muzyka equation (5.7) can be written as:

$$\mathrm{Y} = \mathrm{a} + \mathrm{bMC} \tag{5.18}$$

Because the solid-to-gas heat capacity was essentially constant in our experiments, the results could be used to define coefficients a and b (which remain constant in the range of gas velocities and solids loadings) and thereafter predict h_m/h_g for various values of *M* and *C*. The results are given in Figure 53, illustrating the fair agreement obtained, with coefficients a and b respectively 3.538 and 0.03406, and with a regression coefficient R^2 = 96.47%.

Figure 53: Comparison of experimental and Molodstof-Muzyka (MM) predicted values of h_m/h_g

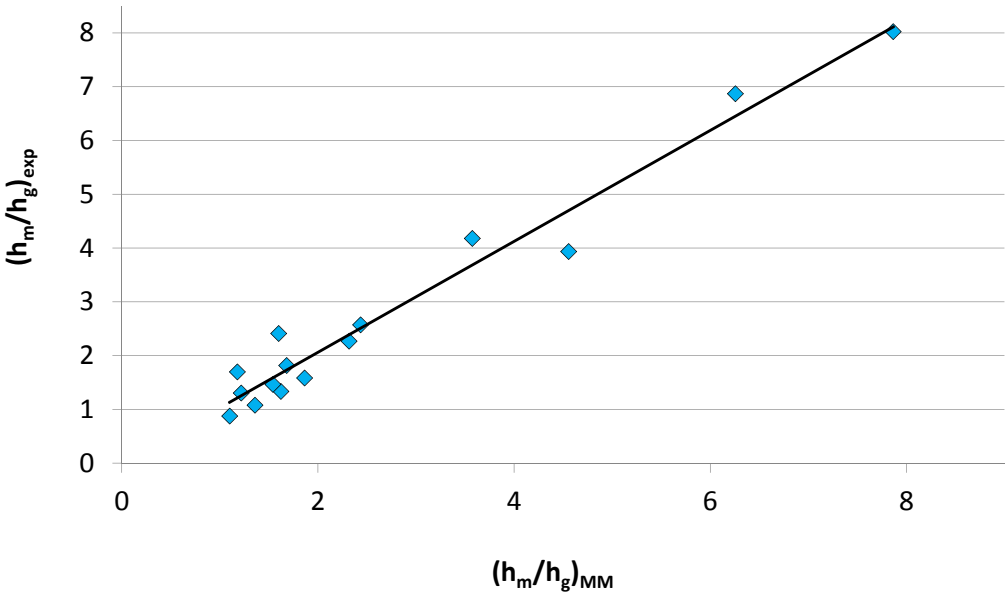

Of course, the design application of the Molodtsof and Muzyka approach needs experimental determination of coefficients a and b.

5.6.3.3 Golriz and Grace

The empirical equations of Golriz and Grace (Golriz and Grace, 2002) can be transformed into the following equation, when radiation is neglected.

$$\frac{h_m}{h_g} = (1-f) + \frac{f}{\left(\frac{1}{G_{sh}C_p} + \frac{1}{k_g/\delta_g}\right)} \tag{5.19}$$

The suspension density was calculated according to Chan *et al.*, with t_p and t_g the residence times of the particles and the gas in the riser respectively (Chan et al., 2010). The values of t_g were calculated by the method presented in Mahmoudi *et al.* (2011), thus a function of U and G.

$$\varepsilon_{sus} = \frac{Ut_g}{Ut_g + Gt_p/\rho_p} \tag{5.20}$$

$$\rho_{sus} = \varepsilon_{sus}\rho_g + (1-\varepsilon_{sus})\rho_p \tag{5.21}$$

Results of the comparison are illustrated in Figure 54.

Although Golriz and Grace only deal with CAF applications (G< ~100 kg/m²s) in large scale risers, experimental results of the CAF regime were compared with predicted values, as illustrated in Figure 54.

Figure 54: Comparison of experimental and Golriz-Grace (GG) predicted values of hm/hg (for G < ~100 kg/m²s)

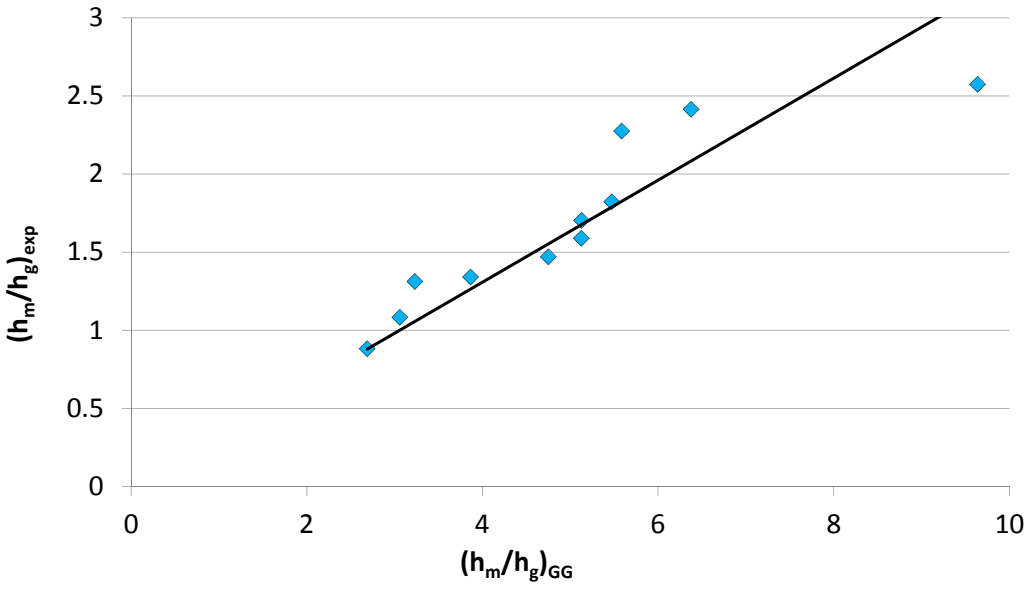

The deviation is between ~250 and 350%. Reasons are inherently linked to the difference in equipment scale, and to the required calculation of the underlying parameters, again on the basis of empirical approaches. A sensitivity analysis of the Gorliz-Grace approach pointed out that the predicted heat transfer coefficient is highly sensitive to the empirical parameter G_{sh}, as predicted by equation (5.16). A very fair agreement of the present experimental and Gorliz-Grace predicted h_m/h_g ratios was obtained, by using a modified equation for G_{sh} as function of the suspension density ρ_{sus}, being:

$$G_{sh} = 0.014 \text{ , for } \rho_{sus} \geq 12 \text{ kg/m}^3 \text{ (hence in the DRU mode)} \quad (5.22)$$

$$G_{sh} = 0.014 + 0.006\,(12-\rho_{sus}), \text{ for } \rho_{sus} < 12 \text{ kg/m}^3 \text{ (hence in CAF or DRF mode)} \quad (5.23)$$

Applying these equations (5.22) and (5.23) into the Gorliz-Grace model, predicts values of the heat transfer coefficient, for all examined flow modes, within +/- 10 % of the experimental value, as illustrated in Figure 55.

Figure 55: Comparison of experimental and Golriz-Grace (GG) predicted values of hm/hg (for G < ~100 kg/m²s) using the modified of equations (5.22) and (5.23)

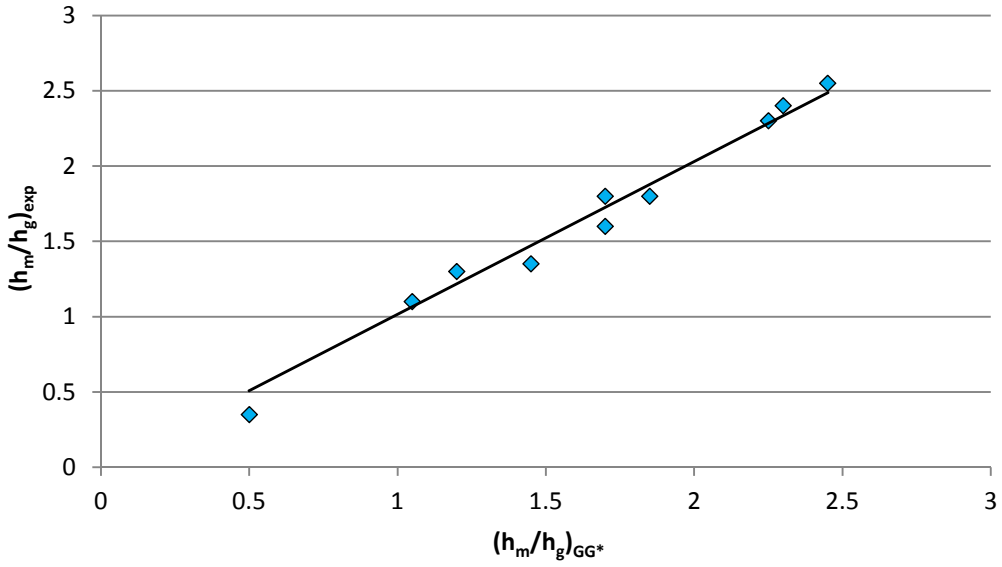

5.6.4 Surface removal model

Comparing experimental h_m values with predictions using equation (5.20) enables the determination of the required fitting $\bar{\theta}$. This $\bar{\theta}$ value is represented in Figure 56

Figure 56: Fitting contact time for different combinations of U and G.

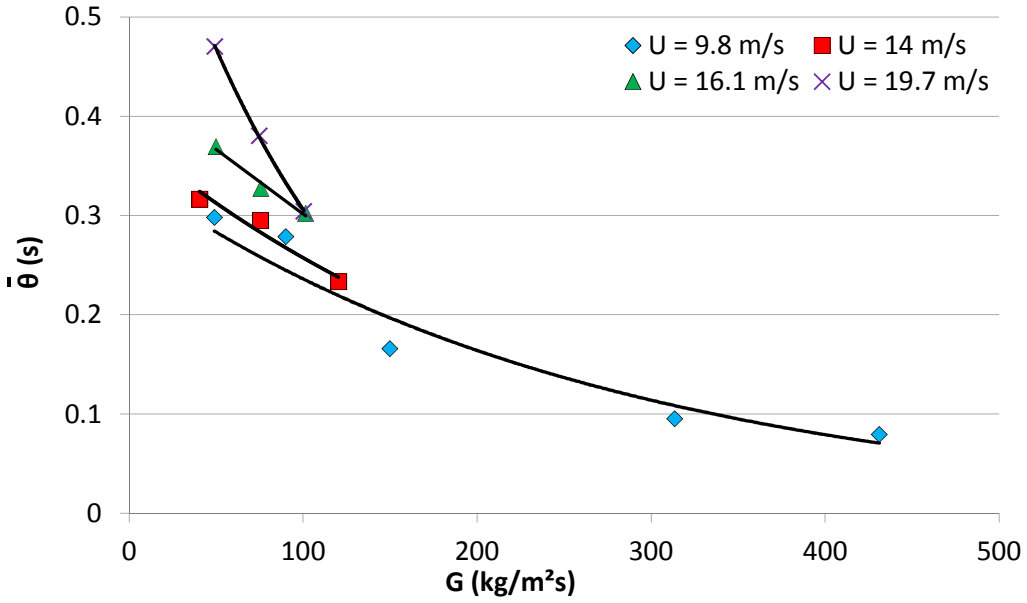

The fitting value of $\bar{\theta}$ and the trend of its dependency on (U,G) again stresses the importance of the riser operating mode. At high values of G, irrespective of U, the riser operates in the DRU (dense upwards flow) mode, and the contact time is determined by the prevailing solids velocity. This velocity is close to the operating gas velocity, according to equation (5.5) with ε ~ 0.9 and φ ~ 0.1s. In the CAF regime, for G< ~ 100 kg/m²s, the contact time is a function of the downward velocity is normally assumed to be close to the terminal velocity of the particles, i.e. 0.38 m/s for the tested particles.

For the heater length of 0.1 m, the contact time should hence be close to 0.26 s, in fair agreement with the experimental fitting results. The application of the contact time approach therefore certainly merits further investigations. These will combine heat transfer measurements and particle residence time measurements by Positron Emission Particle Tracking.

5.6.5 Contribution of radiant heat transfer

The effects of an increasing temperature are twofold: (i) the particle convective heat transfer coefficient will increase due to the increasing thermal conductivity of the gas phase, included in

the contact transfer resistance, h_c, of equation (5.20). In general, the convective heat transfer coefficient will increase proportional to $\sqrt{k_g}$ (Baeyens and Geldart, 1980).

(ii) At $T>600\,℃$, radiation itself becomes important and can be calculated by using the well-known Stefan-Boltzman equation (Baeyens and Geldart, 1980). In general, the contribution of radiation to the overall total heat transfer coefficient will increase from ~10% at 600° C to ~20% at 800°C (Baeyens and Geldart, 1980).

Both effects of k_g and radiation from wall-to-bed will significantly increase the heat transfer coefficient at bed temperatures of 500°C to 750°C, and wall temperatures > 850 °C, as encountered in solar energy capture beds.

5.6.6 The advantages of using PCM-particles in the CFB solar energy capture

Despite the excellent heat transfer coefficient to common heat carrier particles such as sand or SiC, these systems suffer from mainly two drawbacks: (i) the progressive increase in bed temperature as the particles are conveyed from the inlet of the riser (*500 °C*) to its outlet (*750 °C*), thus affecting the driving heat transfer temperature difference between wall and bed; and (ii) the sole heat capture in the form of sensible heat, where the amount of heat to be removed, (Q), necessitates a high circulation rate (*kg/h*) of particles, being $Q \,/\, C_p\ (T_{out} - T_{in})$. High circulation rates involve high associated conveying operation costs.

When using PCM-materials, (i) the bed temperature will achieve its (constant) maximum at the temperature of fusion of the PCM, thus maintaining a slightly higher driving temperature difference; but most importantly (ii) sensible and latent heat (of fusion) will take part in absorbing Q, thus reducing the required circulation rate of particles by a factor of > ~*3* at the given temperature ranges. This significant reduction also reduces the required conveying power and associated costs by the same factor. The development of PCM-coated particles, that can withstand both the thermal stress of temperature and phase variations, but also the erosive nature of the CFB is of paramount importance. According to the results of the present research,

these PCM particles, still to be developed and manufactured, should be of particle size well below 400 µm to avoid the internal conduction resistance, while offering advantages of a high composite specific heat capacity, affecting both the heat capacity ratio, C, in the Molodtsof-Muzyka equation (5.7), and the denominator of equation (5.14).

5.7 Conclusions and recommendations

The present research measured the wall-to-bed heat transfer coefficient in the riser. Measured heat transfer coefficients increase with increasing solid flux at equal values of the gas velocity, and achieve values of ~ 60 W/m²K at low G and high U values, and up to 350 W/m²K at G ~500 kg/m²s.

The ratio of the suspension heat transfer coefficient and the convective transfer coefficient for the sole gas flow is confirmed as a valid fitting parameter. The application of Molodtsof and Muzyka requires the determination of 2 empirical constants by using the experimental results. Once best fit values of these coefficients are obtained, the correlation predicts the correct trend of the evolution in heat transfer coefficient with U and G.

Within the core-annulus flow regime, the equation of Golriz and Grace, together with the assumptions of its composing parameters, overestimates the experimental results by a factor of about 3. The equations are very sensitive to the values of the estimated parameters; especially G_{sh}. Modified equations for G_{sh} were proposed to fit experimental and predicted results.

When applying a packet renewal mechanism to predict the heat transfer coefficient, the definition of a contact time on the basis of particle velocities in the riser, highly different in function of the riser operating regime, very fairly predicts heat transfer coefficient values. Further research coupling heat transfer measurements and particle contact times (as measured by Positron Emission Particle Tracking) are needed to improve the renewal approach.

If e.g. a CSP of 10 MW needs to be built, with a tube surface temperature of 950 °C (Torresol Energy Investments, 2012), and a solid circulation system at 200 kg/m²s between 500

and 650 °C circulating in collector pipes of 0.01 m ID, the previous results demonstrate that the following design parameters prevail :

- Heat to be captured : 10 MW = 10,000 kJ/s
- Solids circulation per pipe : 200 x π x 0.1²/4 = 1.56 kg/s
- Heat captured per pipe : 1.56 x 1.05 (kJ/kg.K) x (650 – 500) = 246 kJ/s
- Number of parallel pipes : 10,000/246 = 41 pipes

With a heat transfer coefficient, radiation included, of 500 W/m²K, the exchange surface area required is:

10,000 / 0.5 x (900 – 575) = 61.5 m².

At 0.1 m I.D., and 41 pipes, each pipe will have a length of 61.5/ (π x 0.1) x 41 = 4.8 m.

Since the solar energy capture window at the Gemasolar CSP towers have a height of about 7 m, 5 m long tubes are certainly acceptable.

If a phase change powder could be applied, the phase change latent heat will about triple the sensible het (C_p x ΔT), and the solids circulation rate can be reduced to about 70 kg/m².s, without significantly affecting the heat transfer coefficient, but reducing the powder pumping power by a factor of 3.

6 CONCLUSIONS AND RECOMMENDATIONS FOR FURTHER RESEARCH

Phase Change Materials (PCMs) have been recognised as having an exceptional potential in applications of thermal energy transport and storage. Their high energy density is the result of the joint contribution of latent and sensible heat. In order to contain, protect and enhance the heat exchange of the PCM with the thermal heat source (solar, waste heat) most usages will require the encapsulation of the material in an inert, mechanically and thermally stable coating, of high thermal conductivity. Commercial applications are available at ambient and moderate temperatures, whereas high temperature processes are still under development. The present thesis focused on a particular high temperature encapsulated PCM.

The **first chapter** provides a general background of the worldwide energy consumption and the need to develop advanced and highly-efficient energy caption/storage systems for both the industry and electricity production. The importance of an efficient use of energy is demonstrated through a short review of opportunities of low grade heat, batch processes, district heating and solid waste. Improving highly effective energy saving solutions is paramount in the current energy demand context. A proper breakthrough in developing highly-efficient materials for energy storage is needed to match the supply and the demand. Concentrated solar plants are given as applications of growing interest.

Chapter 2 reviewed the logical sequence needed to link the general ideas and needs of saving energy with the specific needs in HTTES, leading to the selection of one particular material. The different technologies available to store energy were described albeit with special focus on thermal energy storage. The state of the art in compact heat energy storage highlighted the PCM as most promising material for the next generation of commercial applications. The main weaknesses of PCMs being their poor thermal conductivity, several improvement solutions were presented. Previous works studied the combination of PCM salts with particle

coating. It appears that ceramic encapsulation of PCM needs further studies in order to confirm their legitimacy as a High Temperature Thermal Energy Storage Material.

In order to predict the thermo-mechanical behaviour of such a material, **Chapter 3** adapted two models to develop the fundamental requirements and properties of the PCMs, again applied to the selected composite material. In a first step, the original model was applied in order to highlight the steps that should be adapted to the new material. Subsequently, continuous mechanic principles were used to develop the modelling of a ceramic encapsulated molten salt PCM. The major result of the analysis was the definition of the conditions of mechanical feasibility of such a spherical shell coating of a melting material i.e. the condition for the PCM to crack the encapsulating shell while melting: $\sqrt[3]{\frac{\rho_{s0}}{\rho_{l0}}} < 1 + \Delta T\,\alpha + (1-5\nu)\frac{\sigma_y}{3E}$. This criterion links the thermal expansion properties of the PCM to the mechanical limits of the coating material. A novel analytical modelling of the temperature-dependent mechanical behaviour of a high temperature melting PCM was performed using MATLAB. It proved that the total energy needed to melt the whole bead of PCM increases with the inner pressure due to the presence of the coating material. The proportion of latent heat energy decreases with the high pressure. Finally, COMSOL was used in a finite element method analysis to examine the time-dependent affects of the temperature-dependent mechanical behaviour of a high temperature melting PCM. It was shown that the considerable increase in pressure reduced the efficiency of the latent heat energy storage for a SiC encapsulated salt bead. The thermal expansion of the shell was shown to have an influence when the salt starts to melt. The main result of the simulation is that the interest of coating a PCM with a SiC shell is strongly determined by the PCM properties, namely the PCM should have a high latent heat but a low volumetric expansion, thus leading to a limited increase of pressure during the melting process.

Chapter 4 illustrated the different techniques for thermal energy storage and/or transfer. The ways in which these could benefit from encapsulated PCM for high temperature purpose were considered. Three potential applications were examined: high temperature concrete, high

temperature slurries, and circulating fluidised beds of the heat capture/storage particles. With minor conceptual changes of the initial processes, new materials would bring major improvements. The circulating fluidised bed was recognised as having a high potential for solar heat capture and storage (CSP). Design parameters were determined and included the solids circulation rate, and the heat transfer coefficient from the CFB-wall to the moving solid-gas suspension.

To determine these essential parameters, **Chapter 5** provided initial insights in the mechanism of circulating fluidised beds, and their use as energy storage systems, with special emphasis on the CFB operating hydrodynamics regimes and previous findings on heat transfer in a CFB. The research was performed at the Katholieke Universiteit Leuven (Belgium), where a pilot-scale experimental rig is available. The wall-to-bed heat transfer coefficient in the riser was measured. These coefficients increase with increasing solid flux at equal values of the gas velocity, and achieve values up to 350 W/m²K at G ~500 kg/m²s. The ratio of the suspension heat transfer coefficient and the convective transfer coefficient for the sole gas flow has been confirmed as a valid fitting parameter. The definition of a contact time on the basis of particle velocities in the riser very fairly predicts heat transfer coefficient. Finally, the required dimensions for an application in CSP were given.

Although the reported findings clearly demonstrate the potential of PCM-coated particles for heat capture and storage, some major issues require further investigation and follow-up research. The present study is limited to the modelling of the thermo-mechanical behaviour of the SiC encapsulated PCM, and lab-scale experiments were used to study the potential heat-transfer behaviour of particles in a CFB.

To generally expand the findings, it is therefore recommended:

(i) To develop a more thorough analysis of the benefits of adding latent heat to sensitive heat storage.

(ii) To further develop the production of SiC-shell encapsulated PCM. Although initial tests using Chemical Vapour Deposition were not conclusive (and un-economical), additional techniques need to be investigated.

(iii) To validate the thermo-mechanical modelling by experimental analysis of SiC coated PCMs with e.g. Differential Scanning Calorimetry.

(iv) To control the life cycle of the coated particles in a mechanically stressing environment (thermal and mechanical stress cycling effects and fatigue, erosion…)

(v) To extend the study of CFB to pre-commercial scale studies, of a fair thermal capacity, recommended by the author as 0.5 to 1MW.

REFERENCES

Acem, Z., Lopez, J., Palomo Del Barrio, E., 2010. KNO3/NaNO3 – Graphite materials for thermal energy storage at high temperature: Part I. – Elaboration methods and thermal properties. *Appl. Therm. Eng.* 30, 1580–1585.

Afanasov, I.M., Savchenko, D.V., Ionov, S.G., Rusakov, D.A., Seleznev, A.N., Avdeev, V.V., 2009. Thermal conductivity and mechanical properties of expanded graphite. *Inorg. Mater.* 45, 486–490.

Agyenim, F., Hewitt, N., Eames, P., Smyth, M., 2010. A review of materials, heat transfer and phase change problem formulation for latent heat thermal energy storage systems (LHTESS). *Renew. Sust. Energ. Rev.* 14, 615–628.

Ahlenius, H., 2008. Natural resource - solar power (potential). *The Environment & Poverty Times* 05, 2–3.

Akorede, M.F., Hizam, H., Pouresmaeil, E., 2010. Distributed energy resources and benefits to the environment. *Renew. Sust. Energ. Rev.* 14, 724–734.

Alkan, Z., Kugeler, K., Kaulbarsch, R., Manter, C., 2001. Silicon carbide encapsulated fuel pellets for light water reactors. *Prog. Nucl. Energ.* 38, 411–414.

Ammar, Y., Joyce, S., Norman, R., Wang, Y., Roskilly, A.P., 2012. Low grade thermal energy sources and uses from the process industry in the UK. *Appl. Energy* 89, 3–20.

Arslan, O., 2010. Exergoeconomic evaluation of electricity generation by the medium temperature geothermal resources, using a Kalina cycle: Simav case study. *Int. J. Therm. Sci.* 49, 1866–1873.

Asif, M., Muneer, T., 2007. Energy supply, its demand and security issues for developed and emerging economies. *Renew. Sust. Energ. Rev.* 11, 1388–1413.

Baeyens, J., Geldart, D., 1980. Modelling approach the effect of equipment scale on fluidized bed heat transfer data. *J. Powder Bulk Solids Technol.* 4, 1–9.

Bai, F., Xu, C., 2011. Performance analysis of a two-stage thermal energy storage system using concrete and steam accumulator. *Appl. Therm. Eng.* 31, 2764–2771.

Barlev, D., Vidu, R., Stroeve, P., 2011. Innovation in concentrated solar power. *Sol. Energ. Mat. Sol. C.* 95, 2703–2725.

Barsky, R.B., Kilian, L., 2004. Oil and the Macroeconomy Since the 1970s. *J Econ Perspect* 18, 115–134.

Baskakov, A.P., 1985. Heat transfer in fluidised beds: radiative heat transfer, Chapter 13B, in: Davidson, J.., Clift, R., Harrison, D. (Eds.), Fluidization. Academic Press, London, pp. 465–472.

Basu, P., Nag, P.K., 1987. An investigation into heat transfer in circulating fluidized beds. *Int. J. Heat Mass Transf.* 30, 2399–2409.

Bauer, T., Tamme, R., Christ, M., Öttinger, O., 2006. PCM-graphite composites for high temperature thermal energy storage, in: ECOSTOCK 2006 *Conference Proceedings. Presented at the Ecostock* 2006, Richard Stockton College of New Jersey.

Bayod-Rújula, A.A., 2009. Future development of the electricity systems with distributed generation. *Energy* 34, 377–383.

BERR, 2008. Heat Call for Evidence (No. URN 08/519). Energy Group, Department for Business, Enterprise and Regulatory Reform (BERR), London, UK,.

Bezian, J.-J., Bounaceur, A., De Ryck, A., El Hafi, M., 2007. Un nouveau concept de centrale solaire thermodynamique basé sur un récepteur à lit fluidisé [WWW Document]. URL http://hal.archives-ouvertes.fr/hal-00166316_v1/ (accessed 2.14.11).

Borsukiewicz-Gozdur, A., Nowak, W., 2010. Geothermal Power Station with Supercritical Organic Cycle, in: *Proceedings World Geothermal Congress 2010*. Presented at the World Geothermal Congress, International Geothermal Association, Bali, Indonesia, p. 2667 1–5.

Bounaceur, A., Ryck, A. de, Bezian, J.-J., El Hafi, M., 2007. Chauffage de gaz par un lit de particules solides insolées, in: 11e Congrès de la SFGP : SFGP2007, Saint-Etienne, *Récents Progrès en Génie des Procédés*.

Bradbury, K., 2010. Energy Storage Technology Review [WWW Document]. Sustainable Energy Modeling. URL http://www.duke.edu (accessed 10.19.11).

Brems, A., Chan, C.W., Seville, J.P.K., Parker, D., Baeyens, J., 2011. Modelling the transport disengagement height in fluidized beds. *Adv. Powder Technol.* 22, 155–161.

Bridges, N.J., Visser, A.E., Fox, E.B., 2011. Potential of Nanoparticle-Enhanced Ionic Liquids (NEILs) as Advanced Heat-Transfer Fluids. *Energy Fuels* 25, 4862–4864.

Brosseau, D., Kelton, J.W., Ray, D., Edgar, M., Chisman, K., Emms, B., 2005. Testing of Thermocline Filler Materials and Molten-Salt Heat Transfer Fluids for Thermal Energy Storage Systems in Parabolic Trough Power Plants. *J. Sol. Energy Eng.* 127, 109–8.

Bujak, J., 2008. Energy savings and heat efficiency in the paper industry: A case study of a corrugated board machine. *Energy* 33, 1597–1608.

Burgaleta, J.I., Arias, S., & Ramirez, D. 2011. GEMASOLAR, the First Tower Thermosolar Commercial Plant With Molten Salt Storage. In *Proceedings of the SolarPACES 2011 Conference on Concentrating Solar Power and Chemical Energy Systems. Granada, Spain*.

Cabeza, L.F., Castell, A., Barreneche, C., De Gracia, A., Fernández, A.I., 2011. Materials used as PCM in thermal energy storage in buildings: A review. *Renew. Sust. Energ. Rev.* 15, 1675–1695.

Cadoret, L., Reuge, N., Pannala, S., Syamlal, M., Rossignol, C., Dexpert-Ghys, J., Coufort, C., Caussat, B., 2009. Silicon Chemical Vapor Deposition on macro and submicron powders in a fluidized bed. *Powder Technol.* 190, 185–191.

Cailletaud, G., n.d. Exercice: Enveloppe sphérique soumise à une pression intérieure [WWW Document]. URL http://mms2.ensmp.fr/ressources/ens_exo.php (accessed 3.10.10).

Carbon Disclosure Project, 2011. CDP Global 500 Report 2011 Accelerating Low Carbon Growth. Carbon Disclosure Project.

Carbon Trust, 2010. Carbon Trust Launches New Service to Help SMEs with Carbon Reduction.

Carslaw, H.S., Jaeger, J.C., 1986. Conduction of heat in solids. Clarendon Press ; Oxford University Press, Oxford [Oxfordshire]; New York.

Castellón, C., Medrano, M., Roca, J., Nogués, M., Castell, A., Cabeza, L.F., 2007. Use of Microencapsulated Phase Change Materials in Building Applications, in*: In Thermal Performance of the Exterior Envelopes of Whole Buildings X International Conference.* Presented at the Thermal Performance of the Exterior Envelopes of Whole Buildings X International Conference, ONRL, Clearwater Beach, Florida.

Chan, C.W., Seville, J.P.K., Parker, D.J., Baeyens, J., 2010. Particle velocities and their residence time distribution in the riser of a CFB. *Powder Technol.* 203, 187–197.

Chan, C.W., Seville, J.P.K., Yang, Z., Baeyens, J., 2009. Particle motion in the CFB riser with special emphasis on PEPT-imaging of the bottom section. *Powder Technol.* 196, 318–325.

Chen, B., Wang, X., Zeng, R., Zhang, Y., Wang, X., Niu, J., Li, Y., Di, H., 2008. An experimental study of convective heat transfer with microencapsulated phase change material suspension: Laminar flow in a circular tube under constant heat flux. *Exp. Therm. Fluid Sci.* 32, 1638–1646.

Chen, H., Cong, T.N., Yang, W., Tan, C., Li, Y., Ding, Y., 2009. Progress in electrical energy storage system: A critical review. *Prog. Nat. Sci.* 19, 291–312.

Chen, H., Goswami, D.Y., Rahman, M.M., Stefanakos, E.K., 2011. A supercritical Rankine cycle using zeotropic mixture working fluids for the conversion of low-grade heat into power. *Energy* 36, 549–555.

Chen, J.C., Grace, J.R., Golriz, M.R., 2005. Heat transfer in fluidized beds: design methods. *Powder Technol.* 150, 123–132.

Choi, J., Lee, J.G., Kim, J.H., Yang, H., 2001. Preparation of microcapsules containing phase change materials as heat transfer media by in-situ polymerization. *J. Ind. Eng. Chem.* 7, 358–362.

Chow, L., 1996. Thermal conductivity enhancement for phase change storage media. *Int Commun Heat Mass* 23, 91–100.

Chu, B., Duncan, S., Papachristodoulou, A., Hepburn, C., 2013. Analysis and control design of sustainable policies for greenhouse gas emissions. *Appl. Therm. Eng.* 53, 420–431.

Chung, C.K., Tsai, M.Q., Tsai, P.H., Lee, C., 2005. Fabrication and characterization of amorphous Si films by PECVD for MEMS. *J Micromech Microeng* 15, 136–142.

Clinton Foundation, n.d. Clinton Climate Initiative [WWW Document]. URL http://www.clintonfoundation.org/main/our-work/by-initiative/clinton-climate-initiative/about.html (accessed 8.22.12).

Colclough, S., Griffiths, P., Hewitt, N., 2011. A year in the life of a Passive House with Solar Energy Stores, in: A year in the life of a Passive House with Solar Energy Store. *Presented at the IC-SES 2001*, Belfast.

Czok, G., Werther, J., 2005. Particle coating by chemical vapor deposition in a fluidized bed reactor. *China Part* 3, 105–112.

Czok, G., Ye, M., Hoef, M.A., Kuipers, J.A.M., 2005. Modeling of chemical vapor deposition in a fluidized bed reactor based on discrete particle simulation. *Int J Chem React Eng* 3 (1).

Dagdag, S., 2005. Matériaux et revêtements céramiques multifonctionnels par PECVD et SPS pour l'intégration de puissance haute température - haute tension [WWW Document]. URL http://ethesis.inp-toulouse.fr/archive/00000221/ (accessed 10.5.09).

Delgado, M., Lázaro, A., Mazo, J., Marín, J.M., Zalba, B., 2012. Experimental analysis of a microencapsulated PCM slurry as thermal storage system and as heat transfer fluid in laminar flow. *Appl Therm Eng* 36, 370–377.

Delogu, F., 2007. Numerical simulation of the thermal response of Al core/Ni shell nanometer-sized particles. *Nanotechnology* 18, 505702.1-505702.7.

Department of Energy & Climate Change, 2012. *Uk Energy In Brief* 2012.

Department of the Environment,, Energy Efficiency Office, 1996. Waste Heat Recovery in *the Process Industries*, Harwell. ed, Good practice guide. Department of Energy, London, UK.

Department of Trade and Industry (UK), 2012. Energy consumption in the United Kingdom. *National Statistics*, UK.

Do Couto Aktay, K.S., Tamme, R., Müller-Steinhagen, H., 2008. Thermal Conductivity of High-Temperature Multicomponent Materials with Phase Change. *Int. J. Thermophys.* 29, 678–692.

Dodman, D., 2009. Blaming cities for climate change? An analysis of urban greenhouse gas emissions inventories. *Environ Urban* 21, 185–201.

Domański, R., Fellah, G., 1998. Thermoeconomic analysis of sensible heat, thermal energy storage systems. *Appl. Therm. Eng.* 18, 693–704.

Dutta, A., Basu, P., 2003. An Improvement of Cluster-Renewal Model for Estimation of Heat Transfer on the Water-Walls of Commercial CFB Boilers, in: *17th International Conference on Fluidized Bed Combustion.* Presented at the 17th International Conference on Fluidized Bed Combustion (FBC2003) May 18–21, 2003, Jacksonville, Florida, USA, ASME, New York, pp. 235–244.

EIA, 2011. EIA - 2011 International Energy Outlook (No. DOE/EIA-0484(2011)). *Energy Information Administration*, Washington, DC.

Elgafy, A., Lafdi, K., 2005. Effect of carbon nanofiber additives on thermal behavior of phase change materials. *Carbon* 43, 3067–3074.

Engelhard, M., 2006. The New Generation Kalina Cycle. *Electricity generation from Enhanced Geothermal Systems* - Strasbourg, France, Workshop5

Eslami, M., Babaei, M., Poultangari, R., 2005. Thermal and mechanical stresses in a functionally graded thick sphere. *Int J Pres Ves Pip* 82, 522–527.

Eslami, M.R., Shakeri, M., Shiari, B., 1997. Coupled thermoelasticity of composite spherical shells. Presented at the Structural Mechanics in *React Technol*, The International & American Associations for Structural Mechanics in Reactor Technology, Lyon, France.

Ettouney, H.M., Alatiqi, I., Al-Sahali, M., Al-Hajirie, K., 2006. Heat transfer enhancement in energy storage in spherical capsules filled with paraffin wax and metal beads. *Energy Conv.* Manag. 47, 211–228.

European Committee for Standardization, 2005. “Solid recovered fuels - Specifications and classes” (No. CEN/TC 343:2005). Technical Committee.

European Union, 2011. 7th. Framework Program for Research and Technical Development CSP2 Concentrated Solar Power in Particles, EU Grant Reference : 282932.

Everaert, K., Baeyens, J., Smolders, K., 2006. Heat Transfer from a Single Tube to the Flowing Gas-Solid Suspension in a CFB Riser. *Heat Transfer Eng* 27, 66–70.

Fernandes, D., Pitié, F., Caceres, G., Baeyens, J., 2012. Thermal energy storage: "How previous findings determine current research priorities". *Energy* 39, 246–257.

Fernandez, A.I., Martínez, M., Segarra, M., Martorell, I., Cabeza, L.F., 2010. Selection of materials with potential in sensible thermal energy storage. *Sol. Energy Mater. Sol. Cells* 94, 1723–1729.

Fletcher, N. 2010. Turn batch to continuous processing. *Manuf Chemist.* June, 24-26.

Fukai, J., Hamada, Y., Morozumi, Y., Miyatake, O., 2002. Effect of carbon-fiber brushes on conductive heat transfer in phase change materials. *Int. J. Heat Mass Transf.* 45, 4781–4792.

Fukai, J., Hamada, Y., Morozumi, Y., Miyatake, O., 2003. Improvement of thermal characteristics of latent heat thermal energy storage units using carbon-fiber brushes: experiments and modeling. *Int. J. Heat Mass Transf.* 46, 4513–4525.

Fukai, J., Kanou, M., Kodama, Y., Miyatake, O., 2000. Thermal conductivity enhancement of energy storage media using carbon fibers. *Energy Conv. Manag.* 41, 1543–1556.

Gao, X., 2003. Strain gradient plasticity solution for an internally pressurized thick-walled spherical shell of an elastic–plastic material. *Mech. Res. Commun.* 30, 411–420.

Gao, X.L., Park, S.K., Ma, H.M., 2009. Analytical Solution for a Pressurized Thick-Walled Spherical Shell Based on a Simplified Strain Gradient Elasticity Theory. *Math. Mech. Solids* 14, 747–758.

Geldart, D., 1973. Types of gas fluidization. *Powder Technol.* 7, 285–292.

Gil, A., Medrano, M., Martorell, I., Lazaro, A., Dolado, P., Zalba, B., Cabeza, L.F., 2010. State of the art on high temperature thermal energy storage for power generation. Part 1--Concepts, materials and modellization. *Renew. Sust. Energ. Rev.* 14, 31–55.

Girardet, H., 1998. Sustainable cities: a contradiction in terms?, in: Fernandes, E. (Ed.), *Environmental strategies for sustainable development in urban areas: lessons from Africa and Latin America*, Ashgate Studies in Environmental Policy and Practice. Ashgate Pub Ltd, p. 212.

Gnielinski, V., 2007. Fundamentals of heat and mass transfer, in: *Fundamentals of heat and mass transfer.* John Wiley, Hoboken, N.J., pp. 514–515.

Golriz, M., Grace, J.R., 2002. Predicting heat transfer in large-scale CFB boilers, in: Grace, J.R., Zhu, J., de Lasa, H.I. (Eds.), *Circulating Fluidized Bed Technology VII.* Presented at the 7th International Conference on Circulating Fluidized Beds, held at Niagara Falls, Ontario, Canada, May 5-8, 2002, Canadian Society for Chemical Engineering, Ottawa, ON, Canada, pp. 121–128.

Grace, J.R., 1990. Heat transfer in high velocity fluidized beds, in: Hetsroni, G. (Ed.), *Heat transfer* 1990. Presented at the Ninth International Heat Transfer Conference, Jerusalem, Israel, Hemisphere, New York, pp. 329–339.

Grimm, N.B., Faeth, S.H., Golubiewski, N.E., Redman, C.L., Wu, J., Bai, X., Briggs, J.M., 2008. Global Change and the Ecology of Cities. *Science* 319, 756–760.

Grimmond, S., 2007. Urbanization and global environmental change: local effects of urban warming. *Geogr J* 173, 83–88.

Hamada, Y., Ohtsu, W., Fukai, J., 2003. Thermal response in thermal energy storage material around heat transfer tubes: effect of additives on heat transfer rates. *Sol. Energy* 75, 317–328.

Hamada, Y., Otsu, W., Fukai, J., Morozumi, Y., Miyatake, O., 2005. Anisotropic heat transfer in composites based on high-thermal conductive carbon fibers. *Energy* 30, 221–233.

Hartge, E.U., Rensner, D., Werther, J., 1988. Solids concentration and velocity patterns in circulating fluidized beds, in: Basu, P., Large, J.F. (Eds.), *Circulating Fluidized Bed Technology II*. Presented at the Second International Conference on Circulating Fluidized Beds, Compiègne, France, 14-18 March 1988, Pergamon Press, Oxford, England, pp. 165–180.

Harth, K., Hibst, H., Mattmann, W., 1997. Coating or surface treatment of solid particles by means of a plasma fluidized bed. *Google Patents.*

Hawlader, M.N.A., Uddin, M.S., Khin, M.M., 2003. Microencapsulated PCM thermal-energy storage system. *Appl. Energy* 74, 195–202.

Hilber, T., Maier, J., Scheffknecht, G., Agraniotis, M., Grammelis, P., Kakaras, E., Glorius, T., Becker, U., Derichs, W., Schiffer, H.-P., De Jong, M., Torri, L., 2007. Advantages and possibilities of solid recovered fuel cocombustion in the European energy sector. *J Air Waste Manag Assoc* 57, 1178–1189.

Hlebnikov, A., Siirde, A., 2008. The major characteristic parameters of the Estonian district heating networks and their efficiency increasing potential. *Energetika* (Lithuania) 54, 67–74.

Hrudey, T., Haddow, J., 1973. Elastic-plastic expansion of a thick spherical shell with finite elastic strain. *Acta Mech* 18, 21–34.

Ibrahim, H., Ilinca, A., Perron, J., 2008. Energy storage systems--Characteristics and comparisons. *Renew. Sust. Energ. Rev.* 12, 1221–1250.

IEA, OECD, 2011. *World energy outlook 2011*. IEA, International Energy Agency : OECD, Paris.

Institution of Electrical Engineers, 1994. Profiting from low-grade heat : thermodynamic cycles for low-temperature heat sources, The Watt Committee on Energy. Institution of Engineering and Technology, London.

Jabbari, M., Sohrabpour, S., Eslami, M.R., 2003. General Solution for Mechanical and Thermal Stresses in a Functionally Graded Hollow Cylinder due to Nonaxisymmetric Steady-State Loads. *J. Appl. Mech.* 70, 111.

Janz, G.J., 1967. Molten salts handbook. Academic Press, New York.

Jegadheeswaran, S., Pohekar, S.D., 2009. Performance enhancement in latent heat thermal storage system: A review. *Renew. Sust. Energ. Rev.* 13, 2225–2244.

Jegadheeswaran, S., Pohekar, S.D., Kousksou, T., 2010. Exergy based performance evaluation of latent heat thermal storage system: A review. *Renew. Sust. Energ. Rev.* 14, 2580–2595.

John, E.E., Hale, W.M., Brown, B., Selvam, R.P., 2011a. Development and performance evaluation of high temperature concrete for thermal energy storage for solar power generation, in: *Proceedings of the ASME 2011 International Mechanical Engineering Congress & Exposition*. Presented at the ASME 2011 International Mechanical Engineering Congress & Exposition, IMECE2011, ASME, Denver, Colorado, USA.

John, E.E., Hale, W.M., Selvam, R.P., 2011b. Development of a High-Performance Concrete to Store Thermal Energy for Concentrating Solar Power Plants. *ASME*, pp. 523–529.

Kearney, D., Herrmann, U., Nava, P., Kelly, B., Mahoney, R., Pacheco, J., Cable, R., Potrovitza, N., Blake, D., Price, H., 2002. Evaluation of a Molten Salt Heat Transfer Fluid in a Parabolic Trough Solar Field, in: *Sol. Energy*. Presented at the ASME Solar 2002: International Solar Energy Conference, Reno, Nevada, USA, pp. 293–299.

Kearney, D., Herrmann, U., Nava, P., Kelly, B., Mahoney, R., Pacheco, J., Cable, R., Potrovitza, N., Blake, D., Price, H., 2003. Assessment of a molten salt heat transfer fluid in a parabolic trough solar field. *J. Sol. Energy Eng. Trans.*-ASME 125, 170–7.

Kearney, D., Kelly, B., Herrmann, U., Cable, R., Pacheco, J., Mahoney, R., Price, H., Blake, D., Nava, P., Potrovitza, N., 2004. Engineering aspects of a molten salt heat transfer fluid in a trough solar field. *Energy* 29, 861–870.

Kenisarin, M.M., 2010. High-temperature phase change materials for thermal energy storage. *Renew. Sust. Energ. Rev.* 14, 955–970.

Khodadadi, J.M., Hosseinizadeh, S.F., 2007. Nanoparticle-enhanced phase change materials (NEPCM) with great potential for improved thermal energy storage. *Int. Commun. Heat Mass Transf.* 34, 534–543.

Kim, B.G., Choi, Y., Lee, J.W., Lee, Y.W., Sohn, D.S., Kim, G.M., 2000. Multi-layer coating of silicon carbide and pyrolytic carbon on UO2 pellets by a combustion reaction. *J. Nucl. Mater.* 281, 163–170.

King, D.F., 1989. Estimation of dense bed voidage in fast and slow fluidized beds of FCC catalyst, in: Grace, J.R., Shemilt, L.W., Bergougnou, M.A., Engineering Foundation (U.S.) (Eds.), *Fluidization VI.* Presented at the International Conference on Fluidization, Banff Centre, Banff, Alberta, Canada, May 7-12, 1989, Engineering Foundation, New York, pp. 1–8.

Kunii, D., Levenspiel, O., 1991. Chapter 11, in: *Fluidization engineering*. Butterworth-Heinemann, Boston (USA), pp. 257–276.

Laing, D., 2007. Concrete Storage Development for Parabolic Trough Power Plants. *Parabolic Trough Technology Workshop, Golden, CO, USA*.

Laing, D., Bahl, C., Bauer, T., Lehmann, D., Steinmann, W.-D., 2011. Thermal energy storage for direct steam generation. *Sol. Energy* 85, 627–633.

Law, R., Harvey, A., Reay, D., 2013. Opportunities for low-grade heat recovery in the UK food processing industry. *Appl. Therm. Eng*. 53, 188-196.

Letsrecycle, 2008. Map launched of all planned UK incinerators — letsrecycle.com - recycling and waste management news and information [WWW Document]. letsrecycle.com. URL http://www.letsrecycle.com/news/latest-news/waste-management/map-launched-of-all-planned-uk-incinerators (accessed 8.22.12).

Lints, M.C.L., Glicksman, L.R., 1993. The structure of particle clusters near the wall of a circulating fluidized bed, in: Weimer, A.W. (Ed.), *Fluid-particle processes, AIChE symposium series* ; no. 296. Presented at the American Institute of Chemical Engineers Annual Meeting in Miami Beach, November 1-6, 1992, American Institute of Chemical Engineers, New York, N.Y., pp. 35–52.

Lopez, J., 2007. Nouveaux matériaux graphite/sel pour le stockage d'énergie à haute température. Étude des propriétés de changement de phase. (Ph,D. Thesis).

Lopez, J., Caceres, G., Palomo Del Barrio, E., Jomaa, W., 2010. Confined melting in deformable porous media: A first attempt to explain the graphite/salt composites behaviour. Int. *J. Heat Mass Transf.* 53, 1195–1207.

Lopez, J., Dumas, J.-P., Palomo del Barrio, E., 2008. Graphite/salt composites for high temperature energy storage: a study of the effects of the graphite and of the microstructure of the composites on the phase change properties of the salts. *C. R. Mécanique* 336, 578–585.

Luptowski, B., 2011. Development of Molten-Salt Heat Transfer Fluid Technology for Parabolic Trough Solar Power Plants. In: *Concentrating Solar Power Program Review 2011*.

Mahmoudi, S., Baeyens, J., Seville, J.P.K., 2011. The solids flow in the CFB-riser quantified by single radioactive particle tracking. *Powder Technol.* 211, 135–143.

Mahmoudi, S., Chan, C.W., Brems, A., Seville, J.P.K., Baeyens, J., 2012. Solids flow diagram of a CFB riser using Geldart B-type powders. *Particuology* 10, 51–61.

Marechal, F., Muller, D., 2008. Energy management methods for the food industry., in: Klemeš, J., Smith, R., Kim, J.K. (Eds.), *Handbook of water and energy management in food processing*. Woodhead Publishing in Food Science, Technology and Nutrition, Ecole Polytechnique Fédérale de Lausanne, pp. 221–255.

Markides, C.N., Smith, T.C.B., 2011. A dynamic model for the efficiency optimization of an oscillatory low grade heat engine. *Energy* 36, 6967–6980.

Maruoka, N., Akiyama, T., 2002. Development of PCM for high temperature application in the steelmaking industry, in: *Annex 17, Advanced Thermal Energy Storage Techniques – Feasibility Studies and Demonstration Projects*. Presented at the 3rd Experts' Meeting and Workshop of Annex 17, Tokyo.

Maruoka, N., Akiyama, T., 2003. Thermal Stress Analysis of PCM Encapsulation for Heat Recovery of High Temperature Waste Heat. *J. Chem. Eng. Jpn*. 36, 794–798.

Maruoka, N., Sato, K., Yagi, J., Akiyama, T., 2002. Development of PCM for Recovering High Temperature Waste Heat and Utilization for Producing Hydrogen by Reforming Reaction of Methane. *ISIJ Int.* 42, 215–219.

Matsen, J.M., 1976. Some characteristics of large solids circulation systems, in: Keairns, D.L. (Ed.), *Fluidization technology*. Presented at the International Conference, Pacific Grove, CA., June 15-20, 1975, Hemisphere Pub. Corp., New York, N.Y., p. 135.

McKenna, R., 2009. Industrial energy efficiency: Interdisciplinary perspectives on the thermodynamic, technical and economic constraints (Ph.D. Thesis).

Medrano, M., Gil, A., Martorell, I., Potau, X., Cabeza, L.F., 2010. State of the art on high-temperature thermal energy storage for power generation. Part 2--Case studies. *Renew. Sust. Energ. Rev.* 14, 56–72.

Mettawee, E.-B.S., Assassa, G.M.R., 2007. Thermal conductivity enhancement in a latent heat storage system. *Sol. Energy* 81, 839–845.

Molodstof, Y., 1985. Equations Générales Probabilistes des Écoulements Polyphasiques et Applications aux Mélanges Gaz-Solides (Ph.D. Thesis).

Molodstof, Y., Muzyka, D.W., Large, J.F., Bergougnou, M.A., 1984. The Use of Asymptotic Similar Solutions to Probabilistic Multiphase Flow Equations to Predict Heat Transfer Rates to Dilute Gas-Solids Suspension, in: *Proceedings of the XVIth I.C.N.M.T. Symposium. Dubrovnik, Yugoslavia*.

Molodtsof, Y., Muzyka, D.W., 1989. General probabilistic multiphase flow equations for analyzing gas-solids mixtures. *Int. J. Eng. Fluid. Mech.* 2, 1–24.

Morisson, V., Rady, M., Palomo, E., Arquis, E., 2008. Thermal energy storage systems for electricity production using solar energy direct steam generation technology. *Chemical Engineering and Processing: Process Intensification* 47, 499–507.

Muzyka, D.W., 1985. Use of probabilistic multiphase flow equations in the study of the hydrodynamics and heat transfer in gas-solids suspensions. (Ph.D. Thesis).

Nag, P.K., Gupta, A.V.S.S.K.S., 1998. Exergy analysis of the Kalina cycle. *Appl. Therm. Eng.* 18, 427–439.

Naish, C., McCubbin, I., Edberg, O., Harfoot, M., 2008. Outlook of energy storage technologies (Study No. IP/A/ITRE/FWC/2006-087/Lot 4/C1/SC2). European Parliament's committee on Industry, Research and Energy.

Nallusamy, N., Sampath, S., Velraj, R., 2007. Experimental investigation on a combined sensible and latent heat storage system integrated with constant/varying (solar) heat sources. *Renew. Energy* 32, 1206–1227.

Nomura, S., Shintomi, T., Akita, S., Nitta, T., Shimada, R., Meguro, S., 2010. Technical and Cost Evaluation on SMES for Electric Power Compensation. IEEE Trans. *Appl. Supercond.* 20, 1373–1378.

Oelert, G., Behret, H., Friedel, W., Hennemann, B., Hodgett, D., Statens Raad foer Byggnadsforskning, S. (Sweden), 1982. Thermochemical heat storage: state-of-the-art report. United States.

Ogriseck, S., 2009. Integration of Kalina cycle in a combined heat and power plant, a case study. *Appl. Therm. Eng.* 29, 2843–2848.

Ouyang, S., Potter, O.E., 1993. Consistency of circulating fluidized bed experimental data. *Ind. Eng. Chem. Res.* 32, 1041–1045.

Pellissier Tanon, A., 1988. Appareils à pression: Base de calcul des enceintes sous pression. *Techniques de l'ingénieur. Génie mécanique* 843–843.

Pepermans, G., Driesen, J., Haeseldonckx, D., Belmans, R., D'haeseleer, W., 2005. Distributed generation: definition, benefits and issues. *Energ. Policy* 33, 787–798.

Pilkington Solar International GmbH, 2000. Survey of Thermal Storage for Parabolic Trough Power Plants; Period of Performance: September 13, 1999 - June 12, 2000.

Pincemin, S., Olives, R., Py, X., Christ, M., 2008a. Highly conductive composites made of phase change materials and graphite for thermal storage. *Sol. Energy Mater. Sol. Cells* 92, 603–613.

Pincemin, S., Py, X., Olives, R., Christ, M., Oettinger, O., 2008b. Elaboration of conductive thermal storage composites made of phase change materials and graphite for solar plant. *J. Sol. Energy Eng. Trans.-ASME* 130, 011005.1–011005.5.

Pitié, F., Zhao, C.Y., Cáceres, G., 2011. Thermo-mechanical analysis of ceramic encapsulated phase-change-material (PCM) particles. *Energy Environ. Sci.* 4, 2117–2124.

Pitié, F., Zhao, C.Y., Tamainot-Telto, Z., Cáceres, G., 2012. Circulating fluidized bed application of coated phase-change-material (PCM) particles: Mathematical modelling and experimental validation., in: *Proceedings of the 12th International conference on Energy Storage (Innostock 2012).* Presented at the 12th International conference on Energy Storage (Innostock 2012), Grea, Lleida, Spain.

Poultangari, R., Jabbari, M., Eslami, M.R., 2008. Functionally graded hollow spheres under non-axisymmetric thermo-mechanical loads. *Int. J. Pres. Ves. Pip.* 85, 295–305.

Price, H., Lupfert, E., Kearney, D., Zarza, E., Cohen, G., Gee, R., Mahoney, R., 2002. Advances in Parabolic Trough Solar Power Technology. *J. Sol. Energy Eng.* 124, 109–125.

Py, X., Calvet, N., Olives, R., Meffre, A., Echegut, P., Bessada, C., Veron, E., Ory, S., 2011. Recycled Material for Sensible Heat Based Thermal Energy Storage to be Used in Concentrated Solar Thermal Power Plants. *J. Sol. Energy Eng.* 133, 031008.

Regin, A.F., Solanki, S.C., Saini, J.S., 2008. Heat transfer characteristics of thermal energy storage system using PCM capsules: A review. *Renew. Sust. Energ. Rev.* 12, 2438–2458.

Rovira, A., Montes, M.J., Valdes, M., Martínez-Val, J.M., 2011. Energy management in solar thermal power plants with double thermal storage system and subdivided solar field. *Appl. Energ.* 88, 4055–4066.

Saleh, B., Koglbauer, G., Wendland, M., Fischer, J., 2007. Working fluids for low-temperature organic Rankine cycles. *Energy* 32, 1210–1221.

Sánchez-Rodríguez, R., Seto, K.C., Simon, D., Solecki, W.D., Kraas, F., Laumann, G., 2011. Urbanization and Global Environmental Change - IHDP (*IHDP Report* No. 15), IHDP Report Series. Bonn.

Sarı, A., Alkan, C., Karaipekli, A., 2010. Preparation, characterization and thermal properties of PMMA/n-heptadecane microcapsules as novel solid–liquid microPCM for thermal energy storage. *Appl. Energy* 87, 1529–1534.

Satterthwaite, D., 1999. The keys issues and the works included, in: Satterthwaite, D. (Ed.), *The Earthscan reader in sustainable cities*. Earthscan, pp. 3–21.

Satterthwaite, D., 2011. How urban societies can adapt to resource shortage and climate change. *Philos. Transact. A. Math. Phys. Eng. Sci.* 369, 1762–1783.

Sharma, A., Tyagi, V.V., Chen, C.R., Buddhi, D., 2009. Review on thermal energy storage with phase change materials and applications. *Renew. Sust. Energ. Rev.* 13, 318–345.

Sharma, S.D., Sagara, K., 2005. Latent Heat Storage Materials and Systems: A Review. *Int. J. Green Energy* 2, 1–56.

Sheffield City Council, n.d. District Heating [WWW Document]. Sheffield City Council. URL https://www.sheffield.gov.uk/environment/waste/reducingrecycling/energyrecovery.html (accessed 8.26.12).

Shengjun, Z., Huaixin, W., Tao, G., 2011. Performance comparison and parametric optimization of subcritical Organic Rankine Cycle (ORC) and transcritical power cycle system for low-temperature geothermal power generation. *Appl. Energ.* 88, 2740–2754.

Smith, T.C.B., 2004. Power dense thermofluidic oscillators for high load applications, in: *Proceedings of the 2nd International Energy Conversion Engineering Conference*. Presented at the 2nd International Energy Conversion Engineering Conference, Energy Conversion Engineering, Providence (RI), pp. 1–15.

Smith, T.C.B., 2006. Thermally Driven Oscillations in Dynamic Applications (Ph.D. Thesis).

Smolders, K., Baeyens, J., 2001a. Gas fluidized beds operating at high velocities: a critical review of occurring regimes. *Powder Technol.* 119, 269–291.

Smolders, K., Baeyens, J., 2001b. Hydrodynamic modelling of the axial density profile in the riser of a low-density circulating fluidized bed. *Can. J. Chem. Eng.* 79, 422–429.

Solanki, R., Galindo, A., Markides, C.N., 2012. Dynamic modelling of a two-phase thermofluidic oscillator for efficient low grade heat utilization: Effect of fluid inertia. Applied *Energy* 89, 156–163.

Stern, N., 2007. The Economics of climate change : Stern review on the economics of climate change. Cambridge University Press, Cambridge.

Tamme, R., 2006. Development of Storage Systems for SP Plants. *DG TREN–DG RTD Consultative Seminar, Concentrating Solar Power ", Brussels.* 27.

Tamme, R., Bauer, T., Buschle, J., Laing, D., Müller-Steinhagen, H., Steinmann, W.-D., 2008. Latent heat storage above 120°C for applications in the industrial process heat sector and solar power generation. *Int. J. Energy Res.* 32, 264–271.

The Economist, 2011. Why firms go green. *The Economist.*

Torresol Energy Investments, 2012. Torresol Energy - Gemasolar thermosolar plant [WWW Document]. URL http://www.torresolenergy.com/TORRESOL/home/en (accessed 8.26.12).

Ubrig, J., 2007. Encapsulation de dispositifs sensibles à l'atmosphère par des dépôts couches minces élaborés par PECVD. (PhD Thesis).

United Nations, Department of Public Information, News and Media Division, 2007. City Planning Will Determine Pace of Global Warming, Un-Habitat Chief Tells Second Committee

as She Links Urban Poverty with Climate Change (General Assembly No. GA/EF/3190), Sixty-second General Assembly Second Committee. United Nations, New York.

United States Environmental Protection Agency, n.d. Renewable Energy Production Incentives [WWW Document]. URL http://epa.gov/osw/hazard/wastemin/minimize/energyrec/rpsinc.htm (accessed 8.22.12).

Upadhyaya, S.K., Cooke, J.R., Rand, R.H., 1985. A fluid-filled spherical shell model of the thermo-elastic behaviour of avian eggs. *J. Agr. Eng. Res.* 32, 95–109.

Valdimarsson, P., 2006. The Kalina power plant in Husavik–Why Kalina and what has been learned. *Electricity Generation from Enhanced Geothermal Systems Conference, Strasburg.*

Van Caneghem, J., Brems, A., Lievens, P., Block, C., Billen, P., Vermeulen, I., Dewil, R., Baeyens, J., Vandecasteele, C., 2012. Fluidized bed waste incinerators: Design, operational and environmental issues. *Progr. Energ. Combust.* 38, 551–582.

Van de Velden, M., Baeyens, J., Dougan, B., McMurdo, A., 2007. Investigation of operational parameters for an industrial CFB combustor of coal, biomass and sludge. *China Part.* 5, 247–254.

Van de Velden, M., Baeyens, J, 2007. Attrition and erosion in particle transport loops *Powder Handl. Process.* 19 (1), 29-33

Velraj, R., Seeniraj, R.V., Hafner, B., Faber, C., Schwarzer, K., 1999. Heat transfer enhancement in a latent heat storage system. Sol. Energy 65, 171–180.

Welty, J.R., 1974. Engineering heat transfer, in: *Engineering heat transfer.* John Wiley and Sons, New York, N.Y., 262.

Wu, B., Reddy, R., Rogers, R., 2001. Novel ionic liquid thermal storage for solar thermal electric power systems, in: *Proceedings of Solar Forum 2001 Solar Energy: The Power to Choose*. Presented at the Solar Energy: The Power to Choose, ASME, Washington, DC.

Wu, R.L., Grace, J.R., Lim, C.J., Brereton, C.M.H., 1989. Suspension-to-Surface heat transfer in a circulating-fluidized-bed combustor. *AIChE J.* 35, 1685–1691.

Wu, Z.G., Zhao, C.Y., 2001. Experimental investigations of porous materials in high temperature thermal energy storage systems. *Sol. Energy* 85, 1371–1380.

Xie, D., Bowen, B.., Grace, J.., Lim, C.., 2003a. Two-dimensional model of heat transfer in circulating fluidized beds. Part II: Heat transfer in a high density CFB and sensitivity analysis. *Int. J. Heat Mass Transf.* 46, 2193–2205.

Xie, D., Bowen, B.D., Grace, J.R., Lim, C.J., 2003b. A three-dimensional model for suspension-to-membrane-wall heat transfer in circulating fluidized beds. *Chem. Eng. Sci.* 58, 4247–4258.

Yamagishi, Y., Takeuchi, H., Pyatenko, A.T., Kayukawa, N., 1999. Characteristics of microencapsulated PCM slurry as a heat-transfer fluid. *AIChE Journal* 45, 696–707.

Yang, M., Yang, X., Yang, X., Ding, J., 2010. Heat transfer enhancement and performance of the molten salt receiver of a solar power tower. *Appl. Energy* 87, 2808–2811.

Zalba, B., Marin, J.M., Cabeza, L.F., Mehling, H., 2003. Review on thermal energy storage with phase change: materials, heat transfer analysis and applications. *Appl. Therm. Eng.* 23, 251–283.

Zeng, J.L., Sun, L.X., Xu, F., Tan, Z.C., Zhang, Z.H., Zhang, J., Zhang, T., 2007. Study of a PCM based energy storage system containing Ag nanoparticles. *J. Therm. Anal. Calorim.* 87, 371–375.

Zhong, Y., Li, S., Wei, X., Liu, Z., Guo, Q., Shi, J., Liu, L., 2010. Heat transfer enhancement of paraffin wax using compressed expanded natural graphite for thermal energy storage. *Carbon* 48, 300–304.

Zhou, Z., Liu, P., Li, Z., Ni, W., 2013. An engineering approach to the optimal design of distributed energy systems in China. *Appl. Therm. Eng.* 53, 387–396.

Zhu, Q., Qiu, X., Ma, C., 1999. Oxidation resistant SiC coating for graphite materials. *Carbon* 37, 1475–1484.

Zou, G.L., Tan, Z.C., Lan, X.Z., Sun, L.X., Zhang, T., 2004. Preparation and characterization of microencapsulated hexadecane used for thermal energy storage. *Chin. Chem. Lett.* 15, 729–732.

APPENDIX

Energy 39 (2012) 246–257

Contents lists available at SciVerse ScienceDirect

Energy

journal homepage: www.elsevier.com/locate/energy

Thermal energy storage: "How previous findings determine current research priorities"

D. Fernandes [a], F. Pitié [b,*], G. Cáceres [a,**], J. Baeyens [c]

[a] Facultad de Ingeniería y Ciencias, Universidad Adolfo Ibáñez, Diagonal Las Torres, 2640, 7941169 Peñanolén, Santiago, Chile
[b] School of Engineering, University of Warwick, Coventry CV8 1JE, United Kingdom
[c] Beijing University of Chemical Technology, College of Life Science and Technology, Beijing, China

ARTICLE INFO

Article history:
Received 1 November 2011
Received in revised form
11 January 2012
Accepted 13 January 2012
Available online 15 February 2012

Keywords:
Thermal energy storage
Heat transfer enhancement
PCM
Metal foam
Energy storage
Composite materials

ABSTRACT

Thermal energy storage is an expanding field within the subject of renewable energy technologies. After a listing of the different possibilities available for energy storage, this paper provides a comparison of various materials for High Temperature Thermal Energy Storage (HTTS). Several attributes and needs of each solution are listed. One in particular is using the latent heat as one of the most efficient ways to store thermal energy. The mixture of phase change material (PCM) embedded in a metal foam is optimising the thermal properties of the material for latent heat energy storage. The results of previous studies show that mechanical and thermal properties of foam were extensively studied separately. This paper highlights the potential for an advanced study of thermo-mechanical properties of metal foams embedded with PCM.

1. Introduction

The efficient use of energy is of growing importance and developing highly effective energy saving solutions are paramount in the current energy demand context. The objective of the current paper is to review the available information on the thermal energy storage (TES), in order to define the priority research objectives to complete the fundamentals needed for their widespread application. The review part of the paper specifically focuses upon (i) the underlying storage mechanisms and its potential, (ii) the essential materials and properties that delineate temperature ranges of application, and (iii) the illustration of particular solutions to high temperature thermal energy storage. After a brief description of thermal energy storage, the advantages of storing both sensible and latent heat are discussed. As a specific case, we show the effectiveness of storage involving latent heat and how it leads to the selection of a phase change material (PCM) for specific applications, whilst highlighting its appropriate characteristics, its current weaknesses, and the multiple solutions to improve the thermal properties of PCM. The selected solution involves a metal foam and a PCM, two materials that have been previously studied, mostly towards their applicability and advantages. From assessing these previous studies, it is clear that there is an urgent need to develop a thermo-mechanical modelling of such a composite, subject of the extensive research program currently carried out by the authors. The layout of the present paper is illustrated in Fig. 1. Each of the parallel topics is subsequently dealt with.

2. Energy storage

Energy Storage (ES) is the storage of some kind of energy that can be drawn upon at a later time and usefully re-applied in a given operation. It has the potential of increasing the effective use of energy equipment and is normally applied to balance the possible mismatch between the supply of, and demand for energy [1]. The imperativeness of ES results from the need of having the energy production decoupled from its supply and distribution, and to support the intermittent nature of producing alternative energy [2]. An energy storage process is based on three fundamental steps: charging (loading), storing and discharging (releasing) [1]. As a result, ES applications facilitate energy management, help bridging power supply/needs and power quality, and increase the

* Corresponding author. Tel.: +44 2476522046; fax: +44 2476522129.
** Corresponding author. Tel.: +56 23311598.
E-mail addresses: f.pitie@warwick.ac.uk (F. Pitié), gustavo.caceres@uai.cl (G. Cáceres).

0360-5442/$ – see front matter © 2012 Elsevier Ltd. All rights reserved.
doi:10.1016/j.energy.2012.01.024

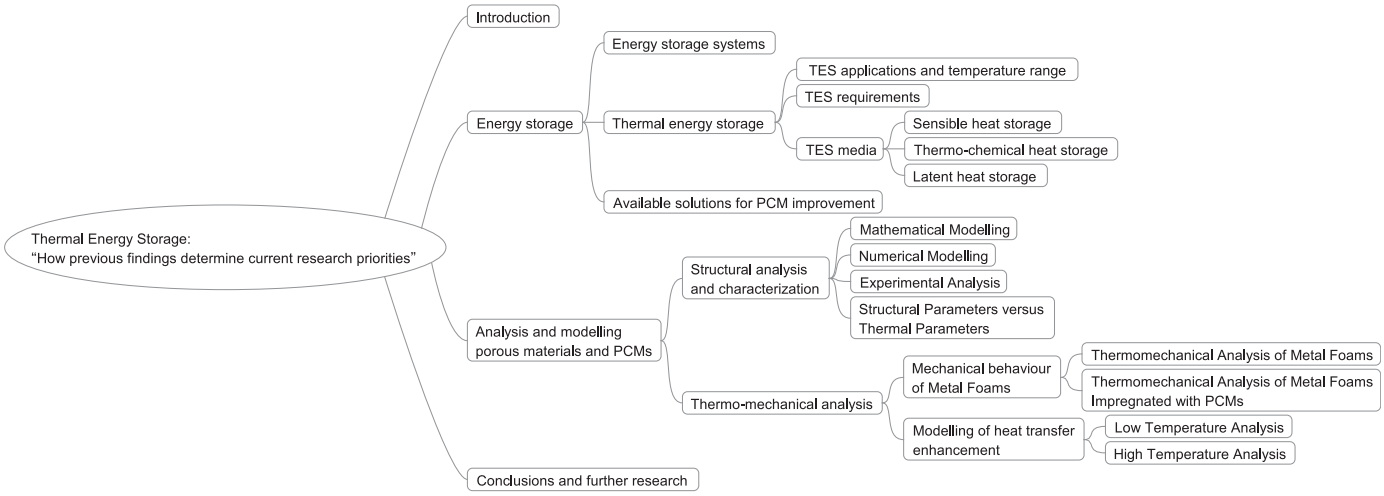

Fig. 1. Layout of the present paper.

system reliability [2]. Energy forms include mainly mechanical, chemical, electrical or thermal energy, and all of them can be stored using an appropriate method, system or technology as described below.

2.1. Energy storage systems

Every system or technology of ES had been developed in order to answer specific needs [2]. They are classified by the form of energy stored, as shown in Fig. 2.

Mechanical ES systems are either of potential or kinetic nature. Kinetic energy storage systems are usually flywheels with low or high rotational speeds (FES) [2]. Potential energy storage systems include pumped hydroelectric (PHS) and compressed air energy systems (CAES) at small and large scale [2]. The electrical ES is the only technology that charges, stores and returns electric energy: it uses standard electrostatic capacitors (CAP), electrochemical capacitors (super-capacitors) (ECC), and superconducting magnetic energy storage (SMES). Chemical ES groups three main types of batteries; i.e. the conventional, molten salt, and flow batteries [2]. The Thermal Energy Storage (TES) systems cover a large range of temperatures and applications [2] and are further detailed in this paper because of their expected high technological strength and market potential.

Several reviews have previously described ES technologies and systems [2,3]. Datas are collected in Table 1 by Bradbury [3]: the wide range of their characteristics, costs and efficiencies illustrates that development and application are at different stages. The comparison shows that each technology has a specific field of applications and answers a specific need. Thermal Energy Storage is presented here as a solution for numerous applications.

2.2. Thermal energy storage

With Thermal Energy Storage (TES), heat is transferred to storage media during the charging period, and released at a later stage during the discharging step, to be usefully applied e.g. in generating high-pressure steam for power block (Rankine cycle) in solar plants, or as heat carrier in high temperature industrial processes, such as metallurgical transformations [4]. In terms of storage media, a variety of choices exists depending on the storage media system selected, the temperature range and the specific application.

2.2.1. TES applications and temperature range

Low temperature thermal energy storage (LTTES) operates in a temperature range below 200 °C and has been extensively investigated and developed. LTTES applications can be found in building heating and cooling [5], in solar cooking, in solar water boilers and air-heating systems, and in solar greenhouses [6,7].

High temperature thermal energy storage (HTTES) plays a vital role in renewable energy technologies and waste heat recovery. There is a wide range of industrial applications where waste heat can be recovered, as in the manufacturing of construction materials (e.g. clay brick or cement kilns) mining and in the metallurgical industry in general [8,9]. Today, most HTTES usages are however focused upon applications of solar thermal energy [10,11].

TES applications are subject of constant innovative research and designs as shown in the numerous reviews [1–3,6,10,12–18]. The current paper presents a guideline in selecting a specific material as TES solution.

2.2.2. TES requirements

In order to make HTTES a more plausible and attractive alternative for improving the efficiency of industrial processes and solar engineering, some requirements must be fulfilled. HTTESs firstly need to stably operate in a high range of temperatures, which in the present context is specified from 200 °C to a as high a temperature limit as possible. Secondly, the material used as storage media must be inexpensive, available in big quantities and compatible with a cost-effective system design [1]. Several additional facts need to be considered when deciding on the storage media for an HTTES, and the most important requirements are presented by Zalba et al. [18]:

(i) Energy capacity: high energy density in the storage material;
(ii) Efficiency: good transfer between the heat transfer fluid (HTF) and the storage medium;
(iii) Mechanical and chemical stability of the storage material during the multiple charging/discharging cycles;
(iv) Safety: compatibility between HTF, heat exchanger and/or storage medium;
(v) Lifespan: complete reversibility in multiple charging/discharging cycles;
(vi) Low heat losses;

(vii) Ease of control;

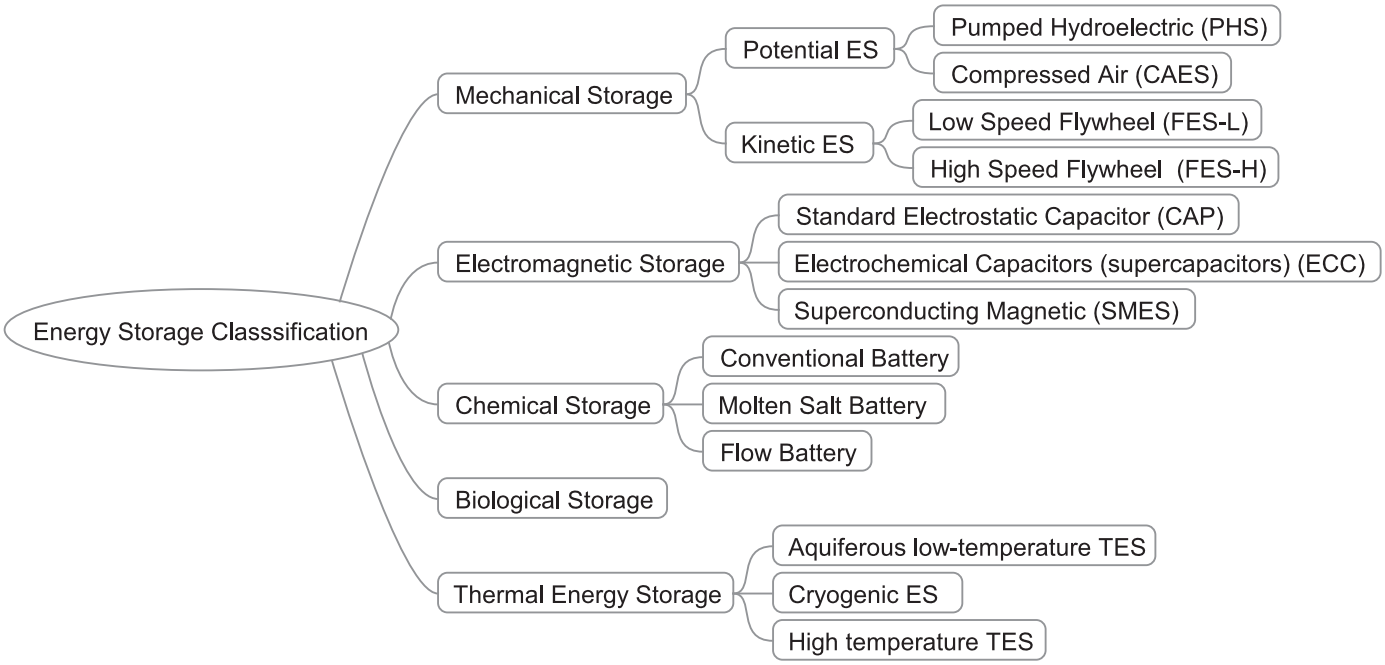

Fig. 2. Classification of energy storage systems [1].

(viii)Adequate maximum load;
(ix) Appropriate nominal temperature and;
(x) Specific enthalpy drops in load.

Meeting all these requirements needs innovative engineering approaches, with a major impact attributed to the development and research into the fields of storage media. The latter is due to the difficulty of selecting an adequate and stable storage material that matches both (i) and (ii) requirements described above. The combination of high efficiency and high energy density requirements can lead to the development of a storage media that makes viable the design of cost-efficient HTTES, and it is a challenge that demands novel ideas and pioneering efforts.

2.2.3. TES media

An assertive material selection involves choosing an adequate form of thermal storage, which can be found in three types, being the thermal storage as sensible heat, the thermal storage as latent heat when phase transformations are accounted for, and the thermo-chemical storage as a result of combining endothermic and exothermic reactions occurring with the media. The energy released or absorbed by a material as its temperature is reduced or increased is called sensible heat, and the specific heat (c_p) is the relevant characteristic. The energy required to convert a solid into a liquid, or a liquid into a gas (material phase change) is called latent heat with e.g. heats of fusion and condensation recognised for their high value. The capacity of energy storage is significantly higher when latent heat storage complements the sensible heat storage. The third and less developed category of heat storage, the thermo-chemical heat storage, uses the reversible endothermic/exothermic reactions of some reactions as detailed below.

2.2.3.1. Sensible heat storage. Sensible heat storage materials undergo no phase change within the temperature range required for the storage application [19]. Table 2 summarizes the main characteristics of the most common solid and liquid sensible HTTS materials [19,20].

Within the indicated solids, concrete and cast ceramics have been extensively studied due to their low costs, good thermal conductivities and moderate specific heats [21,22]. In terms of liquids, molten salts are widely used in power tower systems [22,23], being liquid at ambient pressure, providing an efficient and low cost medium, having their operating temperatures compatible with current high-pressure and high temperature turbines (temperature range over 120 °C–600 °C), whilst being non-flammable and non-toxic. These molten salts are already used in the chemical and metallurgical industries as heat-transport fluid, hence providing experience and knowledge for their use in other fields than solar plants [24]. From Table 2, it is clear that the main candidates for liquid sensible heat storage are either a solar salt, i.e. a binary salt consisting of 60% of $NaNO_3$ and 40% of KNO_3, that melts at 221 °C and is kept liquid at 288 °C in an insulated storage tank; or HitecXL, a ternary salt consisting of 48% $Ca(NO_3)_2$, 7% $NaNO_3$, and 45% of KNO_3 operating beyond its melting point of 130 °C [25].

Sensible heat materials have been widely studied and are currently applied in solar thermal plant applications, despite important disadvantages that can affect the storage system design and stability. Kearny et al. [26] investigated molten salts and demonstrated such disadvantages. Most molten salts have a high freezing point (around 100 °C), and the high outlet temperature results in heat losses and in requiring more expensive piping and materials [26,27]. The high freezing point may be a problem for solar power plants because of the required heat trace during non-functioning periods. Furthermore, the sensible fraction of thermal energy is seldom fully recovered due to the required temperature difference as heat transfer driving force. Another important disadvantage consists in the low energy storage density of sensible heat materials, which are required in large volumes or quantities in order to deliver the amount of energy storage necessary for HTTES applications. The above mentioned problems can imply significant increments in the costs of sensible heat storage systems.

2.2.3.2. Thermo-chemical heat storage. The main advantage of the thermo-chemical heat storage systems consists in the potentially high energy density of the occurring reversible chemical reactions,

Table 1
Main characteristics of energy storage systems [3].

	Mechanical storage			
	PHS	CAES	FES-LS	FES-HS
Parameter				
Roundtrip efficiency [%]	70–85	57–85	70–95	70–95
Self-discharge [%energy/day]	~0	~0	100	1.3–100
Cycle lifetime [cycles]	N/A	N/A	20k–100k	20k–100k
Expected lifetime [years]	30–60	20–40	15–20	15–20
Specific energy [Wh/kg]	0.5–1.5	30–60	10–30	10–30
Specific power [W/kg]	0	0	400–1.5k	400–1.5k
Energy density [kWh/m^3]	0.5–1.5	3–6	20–80	20–80
Power density [kW/m^3]	0	0.5–2	1k–2k	1k–2k
Costs				
Power cost [$/kW]	600–2k	400–800	250–360	250–400
Energy cost [$/kWh]	0–23	2–140	230–60k	580–150k
Balance of plant costs (BOP) [$/kW]	270–580	270–580	110–600	110–600
Power conversion system costs (PCS) [$/kW]	0–4.8	46–190	0–120	0–1200
Operation and maintenance (OM) fixed cost [$/kW-y]	3–4.4	1.6–29	6–22	6–22

	Electrical storage		
	CAP	ECC	SMES
Parameter			
Roundtrip efficiency [%]	60–70	90–98	90–98
Self-discharge [%energy/day]	40	20–40	10–15
Cycle lifetime [cycles]	50k	10k–100k	100k
Expected lifetime [Years]	5	20	20–30
Specific energy [Wh/kg]	0.05–5	2.5–15	0.5–5
Specific power [W/kg]	100k	500–5k	500–2k
Energy density [kWh/m^3]	2–10	0	0.2–2.5
Power density [kW/m^3]	100k	100k	1k–4k
Costs			
Power cost [$/kW]	200–400	100–360	200–350
Energy cost [$/kWh]	500–1k	300–94k	1k–83k
BOP cost [$/kW]	180–580	180–580	140–650
PCS cost [$/kW]	50–12k	50–12k	60–12k
O&M fixed cost [$/kW-y]	6–16	6–16	9.2–30

	Chemical storage				
	Conventional battery			Molten salt battery	
	Lead acid	NiCd	Li-ion	NaS	ZEBRA
Parameters					
Roundtrip efficiency [%]	70–82	60–70	85–98	70–90	85–90
Self-discharge [%energy/day]	0.033–0.3	0.067–0.6	0.1–0.3	0.05–20	15
Cycle lifetime [cycles]	100–2k	800–3.5k	1k–10k	2.5k–2.5k	2.5k
Expected lifetime [Years]	3–20	5–20	5–15	5–15	10–14
Specific energy [Wh/kg]	30–50	50–75	75–200	150–240	100–120
Specific power [W/kg]	75–300	150–300	150–315	150–230	150–200
Energy density [kWh/m^3]	50–80	60–150	200–500	150–250	150–180
Power density [kW/m^3]	10–400	0	0	0	220–300
Costs					
Power cost [$/kW]	175–600	150–1500	175–4000	150–3000	150–300
Energy cost [$/kWh]	150–400	600–1500	500–2500	250–500	100–200
BOP cost [$/kWh]	120–600	120–600	120–600	120–600	120–600
PCS cost [$/kW]	58–180	50–180	0	0–120	0–120
O&M fixed cost [$/kW-y]	1.8–52	6–32	12–30	23–61	23–61

	Chemical storage		
	Flow battery		
	ZnBr	Polysulfide-bromide	Vanadium Redox
Parameters			
Roundtrip efficiency [%]	60–75	57–75	60–85
Self-discharge [%energy/day]	0.24	~0	0.2
Cycle lifetime [cycles]	2k	2k	12k–14k
Expected lifetime [Years]	5–10	10–15	5–15
Specific energy [Wh/kg]	30–50	10–50	10–30
Specific power [W/kg]	0	0	0
Energy density [kWh/m^3]	30–60	16–60	16–33
Power density [kW/m^3]	0	0	0
Costs			
Power cost [$/kW]	175–2500	330–2500	175–1500
Energy cost [$/kWh]	150–1000	120–1000	150–1000
BOP cost [$/kWh]	120–600	120–600	120–610
PCS cost [$/kW]	0–120	60–120	36–120
O&M fixed cost [$/kW-y]	15–47	18–96	24–65

Table 2
Main characteristics of sensible heat storage solid and liquid materials.

Storage medium	Temperature		Average density (kg/m^3)	Average heat conductivity (W/m K)	Average heat capacity (kJ/kg K)	Volume specific heat capacity (kWh_t/m^3)	Costs per kg (US$/kg)	Costs per kWh_t (US/kWh_t$)
	Cold (°C)	Hot (°C)						
Solid storage medium								
Sand-rock-mineral oil	200	300	1700	1	1.3	60	0.15	4.2
Reinforced Concrete	200	400	2200	1.5	0.85	100	0.05	1
NaCl (solid)	200	500	2160	7	0.85	150	0.15	1.5
Cast iron	200	400	7200	37	0.56	160	1	32
Silica fire bricks	200	700	1820	1.5	1	150	1	7
Magnesia fire bricks	200	1200	3000	1	1.15	600	2	6
Liquid storage medium								
HITEC solar salt	120	133	1990	0.60	–	–	–	–
Mineral oil	200	300	770	0.12	2.6	55	0.3	4.2
Synthetic oil	250	350	900	0.11	2.3	57	3	42
Silicon oil	300	400	900	0.1	2.1	52	5	80
Nitrite salts	250	450	1825	0.57	1.5	152	1	12
Nitrate salts	265	565	1870	0.52	1.6	250	0.5	3.7
Carbonate salts	450	850	2100	2	1.8	430	2.4	11
Liquid sodium	270	530	850	71	1.3	80	2	21

which can be even higher than what is usually encountered for the other thermal storage processes [1,28]. Materials that have been mostly investigated for chemical storage are the SnO_x/Sn and ammonia system. In the former case, the metal oxide/metal reactions are possible and technically feasible, occurring at a temperature of 980 K, and SnO_2 (solid) is reduced with CH_4 while it floats on top of liquid Sn. For the latter case, ammonia is dissociated producing hydrogen and nitrogen. The exothermic reaction heat from ammonia synthesis is suitable for electric power generation in conventional Rankine Cycles. Despite its high energy density, thermo-chemical heat storage is considered to be an expensive alternative and is, at the present, at early stages of development [28].

2.2.3.3. Latent heat storage. Latent heat storage is based on the heat absorption or heat release that occurs when a storage material undergoes a phase change. Latent storage systems based on phase change materials (PCMs) with solid–liquid transition are considered to be very efficient in comparison to liquid–vapour and solid–solid transitions [7]. Liquid-gas transition requires a large volume recipient for the PCM and the solid–solid transition presents a low value of latent heat. Therefore these last two alternatives are not considered appropriated choices [29]. A large number of materials are known to melt with a high heat of fusion within different ranges of temperature. No material yet studied has all the optimal characteristics required for a PCM, and the selection of a PCM for a given application requires careful consideration of the properties of the various substances and/or mixtures [16]. The main characteristics required for PCMs are indicated in Table 3 [7]. As an example, commercial or potential substances used as PCM are shown in Tables 4, 5 and 6 [20].

Current experimented uses of PCMs for thermal storage involve low to moderate temperatures (10–100 °C) and include solar water-heating systems, solar air-heating systems, solar cookers, solar greenhouses (for curing and drying processes), building acclimatization as in a PCM Trombe wall, PCM wallboards [5], under-floor heating systems and ceiling boards [6,7]. Though PCMs usage in HTTES has been experimented for solar plant applications, it has not yet been commercially used in a solar plant [1,11].

The development of high temperature thermal storage using PCMs is of increasing interest since they are moderately expensive, have high energy density, can in the future be available in large quantities [18], and are able to store and release thermal energy at a constant temperature most of the times [6,7]. However, most of PCMs have a low thermal conductivity, leading to low charging and discharging rates and sometimes non suitable field of temperature in the material. Therefore, using PCMs for energy storage in high temperature range applications requires considering new aspects of material selection and development. In addition to adapt PCM's melting points to a high temperature range, their characteristics need to be improved in order to increase the *efficiency of the charging and discharging* processes.

Based on this information, several studies or papers consider the development of novel phase change materials for high temperature purpose a very important subject of study, and the team of authors is engaged in an extensive programme of research to provide an adequate theoretical background and a description of the fundamentals. The successful completion of this research will help create fundamental and advanced knowledge on the subject, as well as support the development of cost-effective high temperature thermal storage systems oriented for the improvement of renewable energy technologies and energy-efficient industrial processes. The facts and findings of previous research form the guidelines to the research priorities, and are dealt with below.

2.3. Available solutions for PCM improvement

To improve the efficiency of the charging and discharging processes of PCMs, the most relevant parameter to be studied is their thermal conductivity. In order to increase the thermal conductivity of PCMs, several heat transfer enhancement techniques have been studied [15], such as:

Table 3
Main desirable characteristics of PCMs.

Thermal properties	Phase change temperature suitable within the desired operating range. High latent heat per unit mass. High specific heat. High thermal conductivity for both solid and liquid phases.
Physical properties	High energy density. Low-density variation during phase change. No supercooling during freezing.
Chemical properties	Chemical stability. No chemical decomposition. Compatibility with container materials construction (e.g. vessels and piping). Non-toxic, non-inflammable and non-explosive.
Economic Factors	Available in large quantities. Inexpensive

Table 4
Organic compounds for potential use as PCM.

Organic compounds	Melting point (°C)	Heat of fusion (kJ/kg)
Ammediol	112	285
Neopentyl glycol	125	45.3
Neopentylglycol diacrylate	126	44.3
Isomalt	147	275
Adipic acid	152	247
Dimethylol propionic acid	153	275
Tromethamine	172	27.6
Trimethylolethan	198	44.6
Pentaerythritol	260	36.9

(i) the micro-encapsulation of PCMs using graphite [30], Silicon Carbide (SiC) [31], nickel film coating of PCM copper spheres [32];
(ii) the use of metal carrier structures made of steel or stainless steel;
(iii) a dispersion of high conductivity material i.e. copper, silver or aluminium particles, within the PCM;
(iv) the use of high conductivity, low-density materials such as carbon fibres and paraffin composites; and
(v) the impregnation of high conductivity porous materials, either as a metal foam (copper, steel or aluminium), or as porous material like graphite.

A general review of these techniques has been undertaken by the authors (Fig. 3), and the impregnation of metal foams in PCM was determined as being one of the most promising and suitable approaches at the present stage of the project investigation. As described below and explained in detail in the following sections, metal foams prove to be a non-expensive, easy to handle, abundantly available material that improves heat transfer rates in PCMs significantly, thus being an attractive approach for developing and improving latent heat storage media.

The reasons behind this selection are the result of the detailed assessment, which summaries as follows:

(i) The thermal performance of *micro-encapsulated PCMs* is expected to exceed conventional PCMs since small PCM particles provide larger heat transfer area per unit volume and will provide a higher heat transfer rate. Micro-encapsulated PCMs moreover add advantages like less reaction of PCM with container material, and the ability to withstand volume change during phase change [33]. This heat transfer enhancement technique has been widely studied for different combinations of PCMs and coating shells [30–37]. These studies mainly focused on the preparation and characterization of micro-encapsulated PCMs, without extensive comparison of the performance of micro-encapsulated PCM with that of pure PCM, and more comparative work is needed in order to assess the performance enhancement due to micro-encapsulation of commonly used PCMs. Such approach requires a great deal of experimental work, only at its incipient stage at present.
(ii) *Incorporating metal structures into the PCM* has also been addressed as one of the thermal conductivity enhancement techniques by some researchers, who investigated metal structures made of steel or stainless steel in different geometries, such as cylindrical and spherical geometries, and in different arrangements [38–41]. In order to achieve a significant reduction of melting/solidification time, an important system volume is necessary, thus associated with an expected increase of costs and a limit of LTTES system usages. Due to the constrains demonstrated by the review, this heat transfer enhancement technique does not fulfil our research interests.
(iii) *Dispersion of high conductivity particles into the PCM* is a relatively simple technique to enhance the thermal conductivity of PCM. Studies involving dispersion of metal particles like copper, silver and aluminium have been undertaken [39,42,43]. They showed that, at any given condition, there is a range of optimum particle fractions and it is suggested to choose lower values in the band to ensure a high mass of PCM to increase the amount of energy stored. Hence, an appropriate combination of particle thermal conductivity and particle mass fraction is quite important when the conductive particles are to be dispersed in the PCM to enhance the performance of the unit. These results conclude that there is a limitation in terms of PCM/particle combination that could be applied, and further research is necessary.

Table 5
Inorganic substances for potential use as PCM and commercial compounds.

Inorganic compounds	Melting point (°C)	Heat of fusion (kJ/kg)	Density (kg/m^3)	Specific heat (kJ/kg K)	Thermal conductivity (W/m K)
$Mg(NO_3)\ 2H_2O$	130	275	n.a	n.a.	n.a
Hitec XL: 48%$Ca(NO_3)_2$–45%KNO_3–7%$NaNO_3$	140	n.a.	1992	1.44	0.519
Hitec: KNO_3-$NaNO_2$-$NaNO_3$	142	84	1990	1.34.	0.6
68%KNO_3–32%$LiNO_3$	144	75	n.a	n.a.	n.a
Isomalt	147	252	n.a	n.a.	n.a
$LiNO_3$-$NaNO_3$	195	n.a.	n.a.	n.a.	n.a.
KNO_3/$NaNO_3$ eutetic	223	105	n.a.	n.a.	0.8
$NaNO_3$	307/308	74	2260/2257	n.a.	0.5
KNO_3/KCl	320	116	2100	1.21	0.5
KNO_3	333/336	266/116	2110	n.a.	0.5
KOH	380	149.7	2044	n.a.	0.5
$MgCL_2$/KCl/NaCl	380	400	1800	0.96	n.a.
$NaCO_3$-$BaCO_3$/MgO	500–850	n.a.	2600	n.a.	5
$AlSi_{12}$	576	560	2700	1.038	160
$AlSi_{20}$	585	460	n.a.	n.a.	n.a
$MgCl_2$	714	542	2140	n.a.	n.a
80.5%LiF-19.5%CaF_2 eutetic	767	790	2100/2670	1.97/1.84	1.7/5.9
NaCL	800/802	492/466.7	2160	n.a.	5
LiF	850	1800 MJ/m^3	n.a.	n.a.	n.a.
Na_2CO_3	854	275.7	2533	n.a.	2
KF	857	452	2370	n.a.	n.a.
K_2CO_3	897	235.8	2290	n.a.	2

Table 6
Inorganic substances for potential commercial compounds.

Commercial compounds	Melting point (°C)	Heat of fusion (kJ/kg)	Density (kg/m^3)	Specific heat (kJ/kg K)	Thermal conductivity (W/m K)
Paraffin RT110	112	213	n.a.	n.a.	n.a.
Inorganic E117	117	169	1450	2.61	0.7
Organic A164	164	306	1500	n.a.	n.a.

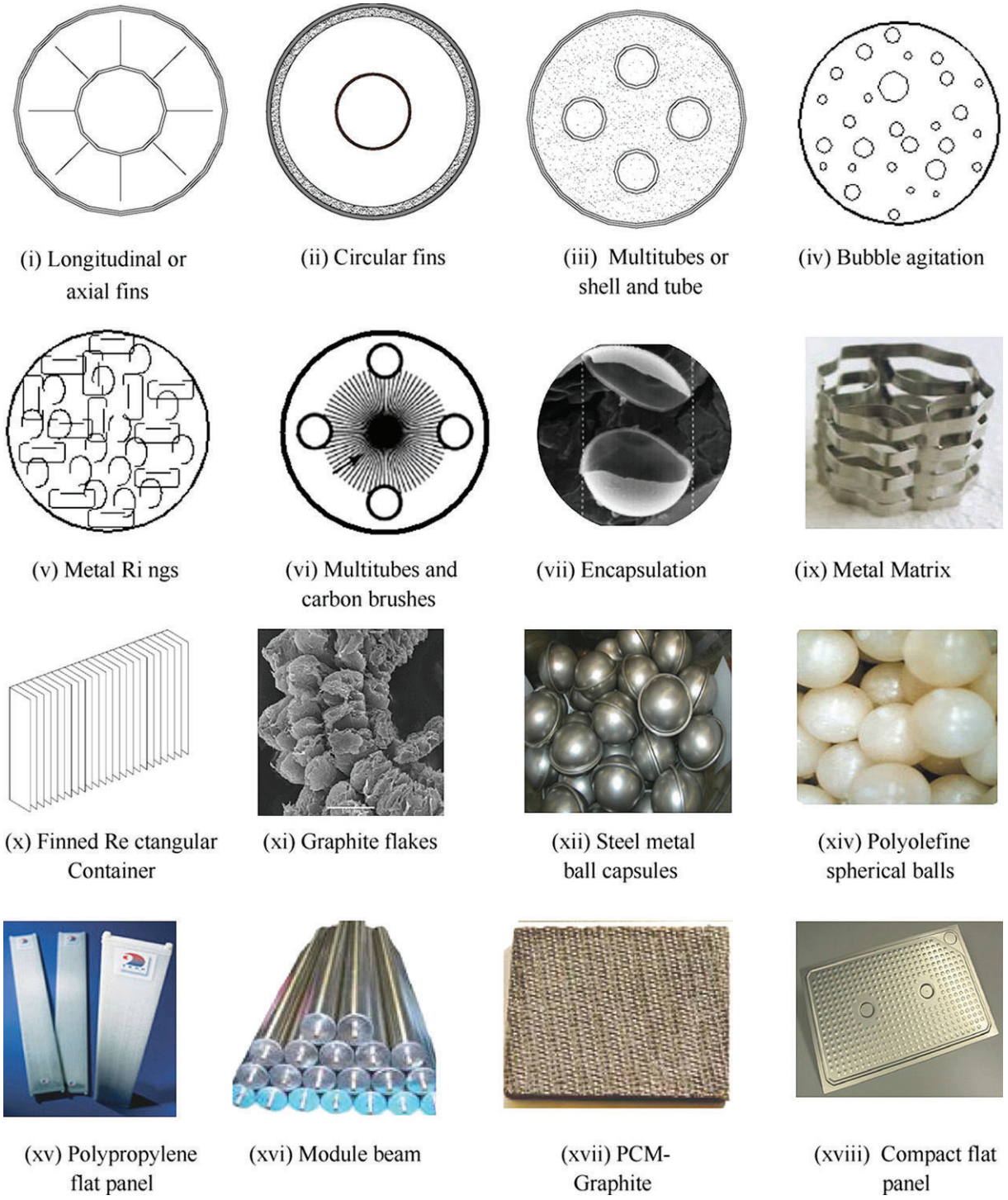

Fig. 3. Heat transfer enhancement methods employed in phase change material research [12].

(iv) High conductivity particles *should also be compatible with all PCMs*. Due to the relatively high density, the metal particles/metal structures may settle at the bottom of the TES container and add considerable weight to the system. According to Fugai et al. [44], not all metal particles are compatible with all PCMs. For example, paraffin and aluminium are compatible, while copper and nickel are not compatible. Similarly, aluminium and copper are not compatible with some salt hydrates. Hence, there has been a search for *low-density high conductivity additives which should be compatible with all PCMs*. Since the densities of carbon fibres are lower than those of metals and the thermal conductivities are almost equal to that of aluminium and copper, carbon fibres can be better alternatives to enhance the thermal performance of LTTES systems. This heat transfer enhancement technique has been widely studied, as previously mentioned [42,45–48]. The review has revealed that both the phase change and/or the charging and discharging rate (melting/solidification) can be increased considerably by adding high conductivity substances. In general, however, these additives may lead to the loss of storage capacity of pure PCM. The loss in storage capacity limits the mass/volume fraction of additives. It should therefore be mentioned that this technique has a limited potential for developing LTTES systems for industrial applications, where a high storage capacity of PCMs is needed to accomplish the industrial requirement of non-intermittent high temperature steam production.

(v) In view of the above mentioned constraints, *impregnation of high conductivity porous materials in PCMs* constitutes an attractive alternative for improving the heat transfer processes in PCMs. The use of a porous matrix has gained increasing attention because of its light weight and high specific surface area for heat transfer [49]. Porous structures can be even matrices made of aluminium, copper, etc., or naturally available porous materials such as graphite. Since the porous material is impregnated in the PCM, the problem of particle segregation at the bottom of the TES container is reduced. The main challenge of this approach would be to develop a compatible and efficient combination of the PCM and porous material, suitable for high temperature purposes. More specifically, the research should provide a proper modelling of copper foam structures embedded in selected salts as PCM. Therefore, *structural* and *thermo-mechanical* parameters need to be studied in conjunction with a *charging/discharging efficiency analysis* of PCMs impregnated in metal foams.

3. Preliminary analysis and modelling of composites metal foam/PCM to be applied as HTTES material

3.1. Structural analysis and characterization

Several studies of isolated metal foam structures have been undertaken over the past years. Efforts have been made to determine the proper modelling of aluminium alloys. However, there are no studies attempting to develop a model specifically to a copper foam structure. The present review presents a few interesting approaches to the micro-structural characterization of metal foams and porous materials in general, which provide starting points for further investigations related to copper foam structures.

3.1.1. Mathematical modelling

Micro-structural modelling of metal foams has been done for tetrakaidecahedron geometry [50–52] and octahedral geometry [53]. The first investigations are considered to be a good approximation to aluminium structures (Fig. 4). The last one states that metallic struts constituting the porous body can be regarded to be regularly connected by the way of diagonals of cubes and, thereby, form a great deal of octahedral units in the form of close-packed Body Centered Cube.

3.1.2. Numerical modelling

Numerical models of metal foams can be found for tetrakaidecahedron geometry [51,52]. The first one was developed in order to predict the heat transfer enhancement capability of a channel filled with metal foam; the last one was generated for estimating the crushing behaviour of dynamically loaded metal foam-filled square columns.

For a spherical geometry [54], an incompressible, hardening, visco-plastic matrix material has been modelled, and the growth of a void in metallic media has been analysed. This approach, similar to the ones described above, is designed to be used in either mechanical or thermo-mechanical evaluations of metal foams structures. In this case specifically, the purpose was the analysis of constitutive relations, shearing and volumetric viscosities for plastic deformation of a porous material.

3.1.3. Experimental analysis

In order to validate the modelling of metal foams structures, Raj et al. [55] have experimentally analysed the microstructure of an aluminium alloy, FeCrAlY, and compared the results with previously modelled geometries.

According to the above mentioned research, modelling of foam cell structures fall into two broad categories: (i) idealized topological models based on minimizing the ratio of the surface free energy to volume free energy that can fill a three-dimensional (3D) space; and (ii) engineering models based on the actual reconstruction of the 3D foam microstructures. Among the several possible idealized topological representations of the foam microstructures [56], the three-dimensional, space-filling Kelvin tetrakaidecahedron [56,57] is often favoured for modelling the foam cellular network. This cell has 14 faces consisting of 6 square and 8 hexagonal faces. In other words, about 43% of the faces are squares, 0% faces are pentagonal and 57% of the faces are hexagonal. Elsewhere, other topological models like Williams and Weaire–Phelan models have been proposed, where pentagonal faces are incorporated in the cell geometry [58,59].

The Raj et al. research [55], belonging to the second category above listed, determined quantitative information on ligament (or struts) dimensions, cell face dimensions, area fractions of open and closed faces, geometric shapes of the cell faces and distribution of ligament [60]. The paper specifically reports statistical data on the geometrical features of the cells faces to determine the validity of the Kelvin [61] and other theoretical space-filling models [57,59,62] in a comprehensive manner.

The shapes of cell faces of the alloy were evaluated by approximating the faces by regular polygons. It was observed that between 24 and 28% of the cell faces were quadrilateral, 50–57% pentagonal and 15–22% hexagonal in morphology. The results agreed with Matzke's observations [63], which suggested that the FeCrAlY foam cells had a total of 11 faces with 3 quadrilateral, 6 pentagonal and 2 hexagonal faces. Both sets of results do not agree with the 14-hedra Kelvin tetrakaidecahedron model [61], which only has 43 and 57% quadrilateral and hexagonal faces, respectively. Neither do the results agree with the Williams and Weaire–Phelan models [58,59]. Their calculations show that the 3–6–2 cell, which probably best describes the FeCrAlY foam cells, has 27 edges and 18 vertices [55]. The Raj et al. studies [55,60] are a very important support for the structural characterization that will be carried out in our further research. However, it will be necessary to analyse if the results need to be taken strictly into account for the investigation of copper foam as a storage material. It could instead be found that the Kelvin model

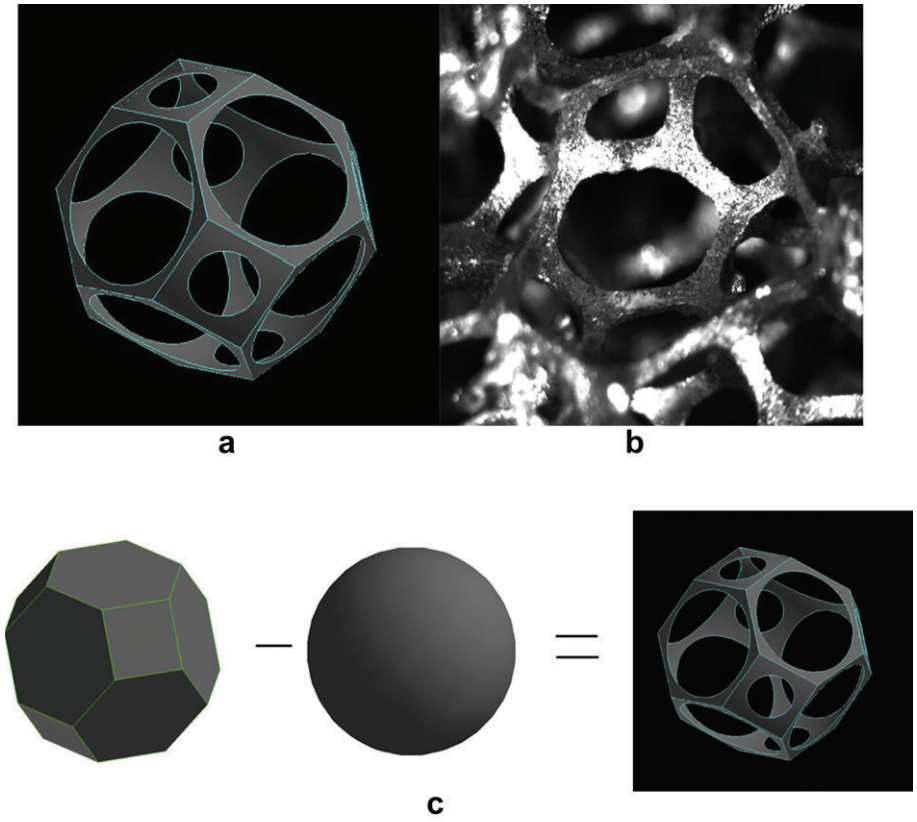

Fig. 4. Comparison of single cell model with actual foam structure, (a) Single cell model used in this study, (b) SEM photo of aluminium foam and (c) Geometry creation of a single cell [51].

assumption (where all cells are of the same size and volume so it can be determined the cell shape that can pack 3D space resulting in a system with the lowest free energy) provides a reasonable approximation. In this case, the mathematical and numerical studies previously mentioned in the other items of this section can be used as reference to evaluate the effects of those approximations in thermo-mechanical analysis results.

3.1.4. Structural parameters versus thermal parameters

The study of the relation of structural parameters with thermal conductivity, thermal diffusivity and latent heat in a porous material impregnated with PCM was done for a graphite foam integrated with paraffin wax [64,65]. The research determined:

(i) an almost linear relation between thermal conductivity and the bulk density of the graphite matrix, as well as between the latent heat of the composite and the mass ratio of the paraffin wax in the matrix;
(ii) a small pore-size and thicker ligament in the matrix resulted in a higher thermal diffusivity;
(iii) a large pore-size and thinner ligament in the matrix resulted in a larger latent heat. A similar analysis relating structural and thermal parameters will be carried out in our research, which will instead consider a metal foam matrix structure impregnated with a selected salt submitted to a high temperature.

3.2. Thermo-mechanical analysis

The thermo-mechanical behaviour analysis is important to predict the effect of various cycles of charging and discharging of thermal energy when the PCM is subjected to high and low temperatures. It also provides information about how this condition influences the stress parameters. The purely mechanical behaviour of isolated porous structures in absence of temperature variation has been widely studied [51–53,66,67] to determine the tensile properties of these materials. The authors consider the understanding of the mechanical behaviour of metal foams a first step to later combine with thermal analysis; therefore the review of particularly relevant literature on this subject has been undertaken. Additionally, the thermo-mechanical review for both isolated porous material and in composite with PCM has also previously been presented.

3.2.1. Mechanical behaviour of metal foams

A mathematical modelling of an octahedral metal foam structure was built to determine how the characteristic parameters, like porosity, are related to the maximum nominal shearing stress [53]. The results show that, when the porous body endures the fracture resulting from shearing loads or from torsion, the maximum nominal shearing stress and the nominal torque for the porous component can be related to the porosity and the inherent characteristic parameters of the metal foam itself. From these mathematical relations, the loading criterions may be directly and conveniently achieved for these materials under the corresponding loads, respectively.

The tetrakaidecahedron geometry, which is the closest approximation used for an aluminium foam, has been mathematic and numerically modelled in order to study the metal's crushing behaviour [52]. An existing fully self-similar Deshpande and Fleck [68] constitutive model for metallic foams is modified assuming

a non-associated plastic flow rule and incremental proportional straining under proportional stressing concept. The research determined a force-deformation curve, a mean force and a folding pattern. The output of the numerical modelling has been compared with available experimental data and the results were found reliable.

3.2.1.1. Thermo-mechanical analysis of metal foams. An experimental and analytical study of the thermal conductivity of compressed expanded graphite (EG) foam was carried out in order to study the density relationships of thermal conductivity and elasticity modulus of compact EG [66]. The compacted EG critical density corresponding to the observed jump in the thermal conductivity coefficient and elasticity modulus was shown to depend on the expandable graphite preparation method, EG bulk density, and degree of dispersion.

A mathematical modelling and numerical simulation of a tetrakaidecahedron open-cell was undertaken for the modelling and simulation of heat transfer enhancement and corresponding pressure drop [51]. A simplified analytical model based on diamond-shaped unit cells has been developed to predict the heat transfer capability of a foamed channel. The heat transfer rates predicted by the analytical model have been compared with available experimental data from other researchers [4] and favourable agreement has been obtained.

3.2.1.2. Thermo-mechanical analysis of metal foams impregnated with PCMs. The thermo-mechanical analysis of porous graphite impregnated with PCMs was also performed in order to develop of a mathematical model [67] of porous materials plastic behaviour. This research is focused on help understanding salt melting within the graphite matrices and for proposing reliable ways for composite materials improvement. The mathematical modelling was able to determine the relation between the pore-elastic-plastic deformation versus temperature and pressure time history, as well as liquid–crystals equilibrium conditions. An important observation was that, under melting, the salt volume expansion will be constrained by the graphite matrix and pressure in pores will thus increase. Main consequences of this pressurization are a progressive increase of the salt melting temperature and a progressive reduction of its latent heat. For melting progress, materials have to be heated up to a melting point which is continuously increasing. Hence, a significant part of the energy supplied to the material will be used to heat it up (sensible heat instead of latent heat). Control of graphite densification during materials elaboration would be an easy way for increasing porosity (voids) within the graphite matrix skeleton and hence to reduce its rigidity and to increase the pore wall thickness. However, this will also lead to a reduction of the effective thermal conductivity. Even though the porous material of this previous study slightly differs from a metal foam, the results could be considered as a preliminary approach of the interaction between the PCM and the embedded foam.

3.2.2. Modelling of heat transfer enhancement

In order to predict how different parameters influence the heat transfer rate in porous materials-PCMs composites, efforts in modelling the thermal conductivity can be divided into three categories: firstly, the mathematical, numerical and experimental modelling of graphite and metal foams in a low temperature range; secondly, mathematical modelling of graphite foam in a high temperature range; and finally, experimental research of metal foams in a high temperature range.

3.2.2.1. Low temperature analysis. The behaviour of graphite and metal foams impregnated with PCMs has been the subject of a variety of studies in the last few years. The discussion of thermal conductivity, diffusivity, convection and radiation has been carried out in order to define the role of structural parameters in the heat transfer rate. Analytical studies found results indicating that the thermal conductivity of the composites can be 28–180 times higher than of the pure paraffin wax [64]. It was moreover found that the thermal diffusivity of the Paraffin-GF can be enhanced 190, 270, 500, and 570 times as compared with that of pure PCM [65].

The combination of an experimental and analytical model was undertaken in order to evaluate the influence of radiation on the heat transfer performance. The analysis showed that radiation accounts up to 50% to the apparent foam conductivity [69,70]. Reduced natural convection was spotted in water-saturated metal foams [58], leaving conduction and buoyant advection as the dominant modes of heat transfer. Suppressed natural convection was also identified in PCM-metal foam composites [71]. The suppression mechanism was given [71]: the PCM was of high viscosity and low thermal expansion coefficient, resulting in both a large resistance force and weak driving force of natural convection. However, relevant studies, combining experiments and numerical modelling demonstrated an opposite tendency in air-saturated metal foams and claimed that natural convection was very significant, accounting for up to 50% of the effective foam conductivity obtained at ambient pressure [72]. These findings are not contradictory, because air tends to have a lower flow resistance and higher buoyancy force due to its low viscosity and high thermal expansion coefficient.

For low temperature analysis, recent research additionally provides experimental, numerical and mathematical modelling of graphite and/or metal foams impregnated with paraffin. Main interest of those studies consists of improving the feasibility of porous material for heat transfer enhancement. A numerical modelling for copper foams was developed and showed that the addition of this type of metal structure to paraffin wax can increase the heat transfer rate in comparison to the pure PCM [73] by 3–10 times. An experimental study comparing copper and graphite foams performances showed that, for a heat storage system of given volume, the PCMs embedded with metal foams usually have higher heat storage capacities than the composites made of PCMs and expanded graphite, since expanded graphite is very low in density [74]. In addition, metal foam composites appeared to have better heat transfer performance than graphite composites, because metal foam composites have continuous inner structures to help evenly distribute heat in PCMs. The research demonstrated that the volumetric heat of fusion decreases with the increase of relative density of metal foam and the mass ratio of expanded graphite.

Finally, an interesting comparison of methods was provided for the mathematical modelling of an aluminium foam embedded in paraffin [75]. The study determined that the heat transfer modelled with a two-temperature model is a better method to predicting the behaviour of energy flux in the metal foam instead of previous studies assuming local thermal equilibrium.

3.2.2.2. High temperature analysis. There are a reduced number of investigations that focus on heat transfer through a porous material embedded in PCMs at high temperature. As occurred in low temperature based studies, the core interest of the investigations resides in proving the feasibility of porous material for increasing heat transfer rates through PCMs subjected to high temperature. Moreover, some of the research aims at establishing a comparison between graphite and copper foam performances for the above mentioned purpose.

A large scale experimentation of graphite and salt composite applied to a thermal solar plant showed a very relevant result [4]; salt leakage was observed during the first cycles of charging/

discharging of the PCM and, therefore, all contact surfaces between PCM and graphite foam were lost. An analysis showed that, under thermal cycling, salt leakage can be mainly attributed to impurities and remaining mechanical stresses. The result points to potential problems that shall be considered in the present and further investigations of metal foams behaviour at high temperatures.

A mathematical model especially relevant for our research was developed for a graphite and salt composite [67]. The methods used for this research were based on energy conservation equations, pressure-dependent liquid–crystal equilibriums, linear elasticity laws and Poiseuille-like flow. The model provided a broad poro-elasto-plastic analysis and was able to determine required actions for achieving more desirable properties of the composite, which are the reduction of the pore wall rigidity, the increase of the pore walls thickness, increasing pores connectivity or, in general, creating void space.

Two very recent high temperature based studies carried out experimentations using both graphite and copper foams filled with $NaNO_3$. A significant advantage of copper foams over graphite in terms of improving heat transfer rates was identified [76]. The performance of the addition of porous materials was proved to increase heat transfer 2–5 times in comparison with pure PCM [49]. Both studies investigated the problem of suppression of natural convection in the liquid region and showed that corrosion stress problems are more intense for copper than for graphite foams.

From this literature review, it is clear that thermo-mechanical and structural parameters play an important role in the heat transfer behaviour of metal foam-PCM composites. However, the few existing approaches lack mathematical modelling to predict how the interaction of those particular parameters will affect the stability and energy flux through the composite subjected to high temperatures.

The present research addresses these issues and tries to present a novel approach to the thermal conductivity predictions by developing a model that incorporates all of the crucial aspects mentioned above and which influence the efficiency of charging and discharging processes of PCMs.

4. Conclusions and further research

The aim of this review was to critically examine the current state of art in order to delineate the required further development of a high temperature model of metal foam embedded with PCM. The parameters involved in the process of loading and releasing of thermal energy have to be investigated and adjustments to improve the material's heat flux behaviour have to be determined.

This paper is leading to focus on the study of one major thermal storage parameter: the rate of loading and releasing of energy in PCMs impregnated in metal foams, and the logical extension of this general work results in the study of (i) the metal foam structure characterization (ii) the analysis of the composites' thermo-mechanical behaviour, and (iii) the combination of these two particular topics to accurately analyse and predict heat transfer processes through copper foam structures embedded in PCMs.

Current research related to heat transfer enhancement by impregnating metal foam to PCMs at high temperatures relies only on experimental studies that were developed without the powerful aid of a mathematical and numerical modelling.

In order to achieve our objectives, research must analyse the thermo-mechanical stress in metal foam structures in order to quantify the influence of stress boundary effects on the effective heat flux. The stress analysis should define conductivity maps as function of pore-size and thickness. Additionally, it has to determine the latent heat storage response to a copper-like micro-structural characterization subjected to high temperature heating conditions during normal operation of loading and releasing of thermal energy in salts. The research has to be carried out by linking each methodology duly selected and adapted for the above mentioned analysis, to then improve the knowledge and insight of heat transfer processes in metal foams impregnated with PCMs.

Metals have in general a good thermal conductivity, but it is not enough to consider metals as good materials because graphite has excellent conductivity also. Then we can consider also the good mechanicals properties as elasticity of metals to support high volume expansion without cracking which is one problem of graphite matrix. Manufacturing metals as foams is correct way to profit better their thermo-mechanical properties.

Acknowledgements

This work is supported by the Centre for the Innovation in Energy (UAI, Chile), FONDECYT Chile (project number:1120490), UK Engineering and Physical Science Research Council (EPSRC grant number: EP/F061439/1), by the National Natural Science Foundation of China (Grant Nos: 51176110 and 51071184). The authors gratefully acknowledge support and advices from Dr. C.Y. Zhao of the School of Mechanical Engineering, Shanghai Jiaotong University, Shanghai 200240, China, and from Mr Y. Tuan of School of Engineering, University of Warwick, Coventry CV7 4AL, UK.

References

[1] Gil A, Medrano M, Martorell I, Lazaro A, Dolado P, Zalba B, et al. State of the art on high temperature thermal energy storage for power generation. Part 1–concepts, materials and modellization. Renewable Sustainable Energy Rev 2010;14:31–55.
[2] Chen H, Cong TN, Yang W, Tan C, Li Y, Ding Y. Progress in electrical energy storage system: a critical review. Prog Nat Sci 2009;19:291–312.
[3] Bradbury K. Energy storage technology review. Sustainable Energy Model; 2010.
[4] Pincemin S, Py X, Olives R, Christ M, Oettinger O. Elaboration of conductive thermal storage composites made of phase change materials and graphite for solar plant. J Sol Energy Eng Trans - ASME 2008;130:011005.1–5.
[5] Castellón C, Medrano M, Roca J, Nogués M, Castell A, Cabeza LF. Use of microencapsulated phase change materials in building applications. In: Buildings X proceedings, clearwater beach. Florida: ONRL; 2007.
[6] Sharma A, Tyagi VV, Chen CR, Buddhi D. Review on thermal energy storage with phase change materials and applications. Renewable Sustainable Energy Rev 2009;13:318–45.
[7] Regin AF, Solanki SC, Saini JS. Heat transfer characteristics of thermal energy storage system using PCM capsules: a review. Renewable Sustainable Energy Rev 2008;12:2438–58.
[8] Tamme R, Bauer T, Buschle J, Laing D, Müller-Steinhagen H, Steinmann W-D. Latent heat storage above 120°C for applications in the industrial process heat sector and solar power generation. Int J Energy Res 2008;32:264–71.
[9] Maruoka N, Sato K, Yagi J-ichiro, Akiyama T. Development of PCM for recovering high temperature waste heat and utilization for producing hydrogen by reforming reaction of methane. ISIJ Int 2002;42:215–9.
[10] Medrano M, Gil A, Martorell I, Potau X, Cabeza LF. State of the art on high-temperature thermal energy storage for power generation. Part 2–Case studies. Renewable Sustainable Energy Rev 2010;14:56–72.
[11] Laing D, Bahl C, Bauer T, Lehmann D, Steinmann W- D. Thermal energy storage for direct steam generation. Sol Energy 2011;85:627–33.
[12] Agyenim F, Hewitt N, Eames P, Smyth M. A review of materials, heat transfer and phase change problem formulation for latent heat thermal energy storage systems (LHTESS). Renewable Sustainable Energy Rev 2010;14:615–28.
[13] Ibrahim H, Ilinca A, Perron J. Energy storage systems–characteristics and comparisons. Renewable Sustainable Energy Rev 2008;12:1221–50.
[14] Jegadheeswaran S, Pohekar SD, Kousksou T. Exergy based performance evaluation of latent heat thermal storage system: a review. Renewable Sustainable Energy Rev 2010;14:2580–95.
[15] Jegadheeswaran S, Pohekar SD. Performance enhancement in latent heat thermal storage system: a review. Renewable Sustainable Energy Rev 2009; 13:2225–44.
[16] Kenisarin MM. High-temperature phase change materials for thermal energy storage. Renewable Sustainable Energy Rev 2010;14:955–70.
[17] Sharma SD, Sagara K. Latent heat storage materials and systems: a review. Int J Green Energy 2005;2:1–56.
[18] Zalba B, Marin JM, Cabeza LF, Mehling H. Review on thermal energy storage with phase change: materials, heat transfer analysis and applications. Appl Therm Eng 2003;23:251–83.

[19] Fernandez AI, Martínez M, Segarra M, Martorell I, Cabeza LF. Selection of materials with potential in sensible thermal energy storage. Sol Energy Mater Sol Cells 2010;94:1723–9.
[20] Nallusamy N, Sampath S, Velraj R. Experimental investigation on a combined sensible and latent heat storage system integrated with constant/varying (solar) heat sources. Renewable Energy 2007;32:1206–27.
[21] Domański R, Fellah G. Thermoeconomic analysis of sensible heat, thermal energy storage systems. Appl Therm Eng 1998;18:693–704.
[22] Tamme R. Development of storage systems for SP plants; 2006.
[23] Yang M, Yang X, Yang X, Ding J. Heat transfer enhancement and performance of the molten salt receiver of a solar power tower. Appl Energy 2010;87: 2808–11.
[24] Kearney D, Herrmann U, Nava P, Kelly B, Mahoney R, Pacheco J, et al. Assessment of a molten salt heat transfer fluid in a parabolic trough solar field. J Sol Energy Eng Trans - ASME 2003;125:170–7.
[25] Kearney D, Kelly B, Herrmann U, Cable R, Pacheco J, Mahoney R, et al. Engineering aspects of a molten salt heat transfer fluid in a trough solar field. Energy 2004;29:861–70.
[26] Kearney D, Herrmann U, Nava P, Kelly B, Mahoney R, Pacheco J, et al. Evaluation of a molten salt heat transfer fluid in a parabolic trough solar field, Solar energy. Nevada, USA: Reno; 2002. 293–299.
[27] Brosseau D, Kelton JW, Ray D, Edgar M, Chisman K, Emms B. Testing of thermocline filler materials and molten-salt heat transfer fluids for thermal energy storage systems in parabolic trough power plants. J Sol Energy Eng 2005;127:109.1–8.
[28] Haselden GG. Thermochemical heat storage. State-of-the-art report: Gerhard Oelert et al., Swedish Council for Building Research, Stockholm, Sweden. Int. J. Refrig - Rev. Int. Froid 1982; vol. 5: 250–250.
[29] do Couto Aktay KS, Tamme R, Müller-Steinhagen H. Thermal conductivity of high-temperature multicomponent materials with phase change. Int J Thermophys 2008;29:678–92.
[30] Lopez J. Nouveaux matériaux graphite/sel pour le stockage d'énergie à haute température. Étude des propriétés de changement de phase. Ph D. thesis. Bordeaux I, 2007.
[31] Pitié F, Zhao CY, Cáceres G. Thermo-mechanical analysis of ceramic encapsulated phase-change-material (PCM) particles. Energy Environ Sci 2011;4: 2117–24.
[32] Maruoka N, Akiyama T. Thermal stress analysis of PCM encapsulation for heat recovery of high temperature waste heat. J Chem Eng Jpn 2003;36:794–8.
[33] Hawlader MNA, Uddin MS, Khin MM. Microencapsulated PCM thermal-energy storage system. Appl Energy 2003;74:195–202.
[34] Chen B, Wang X, Zeng R, Zhang Y, Wang X, Niu J, et al. An experimental study of convective heat transfer with microencapsulated phase change material suspension: Laminar flow in a circular tube under constant heat flux. Exp Therm Fluid Sci 2008;32:1638–46.
[35] Sari A, Alkan C, Karaipekli A. Preparation, characterization and thermal properties of PMMA/n-heptadecane microcapsules as novel solid-liquid microPCM for thermal energy storage. Appl Energy 2010;87:1529–34.
[36] Zou GL, Tan ZC, Lan XZ, Sun LX, Zhang T. Preparation and characterization of microencapsulated hexadecane used for thermal energy storage. Chin Chem Lett 2004;15:729–32.
[37] J-kyu Choi, Lee JG, Kim JH, Yang H-soo. Preparation of microcapsules containing phase change materials as heat transfer media by in-situ polymerization. J Ind Eng Chem 2001;7:358–62.
[38] Velraj R, Seeniraj RV, Hafner B, Faber C, Schwarzer K. Heat transfer enhancement in a latent heat storage system. Sol Energy 1999;65:171–80.
[39] Khodadadi JM, Hosseinizadeh SF. Nanoparticle-enhanced phase change materials (NEPCM) with great potential for improved thermal energy storage. Int Commun Heat Mass Transfer 2007;34:534–43.
[40] Ettouney HM, Alatiqi I, Al-Sahali M, Al-Hajirie K. Heat transfer enhancement in energy storage in spherical capsules filled with paraffin wax and metal beads. Energy Convers Manag 2006;47:211–28.
[41] Zeng JL, Sun LX, Xu F, Tan ZC, Zhang ZH, Zhang J, et al. Study of a PCM based energy storage system containing Ag nanoparticles. J Therm Anal Calorim 2007;87:371–5.
[42] Elgafy A, Lafdi K. Effect of carbon nanofiber additives on thermal behavior of phase change materials. Carbon 2005;43:3067–74.
[43] Mettawee EB, Assassa GM. Thermal conductivity enhancement in a latent heat storage system. Sol Energy 2007;81:839–45.
[44] Fukai J, Kanou M, Kodama Y, Miyatake O. Thermal conductivity enhancement of energy storage media using carbon fibers. Energy Convers Manag 2000;41: 1543–56.
[45] Hamada Y, Otsu W, Fukai J, Morozumi Y, Miyatake O. Anisotropic heat transfer in composites based on high-thermal conductive carbon fibers. Energy 2005; 30:221–33.
[46] Fukai J, Hamada Y, Morozumi Y, Miyatake O. Effect of carbon-fiber brushes on conductive heat transfer in phase change materials. Int J Heat Mass Transfer 2002;45:4781–92.
[47] Fukai J, Hamada Y, Morozumi Y, Miyatake O. Improvement of thermal characteristics of latent heat thermal energy storage units using carbon-fiber brushes: experiments and modeling. Int J Heat Mass Transfer 2003;46: 4513–25.
[48] Hamada Y, Ohtsu W, Fukai J. Thermal response in thermal energy storage material around heat transfer tubes: effect of additives on heat transfer rates. Sol Energy 2003;75:317–28.
[49] Wu ZG, Zhao CY. Experimental investigations of porous materials in high temperature thermal energy storage systems. Sol Energy 2001;85:1371–80.
[50] Demiray S, Becker W, Hohe J. Numerical determination of initial and subsequent yield surfaces of open-celled model foams. Int J Solids Struct 2007;44: 2093–108.
[51] Bai M, Chung JN. Analytical and numerical prediction of heat transfer and pressure drop in open-cell metal foams. Int J Therm Sci 2011;50:869–80.
[52] Shahbeyk S, Petrinic N, Vafai A. Numerical modelling of dynamically loaded metal foam-filled square columns. Int J Impact Eng 2007;34:573–86.
[53] Liu PS. Mechanical relations for porous metal foams under several typical loads of shearing, torsion and bending. Mater Sci Eng A-Struct Mater Prop Microstruct Process 2010;527:7961–6.
[54] Lee Y- S. Development of constitutive equations for plastic deformation of a porous material using numerical experiments. J Mater Process Technol 2002;130–131:161–7.
[55] Raj SV. Microstructural characterization of metal foams: an examination of the applicability of the theoretical models for modeling foams. Mater Sci Eng A-Struct Mater Prop Microstruct Process 2011;528:5289–95.
[56] Gibson LJ, Ashby MF. Cellular solids: structure and properties. 2 ed., 1. paperback ed. (with corr.) ed. Cambridge: Cambridge Univ. Press; 1999.
[57] Weaire D, Hutzler S. The physics of foams. Oxford: Oxford University Press; 2001. USA.
[58] Williams RE. Space-filling polyhedron: its relation to aggregates of soap bubbles, plant cells, and metal crystallites. Science 1968;161:276–7.
[59] Weaire D, Fhelan R. The structure of monodisperse foam. Philos Mag Lett 1994;70:345–50.
[60] Raj SV, Kerr JA. Effect of microstructural parameters on the relative densities of metal foams. Metall Mater Trans A-Phys Metall Mater Sci 2011;42: 2017–27.
[61] Thomson III WLX. On the division of space with minimum partitional area. Philos Mag Lett 2008;88:103–14.
[62] Williams DF, Toth LM, Clarno KT. Assessment of candidate molten salt coolants for the advanced high-temperature reactor (AHTR). Oak Ridge (TN): ORNL, USDOE; 2006.
[63] Matzke EB, Nestler J. Volume-shape relationships in variant foams. A further study of the role of surface forces in three-dimensional cell shape determination. Am J Bot 1946;33:130–44.
[64] Zhong Y, Li S, Wei X, Liu Z, Guo Q, Shi J, et al. Heat transfer enhancement of paraffin wax using compressed expanded natural graphite for thermal energy storage. Carbon 2010;48:300–4.
[65] Zhong Y, Guo Q, Li S, Shi J, Liu L. Heat transfer enhancement of paraffin wax using graphite foam for thermal energy storage. Sol Energy Mater Sol Cells 2010;94:1011–4.
[66] Afanasov IM, Savchenko DV, Ionov SG, Rusakov DA, Seleznev AN, Avdeev VV. Thermal conductivity and mechanical properties of expanded graphite. Inorg Mater 2009;45:486–90.
[67] Lopez J, Caceres G, Palomo Del Barrio E, Jomaa W. Confined melting in deformable porous media: a first attempt to explain the graphite/salt composites behaviour. Int J Heat Mass Transfer 2010;53:1195–207.
[68] Deshpande VS, Fleck NA. Isotropic constitutive models for metallic foams. J Mech Phys Solids 2000;48:1253–83.
[69] Zhao CY, Lu TJ, Hodson HP. Thermal radiation in ultralight metal foams with open cells. Int J Heat Mass Transfer 2004;47:2927–39.
[70] Zhao CY, Tassou SA, Lu TJ. Analytical considerations of thermal radiation in cellular metal foams with open cells. Int J Heat Mass Transfer 2008;51:929–40.
[71] Tian Y, Zhao CY. A numerical investigation of heat transfer in phase change materials (PCMs) embedded in porous metals. Energy 2011;36:5539–46.
[72] Zhao CY, Lu TJ, Hodson HP. Natural convection in metal foams with open cells. Int J Heat Mass Transfer 2005;48:2452–63.
[73] Zhao CY, Lu W, Tian Y. Heat transfer enhancement for thermal energy storage using metal foams embedded within phase change materials (PCMs). Sol Energy 2010;84:1402–12.
[74] Zhou D, Zhao CY. Experimental investigations on heat transfer in phase change materials (PCMs) embedded in porous materials. Appl Therm Eng 2011;31:970–7.
[75] Chen Z, Gu M, Peng D. Heat transfer performance analysis of a solar flat-plate collector with an integrated metal foam porous structure filled with paraffin. Appl Therm Eng 2010;30:1967–73.
[76] Zhao CY, Wu ZG. Heat transfer enhancement of high temperature thermal energy storage using metal foams and expanded graphite. Sol Energy Mater Sol Cells 2011;95:636–43.

Energy &
Environmental Science

View Online
Dynamic Article Links

Cite this: *Energy Environ. Sci.*, 2011, **4**, 2117

www.rsc.org/ees

PAPER

Thermo-mechanical analysis of ceramic encapsulated phase-change-material (PCM) particles

F. Pitié, C.Y. Zhao* and G. Cáceres

Received 15th November 2010, Accepted 12th March 2011
DOI: 10.1039/c0ee00672f

Thermal energy storage (TES) is of growing importance, and involves the storage of both sensible and latent heat. Latent heat storage is particularly attractive, since it can store the energy as the latent heat of fusion at a constant temperature, thus providing a high energy storage density. The low temperature encapsulated phase change materials (PCM) in buildings have been extensively investigated mostly in rigid cells. The present paper studied the encapsulation of salts PCM material within elastic shells. The mechanical feasibility of such a spherical shell coating of a melting material is first investigated. The influence of encapsulation on the melting process of PCMs is thereafter studied for this particular geometrical case, including the complicated interactions with melting temperature of PCMs. The stored energy and pressure variation due to the volume change during the melting process are examined. It is shown that the encapsulated PCM particles can melt without cracking the coating shell only under specific conditions.

Introduction

High temperature thermal energy storage (HTTES) has a vital role in renewable energy and waste heat recovery. Although there is a wide range of industrial applications, most HTTES usages are found in solar thermal technologies,[1,2] aerospace applications,[3] and steelmaking industry.[4] One of HTTES solutions proposed is using latent heat of phase change materials (PCM); different salts are used as PCMs, since they are cheap, available in large quantities, and have good thermal storage properties.[5] Despite these advantages, salts have low thermal conductivities, leading to slow heat charging and discharging rates with low heat energy storage efficiency.[6]

In order to increase the thermal conductivity, several heat transfer enhancement techniques have been studied,[6,7] such as mixing graphite and nitrate salts under isotropic pressure.[8–10] The graphite has naturally good thermal properties, and its mixture with nitrate salts compensates the low thermal conductivity of PCM.[11,12] This composite material has been widely studied by Lopez *et al.*,[13,14] and referred to as graphite encapsulated PCM salt. This studied composite is considered as a solid sphere of PCM nitrate salts encapsulated in a thick shell of graphite. Since the graphite shell is part of a plain material, it is modelled as an elastic material with a mobile internal wall and a non-moving external wall, leading to variations of melting temperature, enthalpy and energy function of this modelled sphere.

The current research is based on the model of the closed solid sphere developed by Lopez *et al.*,[14] and their results have been used to verify the code used in the current paper. The starting hypotheses are thereafter extended to a shell of Silicon Carbide (SiC) with a free mobile external wall:

• Encapsulating a salt bead (diameter ≈ 1mm) into a SiC shell as a HTTES material is proven to be more efficient for heat

School of Engineering, University of Warwick, Coventry, CV4 7AL, UK. E-mail: c.y.zhao@warwick.ac.uk; Tel: +44 (0)24 76522339

Broader context

Thermal energy storage (TES) is of growing importance, and involves the storage of both sensible and latent heat. Latent heat storage is particularly attractive, since it can store the energy as the latent heat of fusion at a constant temperature, thus providing a high energy storage density. The present paper studied the encapsulation of high-temperature salt PCM material within elastic shells. The mechanical feasibility of such a spherical shell coating of a melting material is first investigated. The influence of encapsulation on the melting process of PCMs is thereafter studied for this particular geometrical case, including the complicated interactions with melting temperature of PCMs. The stored energy and pressure variation due to the volume change during the melting process are examined. It is shown that the encapsulated PCM particles can melt without cracking the coating shell only under specific conditions.

transfer by increasing the surface area of heat exchange.[15,16] Because the SiC shell is a free surface, no strain and displacement are imposed on the external wall for initial conditions.

• SiC is already used in nuclear energy processes as a coating material: it protects fissionable fuel material from the chemical corrosive and mechanical erosive environment.[17] The better mechanical strength, extreme chemical resistance, and high thermal conductivity of SiC compared to graphite[18] could offer major advantages when coating PCM pellets with SiC.

The mechanical stress analysis of a shell under inner pressure due to the volume expansion of a coated material has already been studied, and the work of *e.g.* Maruoka and Akiyama[19] assesses the thermal-stress while the coating material is strained by the volumetric expansion of the melting PCM. In the research of Maruoka *et al.*, the PCM is a pellet of lead or copper encapsulated by a nickel coating shell. The experiments and modelling evaluate the required conditions to avoid the cracking of the shell under the inner pressure, without considering the heat storage efficiency of the PCM. The coating material has an elastoplastic behaviour while the SiC shell of the present study has a pure elastic behaviour.

Upadhyaya *et al.*[20] developed a stress analysis of an eggshell strained by the volumetric expansion of its content, whereby the thermo-elastic behaviour of the coating is modelled by applying a thin shell theory. Upadhyaya *et al.* showed that it is possible to use Hooke's laws to make a simple model of the full-filled shell stress–strain behaviour. The difference of the current paper with that of Upadhyaya *et al.* is that the eggshell does not coat a PCM. This study is used as a first step to model the SiC shell fully filled with a melting PCM.

The thermo-mechanical behaviour of encapsulated PCMs has not yet been fully studied for HTTES purposes. Encapsulation of free PCM particles may be a solution to increase the low thermal conductivity and protect the salt, with a coating film of silicon carbide (SiC) being a possible example.[17] The high thermal resistance of such a material would protect the PCM of aggressive external conditions, although the coating is subjected to volumetric expansion. The aim of this work is to investigate the thermo-mechanical conditions for an elastic material shell as coating of PCM without cracking. This attempt studies the thermo-dependent mechanical model of a PCM sphere with a SiC coating in a free surface shell rather than with fixed walls.

Objectives

The main objective is to provide a thermo-mechanical model to describe the behaviour of a free spherical PCM coated by SiC.

Previous work of Lopez *et al.*[14] presents a model of confined melting in composite materials made of graphite and a PCM. The present paper extends it to PCM coated by SiC. This modelling defines respectively (i) stress and expansion of the coating shell, and (ii) inner pressure, melting temperature, enthalpy, entropy, and total energy of the coated particle. The final target is to design and proportion a SiC encapsulation of PCM by using the modelled strengths.

Expansion and stress of the coating shell

The geometry of the problem and the analysis of the stress–strain behaviour of the shell are developed for three different cases. The first spherical shell with a fixed external wall as presented in the work of Lopez *et al.*[14] is used as a reference to validate our code. Then a thermo-mechanical stress analysis with the thin shell theory is used to express the inner pressure function of volumetric expansion.[20] The Lame's equations, extended to a thick spherical shell,[21] are then used to develop a more accurate model. Finally, the maximum pressure supported by a thick shell is calculated with the von Mises yield criterion (or octahedral shear stress criterion).[22]

Geometry and initial hypotheses

The geometry of a coated particles is shown in Fig. 1. The study develops the model of a salt spherical particle coated in a graphite shell with a non-moving external wall ($R(t)/\mathrm{d}t = 0$) to validate the code, thanks to the results of Lopez *et al.*[14] The current work thereafter uses a silicon carbide (SiC) free surface shell instead of the graphite fixed wall.

The present paper uses the hypotheses of Lopez *et al.*[14] to validate the code, thanks to the study of the non-moving external wall of the graphite coating shell. The main hypotheses applied in the model of Lopez concerning the *liquid phase of the salt* are:

(a) The density ρ_l, specific heat c_{pl} and thermal conductivity λ_l are constant, independent of pressure and temperature.

(b) The liquid pressure within the shell is uniform.

(c) As a result of the salt viscosity in its liquid state ($\sim 6 \times 10^{-3}$ kg m^{-1} s^{-1}) and shell size ($\sim$mm), convective heat transfer will be negligible.

(d) The viscous energy dissipation is also neglected.

For the *salt in the solid state* it is assumed that:

(e) It can be considered as homogeneous, with constant values of density ρ_s, specific heat c_{ps}, and thermal conductivity λ_s.

(f) It is non-deformable.

The *shell wall* (graphite or silicon carbide) is considered to be:

(g) homogeneous, isotropic and exhibiting a linear elastic behaviour;

(h) at known and uniform temperature.

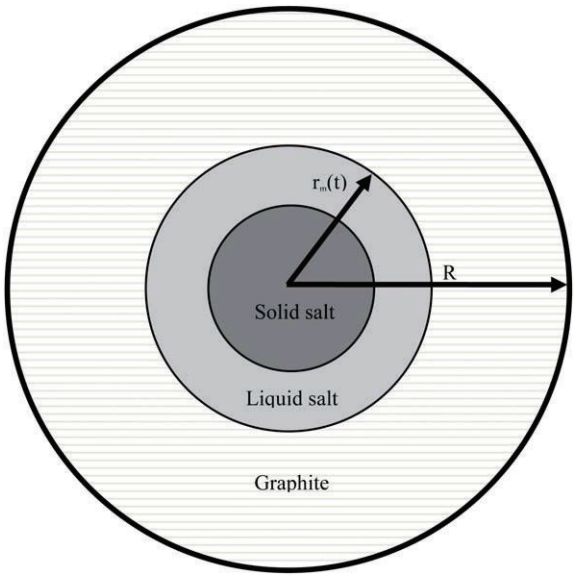

Fig. 1 Salt particles coated in a graphite matrix.[14]

At the *interfaces*, the following conditions are proposed:

(i) an equality of phase temperature and heat flux continuity at the melting front;

(j) an equality of temperature and pressure at the graphite/salt interface.

Spherical symmetry coming from hypotheses (b) and (h) allows reducing the original three-dimensional problem of transfer to a one-dimensional one.[14]

In the present work, the new hypothesis of a SiC shell with an external free surface does not modify any other hypotheses.

Volume expansion of the PCM bead

In the different following cases, the volume expansion of the PCM at a time t is:

$$\Delta V = V_{s0}\left(\frac{\rho_s - \rho_l}{\rho_l}\right)f^* \quad (1)$$

where f^* is, at a time t, the fraction of the initial volume of salt V_{s0} which has been molten (molten salt fraction in the following), and ρ_i ($i = [s,l]$) represents the phase density.[14]

Expression of pressure as a function of volume expansion

Shell with a non-moving external wall. In this first case, a spherical closed shell is delimited by an elastic wall which satisfies Hooke's law.[23] The external wall (initial radius R) is supposed to be fixed; the internal wall (initial radius r_{m0}) is under a uniform increasing pressure due to the volume expansion of the melting salt (ΔV). From the hypotheses that the wall is homogeneous, isotropic and showing a linear elastic behaviour and that the liquid pressure within the shell is uniform, the inner pressure is:

$$P = P_0 - K\frac{V_m - V_{m0}}{V_{m0}} \quad (2)$$

where P_0 represents the initial shell pressure (atmospheric), K is the bulk modulus of the shell wall, V_{m0} is the initial volume of the wall (before its deformation) and V_m is the wall volume at shell pressure P.[14]

$$\Delta V = -(V_m - V_{m0}) \quad (3)$$

Introducing this expression in eqn (1) yields:

$$P(t) = P_0 + K\left(\frac{\rho_s - \rho_l}{\rho_l}\right)\left(\frac{V_{s0}}{V_{m0}}\right)f^*(t) \quad (4)$$

This equation allows calculating the pressure in the closed graphite non-moving wall shell as a function of the fraction of molten salt in the model.[14] The current work uses this formula as a basis to validate the used code. Once the code is validated for a non-moving external wall, the next step is to extend it to a moving wall.

Shell with a thin wall. The second case is a free surface thin shell. The external wall is no longer fixed, R can increase. The thin shell theory is used to validate the change in the code between moving and non-moving wall. The thin shell theory is a classical approximation in mechanical studies when the shell thickness is a maximum 10% of the inner radius.[20]

According to the thin shell model,[20] the relation between the pressure and volume variation is:

$$\Delta V = 3V_{s0}\left(\alpha\Delta T + P\left(\frac{1-\nu}{2E}\right)\left(\frac{r_{m0}}{R - r_{m0}}\right)\right) \quad (5)$$

with the value of ΔV from eqn (1) it becomes:

$$P(t) = \frac{2}{3}\left(\frac{E}{1-\nu}\right)\left(\frac{R - r_{m0}}{r_{m0}}\right)\left(\frac{\rho_s - \rho_l}{\rho_l}f^*(t) - 3\alpha\Delta T\right) \quad (6)$$

where E, ν, α, and ΔT are, respectively, the Young's modulus, the Poisson's ratio, the coefficient of linear expansion, and the change of temperature of the shell material, R and r_{m0} are, respectively, the external and the internal radius of the shell. This equivalence is true under the condition of thin shells, *i.e.* $r_{m0} \gg R - r_{m0}$.

This equation allows calculating the pressure in the closed SiC free surface shell as a function of the fraction of molten salt in the model. The current work uses this formula to validate its code for a free surface SiC shell. Once the code is validated for a thin shell, the next step is to extend it to a thick shell to increase the accuracy of the model.

Shell with a thick wall. In the case of a thick shell, the Lamé's equations are solved without ignoring the radial component of the stress. The approximation of the mechanical model of the current work is more accurate.

In a spherical coordinates system r,θ,ϕ the studied volume has a spherical symmetry, and it includes a homogenous and isotropic material; the boundary conditions have also a spherical symmetry. In this case, the displacement, strain, and stress fields are:

$$u = u_r = f(r),\ u_\theta = u_\phi = 0 \quad (7)$$

$$\varepsilon_{rr} = g_1(r),\ \varepsilon_{\theta\theta} = \varepsilon_{\phi\phi} = g_2(r),\ \varepsilon_{r\theta} = \varepsilon_{r\phi} = \varepsilon_{\phi\theta} = 0 \quad (8)$$

$$\sigma_{rr} = h_1(r),\ \sigma_{\theta\theta} = \sigma_{\phi\phi} = h_2(r), \text{ and } \sigma_{r\theta} = \sigma_{r\phi} = \sigma_{\phi\theta} = 0 \quad (9)$$

The strain–displacement relations are:

$$\varepsilon_{rr} = u',\quad \varepsilon_{\theta\theta} = \frac{u}{r} \quad (10)$$

where ($'$) denotes differentiation with respect to r.[21] The stress–strain relations are:

$$\sigma_{rr} = \lambda(\varepsilon_{rr} + 2\varepsilon_{\theta\theta}) + 2\mu\varepsilon_{rr} - (3\lambda + 2\mu)\alpha\Delta T,\ \sigma_{\theta\theta} = \lambda(\varepsilon_{rr} + 2\varepsilon_{\theta\theta}) + 2\mu\varepsilon_{\theta\theta} - (3\lambda + 2\mu)\alpha\Delta T \quad (11)$$

where λ and μ are Lamé constants related to the modulus of elasticity E and Poisson's ratio ν as[21]

$$\lambda = \frac{E\nu}{(1+\nu)(1-2\nu)},\ \mu = \frac{E}{2(1-\nu)} \quad (12)$$

The equilibrium equation in the radial direction, disregarding the body force and the inertia term is

$$\sigma_{rr} + \frac{2}{r}(\sigma_{rr} - \sigma_{\theta\theta}) = 0 \quad (13)$$

The boundary conditions are:

$$\sigma_{rr}(r = r_{m0}) = -P, \text{ and } \sigma_{rr}(r = R) = 0 \quad (14)$$

Solving the eqn (7)–(12), and with the boundary conditions (14), yields the elastic description of the system as:

$$u(r) = r\Delta T\alpha + \frac{r_{m0}^3}{R^3 - r_{m0}^3}\left(\frac{R^3}{4r^2\mu} + \frac{r}{3\lambda + 2\mu}\right)P \quad (15)$$

$$\varepsilon_{rr}(r) = \Delta T\alpha + \frac{r_{m0}^3}{R^3 - r_{m0}^3}\left(-\frac{R^3}{2r^3\mu} + \frac{1}{3\lambda + 2\mu}\right)P \quad (16)$$

$$\varepsilon_{\theta\theta}(r) = \Delta T\alpha + \frac{r_{m0}^3}{R^3 - r_{m0}^3}\left(\frac{R^3}{4r^3\mu} + \frac{1}{3\lambda + 2\mu}\right)P \quad (17)$$

$$\sigma_{rr}(r) = -\frac{r_{m0}^3}{R^3 - r_{m0}^3}\left(\frac{R^3}{r^3} - 1\right)P \quad (18)$$

$$\sigma_{\theta\theta}(r) = \frac{r_{m0}^3}{R - r_{m0}^3}\left(\frac{R^3}{2r^3} + 1\right)P \quad (19)$$

For $r = r_{m0}$, the volume displacement is written:

$$\Delta V = \frac{4}{3}\pi\left[\left(u(r_{m0}) + r_{m0}\right)^3 - r_{m0}^3\right] \quad (20)$$

re-arranged using eqn (1):

$$u(r = r_{m0}) = r_{m0}\left(\sqrt[3]{\frac{\rho_s - \rho_l}{\rho_l}f^*(t) + 1} - 1\right) \quad (21)$$

which combined with eqn (15) gives:

$$P(t) = \frac{2\left(R^3 - r_{m0}^3\right)E\left(\sqrt[3]{\frac{\rho_s - \rho_l}{\rho_l}f^*(t) + 1} - (1 + \alpha\Delta T)\right)}{r_{m0}^3(1 + \nu) + R^3(2 - 4\nu)} \quad (22)$$

This equation allows calculating the pressure in the closed SiC free surface shell as a function of the fraction of molten salt in the model. Once the code is validated for a thick shell, the next step is to estimate the critical pressure that will make the shell crack.

Equivalent critical pressure. Under a maximum stress, the shell will crack and loose the encapsulated PCM.[19] According to the Von Mises criterion, the yield condition of pressure, named equivalent pressure P_e, in the shell is:

$$P_e = \frac{2}{3}\left(1 - \frac{r_{m0}^2}{R^3}\right)\sigma y \quad (23)$$

where σ_y is the yield strength of the coating material.[23] The Von Mises' criterion describes the stress equivalent to the elastic limit of the material. According to the fact that ceramics are non-plastic materials, the tensile strength is taken as yield strength.

Knowing this criteria, the hypothesis is that the maximum tensile strength is reached at the maximum volumetric expansion *i.e.* when all the PCM is molten ($f^*(t) = 1$) For fixed PCM material properties and volume, and fixed coating material properties, the external radius, chosen as a variable, can be optimised to reduce the shell stress to the minimum value possible. Then, solving the equation $P(R) = P_e(R)$, for any values of t, gives:

$$R_{min\,0} = \sqrt[3]{\frac{4\nu - 2}{3\frac{E}{\sigma_y}\left(1 + \Delta T\alpha - \sqrt[3]{\frac{\rho_{s0}}{\rho_{l0}}}\right) + (1 + \nu)}}\, r_{m0} \quad (24)$$

R_{min0} is the minimum value of the external radius of the shell under the maximum acceptable pressure P_0 that prevents the shell from cracking. The condition for the existence of the shell is then $\frac{R_{min\,0}}{r_{m\,0}} > 1$ which, according to (24), can be simplified as:

$$\sqrt[3]{\frac{\rho_{s\,0}}{\rho_{l0}}} < 1 + \Delta T\alpha + (1 - 5\nu)\frac{\sigma_y}{3E} \quad (25)$$

This final criterion expresses the fact that the spherical shell will not crack under the condition that the change of densities of the melting PCM, written $\sqrt[3]{\frac{\rho_{s\,0}}{\rho_{l0}}}$, is less than the combination of the thermo-mechanical properties of the shell material.

In the current paper, the mechanical stress analysis of the spherical shell proceeds according to three steps: (i) the study from the work of Lopez *et al.*[14] gives the relation between volume expansion and inner pressure of a graphite shell with a non-moving external wall. The current work takes this expression as a basis to start the discussion about a free surface particle. (ii) The relation between volume expansion and inner pressure of a SiC shell with a moving external wall is calculated using the theory of thin shells. This relation is used to estimate the mechanical behaviour of the shell. (iii) A more accurate description is given by the thick shell model. The maximum pressure that the shell can support before cracking is estimated using the von Mises criterion. This estimation is used to calculate the minimum external radius possible. The condition of existence of this external radius is used to set a thermo-mechanical criterion for SiC coating of PCM.

The new description of pressure as a function of the fraction of molten salt in a SiC shell is used to compare the thermal behaviour of PCM in two case: one with a graphite non-moving external wall shell and other with a SiC thick shell.

Full description of PCM in a closed shell at thermodynamical equilibrium

Equations governing salt melting of a solid sphere (Fig. 1) are established in the research of Lopez:[14] the external shell radius is noted as R and is assumed to be constant during melting. This hypothesis is due to the geometry chosen of a graphite matrix. In the current paper with a selected free surface SiC shell, R is not constant. Both cases are reproduced in the following demonstration. The position of the shell/salt interface and the melting front at time t are referred to as $r_m(t)$ and $r_f(t)$ respectively.[14]

The different variables of a first order solid ↔ liquid transformation were demonstrated,[14] and the approach deals with simple univariant equilibrium because no component changes occur during the transformation. In that case, both phases exist along a single curve in the temperature–pressure domain (T,P).[14]

The system of PCM encapsulated in a closed shell is fully described by the following equations:[14]

The conservation of energy is written:

$$\frac{\partial\left[\left(\rho c_p\right)_{eq}T(r,T)\right]}{\partial t} = \frac{1}{r^2}\frac{\partial}{\partial r}\left(\lambda_{eq}r^2\frac{\partial T(r,t)}{\partial r}\right) - \rho_s\Delta h_m\frac{df_s(r,t)}{dt} \quad (26)$$

where $(0 < r < r_m(t))$, $(\rho c_p)_{eq}$ and λ_{eq} are, respectively, the equivalent heat capacity and the equivalent thermal conductivity. They are given by:

$$(\rho c_p)_{eq} = \rho_l c_{pl}(1 - f_s) + \rho_s c_{ps} f_s,\ \lambda_{eq} = \lambda_l(1 - f_s) + \lambda_s f_s \quad (27)$$

Boundary conditions of the problem are:

$$\forall t, \begin{cases} T(r,t) = T_m(t) r = r_m(t) \\ -\lambda_{eq} \left.\dfrac{\partial T(r,t)}{\partial r}\right|_{r=0} = 0, r = 0 \end{cases} \quad (28)$$

where $T_m(t)$ is the temperature of the shell wall (assumed to be known and uniform).

With the solid fraction $f_s(r,t)$:

$$f_s(r,t) = 0.5\left[\tanh\left(\frac{T_m(P) - T(r,t)}{\Delta T}\right) + 1\right] \quad (29)$$

where ΔT defines the interval where the curve is smoothed. The global variables are:

$$f^*(t) = 1 - \frac{3}{r_{m0}^3}\int_0^{r_m(t)} r^2 f_s(r,t)\,dr \quad (30)$$

$$\begin{aligned} P(t) &= P_0 + K\left(\frac{\rho_s - \rho_l}{\rho_l}\right)\left(\frac{V_{s0}}{V_{m0}}\right) f^*(t),\ P(t) \\ &= \frac{2(R^3 - r_{m0}^3)E}{r_{m0}^3(1+\nu) + R^3(2-4\nu)}\left(\sqrt[3]{\frac{\rho_s - \rho_l}{\rho_l} f^*(t) + 1} \right. \\ &\quad \left. - (1 + \alpha\Delta T)\right) \end{aligned} \quad (31)$$

The two different expressions of the pressure stem from the different cases studied earlier. The first one describes the pressure in a non-moving external wall shell, and the second expression gives the pressure in a free surface shell.

The displacement of the internal wall is:

$$\Delta r_m(t) = r_{s0}\left[\sqrt[3]{\frac{\rho_l - \rho_s}{\rho_s} f^*(t) + 1} - 1\right] \quad (32)$$

$\Delta r_m(t) = r_m(t) - r_{m0}$ represents the displacement of the interface graphite/salt with respect to its initial position $r_{m0} = r_{s0} = r_m(t = 0)$.

The melting temperature function of the pressure equation is

$$T_m(P) = T_0 + \frac{-b + \sqrt{b^2 - 4ac}}{2a} \text{ with}$$

$$\begin{cases} a = -\dfrac{1}{2}\left(\dfrac{c_{pl0} - c_{ps0}}{T_0}\right), \\ b = -(s_{l0} - s_{s0}) + \left(\dfrac{\alpha_{l0}}{\rho_{l0}} - \dfrac{\alpha_{so}}{\rho_{so}}\right)(P - P_0), \\ c = \left(\dfrac{1}{\rho_{l0}} - \dfrac{1}{\rho_{s0}}\right)(P - P_0) - \dfrac{1}{2}\left(\dfrac{\beta_{l0}}{\beta_{l0}} - \dfrac{\beta_{so}}{\rho_{so}}\right)(P - P_0)^2, \end{cases} \quad (33)$$

Values of parameters s_{l0}, s_{s0}, ρ_{l0}, ρ_{s0}, c_{pl0}, c_{ps0}, α_{l0}, α_{s0}, β_{l0}, and β_{so} are usually available in standard thermodynamic databases.

The enthalpy and entropy function of the pressure at thermodynamic equilibrium are:

$$\Delta h_m(T_m,P) = -\Delta s_m(T_m,P)T \quad (34)$$

with:

$$\Delta s_m = (s_{l0} - s_{s0}) + \left(\frac{c_{pl0} - c_{ps0}}{T_0}\right)(T_m - T_0) - \left(\frac{\alpha_{l0}}{\rho_{l0}} - \frac{\alpha_{s0}}{\rho_{l0}}\right)(P - P_0) \quad (35)$$

The equation of density, admitting that values of state of reference are T_0 and P_0, is:

$$\frac{1}{\rho_i} = \frac{1}{\rho_{i0}}[1 + \alpha_i(T - T_0) - \beta_i(P - P_0)] \quad (36)$$

Fig. 2 shows the relative evolution of the density of molten salt as a function of the fraction of molten salt: $\frac{\rho_i - \rho_{i0}}{\rho_{i0}}$

As shown later (Fig. 3), and due to the higher mechanical strength of SiC, the inner pressure is 6.3 times higher than in a graphite shell. The density of the liquid phase ρ_l is then increased and is no longer considered as a constant as shown in Fig. 2. This graph shows that the variation of density can be ignored at low pressures but not at high pressures.

The full energy stored during the fusion in the shell is given by:[14]

$$\begin{aligned} E(f^*) &= \int_0^{f^*} V_{s0}\frac{\rho_s - \rho_l}{\rho_l} P d\xi + \int_0^{f^*} \rho_s V_{s0}\Delta h_f\, d\xi \\ &\quad + \int_{T(f=0)}^{T(f^*)} V_{s0}(\rho_l Cp_l f + \rho_s Cp_s(1-f))d\xi \end{aligned} \quad (37)$$

The first term represents the energy used for shell deformation, the second term represents the energy required for melting a volume fraction f^* of salt, and the third term is the sensible heat accumulation. This expression intends to describe the ratio of each type of energy in the global system of the PCM closed shell.

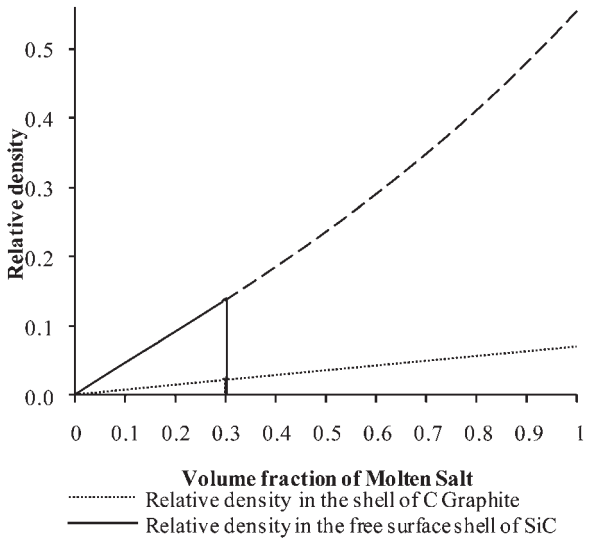

Fig. 2 Relative density function of fraction of molten salt.

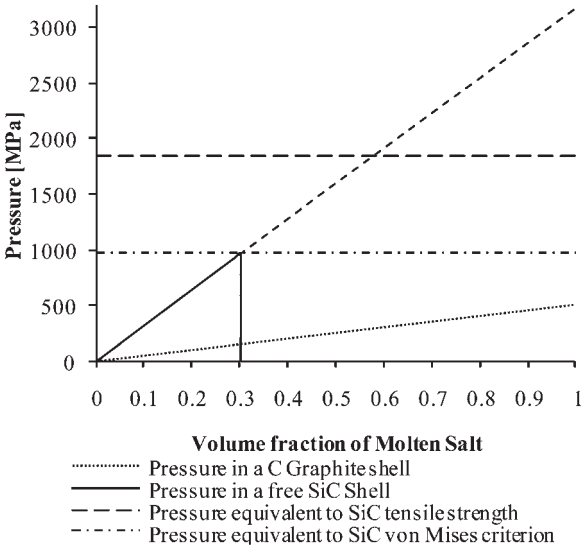

Fig. 3 Inner pressure of the shell as a function of fraction of molten salt.

The mechanical, thermal and thermodynamical behaviour of the PCM coated in a graphite wall or a SiC shell is fully given by the equations listed before. The two behaviours are now analysed and compared.

Results and discussion

In a first attempt to validate the understanding of the Lopez model,[14] the thermodynamical properties at $P_0 = 10^5$ Pa of the $KNO_3/NaNO_3$ salt are listed in the Table 1.

The following study will focus on two sets of geometrical and mechanical values of the shell:

- $K_m = 8 \times 10^9$ Pa representing the graphite matrix properties.
- $E_{SiC} = 476 \times 10^9$ Pa, $\nu_{SiC} = 0.19$, and $\alpha_{SiC} = 3.8\ 10^{-6}\ K^{-1}$ representing the SiC shell properties.
- $R = 1.1$ mm and $r_m = 1$ mm.

An analytical computation provides a first estimation of the results. The calculation of the inner pressures is illustrated in Fig. 3. The inner pressure of the graphite non-moving wall is traced according to the data of the original work of Lopez,[14] and used as a reference to validate the code. The pressures' equivalent respectively to the tensile strength and the von Mises criterion strength of SiC are traced as to compare the evolution of the inner pressure in the SiC shell to the limits of the material.

The pressures are important in both cases. The value of pressure in the graphite is the same as the value presented in the original results. The SiC shell pressure is 6.3 times higher than the pressure in graphite while the ratio of the bulk modulus exceeds 32. The shell shape reduces the inner pressure compared to the non-moving external wall. Once a third of the salt is molten, the shell is strained up to its maximum octahedral shear stress criterion equivalent or von Mises criterion. Later in the paper, the proportion of molten salt that sets the inner pressure equivalent to von Mises criterion stress is referred to as the cracking limit. The SiC shell presents a maximum pressure when the cracking limit indicates an impossibility to encapsulate a PCM with a SiC coating, and it becomes impossible to consider the PCM trapped in a closed shell anymore.

The following figures are still considering up to 100% of molten salt to compare the SiC case to the graphite one.

While considering the melting temperature (Fig. 4), the theoretical model in the graphite cell is not in conformity with the original model.[14] The melting temperature found here is lower than in the original work. This phenomenon results from the difference between the original values of the thermal properties of the salt and the values used in the present work. Despite the difference, the increase of melting temperature of the PCM bead coated in a graphite wall is visible. The coated PCM does no longer melt at constant temperature. For achieving a complete melting in the graphite cell, the salt should be heated up to 567 K, while the maximum temperature before the SiC shell cracks is 651 K.

The problem of the high temperature needed for a free SiC shell appears. Considering the fact that only a third of the PCM can melt before the shell cracks, the maximum temperature reached by the salt is still below the maximum acceptable temperature for the material.

In Fig. 5, the data of latent heat in a graphite shell do not match the original model.[14] Despite that this graph shows the impact of too high a pressure on the latent heat. As the melting

Table 1 Properties of salt[14]

	Properties	Symbol	Value	Unit
Salt in liquid state	Density	ρ_{l0}	2096	kg m^{-3}
	Specific heat	c_{pl}	1500	J kg^{-1} K^{-1}
	Compressibility	β_l	1.86×10^{-10}	Pa^{-1}
	Thermal expansion	α_l	3.7×10^{-4}	K^{-1}
	Thermal conductivity	λ_l	0.8	W m^{-1}
Salt in solid state	Density	ρ_{s0}	2192	kg m^{-3}
	Specific heat	c_{ps}	1430	J kg^{-1} K^{-1}
	Compressibility	β_s	0	Pa^{-1}
	Thermal expansion	α_s	0	K^{-1}
	Thermal conductivity	λ_s	1	W m^{-1}
S ↔ L	Melting temperature at P_0	T_{f0}	223	°C
	Melting enthalpy at (T_{f0},P_0)	Δh_{f0}	105	kJ kg^{-1}

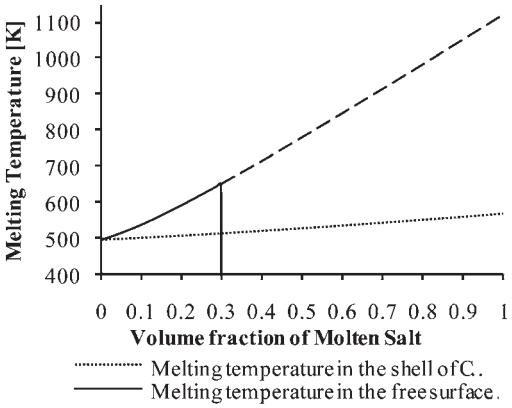

Fig. 4 Melting temperature of the PCM as a function of fraction of molten salt.

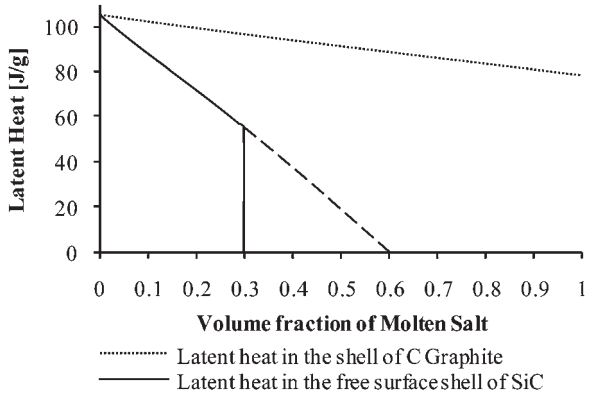

Fig. 5 Latent heat of the PCM bead as a function of fraction of molten salt.

temperature and inner pressure rise, the latent heat decreases. For the SiC shell, until a third of the shell melts, the latent heat decreases by almost 50%. The effect of a loss of latent heat storage energy is observed, and the high pressures impact it significantly. Once 60% of the salt is molten, the pressure is higher than what PCM is allowing, and it is not capable of melting anymore, which explains the nil latent heat.

Fig. 6 and 7, respectively, illustrate the energy stored within the graphite and SiC shells. In both types of shell, the mechanical energy is negligible compared to the total energy. Sensible energy and latent energy represent an average identical share of the total of the energy needed to melt a PCM bead coated in a graphite shell. According to Lopez,[14] the energy required to melt the bead of PCM coated graphite is higher than an equivalent volume of PCM at constant temperature. In the SiC shell coating, the high pressure renders the capacities of latent heat energy storage of the less efficient, and the sensible energy PCM is more important than the latent one.

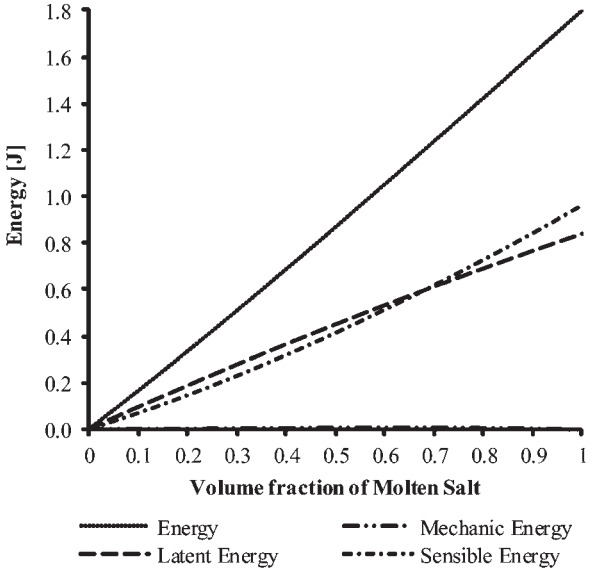

Fig. 6 Energy of the PCM bead coated in a graphite shell as a function of fraction of molten salt.

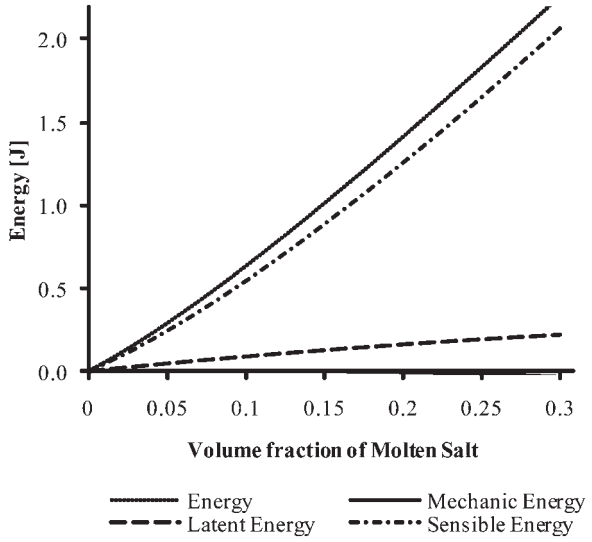

Fig. 7 Energy of the PCM bead coated in a SiC shell as a function of fraction of molten salt.

The pressure that the SiC shell imposes on the PCM is 6.3 times higher than the pressure in a graphite shell. This higher pressure involves an increasing melting temperature, a decreasing latent heat, and a reduction of the energy stored by the PCM bead.

Conclusions

The mechanical model of a PCM coated in a spherical shell was calculated in three cases. A non-moving external wall graphite shell refers to the work of Lopez *et al.*[14] which is taken as a reference to this work. A thin SiC free surface shell is used to estimate the inner pressure of the shell under volumetric expansion of PCM. The thick shell model of a shell coating melting PCM is finally used to estimate with the von Mises criterion to define the conditions when the shell cracks under the inner pressure. The computed inner pressure is higher than the limit of the SiC material, which tends to show that this kind of encapsulation for such a material is not possible with this particular PCM.

In a second part of the paper, the thermal dependent mechanical behaviour of a high temperature melting PCM is studied. The original work is fully adapted to the new hypotheses. Despite the fact that the energy traced in the first diagram does not match with the original model, the model seems to be viable. This mismatch is the result of the fact that the data used in the article have been estimated from the thermal properties of separate elements of the PCM. The expression of the energy of the system is proven to be adapted to a free surface coated particle. The study in high pressure conditions shows that the density of the PCM cannot be considered as a constant with the new hypotheses. The total energy needed to melt the whole bead of PCM increases with the inner pressure due to the coating material. The proportion of latent heat energy decreases with the high pressure.

The research indicates that the interest of coating a PCM with a SiC shell is strongly determined by the PCM properties, namely the PCM should have a high latent heat but a low volumetric

expansion, thus leading to a less pressure increase during the melting process.

Nomenclature

c_{pi}	specific heat, J kg^{-1} K^{-1}
E	energy, J
f	fraction
h	enthalpy, kJ kg^{-1}
K	bulk modulus, Pa
P	pressure, Pa
R, r	radius, m
s_i	entropy, J kg^{-1} K^{-1}
T	temperature, K
u	displacement
V	volume, m^3
α	coefficient of linear expansion, K^{-1}
β_i	isothermal compressibility
ε	strain
E	Young's modulus, Pa
λ, μ	Lamé's constant
λ_I	thermal conductivity, W m^{-1} K^{-1}
ν	poisson ratio
ρ_i	density of phase, kg m^{-3}
θ, ϕ	angulus, *rad*
σ	stress, Pa

Acknowledgements

This work is supported by the UK Engineering and Physical Science Research Council (EPSRC grant number: EP/F061439/1), National Natural Science Foundation of China (grant no: 51071184).

References

1 A. Gil, I. Martorell, A. Lazaro, P. Dolado, B. Zalba, L. F. Cabeza and M. Medrano, *Renewable Sustainable Energy Rev.*, 2010, **14**, 31–55.
2 R. Tamme, T. Bauer, J. Buschle, D. Laing, H. Müller-Steinhagen and W. Steinmann, 2008, **32**, 264–271.
3 L. Chow, *Int. Commun. Heat Mass Transfer*, 1996, **23**, 91–100.
4 N. Maruoka, K. Sato, J. Yagi and T. Akiyama, *ISIJ Int.*, 2002, **42**, 215–219.
5 A. F. Regin, S. Solanki and J. Saini, *Renewable Sustainable Energy Rev.*, 2008, **12**, 2438–2458.
6 F. Agyenim, N. Hewitt, P. Eames and M. Smyth, *Renewable Sustainable Energy Rev.*, 2010, **14**, 615–628.
7 T. Bauer, R. Tamme, M. Christ and O. Öttinger, Tenth International Conference on Thermal Energy Storage, Ecostock 2006, 31 May to 2 June 2006, Pomona, NJ, USA.
8 S. Pincemin, X. Py, R. Olives, M. Christ and O. Oettinger, *J. Sol. Energy Eng.*, 2008, **130**, 011005.
9 S. Pincemin, R. Olives, X. Py and M. Christ, *Sol. Energy Mater. Sol. Cells*, 2008, **92**, 603–613.
10 V. Morisson, M. Rady, E. Palomo and E. Arquis, *Chem. Eng. Process.*, 2008, **47**, 499–507.
11 K. do Couto Aktay, R. Tamme and H. Müller-Steinhagen, *Int. J. Thermophys.*, 2007, **29**, 678–692.
12 I. M. Afanasov, D. V. Savchenko, S. G. Ionov, D. A. Rusakov, A. N. Seleznev and V. V. Avdeev, *Inorg. Mater.*, 2009, **45**, 486–490.
13 J. Lopez, J. Dumas and E. Palomo del Barrio, *C. R. Mec.*, 2008, **336**, 578–585.
14 J. Lopez, G. Caceres, E. Palomo Del Barrio and W. Jomaa, *Int. J. Heat Mass Transfer*, 2010, **53**, 1195–1207.
15 A. Bounaceur, A. D. Ryck, J. Bezian and M. El Hafi, in *11e Congrès de la SFGP: SFGP2007*, SFGP., Saint-Etienne, 2007, vol. 96.
16 J. Bezian, A. Bounaceur, A. De Ryck, and M. El Hafi, *Proceedings IJTH*, 2007, Albi France, 346–350.
17 Z. Alkan, K. Kugeler, R. Kaulbarsch and C. Manter, *Prog. Nucl. Energy*, 2001, **38**, 411–414.
18 Q. Zhu, X. Qiu and C. Ma, *Carbon*, 1999, **37**, 1475–1484.
19 N. Maruoka and T. Akiyama, *J. Chem. Eng. Jpn.*, 2003, **36**, 794–798.
20 S. Upadhyaya, J. R. Cooke and R. H. Rand, *J. Agric. Eng. Res.*, 1985, **32**, 95–109.
21 M. Eslami, M. Babaei and R. Poultangari, *Int. J. Pressure Vessels Piping*, 2005, **82**, 522–527.
22 A. Pellissier Tanon, *Techniques de l'ingénieur. Génie mécanique*, 1988, pp. 843–843.
23 X. Gao, *Mech. Res. Commun.*, 2003, **30**, 411–420.

Applied Energy xxx (2013) xxx–xxx

Contents lists available at SciVerse ScienceDirect

Applied Energy

journal homepage: www.elsevier.com/locate/apenergy

Circulating fluidized bed heat recovery/storage and its potential to use coated phase-change-material (PCM) particles

F. Pitié [a,b], C.Y. Zhao [c], J. Baeyens [b], J. Degrève [d], H.L. Zhang [d,*]

[a] Whittaker Engineering Ltd., Stonehaven, UK
[b] University of Warwick, School of Engineering, Coventry, UK
[c] School of Mechanical Engineering, Shanghai Jiaotong University, Shanghai 200240, China
[d] Department of Chemical Engineering, Chemical and Biochemical Process Technology and Control Section, Katholieke Universiteit Leuven, Heverlee, Belgium

HIGHLIGHTS

- Within the thermal storage systems available or investigated, PCMs are the sole latent heat stores.
- PCMs have a high potential in energy capture and storage, using a circulating fluidized bed (CFB) as transfer/storage mode.
- Thermal considerations determine the optimum size range for the applied PCM particles (<400 μm).
- The wall-to-CFB heat transfer is measured, and compared with both empirical and model predictions.

ARTICLE INFO

Article history:
Received 14 August 2012
Received in revised form 5 November 2012
Accepted 13 December 2012
Available online xxxx

Keywords:
Heat transfer
Coated phase-change material
Convection
Conduction
Radiation
Solar energy collectors

ABSTRACT

Within the thermal energy capture and/or storage systems currently available or investigated, PCMs are the sole latent heat stores. Despite their low thermal conductivity, that limits charging and discharging times, the higher energy storage capacity per unit weight in comparison with sensible heat stores, makes them increasingly attractive for high temperature applications, resulting in reduced storage volumes and required circulation rates within the heat collector. The present paper introduces these PCMs, and their potential application in high temperature energy capture and storage, using a circulating fluidized bed (CFB) as transfer/storage mode. Thermal considerations determine the optimum size range for the applied particles (<400 μm). The heat transfer from the wall of the CFB to the flowing gas–solid suspension is a major design parameter of the collector, and studied for different operating conditions as determined by the gas velocity and solids circulation flux. Measured values of the heat transfer coefficients are discussed, and compared with empirical predictions of Molodtsof–Muzyka, and Gorliz–Grace. Fair agreement is obtained only when the empirical parameters are carefully predicted. The application of a packet renewal mechanism at the wall is also investigated, with a fair prediction of the heat transfer coefficient in terms of the expected solid contact time at the wall.

1. Introduction

1.1. Phase change materials (PCMs)

Latent heat thermal energy storage and associated phase change materials (PCMs) are attractive as they provide a high energy density storage due to the phase transformation, and mostly applied by solidification/fusion, or to a lesser extent by boiling/condensing. PCMs can involve organic or inorganic materials, coated by (or embedded in) a stable and inert shell (or matrix). Various examples were recently reviewed by Fernandes et al. [1].

Relative to sensible heat energy storage systems, a PCM requires a lower weight and volume of material for a given amount of stored energy and has the capacity to store the heat at a constant or near-constant phase-transition temperature. Considering the latent heat of phase transition and the sensible heat related to the specific heat capacity (C_p) and the applied temperature difference (ΔT), it is obvious that an inorganic PCM can store the same amount of energy in 25–30% of the weight of a pure inorganic solid; whereas an organic paraffin-based PCM stores about seven times more energy per unit weight than the pure mineral or metal used to coat the paraffin. The main disadvantage with regards to PCMs is the low thermal conductivity and the phase change itself: during extraction of energy from storage, the liquid solidifies at the heat transfer surfaces and an immobile layer of solid material

* Corresponding author.
E-mail address: Zhanghl.lily@gmail.com (H.L. Zhang).

0306-2619/$ - see front matter © 2013 Elsevier Ltd. All rights reserved.
http://dx.doi.org/10.1016/j.apenergy.2012.12.048

Nomenclature

a, b	dimensionless parameters
A_{ex}	surface area of the heat exchanging wall, m
Bi	Biot number
C	solid to gas heat capacity, C_p/C_g
C_p, C_g	specific heat capacity of solid and gas respectively, J g^{-1} K^{-1}
CAF, CFB, BFB	core-annulus flow, circulating and bubbling fluidized bed, respectively
ID, OD	inner and outside diameter respectively, mm
D	riser equivalent diameter, m
d_p	average particle diameter, m
DRF, DRU	dilute riser flow, dense riser flow, respectively
f_d	time fraction of contact by the dense phase
G	solids circulation flux, kg m^{-2} s^{-1}
G_{sh}	particles horizontal exchange flux, kg m^{-2} s^{-1}
h_c	contact transfer resistance, W m^{-2} K^{-1}
h_d	heat transfer coefficient during dense phase contact, W m^{-2} K^{-1}
h_{ij}^{rad}	radiation heat transfer coefficient, W m^{-2} K^{-1}
h_g, h_{gc}	gas convective heat transfer coefficient, W m^{-2} K^{-1}
h_l	heat transfer coefficient of lean gas phase contact, W m^{-2} K^{-1}
h_m, h	average heat transfer coefficient from riser wall to the suspension, W m^{-2} K^{-1}
h_r	heat transfer coefficient by radiation, W m^{-2} K^{-1}
h_{sr}	heat transfer coefficient by radiation from the suspension to the wall, W m^{-2} K^{-1}
h_{tot}	total effective heat transfer coefficient, W m^{-2} K^{-1}
$h(\bar{\theta})$	average heat transfer coefficient as function of contact time at the wall, W m^{-2} K^{-1}
k_g, k_p	thermal conductivity of gas and particles, respectively, W m^{-1} K^{-1}
M	loading ratio
Nu, Re	Nusselt and Reynolds number respectively
r	radial position in a sphere of radius R, m
T_b, T_w	bulk temperature and wall temperature respectively, K
T_R, T_c	temperature at the outer surface or core of a sphere, respectively, K
t_g, t_p	residence time of gas and particles, respectively, s
TFBB	Turbulent Fluidized Bed at the Bottom of the CFB riser.
U, U_{TR}	superficial air velocity through the riser and transport velocity respectively, m s^{-1}
$\bar{v}_p$	average velocity of particle, m s^{-1}
δ_g	gas gap thickness, μm
ΔT	temperature difference, K
α	thermal diffusivity of the particle $[k_p/\rho_p\, C_p]$, m^2 s^{-1}
β	heating rate, K s^{-1}
ε	voidage of the riser
ε_{sus}	cross sectional average suspension voidage
φ	slip factor
$\bar{\theta}$	average contact time of the particle packets at the wall, s
ρ_g, ρ_p	gas and particle density respectively, kg m^{-3}
ρ_{sus}	suspension density, kg m^{-3}
ζ	$\zeta = \sqrt{1.82\log(\mathrm{Re}) - 1.64}$ Eq. (13)

grows as it gives up its heat of fusion. Both factors lead to slow charging and discharging rates, hence contacting techniques with a high heat transfer rate are required.

Although the development of PCM applications is increasingly reported upon in the literature, the manufacturing of PCM-particles is at its early stage and commercial small-size particles are not yet available. Fundamental studies on PCM materials towards their properties and behaviour have been presented by Pitié et al. [2], Joulin et al. [3] and Li et al. [4]. Applications of PCM cold storage systems have been investigated by Castell et al. [5], Martin et al. [6], Rady [7] and Oró et al. [8]. Building applications have been assessed by e.g. Zhou et al. [9] and Borreguero et al. [10]. Additional research investigated the use of PCM materials in tubular heat exchangers [11–13] and in specific applications, such as in a finned storage [14] or in packed bed storage [7].

The potential of using a suspension flow of PCM-particles in energy capture/storage has not previously been assessed, and is studied in the present paper, with the main focus upon the dominant heat transfer mode and upon the heat transfer coefficients obtained in such a suspension flow system.

The variation of the surface heat flux depends upon the relative importance of the convective resistance (fixed resistance) and the conductive resistance (variable resistance). A dominant convective resistance achieves a nearly uniform surface heat flux with time, whereas a conductive resistance will create a time-decreasing heat flux. In view of the relative importance of convection and conduction, it is therefore important, as a *first objective*, to consider the heat transfer mode to the PCM particles, as discussed in Section 2. To achieve the dominant convection heat transfer, the analysis will determine that systems with a high heat transfer coefficient are required. The *second objective* of the research subsequently quantifies the heat transfer coefficients obtained between the wall of a CFB riser and the circulating gas–solid suspension of particles. This heat transfer coefficient is assessed in terms of the different hydrodynamic regimes that occur in a CFB riser. The high heat transfer coefficient obtained will demonstrate that convection heat transfer dominates.

1.2. The CFB and heat transfer

The circulating fluidized bed (CFB) is increasingly used in chemical reactors and in physical gas–solid processes (e.g. drying). Recent developments propose its use in concentrated solar energy capture/storage systems or industrial waste heat recovery, to replace thermal fluids or molten salts as transfer and storage medium [15]. A circulating fluidised bed consists of various essential components, i.e. (i) a riser where generally most of the important industrial reactions or thermal processes occur, (ii) a cyclone which separates solids from air, allowing only very fine solids to be carried out of the system; (iii) a standpipe to collect solids from the cyclone and provides a solids reservoir; and (iv) a solids re-circulation valve, that feeds solids back into the riser. The riser is the key part the CFB system. A CFB system commonly uses small Geldart A-Type particles, also used in the present experiments. The typical set-up of Fig. 1, applicable in solar towers [16] and in high temperature waste heat recovery, applies a dense particle bed conveyed within a tube bundle to capture the heat at bed temperatures between e.g. 500 and 750 °C, thereafter using the stored heat in a subsequent bubbling fluidized bed steam boiler. A CFB shares many of its advantages with traditional bubbling fluidized beds (BFBs), including temperature uniformity and excellent heat transfer. The continuous carry-over of particles implies solids' collection and return equipment. In solar energy capture systems, solar heat will be captured at the outside tube wall, and subsequently transferred to the circulating solids.

Please cite this article in press as: Pitié F et al. Circulating fluidized bed heat recovery/storage and its potential to use coated phase-change-material (PCM) particles. Appl Energy (2013), http://dx.doi.org/10.1016/j.apenergy.2012.12.048

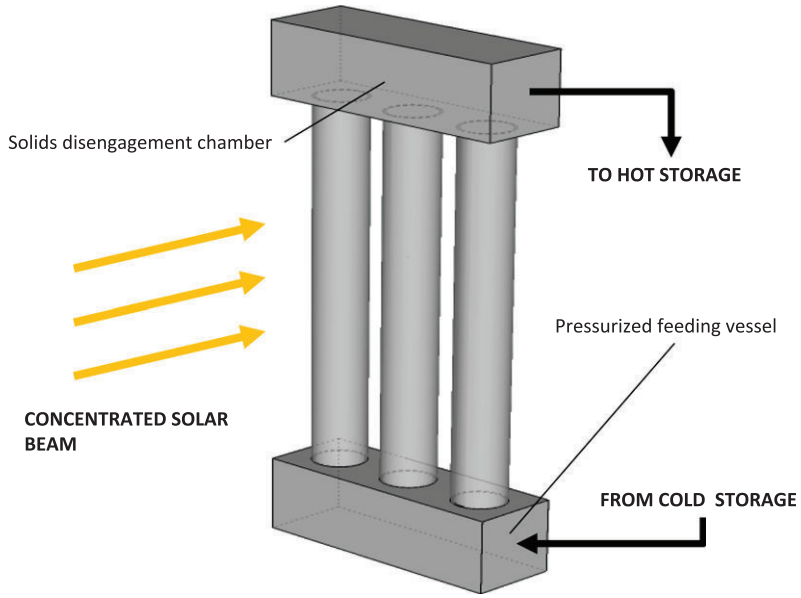

Fig. 1. Illustration of the riser solar energy capture and storage.

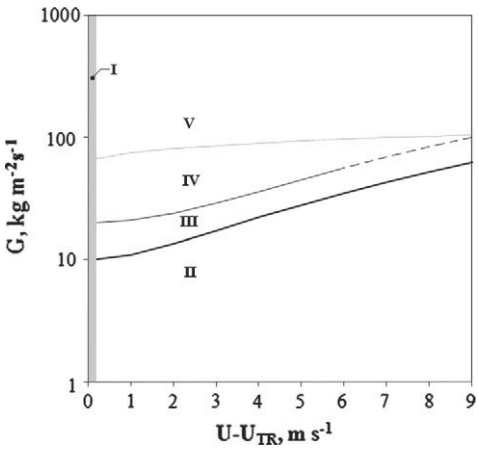

Zone I: Transition zone and/or inaccuracy in UTR prediction
Zone II: dilute riser flow (DRF)
Zone III: core-annulus flow (CAF) only
Zone IV: CAF with turbulent fluidized bed at the bottom (TFBB)
Zone V: dense riser up-flow (DRU)
——transition DRF - CAF: G = 10 + (U - UTR)1.8
——transition CAF - CAF with TFBB: G = 20 + (U - UTR)2
.....transition CAF with TFBB - DRU: G = 60 +15 (U - UTR)0.5
– – –Range of operating conditions where CAF mode is no longer reported and only DRF and DRU prevail.

Fig. 2. Hydrodynamic operating modes of a CFB riser, expressed as G versus $U–U_{TR}$ depending on the different hydrodynamic flow modes [17].

The riser operating modes are vital to design a CFB, since producing different solid residence times and mixing behaviour and determining the efficiency of the heat transfer. Fig. 2 depicts the existence of four different operating modes (dilute, dense, core-annulus, combined) as a function of U and G in the riser [16]. The various flow regimes have distinct characteristics towards solids flow. In general, the particle velocity is defined as:

$$\overline{v}_p = \frac{U}{\varepsilon\varphi} \tag{1}$$

In the *Dilute Riser Flow (DRF)*-regime, the slip factor, φ, has a previously reported value between 1 and 1.2 [16,17]. In *Dense Riser Upflow (DRU)*, Chan et al. [17] found that the φ values are fractionally higher, ranging between 1.2 and 1.6 with an average of 1.3. In *Core-annulus Flow (CAF)*, cluster formation reduces the net velocity and φ values are close to 2 [17,18]. *CAF with Turbulent Fluidised Bottom Bed (TFBB)* is an intermediate regime. The residence time for CAF with TFBB is significantly longer than CAF itself and DRF due to the existence of the fully mixed TFBB. Chan et al. [19] demonstrated that the residence time for solids in TFBB alone can range from 10 to 20 s. The characteristics of the CAF region above the TFBB are similar to the above sole CAF flow, as described before. Together with the particle velocity, also the bed voidage is distinct, ranging respectively from about 0.99 in DRF; 0.7–0.9 in a TFBB, 0.95–0.98 in CAF, to ~0.9 in dense riser up-flow DRU [20,21].

The design of a heat capturing CFB riser requires a prediction of the heat transfer coefficient between the wall of the riser and the

Please cite this article in press as: Pitié F et al. Circulating fluidized bed heat recovery/storage and its potential to use coated phase-change-material (PCM) particles. Appl Energy (2013), http://dx.doi.org/10.1016/j.apenergy.2012.12.048

particle-gas suspension flow. The wall-to-bed heat transfer coefficient will be measured for different operating conditions of gas flow (U) and solids' circulation rate (G) and will cover the different operating modes of the riser flow (dilute, core-annulus, dense), which will be shown to have a marked influence on the heat transfer coefficient.

Heat transfer to the wall of a CFB riser can be assumed to involve additive components due to conduction, convection and radiation, similar to that described for bubbling beds [22], different since no bubbles are present, but with the flow at the wall dominated by streamers or clusters travelling upward and downward. The processes governing heat transfer are however similar, with packets of particles contacting the wall, and exchanging heat according to the known film penetration model [22]. Published empirical correlations, widely used in bubbling fluidized beds, are not common for circulating fluidized beds. Instead, a number of semi-empirical models have been proposed in the literature and discussed below. As indicated in Eq. (2), one treats the heat transfer as being composed of additive conduction/convection and radiation.

$$h_{tot} = f_d h_d + (1 - f_d) h_1 + h_r \tag{2}$$

where h_{tot}, h_d, h_l and h_r are the total effective heat transfer coefficient, the heat transfer coefficient during dense (particle) phase contact, the heat transfer coefficient during lean gas phase contact, and the heat transfer coefficient for radiation, respectively, while f_d is the time fraction of contact by the dense phase [22,23].

Previous work on heat transfer in vertically flowing gas–solid suspensions, as occurring in a CFB riser, has been extensively reviewed by Muzyka [24] and Grace [25]. As long as convective heat transfer between the suspension and the surface is considered, with the exclusion of radiant heat transfer, the major concern is to predict the variation of the heat transfer coefficient with solids loading and gas velocity in various riser geometries. Different empirical correlations and models (mostly for bed-to-wall heat transfer) have been proposed, but Grace [25] summarised the situation as follows: "no existing correlations give consistent agreement with the available data".

The theoretical approach proposed by Molodtsof and Muzyka [26] predicts the wall-to-suspension heat transfer coefficient (h_m) as a function of loading ratio (M), heat capacity ratio (C), and the gas convective transfer coefficient (h_g).

$$\frac{h_m}{h_g} = \frac{(1 + MC)^2}{1 + aMC + b(MC)^2} \tag{3}$$

The dimensionless parameters a and b in Eq. (3) are compound factors involving dimensionless radial concentration, velocity, and temperature profiles. They are generally unknowns, as the profiles are unknown. Apart from design parameters (pipe diameter, particle size distribution and physical properties), they only depend on the superficial gas velocity, and need to be fitted from experimental results for the specific gas–solid system under scrutiny.

Golriz and Grace [27] proposed a model for large units (>1 m ID) based on the assumptions of fully developed conditions and radially uniform clusters at the wall, hence valid for CAF operation. At any instant, some portions of the surface are bare, while other portions of the surface are covered by clusters, each separated from the wall by a thin gas gap of thickness δ_g. Different heat transfer mechanisms are assumed for the bare and covered portions. For the bare sections, transfer is by gas convection (denoted by subscript '*gc*') and by radiation from the suspension to the wall (subscript '*sr*'). The rest of the wall is covered by clusters/streamers providing a parallel transfer path. The transfer rate is then assumed to be controlled by a particle horizontal exchange flux, G_{sh}. The combined expression of the heat transfer coefficient is given as a total heat transfer coefficient, h_{tot}, as follows:

$$h_{tot} = (h_{gc} + h_{sr})(1 - f) + \frac{f}{\frac{1}{G_{sh} C_p + h_{be}^{rad}} + \frac{1}{(k_g/\delta_g) + h_{ew}^{rad}}} \tag{4}$$

For operation at temperatures below 600 °C, the radiation contribution can be omitted [22]. The parameters of the equation are then estimated, with an expression for the fractional coverage, f, accounting for the scale of the unit:

$$f = 1 - \exp\left[-25000\left(1 - \frac{2}{\exp(0.5D) + \exp(-0.5D)}\right)(1 - \varepsilon_{sus})\right] \tag{5}$$

where D(m) is the riser equivalent diameter (4 × cross sectional area/perimeter). For large units, f approaches unity, meaning that the entire wall becomes covered by clusters. The gas convective transfer coefficient, h_{gc}, was obtained from the well-known Dittus–Boelter correlation. If a contribution by radiation between the suspension and the bare wall is important, its contribution can be predicted as proposed in the Gorliz and Grace paper [27], or by an alternative estimation as presented in Section 5.5. of the present paper.

The gas gap thickness is estimated [28] from:

$$\delta_g = 0.0282 d_p (1 - \varepsilon_{sus})^{-0.59} \tag{6}$$

where d_p is the average particle diameter and ε_{sus} is the cross sectional average suspension void fraction. An expression for the lateral solids flux was obtained by fitting all heat transfer data for units of $D \geqslant 1$ m where the suspension densities, $\rho_{sus} = \rho_p(1 - \varepsilon_{sus}) + \rho_g \varepsilon_{sus}$, exceeded 5 kg m^{-3}, leading to:

$$G_{sh} = 0.0225 \ln(\rho_{sus}) + 0.1093 \tag{7}$$

Since the heat transfer is determined by the transient heat transfer from the wall to clusters of particles in contact, a *surface renewal model* can be applied, as initially developed by Baeyens and Geldart [22] for BFB applications.

$$h(\bar{\theta}) = \frac{h_c}{1 + \frac{6h_c}{\rho_p C_p d_p}\bar{\theta}} \tag{8}$$

2. The heat transfer mode and possible reduction of thermal gradients

The present section assesses objective 1 of the study: "how can thermal gradients in and around the particle be avoided?" Application of the basic principles of both heat transfer to the particle and of heat conduction within the particle, allows to determine the required working conditions. The temperature uniformity throughout the particles can be determined by the heat conduction law of Fourier, here applied in non-stationary regime and for the simple case of a spherical particle:

$$\frac{\partial T}{\partial t} = \frac{k_p}{\rho_p c_p}\left(\frac{\partial^2 T}{\partial r^2} + \frac{2}{r}\frac{\partial T}{\partial r}\right) \tag{9}$$

with symbols defined in the Nomenclature.

$\partial T/\partial t = \beta$ for $r = 0$ to R ($=d_p/2$) and $\partial T/\partial r = 0$ for $r = 0$ (in the core)

The solution is given by Carslaw and Jaeger [29] as:

$$\Delta T_{\max} = (T_R - T_c) = \beta d_p^2/(24\alpha) \tag{10}$$

Applied for various values of β and with e.g. the characteristic properties of an inorganic particle at 773 K, i.e. $k_p = 0.60$ W m^{-1} K^{-1}, $c_p = 1150$ J kg^{-1} K^{-1} and $\rho_p = 2800$ kg m^{-3}, results are a set of curves in function of the diameter as shown in Fig. 3.

Please cite this article in press as: Pitié F et al. Circulating fluidized bed heat recovery/storage and its potential to use coated phase-change-material (PCM) particles. Appl Energy (2013), http://dx.doi.org/10.1016/j.apenergy.2012.12.048

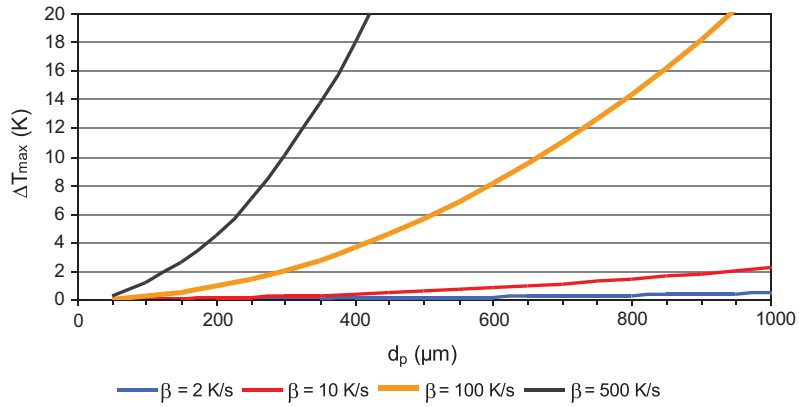

Fig. 3. Maximum temperature difference (ΔT_{max}) between the surface and core of the particle in function of the particle diameter at different heating rates (β).

These calculations show that the temperature differences between the particle surface and core are very limited, certainly when considering that the surrounding temperature is 773 K.

The heating rate will vary with the heating technique applied, between minimally 1.5 K s^{-1} in a TGA (thermogravimetic analysis), to >>100 K s^{-1} in a BFB or CFB [22]. In order to minimise ΔT_{max} (<10 K) even at high heating rates, it is appropriate to use small inorganic particles (sand, SiC, etc.) below 400 μm. No significant thermal gradient will occur in these small particles, even when working at slow heating rates: the core and the surface of the particle will behave thermally in a similar way.

Solar energy capture and subsequent heat release require a fast heat transfer from the exchanger wall to/from the particles. This heat transfer is conditioned by the degree of gas and solid turbulence achieved in the collector. The heat transfer coefficient depends on the gas–solid contacting mode. It ranges from 10 W m^{-2} K^{-1} for a static bed, to 50–100 W m^{-2} K^{-1} in a fixed bed with forced gas circulation (as in TGA), and several hundreds of W m^{-2} K^{-1} for BFB and CFB [22]. This explains why fluidized beds are specifically considered as top technologies for solar energy systems. The value of the heat transfer coefficient in a CFB was previously reported between 150 and 600 W m^{-2} K^{-1}. The experimental results of the present research are given in Section 4 below,

Since not only external convection but also internal conduction is important, the overall picture is expressed by the Biot-number, as the ratio of the internal resistance to heat penetration and the external convection resistance to heat transfer.

$$Bi = (d_p/k_p)/(1/h) \tag{11}$$

For the 100 μm particle at 773 K, the values are as follows:

$h = 150$ W m^{-2} K^{-1} Bi $= 100.10^{-6}$. $150/0.60 = 0.025$

$h = 300$ W m^{-2} K^{-1} Bi $= 100.10^{-6}$. $300/0.60 = 0.05$

$h = 500$ W m^{-2} K^{-1} Bi $= 100.10^{-6}$. $500/0.60 = 0.08$

The Biot-number is <<1 in all cases, implying that the external resistance associated with convection heat transfer largely dominates for smaller particles. This remains valid for particle sizes below ~700 μm. Bi is only >1 for coarser particles. This result confirms Fig. 3 where limited increasing ΔT_{max} values are noticed with increasing β values (achieved at high convection heat transfer rates), for smaller particles, but significant differences occur for coarser particles. Operating a CFB collector at $d_p <$ ~400 μm is hence certainly indicated to avoid thermal gradients within the particle. Fortunately, CFB operations are restricted to particle sizes of similar magnitude [16].

3. Experimental setup and procedure: wall-to-bed heat transfer

The experimental riser and CFB are depicted in Fig. 4.

The riser consists of a 50 mm ID pipe approximately 2.5 m high. Solids circulation was achieved via a 100 mm ID downcomer and 50 mm ID L-valve. Air is supplied through a distributor plate and leaves the system through a cyclone after the riser exit. Pressure taps are located along the height of the riser and connected to a data acquisition system. Flow rates and pressure drops were monitored. A concentric wall heater of 10 cm length was installed at 1.2 m above the re-entry joint of the L-valve. Heat supply was by hot water (60–90 °C) or by thermal fluid (Santotherm 350). The downcomer was water-cooled through a 0.2 m long concentric cooler. The bed temperature was kept within the range of 30–40 °C. The wall surface temperature was measured using a resistance thermocouple welded onto the wall. Additional Thermocoax thermocouples (0.1 mm OD) were installed at various locations in the riser and downcomer, as well as in the feeding and overflow lines of the fluid, as indicated in Fig. 4. The flow rates of gas and solids were set to the desired values, the heat input into the system was fixed, and the system was allowed to stabilize over a period of about one hour, during which flow rate, temperatures, and pressures were monitored and recorded.

The axial pressure profile was recorded during each experiment in order to make sure that the suspension entering the heated section was in fully developed flow conditions. From the known exposed surface area, A_{ex}, and measured wall-to-bed temperature difference, ΔT, the heat transfer coefficient was calculated for the given heat input as:

$$h_m = \frac{Q}{A_{ex}\Delta T} \tag{12}$$

The measurements were performed for the gas flow alone (h_g) and for the gas–solid suspension at various solid/gas ratios (h_m). The heat transfer coefficient to the gas–solid suspension, h_m, was also expressed as h_m/h_g ratio. The bed material used was rounded sand of the following characteristics: d_{sv} = 75 μm, ρ_p = 2260 kg/m^3, and C_p = 1.05 kJ/kg K.

Various combined (U,G) values were tested in order to scan the different riser hydrodynamic regimes: these experimental conditions are illustrated in Fig. 5, using the Mahmoudi et al. [16] regime diagram as a basis. Clearly DRF, CAF and DRU hydrodynamic regimes were investigated.

Please cite this article in press as: Pitié F et al. Circulating fluidized bed heat recovery/storage and its potential to use coated phase-change-material (PCM) particles. Appl Energy (2013), http://dx.doi.org/10.1016/j.apenergy.2012.12.048

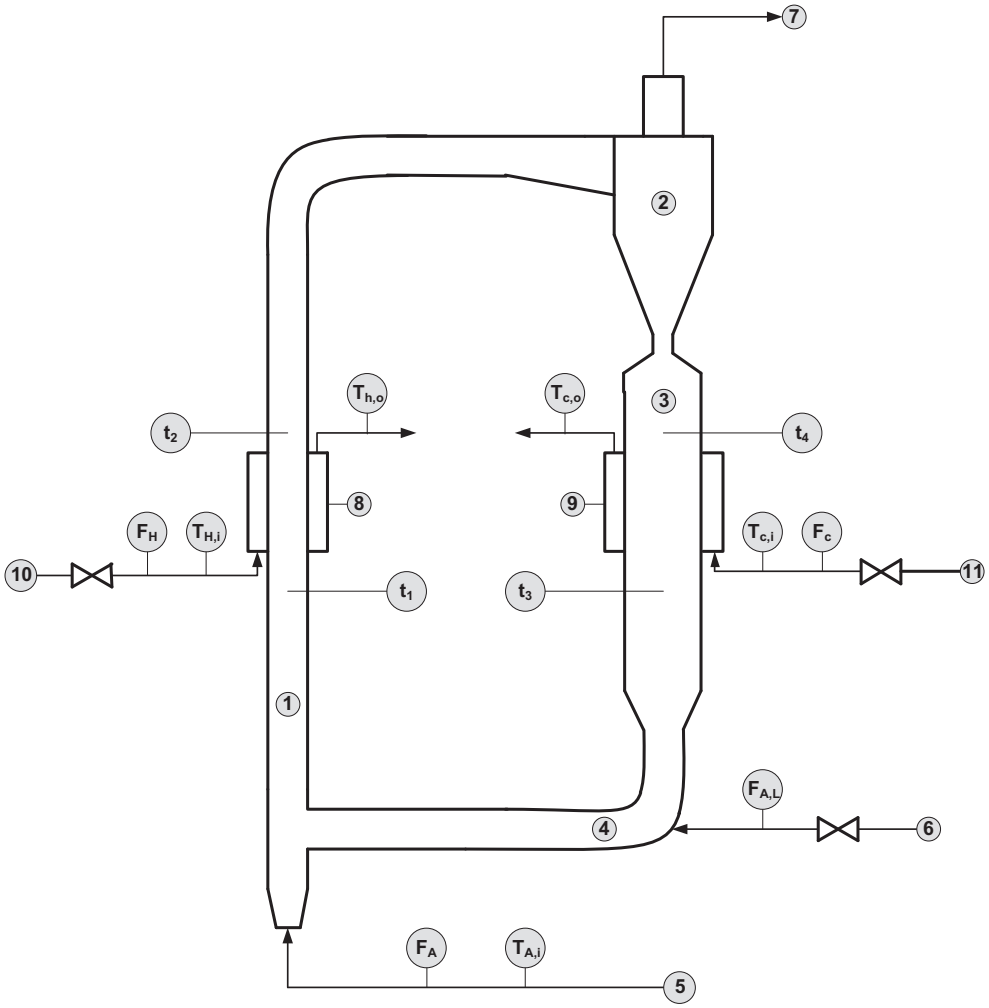

(1) riser 50 mm I.D., (2) HE Stairmand cyclone, (3) downcomer 100 mm I.D.,(4) L-valve 50 mm I.D., (5) air from speed-controlled blower,(6) compressed air, (7) vent to baghouse filter, (8) co-axial heating section, (9) co-axial cooling section, (10) supply of thermal fluid, (11) supply of cooling water;F_H, F_C, F_A, $F_{A,L}$: respectively flow meters of thermal fluid, cooling water, riser air, L-valve air;T: temperature probes for respective fluids;t : temperature probes inside riser and downcomer.

Fig. 4. Layout of the experimental set-up.

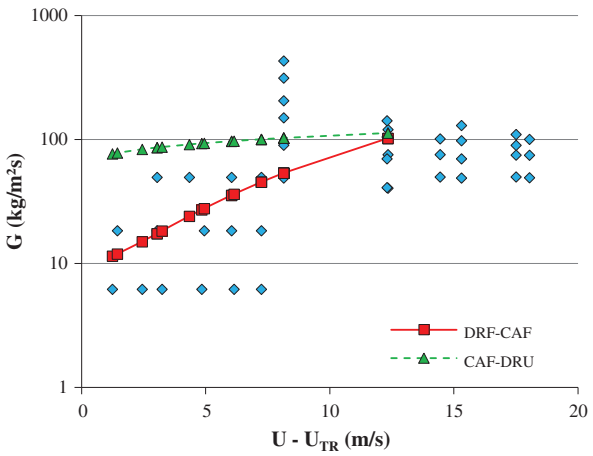

Fig. 5. Experimental (*U*,*G*) conditions in comparison with the riser flow modes.

4. Results and discussion

4.1. The gas convection coefficient

Essential in the use of the semi-experimental equations, is the prediction of the heat transfer coefficient when solids are absent, i.e. the heat transfer coefficient between the heat transfer surface and a pure gas flow at velocity *U*, in the riser, h_g. The Gnielinski equation [30] is used to predict h_g in the present treatment, to cover gas flow in the transitional and turbulent flow regime.

$$\mathrm{Nu} = \frac{h_g D}{k_g} = \frac{(\frac{\zeta}{8})(\mathrm{Re} - 1000)\mathrm{Pr}}{1 + 12.7\sqrt{\frac{\zeta}{8}}(\mathrm{Pr}^{2/3} - 1)}\left(1 + \left(\frac{D}{L}\right)^{2/3}\right) \tag{13}$$

with $\zeta = \sqrt{1.82\log(\mathrm{Re}) - 1.64}$ and other symbols defined in the Nomenclature.

Please cite this article in press as: Pitié F et al. Circulating fluidized bed heat recovery/storage and its potential to use coated phase-change-material (PCM) particles. Appl Energy (2013), http://dx.doi.org/10.1016/j.apenergy.2012.12.048

4.2. Experimental results for the riser-wall to bed heat transfer coefficient, h_m

Experimental results, expressed as the ratio of h_m/h_g, are illustrated in Fig. 6. Clearly, h_m is a strong function of the (U,G) combination, especially at lower G values, thus also of the hydrodynamic operating mode of the riser. Experimental results will further be developed in terms of the empirical and model approaches of Section 1.2. At $G = 0$, h_m should assume the h_g heat transfer coefficient, only a function of U.

4.3. Preliminary literature findings

In a previous research, Everaert et al. [31] studied the heat transfer coefficient to an in-bed heat transfer surface in a 0.1 m I.D. riser. Experiments were carried out in the DRF and CAF operating modes. Relevant results with respect to the present research determine that: (i) the core region extends to approximately 85% of the riser radius (0.05 m) with an annulus thickness of approximately 7.5 mm; (ii) increasing the gas flow rate at a given solid circulation rate significantly reduces the suspension heat transfer coefficient; (iii) the heat transfer coefficient is a function of the radial position in the riser, as illustrated in Fig. 6: the heat transfer coefficient in the core is significantly higher than at the wall; and (iv) even in dilute flow, i.e. at the low G values of Fig. 7, the solids contribute significantly to the overall heat transfer coefficient, since the ratio h_m/h_g exceeds ~2.

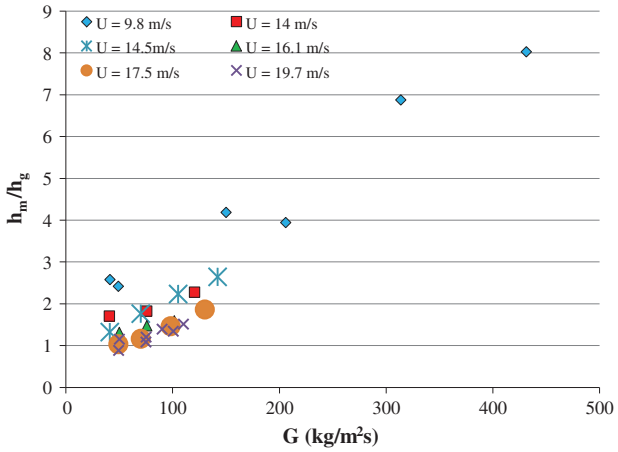

Fig. 6. Experimental results, expressed as h_m/h_g, for different (U,G) combinations.

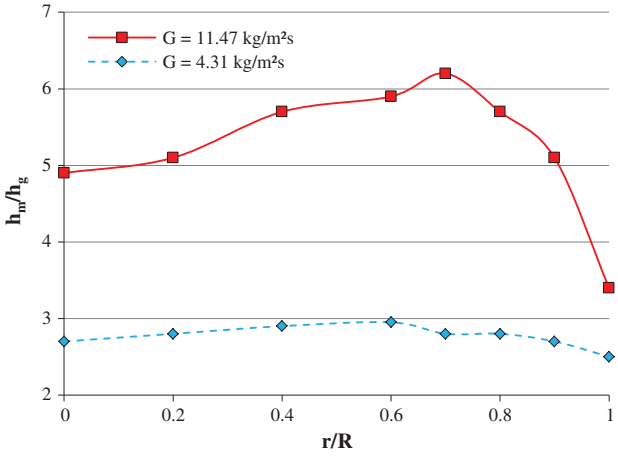

Fig. 7. Effect of the radial position of the heater in the riser on the heat transfer coefficient h_m (expressed as ratio) at $U_g = 7.8$ m/s.

5. Transformation of experimental results into design equations

5.1. Molodtsof and Muzyka

All results were expressed as h_m/h_g values. Experimental h_m/h_g-ratios can be fitted by Eq. (6), to determine the unknown coefficients a and b.

Since the solid-to-gas heat capacity was constant in our experiments, the results could be used to define coefficients a and b (which remain constant in the range of gas velocities and solids loadings) and thereafter predict h_m/h_g for various values of M and C. The results are given in Fig. 8, illustrating the fair agreement obtained, with coefficients a and b respectively 3.37 and 0.028 ($R^2 = 96.5\%$). Of course, the design application of the Molodtsof and Muzyka approach needs the experimental determination of the fitting coefficients a and b.

5.2. Golriz and Grace

The empirical equations of Golriz and Grace [27]can be transformed into the following equation, when radiation is neglected.

$$\frac{h_m}{h_g} = (1-f) + \frac{f}{\left(\frac{1}{G_{sh}C_p} + \frac{1}{k_g/\delta_g}\right)} \tag{14}$$

The suspension density and particle residence time (t_p) were calculated according to Chan et al. [19]. The values of the gas residence time (t_g) was calculated by the method presented in Mahmoudi et al. [32], thus a function of U and G.

$$\varepsilon_{sus} = \frac{Ut_g}{Ut_g + Gt_p/\rho_p} \tag{15}$$

$$\rho_{sus} = \varepsilon_{sus}\rho_g + (1-\varepsilon_{sus})\rho_p \tag{16}$$

Although outside the range of applicability of the initial Gorliz and Grace correlations (experimental $D << 1$ m), the comparison between experimental and predicted values is illustrated in Fig. 9A. Since Golriz and Grace only deal with CAF applications ($G \lesssim 100$ kg/m^2 s), the experimental results of the CAF regime were only used for the comparison. The deviation is between ~250% and 400%. This deviation is not only due to the scale of the riser, but also inherently linked to the required calculation of the underlying empirical parameters. The Gorliz–Grace equations are indeed very sensitive to the predicted value of G_{sh}.

A very fair agreement of the experimental and predicted heat transfer coefficient ratios, covering all of the different CFB operat-

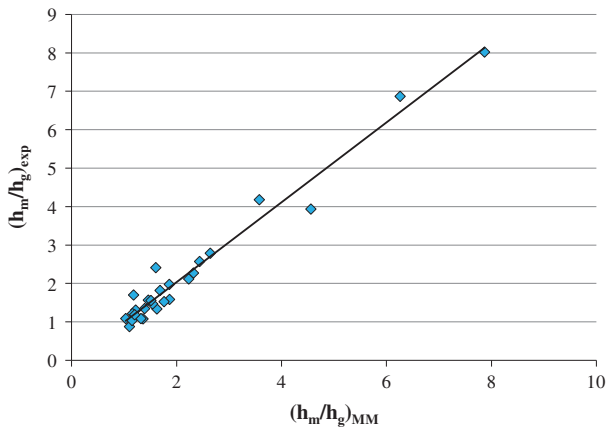

Fig. 8. Comparison of experimental and Molodstof–Muzyka (MM) predicted values of h_m/h_g.

Please cite this article in press as: Pitié F et al. Circulating fluidized bed heat recovery/storage and its potential to use coated phase-change-material (PCM) particles. Appl Energy (2013), http://dx.doi.org/10.1016/j.apenergy.2012.12.048

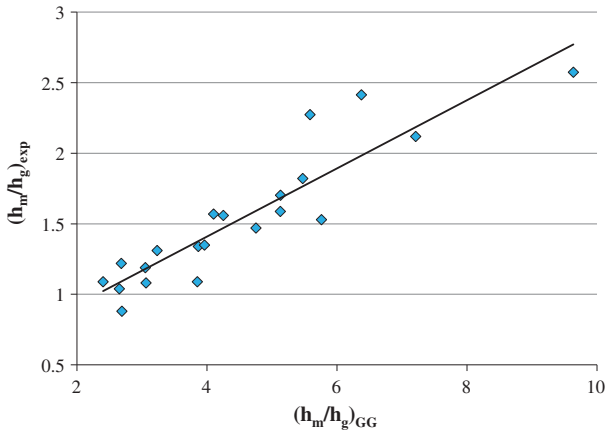

Fig. 9A. Comparison of experimental and Golriz–Grace (GG) predicted values of h_m/h_g (for $G \lesssim 00$ kg/m^2 s), according to the estimated parameters of the initial equations.

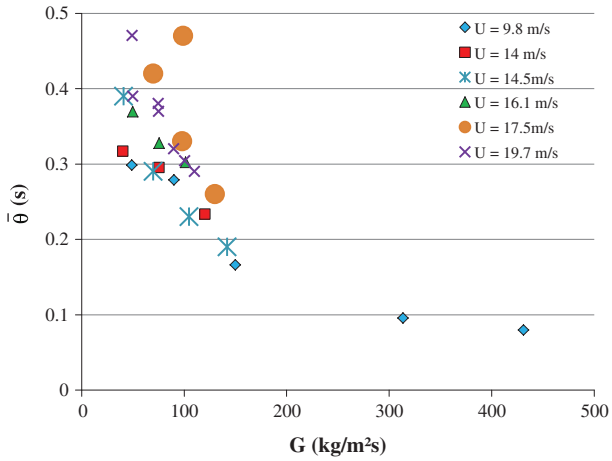

Fig. 10. Fitting contact time $\bar{\theta}$ for different combinations of U and G.

ing regimes, was obtained by using a modified dependency of G_{sh} and ρ_{sus} according to:

$$G_{sh} = 0.014 \text{ for } \rho_{sus} \geq 12 \text{ kg m}^{-3}, \text{ hence in the DRU operating mode} \quad (17)$$

$$\text{And } G_{sh} = 0.014 + 0.006(12 - \rho_{sus}) \text{ for } \rho_{sus} < 12 \text{ kg m}^{-3} \quad (18)$$

When applying these G_{sh} values, a very good fitting is obtained, as illustrated in Fig. 9B.

5.3. Surface renewal model

Comparing experimental h_m values with predictions using Eq. (8) enables the determination of the required fitting $\bar{\theta}$. This $\bar{\theta}$ value is represented in Fig. 10, the fitting value of $\bar{\theta}$ and the trend of its dependency on (U,G) again stresses the importance of the riser operating mode. At high values of G, irrespective of U, the riser operates in the DRU (dense upwards flow) mode, and the contact time is determined by the prevailing solids velocity. This velocity is close to the operating gas velocity: according to Eq. (5) with $\varepsilon \sim 0.9$ and $\varphi \sim 1.3$, $\bar{\theta} \sim 0.1$ s. This particle velocity defined contact time is in fair agreement with the calculated fitting time.

In the CAF regime, for $G \lesssim 100$ kg/m^2 s, the contact time is a function of the downward velocity, normally assumed to be close to the terminal velocity of the particles, i.e. 0.38 m/s for the tested particles. For the heater length of 0.1 m, the contact time should hence be close to 0.26 s, again in fair agreement with the experimental fitting results. The application of the contact time approach therefore certainly merits further investigations. These will combine heat transfer measurements and particle residence time measurements by Positron Emission Particle Tracking. These experiments are programmed and will be subsequently reported upon.

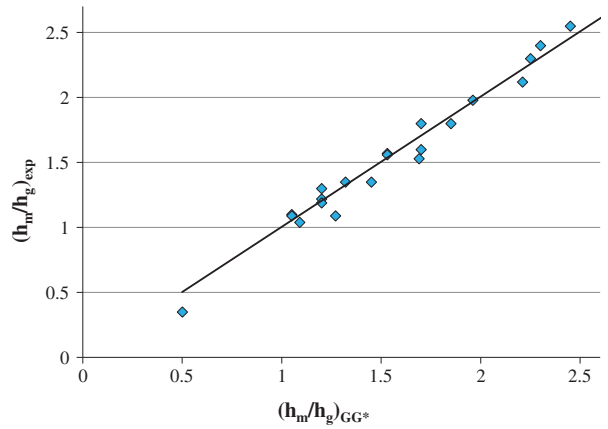

Fig. 9B. Comparison of experimental and Golriz–Grace (GG) predicted values of h_m/h_g, according to G_{sh} predictions of Eqs. (17) and (18).

5.4. Contribution of radiant heat transfer

The effects of an increasing temperature are twofold:

(i) The particle convective heat transfer coefficient will increase due to the increasing thermal conductivity of the gas phase, included in the contact transfer resistance, h_c, of Eq. (8). In general [22], the convective heat transfer coefficient will increase proportional to $\sqrt{k_g}$.
(ii) At $T > 600$ °C [22], radiation itself becomes important and can be calculated by using the well-known Stefan–Boltzman equation. In general, the contribution of radiation to the overall total heat transfer coefficient will increase from ~10% at 600 °C to ~20% at 800 °C [22].

Both the effects of k_g and of radiation from wall-to-bed will significantly increase the heat transfer coefficient at bed temperatures of 500–750 °C and wall temperatures >850 °C, as encountered in solar energy capture beds.

5.5. The advantages of using PCM-particles in the CFB solar energy capture

Despite the excellent heat transfer coefficient to common heat carrier particles such as sand or SiC, these systems suffer from some drawbacks, being mainly: (i) the progressive increase in bed temperature as the particles are conveyed from the inlet of the riser (500 °C) to its outlet (750 °C), thus progressively reducing the driving heat transfer temperature difference between wall and bed; and (ii) the sole heat capture in the form of sensible heat, where the amount of heat to be removed, (Q), necessitates a high circulation rate (kg/h) of particles, being $Q/C_p\,(T_{out} - T_{in})$. High circulation rates involve high associated conveying operation costs.

When using PCM-materials, (i) the bed temperature will achieve its (constant) maximum at the temperature of fusion of the PCM, thus maintaining a slightly higher driving temperature difference; but most importantly, and (ii) sensible and latent heat

Please cite this article in press as: Pitié F et al. Circulating fluidized bed heat recovery/storage and its potential to use coated phase-change-material (PCM) particles. Appl Energy (2013), http://dx.doi.org/10.1016/j.apenergy.2012.12.048

(of fusion) will take part in absorbing Q, thus reducing the required circulation rate of particles by a factor of $\gtrsim 3$ at the given temperature ranges. This significant reduction also reduces the required conveying power and associated costs by the same factor. The development of PCM-coated particles, that can withstand both the thermal stress of temperature and phase variations, but also the erosive nature of the CFB is of paramount importance, and currently investigated. According to the results of the present research, these PCM particles, still to be developed and manufactured, should be of particle size well below 400 μm to avoid the internal conduction resistance, while offering advantages of a high composite specific heat capacity, affecting both the heat capacity ratio, C, in the Molodtsof–Muzyka Eq. (3), and the denominator of Eqs. (7) and (8).

6. Conclusions and recommendations

Within the thermal energy capture and/or storage systems currently available or investigated, PCMs are the sole latent heat stores. The present paper introduces these PCMs, and their potential application in high temperature energy capture and storage, using a circulating fluidized bed (CFB) as transfer/storage mode. Thermal considerations determine the optimum size range for the applied particles (<400 μm), when convection heat transfer dominates. In the design of a CFB heat collector, the heat transfer coefficient between the riser wall and the flowing suspension is an important design parameter to determine the required heat exchange surface area. The present research measured the wall-to-bed heat transfer coefficient in the riser, with values of $\sim$60 W m^{-2} K^{-1} at low G and high U values, and up to 350 W m^{-2} K^{-1} at higher G values. The ratio of the suspension heat transfer coefficient and the convective transfer coefficient for the sole gas flow, is confirmed as a valid fitting parameter. Experimental results are expressed in terms of this ratio. The application of Molodtsof and Muzyka requires the determination of two empirical constants by using the experimental results. Once best fit values of these coefficients are obtained, the correlation predicts the correct trend of the evolution in heat transfer coefficient with U and G.

The initial set of equations of Golriz and Grace, overestimates the experimental results by a factor of about three. A very good fit is obtained with a modified expression for G_{sh}.

When applying a packet renewal mechanism to predict the heat transfer coefficient, the definition of a contact time on the basis of particle velocities in the riser, highly different in function of the riser operating regime, appears to predict heat transfer coefficient values of the correct order of magnitude. Further research coupling heat transfer measurements and particle contact times (as measured by Positron Emission Particle Tracking) are needed to improve the renewal approach.

Acknowledgements

This work was partly developed in the frame of the CSP2 European project. Authors acknowledge the European Commission for co-funding the "CSP2" Project-Concentrated Solar Power in Particles – (FP7, Project No. 282 932). It is also partly supported by the UK Engineering and Physical Science Research Council (EPSRC grant number: EP/F061439/1), and by the National Natural Science Foundation of China (Grant Nos. 51176110 and 51071184). The authors gratefully acknowledge support and advice from Prof. G. Cacères (Faculdad de Ingenierià y Ciencias, Universidad Adolfo Ibánez, Santiago, Chile), and Prof. Z. Tamainot Telto of the School of Engineering, University of Warwick, Coventry, UK.

References

[1] Fernandes D, Pitié F, Caceres G, Baeyens J. Thermal energy storage: how previous findings determine current research priorities. Energy 2012;39:246–57.
[2] Pitié F, Zhao CY, Cáceres G. Thermo-mechanical analysis of ceramic encapsulated phase-change-material (PCM) particles. Energy Environ Sci 2011;4:2117–24.
[3] Joulin A, Younsi Z, Zalewski L, Lassue S, Rousse DR, Cavrot J-P. Experimental and numerical investigation of a phase change material: thermal-energy storage and release. Appl Energy 2011;88:2454–62.
[4] Li M, Wu Z, Tan J. Properties of form-stable paraffin/silicon dioxide/expanded graphite phase change composites prepared by sol–gel method. Appl Energy 2012;92:456–61.
[5] Castell A, Belusko M, Bruno F, Cabeza LF. Maximisation of heat transfer in a coil in tank PCM cold storage system. Appl Energy 2011;88:4120–7.
[6] Martin V, He B, Setterwall F. Direct contact PCM–water cold storage. Appl Energy 2010;87:2652–9.
[7] Rady M. Thermal performance of packed bed thermal energy storage units using multiple granular phase change composites. Appl Energy 2009;86:2704–20.
[8] Oró E, de Gracia A, Castell A, Farid MM, Cabeza LF. Review on phase change materials (PCMs) for cold thermal energy storage applications. Appl Energy 2012;99:513–33.
[9] Zhou D, Zhao CY, Tian Y. Review on thermal energy storage with phase change materials (PCMs) in building applications. Appl Energy 2012;92:593–605.
[10] Borreguero AM, Luz Sánchez M, Valverde JL, Carmona M, Rodríguez JF. Thermal testing and numerical simulation of gypsum wallboards incorporated with different PCMs content. Appl Energy 2011;88:930–7.
[11] Tay NHS, Belusko M, Bruno F. Experimental investigation of tubes in a phase change thermal energy storage system. Appl Energy 2012;90:288–97.
[12] Pavel PM, Constantinescu M, Anghel EM, Olteanu M. Solidification of a PEG 1500-epoxy nanocomposite around a horizontal pipe. Appl Energy 2012;89:482–9.
[13] Medrano M, Yilmaz MO, Nogués M, Martorell I, Roca J, Cabeza LF. Experimental evaluation of commercial heat exchangers for use as PCM thermal storage systems. Appl Energy 2009;86:2047–55.
[14] Lamberg P. Approximate analytical model for two-phase solidification problem in a finned phase-change material storage. Appl Energy 2004;77:131–52.
[15] European Union. 7th. Framework program for research and technical development CSP2 concentrated solar power in particles. EU Grant Reference: 282932; 2011.
[16] Mahmoudi S, Chan CW, Brems A, Seville JPK, Baeyens J. Solids flow diagram of a CFB riser using Geldart B-type powders. Particuology 2012;10:51–61.
[17] Chan CW, Seville JPK, Parker DJ, Baeyens J. Particle velocities and their residence time distribution in the riser of a CFB. Powder Technol 2010;203:187–97.
[18] Ouyang S, Potter OE. Consistency of circulating fluidized bed experimental data. Ind Eng Chem Res 1993;32:1041–5.
[19] Chan CW, Seville JPK, Yang Z, Baeyens J. Particle motion in the CFB riser with special emphasis on PEPT-imaging of the bottom section. Powder Technol 2009;196:318–25.
[20] Smolders K, Baeyens J. Gas fluidized beds operating at high velocities: a critical review of occurring regimes. Powder Technol 2001;119:269–91.
[21] Smolders K, Baeyens J. Hydrodynamic modelling of the axial density profile in the riser of a low-density circulating fluidized bed. Can J Chem Eng 2001;79:422–9.
[22] Baeyens J, Geldart D. Modelling approach the effect of equipment scale on fluidized bed heat transfer data. J Powder Bulk Solids Technol 1980;4:1–9.
[23] Chen JC, Grace JR, Golriz MR. Heat transfer in fluidized beds: design methods. Powder Technol 2005;150:123–32.
[24] Muzyka DW. Use of probabilistic multiphase flow equations in the study of the hydrodynamics and heat transfer in gas–solids suspensions. Ph.D. thesis. University of Western Ontario; 1985.
[25] Grace JR. Heat transfer in high velocity fluidized beds. In: Hetsroni G, editor. Heat transfer 1990, vol. 4. New York: Hemisphere; 1990. p. 329–39.
[26] Molodtsof Y, Muzyka DW. General probabilistic multiphase flow equations for analyzing gas–solids mixtures. Int J Eng Fluid Mech 1989;2:1–24.
[27] Golriz M, Grace JR. Predicting heat transfer in large-scale CFB boilers. In: Grace JR, Zhu J, de Lasa HI, editors. Circulating fluidized bed technology VII. Ottawa, ON, Canada: Canadian Society for Chemical Engineering; 2002. p. 121–8.
[28] Lints MCL, Glicksman LR. The structure of particle clusters near the wall of a circulating fluidized bed. In: Weimer AW, editor. Fluid-particle processes, vol. 89. New York (NY): American Institute of Chemical Engineers; 1993. p. 35–52.
[29] Carslaw HS, Jaeger JC. Conduction of heat in solids. Oxford [Oxfordshire]: Oxford University Press; 1986.
[30] Gnielinski V. Fundamentals of heat and mass transfer. Fundamentals of heat and mass transfer. Hoboken (NJ): John Wiley; 2007. pp. 514–5.
[31] Everaert K, Baeyens J, Smolders K. Heat transfer from a single tube to the flowing gas–solid suspension in a CFB riser. Heat Transfer Eng 2006;27:66–70.
[32] Mahmoudi S, Seville JPK, Baeyens J. The residence time distribution and mixing of the gas phase in the riser of a circulating fluidized bed. Powder Technol 2010;203:322–30.

Please cite this article in press as: Pitié F et al. Circulating fluidized bed heat recovery/storage and its potential to use coated phase-change-material (PCM) particles. Appl Energy (2013), http://dx.doi.org/10.1016/j.apenergy.2012.12.048